# Three-Dimensional Numerical Modelling of Geo-Electromagnetic Induction Phenomena

by

Xing-Hua Pu

B.Sc., University of Science & Technology of China, 1982
M.Sc., Institute of Geology of the State Seismological Bureau of China, 1986

A Dissertation Submitted in Partial Fulfillment of the Requirements for the Degree of
DOCTOR OF PHILOSOPHY
in the Department of Physics and Astronomy

We accept this dissertation as conforming to the required standard

---

Dr. J.T. Weaver, Supervisor (Department of Physics and Astronomy)

---

Dr. H.W. Dosso, Departmental Member (Department of Physics and Astronomy)

---

Dr. R.E. Horita, Departmental Member (Department of Physics and Astronomy)

---

Dr. F.H. El Guibaly, Outside Member (Department of Electrical Engineering)

---

Dr. D.E. Hewgill, Outside Member (Department of Mathematics)

---

Dr. F.W. Jones, External Examiner (Department of Physics and the Institute of Geophysics, Meteorology and Space Physics, University of Alberta)

# Abstract

A finite difference algorithm for solving the forward modelling problem of geo-electromagnetic induction in three-dimensional structures has been developed in this thesis. Novel features of the method include the incorporation of a thin sheet of anomalous conductance at the surface of an otherwise quite general three-dimensional structure in which the anomalous region is allowed to approach two-dimensional configurations at infinity; the use of magnetic rather than the electric field components for obtaining the solution; the use of integral boundary conditions at the top and bottom of the model; and the application of new cell-integral finite difference equations to the main body of the model.

The algorithm has been tested for synthetic models against results delivered by existing two and three dimensional modelling programs which are already well established. The results are found to be very satisfactory. Applications of the algorithm have been shown for two cases. First, the dependence of the induction vectors on the period ranging from 10 to 10000 s has been studied for a model with two perpendicular lateral conductivity contrasts; the directions of induction vectors vary from site to site reflecting the combined effect of the two perpendicular contrasts. In the second case, the distortion effect due to small surface inhomogeneities over a buried 2D anomaly was studied using induction vectors and difference vectors. There is evidence of mutual coupling in a certain region which invalidates a simple subtraction of the vectors to reveal the form of the buried anomaly, but elsewhere the procedure appears to be quite valid.

Since surface anomalies can be simulated by an anomalous thin sheet over the general 3D structure, it is suggested that this algorithm could be very useful

for testing the validity of existing schemes for impedance tensor decompositions used in MT studies when surface anomalies are thought to be distorting the real data.

Examiners:

Dr. J.T. Weaver, Supervisor (Dept. of Physics and Astronomy)

Dr. H.W. Dosso, Departmental Member (Dept. of Physics and Astronomy)

Dr. R.E. Horita, Departmental Member (Dept. of Physics and Astronomy)

Dr. F.H. El Gamaly, Outside Member (Dept. of Electrical Engineering)

Dr. D.E. Hewgill, Outside Member (Dept. of Mathematics)

Dr. F.W. Jones, External Examiner (Dept. of Physics and the Institute of Geophysics, Meteorology and Space Physics, University of Alberta)

# Contents

# List of Figures

# Acknowledgements

With great pleasure, I thank my supervisor, Dr. J.T. Weaver for his invaluable guidance, assistance and encouragement throughout the course of this study. The help from Dr. Weaver not only comes from him personally, but also from the book he has just finished recently, both from its contents and its LaTeXfiles for many equations, graphs and bibliography.

I sincerely wish to thank my colleague, Dr. A.K. Agarwal for checking my equations and computer programs and providing numerical results obtained by other established programs for comparison. His encouragement, persistence and even direct involvement at times when progress was stalled was both helpful and fruitful.

I also want to thank Bob Allen, Melvin Klassen and Terry Slater for their advice and assistance on computer-related matters, Dr. D.E. Hewgill for his assistance in using the MAPLE symbolic computation system and Dr. H.W. Dosso for his helpful suggestions in the writing of this thesis. Many other people have also helped me one way or another, it is not practical to list all their names, but their assistances are greatly valued.

The patience and moral support from my wife, Shi Ning, during the years of my study and writing this thesis are highly appreciated.

At last, financial support provided by a University of Victoria Graduate Fellowship, and from my supervisor's Natural Sciences and Engineering Research Council of Canada research grant are gratefully acknowledged.

# Dedication

---

谨以此论文敬献给我的父母蒲一平，王玲慧。

是你们在社会动荡不安及物质极其匮乏的年代把我和弟弟们带大；在读书无用的浪潮中，鼓励我们努力学习，并以身作则。是你们在重重经济困难中坚强地挑起了供养我们同时上大学的重担。是你们的智慧，引导及无私的奉献使我的今天成为可能。但愿这篇论文——这颗经由你们的儿子辛勤浇灌，并成熟於异国他乡的劳动果实——能够在你们回忆往日的艰辛时，为你们带来一丝心灵上的宽慰。

To my beloved parents, PU Yi-Ping and WANG Ling-Hui.

Without their selfless sacrifices and wise guidance, the present work would not have been possible. They struggled to bring up me and my brothers during a time of great political turmoil and economic hardship in China. They guided us into the realm of intellectual inquiry at a time when in China knowledge was condemned and academic learning was deemed useless. Further more, they tenaciously shouldered the enormous financial responsibility of putting me and my brothers (at one time simultaneously) through undergraduate studies at university. It is my sincere hope that this dissertation will bring some comfort to their hearts when they remember the hardship they have endured for us in those past years.

# Chapter 1

# INTRODUCTION AND BASIC EM INDUCTION PROBLEMS

## 1.1 History of Geoelectromagnetic Induction

According to Faraday's Law, any time-varying external electromagnetic (EM) field will induce electric current within a conducting body. The EM field associated with the induced current varies with the conductivity structure of the conducting body. By measuring these fields (usually on the surface), the interior structure of the body can be revealed. The earth can be considered as a conducting body, and is exposed to the external geomagnetic field, which can be generated by the current systems located in the ionosphere and magnetosphere. It should, therefore, be possible that the earth's interior can be inferred from the EM field observed on its surface. The question is how? A natural way is to match the field data (the EM response actually collected on the earth's surface) with the theoretical data ( the EM response of given conducting models obtained by analytical solution, analogue modelling or numerical modelling). Once the data match, the given model might represent the real conductivity distribution in the earth to a certain degree.

This study is called geo-electromagetic induction and it can be divided into two types: global studies and local studies (Price, 1964). In the global studies, the earth is treated as a whole and the induced current system has a world wide dimension. Rikitake (1973) reviewed the global conductivity measurements for the spherical earth. He indicated how the frequency range (0.0001-0.2 cy-

cles/day) can be used to obtain estimates of the conductivity as a function of depth from about (400 - 1500) km. The generally accepted picture for the earth is that there is a near-surface layer about 400 km thick with conductivity no greater than 0.1 S/m, below which the conductivity rises rapidly to 1 S/m and subsequently increases to about 100 S/m at about 2000 km.

In local studies, the earth is treated as a flat half space, and the anomalous features for transient geomagnetic variations over a limited region (usually a few hundred kilometers) are investigated. According to the distribution of the conductivity, geomagnetic induction studies can be categorized as one-dimensional (1D), two-dimensional (2D) and three-dimensional (3D) problems.

The induction in a uniform conducting half-space by external magnetic sources was thoroughly studied by Price (1950). A parallel treatment by Gordon (1951) investigated the induction by both external electric and magnetic sources and retained the time dependence of the fields. Weaver (1971) simplified Price's study by employing electric and magnetic Hertz potential vectors normal to the surface and expressed the solutions in terms of the known source at the surface through a systematic application of integrals. This method was later extended to a half-space consisting of N horizontal layers by Summers and Weaver (1973). The layered conductor problem has been reviewed by Weaver (1973).

When the conductivity of the earth varies only along the vertical direction, it is called a one-dimensional (1D) problem. For such a 1D problem, e.g. a stratified earth, the magneto-telluric method (MT) is particularly interesting. Cagniard (1953) initiated this study with a discussion of a plane wave falling on a layered conductor. Wait (1954) discussed the extension to complex angles of incidence, thus allowing more general sources to be considered, and indicated to what extent Cagniard's method was valid for a uniform half-space. Price (1962) discussed the MT method accounting for the source distribution and pointed out how source inhomogeneities are of greater consequence for a true layered

structure than a uniform one. After many years of work, for the 1D model, not only the forward modelling problem is fully solved, even the inversion problem is probably regarded as a closed book by many practioners in the field of EM induction. The inversion of MT data can now be performed automatically by computer (Weaver and Agarwal, 1993).

When the conductivity of the earth varies in one horizontal direction only, it is a two-dimensional (2D) problem. For 2D structures, only a few special models have been solved analytically, such as a vertical outcropping fault over either a perfect insulator or a perfect conductor (d'Erceville and Kunetz 1962), an outcropping dike (Rankin, 1962), and infinite vertical fault ( Weaver, 1963) and segmented overburden model (Weaver LeQuang and Fischer, 1985, 1986). Although analytic solutions can be obtained only for a handful of simple cases, the solutions do serve as a check on more general numerical methods and may indicate properties not so evident in numerical solutions. On the other hand, numerical methods, based on finite difference (FD), finite element (FE), integral equation (IE) or other techniques are quite powerful and general. 2D forward modelling problems can now be routinely undertaken by most research groups with the aid of a number of computer programs that have been developed over the past two decades or so (e.g. Madden & Swift, 1969; Coggon, 1971; Hohmann, 1971; Jones, 1973; Kisak & Silvester, 1975; Brewitt-Taylor & Weaver, 1976; Kaikkonen, 1977; Wannanaker *et al.*, 1987; Travis & Chave, 1989). The 2D inversion problem is still a challenging one. Contributions have been made by many authors (e.g. Weidelt, 1975a; Jupp and Vozoff, 1977; deGroot-Hedlin & Constable, 1990; Zhao & Liu, 1990; Smith & Booker, 1991; Oldenburg & Ellis, 1991; Schmucker, 1993; Agarwal & Weaver, 1991; Uchida, 1993; Schnegg, 1993; Everett & Schult, 1993; and Agarwal, Poll & Weaver, 1994).

When the conductivity varies along both of the two perpendicular horizontal directions, it is a three-dimensional (3D) problem. No analytical solution has

been reported for any 3D problem yet. Laboratory analogue modelling methods can be used to study complicated full 3D induction problems. The work in this field was reviewed by Dosso (1973) and also in Dosso and Weaver (1983). In this method, a linear isotropic geophysical system is represented and studied by a laboratory analogue model which satisfies the scaling condition (e.g. Dosso, 1966)

$$(\sigma_g/\sigma_m)(f_g/f_m)(L_g/L_m)^2 = 1,$$

where $\sigma_g$, $f_g$, $L_g$ are respectively the conductivity, frequency of the time harmonic field, the length of the geophysical system while $\sigma_m$, $f_m$ and $L_m$ are the corresponding values of the analogue model. In practice, the conductivity scaling factor $\sigma_g/\sigma_m$ and the length scaling factor $L_g/L_m$ are constrained by the model materials, the area of geophysical interest and the size of the analogue facility, thus leaving the frequency scaling factor $f_g/f_m$ to be adjusted according to the frequency range of the instrumental capability. One advantage of this method is the ability to model real geophysical structures in much greater detail than is possible with numerical methods. The usefulness and effectiveness of analogue modelling in MT interpretation, particularly for 3D cases is distinct and recognized; many results have been obtained using this method, e.g. Dosso, Jones and Thomson (1974); Dosso, Nienaber and Hutton (1980); Dosso, Nienaber and Parkinson (1985); Dosso, Nienaber and Chen (1989); Dosso, Agarwal and Chen (1992); Nienaber *et al.* (1977, 1979); Chan, Dosso and Law (1981); Hu, Dosso and Nienaber (1983); Chen, Dosso and Nienaber (1989); Chen, Dosso and Ingham (1990); Meng, Dosso and Nienaber (1990); Meng and Dosso (1990) and Meng (1991). But certain limitations, such as material problems, make it difficult to model intermediate conductivity contrasts.

## 1.2 Three-dimensional Numerical Modelling

With the rapid growth of computing power, the 3D numerical modelling becomes more and more practical, useful and important in the interpretation of EM field data. Several review papers have summarized the achievement made towards 3D modelling. From the point of view of methodology, there are Hohmann (1983), Varentsov (1983), and Kaikkonen (1986) and from the point of view of 3D effects, there are Jones (1983) and Menvielle (1988). A recent review paper by Červ and Pek (1990) summarized the main progress in 3D modelling that had been achieved in the previous few years. They described and compared the possibilities and efficiency of various 3D numerical modelling techniques. There are two major different approaches to 3D problems; one is for modelling the near surface conductivity anomalies, known as the "thin Sheet" approximation; the other one is for modelling the deep buried conductivity anomalies, in which either Differential Equations (DE) or Integral Equations (IE) are used.

First introduced by Price (1949), the "Thin Sheet" approximation has significantly simplified the study of near-surface inhomogeneities. In this approximation a physically thin region of arbitrarily varying conductivity is mathematically replaced by an interface that has zero thickness and a conductance equivalent to the integrated conductivity over the z coordinates of the thin region. Beneath the interface, the conductivity varies in depth only. The analytical solution can be obtained in this region, and is subsequently coupled across the interface by boundary conditions. Therefore the resulting equations have one less variable and the numerical computation required to solve the equations is much reduced. The limitation of this technique is discussed by Schmucker (1970). Many authors have contributed in the 2D aspect of thin sheet approximation, e.g. Green and Weaver (1978). The full 3D thin sheet problems present greater mathematical difficulty. Ashour and Chapman (1965) considered the simple geometries

of an infinite plane sheet whose conductance is uniform except for a circular or elliptical region. Vasseur and Weidelt (1977) formulated a fairly general thin sheet problem in 3D. Their models (Fig. 1.1a) consist of a bounded region with arbitrary variations of conductance which is surrounded by an unbounded sheet of uniform conductance. A two-component vector integral equation for the two horizontal electrical field components in the sheet was derived which could be solved numerically. But in their model, the conductivity anomaly was confined to a limited region and surrounded by a uniform region, which sometimes is not realistic. The technique was further developed by McKirdy and Weaver (1984) and McKirdy, Weaver and Dawson (1985) (Fig. 1.1b) so that 2D structures could be allowed at the boundaries, e.g. when there is a long coastline intersecting the model. For deep seated anomalies, the problems can be solved either by differential equations (DE) or integral equations (IE). Both procedures lead to a set of linear algebraic equations for solution. In the DE techniques, since the unknown field quantities used in the equations have to be solved at every node of a mesh which generally covers a large space, there result large but sparse and banded matrices. In the IE approach, since the unknown fields only have to be solved for in the anomalous regions, only they are covered by the mesh, and it follows that the dimensions of the matrices, and hence the computer storage requirements, are smaller than in the DE methods, even though the matrices in the IE method are full.

Much work has been done on the IE method. Due to the properties mentioned above, this method is most likely the best numerical method in solving 3D EM problems, provided that the inhomogeneity is not too large and that there are only a few of them (Raiche, 1974; Weidelt, 1975b; Hohmann, 1975; Ting and Hohmann, 1981; Das and Verma, 1981, 1982).

When the geological structures are really complex or inhomogeneities extend to infinity, some DE approaches are more appropriate. One of the commonly

used DE approaches is the Finite Element (FE) method. After the pioneering work by Coggon (1971), numerous papers that use this method in the EM study have been presented (e.g., Silvester and Haslam, 1972; Reddy and Rankin, 1973; Rodi, 1976; Kaikkonen, 1977, 1980; Reddy *et al.*, 1977; Pridmore *et al.*, 1981).

The other DE approach is the Finite Difference (FD) method in which the derivatives are substituted by their corresponding finite difference formulas. Simplicity and straightforwardness are the merits of this method. In fact FD was the first DE approach used in numerical MT solutions (Neves, 1957) and since then it has been probably the most popular and widely used method among the induction community. Although this popularity is most likely due to the FD program listing published by Jones and Pascoe (1971) at the beginning, the rapid advance of computer techniques also plays an important role. The fast expansion of computer storage offsets the drawback of the FD method that a larger storage space is needed and makes it more meritorious than before. Other FD works either directly attack the 3D problem itself or lead to this aspect include Jones and Price (1970), Lines and Jones (1973a, b), Jones and Pascoe (1972), Jones (1974a, b, c), Brewitt-Taylor and Weaver (1976), Praus (1976), Jones and Vozoff (1978), Zhdanov *et al.* (1982).

The above algorithms have certainly contributed to the progress of the EM 3D modelling, but none of them are entirely satisfactory; they all suffer from one or another limitation. The "Thin Sheet" program by McKirdy, Weaver and Dawson (1985) can solve a variety of near surface problems (Fig. 1.1b), but its application is limited to the near surface inhomogeneity only. The programs based on the integral equation method such as that of Raiche (1974) and Weidelt (1975) (Fig. 1.1c) can solve deep seated anomalies, but the anomalies must be confined and surrounded by a 1D region which is not always realistic. Programs by Lines and Jones (1973b), Jones (1974c) and Jones & Vozoff (1978) (Fig. 1.1d) allow the inhomogeneity to extend to the boundary but only in one

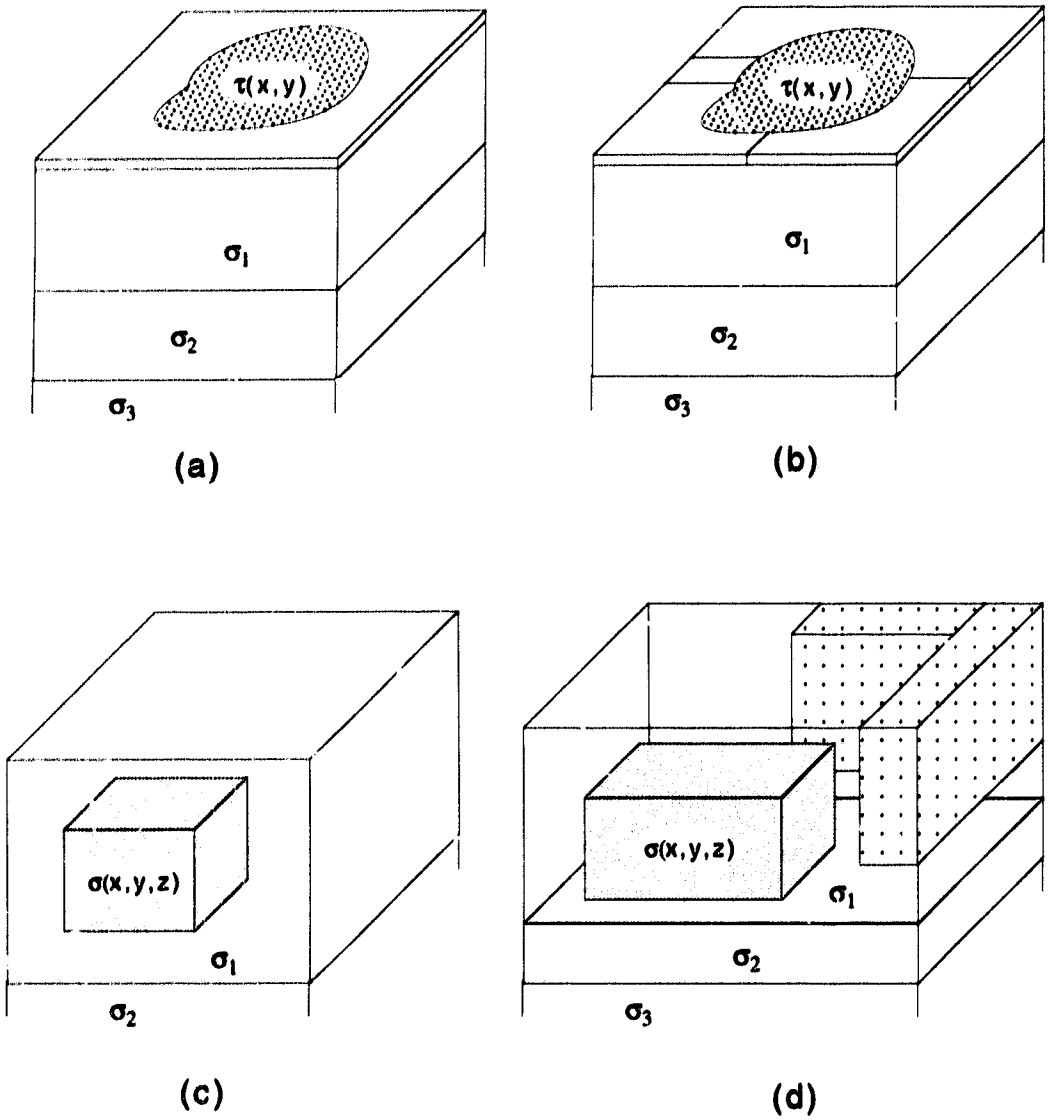


Figure 1.1: 3D models that have been solved by different authors. (a) Vasseur & Weidelt (1977); (b) McKirdy, Weaver & Dawson (1985); (c) Raiche (1974) and Weidelt (1975b); (d) Lines & Jones (1973b), Jones (1974c) and Jones & Vozoff (1978).

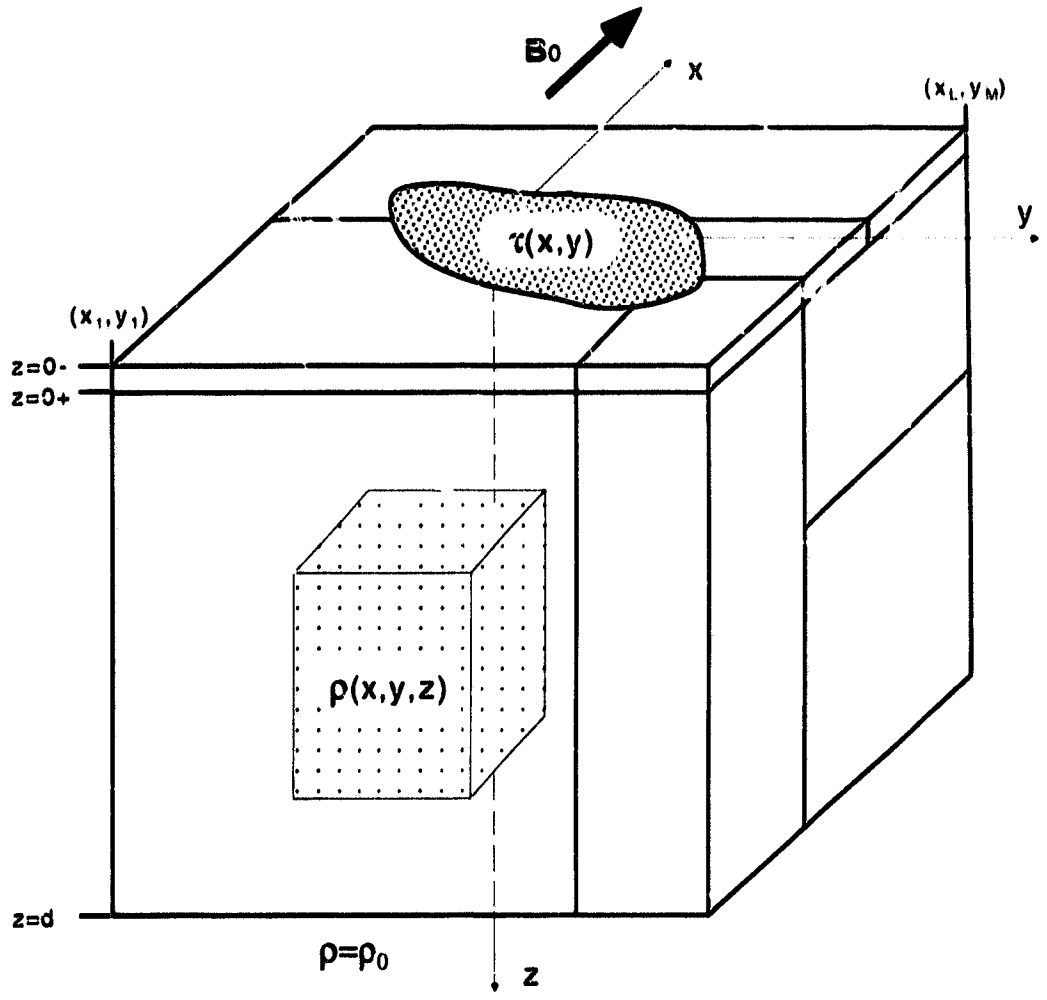


Figure 1.2: The 3D model solved by the new algorithm developed in this thesis. An anomalous thin sheet layer is incorporated at the surface of a general 3D structure. Both thin sheet layer and 3D structure may approach 2D configuration at infinity. Integral boundary conditions are used on both the surface and bottom boundaries.

direction. Furthermore, all the above programs are either for the near surface anomalies only or deep seated ones only. But in certain problems, such as when a surface geomagnetic coast-effect contaminates the EM response of a deeper lying structure, these two distinct phenomena (with different grid requirements) must be incorporated within the same model. This causes considerable difficulty with grid design in the conventional programs mentioned above.

Considering the limitations of the other programs and the enormous computer power offered by modern workstations and mainframes, we have developed a new FD algorithm for solving 3D forward modelling problems as shown in Fig. 1.2, which has the following properties:

1) It overcomes the difficulty of grid design by permitting the inclusion of a surface thin sheet of variable conductance above the conventional 3D structure all within the same finite difference program.

2) The 3D geoelectric structure may approach 2D configurations on all sides of the grid, which allows a wide range of models to be handled.

3) It uses integral boundary conditions both on the surface (Weaver, 1964) and at the bottom. This reduces the size of the mesh, removes the air layer above the surface (the height of that layer is normally difficult to determine) and makes it easier to design the model.

4) By using the surface boundary condition, it also makes the handling of the non-uniform source much easier. Since no grid points are needed in the air layer, any source above the earth is considered 'external'. The non-uniform source in consideration can be adapted by replacing the constant primary field $B_0$ with the corresponding horizontal component of the primary field $B_0(x, y)$.

5) It obtains solutions in terms of the magnetic field rather than the electric field. The magnetic field is of primary interest in many of the EM methods used to investigate the structure of the earth. In previous programs the solutions were obtained from E field, so that an extra step of numerical differentiation is

required to obtain the magnetic fields.

## 1.3 The Basic Equations

The laws that govern most general electromagnetic phenomena in a source free medium are expressed in the form of Maxwell equations. In SI units, these equations are

$$\nabla \times \mathbf{E} = -\frac{\partial \mathbf{B}}{\partial t} \tag{1.1}$$

$$\nabla \times \mathbf{H} = \mathbf{J} + \frac{\partial \mathbf{D}}{\partial t} \tag{1.2}$$

$$\nabla \cdot \mathbf{D} = \rho \tag{1.3}$$

$$\nabla \cdot \mathbf{B} = 0 \tag{1.4}$$

where $\mathbf{J}$ and $\rho$ are respectively the volume current and volume free charge densities, $\mathbf{D}$ and $\mathbf{B}$ the electric and magnetic flux densities, $\mathbf{E}$ and $\mathbf{H}$ the electric and magnetic field intensities. Strictly speaking, $\mathbf{E}$ and $\mathbf{B}$ are the fundamental physical measurements of an EM field, while $\mathbf{D}$ and $\mathbf{H}$ are only auxiliary variables. But, historically, people have mistaken $\mathbf{H}$ as the basic property of a magnetic field and made it a peer of $\mathbf{E}$. Although this point has been realized now, people are still sticking on the original names given to $\mathbf{B}$ and $\mathbf{H}$ for the sake of history. From now on in this thesis, all equations will be deliberately written in terms of $\mathbf{B}$ and $\mathbf{E}$ alone, and $\mathbf{B}$ and $\mathbf{E}$ will be called the magnetic and electric fields respectively.

Since our object to be studied is the earth, some geophysical properties can be used to simplify the Maxwell equations. Firstly, we are investigating the induction between the earth and natural electromagnetic sources which are located in the ionosphere or even higher. It can then be assumed that the earth and lower atmosphere are free of the primary source. So Maxwell equations (1.1) to (1.4) can be applied to these regions. Secondly, these regions can be assumed

to be linear and isotropic. Therefore the relations that apply to the region are

$$\mathbf{D} = \epsilon\mathbf{E}, \qquad \mathbf{H} = \mathbf{B}/\mu \tag{1.5}$$

$$\mathbf{J} = \sigma\mathbf{E} \tag{1.6}$$

where $\epsilon$ is the permittivity, $\mu$ the permeability and $\sigma$ the conductivity of the medium under consideration. Thirdly, for most materials, the permeability $\mu$ does not differ appreciably from its free space value $\mu_0 = 4\pi \times 10^{-7}$ N/A$^2$ (Jackson, 1975, p189). Exceptions are some ferromagnetic minerals with $\mu \gg \mu_0$; however materials with permeability more than an order of magnitude greater than $\mu_0$ are expected in only insignificant quantities in the earth. We can therefore assume the area to be studied to have $\mu = \mu_0$. Fourthly, it is assumed that the earth is piecewise homogeneous; it may be broken up into a number of homogeneous regions where $\epsilon$ and $\sigma$ are spatially constant. The permittivity $\epsilon$ is taken as constant in time. For most materials, $\epsilon$ is about the same as its free space value $\epsilon_0 = 8.85 \times 10^{-12}$ C$^2$/N.m$^2$. An exception is water whose permittivity is about 80 times that of $\epsilon_0$.

Finally, it is assumed that the sources have a common harmonic time dependence with angular frequency $\omega$ and that all subsequent electromagnetic quantities have this same time dependence. Thus

$$\mathbf{E} = \mathbf{E}(x,y,z)\exp(i\omega t), \quad \mathbf{B} = \mathbf{B}(x,y,z)\exp(i\omega t)$$

where from here on $\mathbf{E} = (U,V,W)$ and $\mathbf{B} = (X,Y,Z)$ are taken to represent the (complex) spatial parts (in cartesian components) of an EM field. After all these operations, the Maxwell equations become

$$\nabla \times \mathbf{E} = -i\omega\mathbf{B} \tag{1.7}$$

$$\nabla \times \mathbf{B} = \mu_0\sigma\mathbf{E} + i\omega\mu_0\epsilon\mathbf{E} \tag{1.8}$$

$$\nabla \cdot \mathbf{E} = \rho/\epsilon \tag{1.9}$$

$$\nabla \cdot \mathbf{B} = 0. \tag{1.10}$$

Next we will show that the displacement current in the Maxwell equations (i.e. $i\omega\mu_0\epsilon\mathbf{E}$ in (1.8) or $\partial\mathbf{D}/\partial t$ in (1.2)) is negligible in the EM induction study of the earth. The displacement current has to be inspected separately for the case of $\sigma = 0$ and $\sigma \neq 0$.

First, we consider the situation when $\sigma = 0$ by following the approach used in Weaver (1994). In this case, (1.8) gives

$$\nabla \times \mathbf{B} - i\omega\mu_0\epsilon\mathbf{E} = 0. \tag{1.11}$$

We are to see that $|i\omega\mu_0\epsilon\mathbf{E}| \ll |\nabla \times \mathbf{B}|$. Take the curl of (1.11) we have

$$\nabla \times \nabla \times \mathbf{B} - \omega^2\mu_0\epsilon\mathbf{B} = 0. \tag{1.12}$$

In order to examine the relative importance of the terms in the equation, it is convenient to cast it into dimensionless form. Let $l$ represent any variable with the dimension of length and let $L$ be a characteristic length of the geomagnetic phenomenon under investigation. A suitably scaled dimensionless variable is $l' = l/L$. For problems involving global electromagnetic induction, $L$ might be taken as the radius of the earth. While in regional induction studies which are confined to a limited area of the earth's surface, $L$ would be a much smaller length representing a typical dimension of the region. A properly scaled variable ensures that in regions where gradients of the magnetic fields exist, the derivatives of the fields have reasonable numerical magnitudes.

Let $\mathbf{r}' = (x', y', z') = \mathbf{r}/L = (x/L, y/L, z/L)$; then

$$\frac{\partial}{\partial \mathbf{r}'} = \frac{\partial}{\partial x'}\hat{\mathbf{x}} + \frac{\partial}{\partial y'}\hat{\mathbf{y}} + \frac{\partial}{\partial z'}\hat{\mathbf{z}} = \frac{\partial}{\partial x}\frac{dx}{dx'}\hat{\mathbf{x}} + \ldots = L\frac{\partial}{\partial x}\hat{\mathbf{x}} + \ldots = L\frac{\partial}{\partial \mathbf{r}}.$$

With $\nabla'$ denoting the gradient operator with respect to the dimensionless space variables, we have $\nabla = \nabla'/L$; the differential equation (1.12) can now be written in the form

$$\nabla' \times \nabla' \times \mathbf{B} - \omega^2\mu_0\epsilon L^2\mathbf{B} = 0. \tag{1.13}$$

Since $\mu_0\epsilon_0 = 1/c^2$ where $c = 3 \times 10^8$ m/s is the speed of light. The condition to neglect the second term is

$$\left(\frac{\omega L}{c}\right)^2 \ll 1, \text{ or } \left(\frac{2\pi L}{Tc}\right)^2 \ll 1. \tag{1.14}$$

where $T$ is the period of the EM field. In most geophysical applications $(2\pi L/Tc)^2$ is indeed very small. For example, in a global investigation for which $L \approx 6.4 \times 10^4$ km, condition (1.14) holds for magnetic variations with period $T \geq 3$ s. Now the periods of most worldwide geomagnectic variations of interest are of the order of several minutes or hours; they are well above the limit. In problems involving induction over a very localized area, such as might be encountered in exploration geophysics for which $L = 30$ km, the condition holds for frequencies less than 1 kHz. Since the values of the relevant parameters always fall somewhere between the extremes of the two examples mentioned above (e.g., a typical application of the magnetolelluric method might cover an area of 500 km$^2$ for periods ranging from a few seconds to an hour or two), (1.14) can be regarded as a valid condition quite generally. Physically, condition (1.14) states that the characteristic length $L$ must be much smaller compared to $Tc$, the wave length of the EM field, so that there is very little spatial change in the EM field due to the propagation of the EM wave within the characteristic length $L$.

Now we turn to the situation when $\sigma \neq 0$, i.e. consider the region in the earth. Inspection of equation (1.8) shows that the additional condition required for neglect of the displacement current is $|i\omega\mu_0\epsilon\mathbf{B}| \ll |\mu_0\sigma\mathbf{B}|$, i.e.

$$\frac{\omega\epsilon}{\sigma} \ll 1. \tag{1.15}$$

Materials within the earth have very different conductivities ranging from $10^{-4}$ S/m for some rocks to 4 S/m for seawater. Taking the lowest value in the range we find that (1.15) holds for $T \geq 10^{-5}$ s. It follows that condition (1.15) holds quite generally within the earth for all frequencies in the induction range.

Returning to equation (1.8), we now see that inside the earth, the second term in the R.H.S. of the equation is always negligible compared with the first and the L.H.S. term. Above the earth's surface where it is assumed that the atmosphere is non-conducting (i.e., $\sigma = 0$), the first R.H.S. term vanishes but the second one still remains negligible compared with the L.H.S. term by virtue of condition (1.14). We conclude that the displacement current, i.e. the second term $i\omega\mu_0\epsilon\mathbf{E}$ in (1.8), can always be neglected when discussing electromagnetic induction in the earth. Thus (1.8) becomes

$$\nabla \times \mathbf{B} = \mu_0\sigma\mathbf{E}. \tag{1.16}$$

The resulting solutions are called quasi-static fields.

One of the results that follows from neglecting the displacement is worth mentioning. Taking the divergence of (1.16), and noting that $\nabla \cdot (\nabla \times ) \equiv 0$, we obtain

$$\nabla \cdot (\sigma\mathbf{E}) = 0 \tag{1.17}$$

or

$$\sigma\nabla \cdot \mathbf{E} + (\nabla\sigma) \cdot \mathbf{E} = 0. \tag{1.18}$$

Combined with (1.9), it gives the expression

$$\rho = -\epsilon(\nabla\sigma) \cdot \mathbf{E}/\sigma \tag{1.19}$$

for the volume charge density in a conductive medium. It can be seen clearly from this equation that electric charges can only accumulate in regions where the conductivity has a non-vanishing gradient. Since we are assuming that the medium under consideration is piecewise homogeneous, it follows that within each uniform conductive block, $\nabla\sigma = 0$, and therefore that $\rho = 0$ by (1.19). Even if a volume charge density $\rho_0$ did initially exist, it would be rapidly dispersed to the boundaries of blocks. This can be seen by taking the divergence

of (1.2) rather than (1.17), combining (1.5) and (1.6) with $\sigma$ held constant, so that

$$\partial\rho/\partial t = -\sigma\rho/\epsilon \tag{1.20}$$

which has the solution

$$\rho = \rho_0 \exp(-\sigma t/\epsilon). \tag{1.21}$$

This shows that the free volume charge $\rho$ decays with a time constant which is independent of the time variations of the electromagnetic field. Take the previous value of $\sigma$ and $\epsilon$, i.e. $\sigma = 10 \times 10^{-4}$ S/m and $\epsilon = \epsilon_0 = 8.85 \times 10^{-12}$ $C^2/N.m^2$, the half decay time is in the order of $10^{-8}$ s. In conclusion, there is no free volume charge in the uniform region of the earth; and the accumulation of charges on the boundaries between regions of uniform conductivity gives rise to a surface charge density.

With all the points discussed above taken into account, the final simplified Maxwell equations for geo-electromagnetic induction become

$$\nabla \times \mathbf{E} = -i\omega\mathbf{B} \tag{1.22}$$

$$\nabla \times \mathbf{B} = \mu_0\sigma\mathbf{E} \tag{1.23}$$

$$\nabla \cdot \mathbf{E} = 0 \tag{1.24}$$

$$\nabla \cdot \mathbf{B} = 0 \tag{1.25}$$

where the earth and lower atmosphere are assumed to be source free, linear, isotropic and piecewise homogeneous.

Taking the curl of equations (1.22) and (1.23), we obtain the basic equations governing the EM fields expressed in $\mathbf{E}$ or $\mathbf{B}$ alone,

$$\nabla \times \nabla \times \mathbf{E} = -i\alpha^2\mathbf{E} \tag{1.26}$$

$$\nabla \times \nabla \times \mathbf{B} + \frac{\nabla\rho}{\rho} \times (\nabla \times \mathbf{B}) = -i\alpha^2\mathbf{B} \tag{1.27}$$

where $\alpha^2 = \omega\mu_0\sigma = \omega\mu_0/\rho$. Since $\nabla \cdot \mathbf{B} = 0$, we have

$$\nabla \times \nabla \times \mathbf{B} = \nabla(\nabla \cdot \mathbf{B}) - \nabla^2\mathbf{B} = -\nabla^2\mathbf{B}.$$

Equation (1.27) becomes

$$\nabla^2\mathbf{B} - \frac{\nabla\rho}{\rho} \times (\nabla \times \mathbf{B}) = i\alpha^2\mathbf{B}, \tag{1.28}$$

or in component form

$$X_{xx} + X_{yy} + X_{zz} + (X_y - Y_x)\bar{\rho}_y + (X_z - Z_x)\bar{\rho}_z = i\alpha^2 X \tag{1.29}$$

$$Y_{xx} + Y_{yy} + Y_{zz} + (Y_z - Z_y)\bar{\rho}_z + (Y_x - X_y)\bar{\rho}_x = i\alpha^2 Y \tag{1.30}$$

$$Z_{xx} + Z_{yy} + Z_{zz} + (Z_x - X_z)\bar{\rho}_x + (Z_y - Y_z)\bar{\rho}_y = i\alpha^2 Z. \tag{1.31}$$

where $X_{xx} = \partial^2 X/\partial x^2$, $X_x = \partial X/\partial x$, $\bar{\rho}_x = (\partial\rho/\partial x)/\rho$, etc. Sometimes, we also denote $X_z$ as $X'$ and $X_{zz}$ as $X''$ and we will use these two notations interchangeably from now on.

In the air layer, we have assumed that $\sigma \equiv 0$; the consequence of which is that

$$\nabla \times \mathbf{B} = 0, \qquad \nabla \cdot \mathbf{B} = 0. \tag{1.32}$$

Therefore the magnetic field $\mathbf{B}$ can be obtained from one scalar potential as follows:

$$\mathbf{B} = -\nabla\Omega, \quad \text{where} \quad \nabla^2\Omega = 0. \tag{1.33}$$

## 1.4 Interface Boundary Conditions

We have assumed that the earth and lower atmosphere are source free, linear, isotropic and piecewise homogeneous, and have discussed the governing equations in these regions. In order to obtain the full solution for the induced EM field in such a model, it is necessary to match the solutions in adjoining regions across their common boundaries.

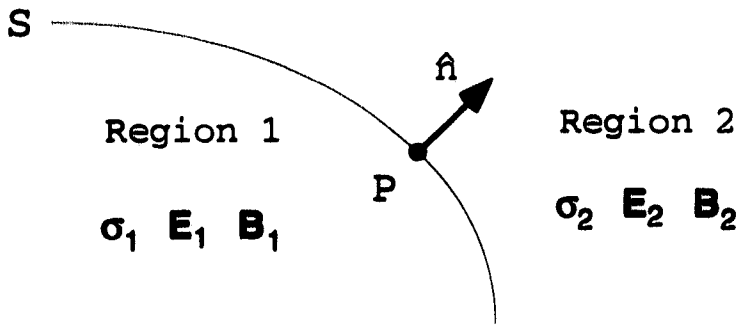


Figure 1.3: Interface boundary

Consider two linear isotropic homogeneous regions separated by an interface boundary $S$ as shown by Fig. 1.3. Let $P$ be a given point on $S$ and $\hat{\mathbf{n}}$ be a unit normal vector at $P$ pointing into region 2. Also, let the limits of the electromagnetic properties when approaching point $P$ within region 1 and 2 be denoted by $\epsilon_1$, $\mu_1$, $\sigma_1$, $\mathbf{E}_1$, $\mathbf{B}_1$ and $\epsilon_2$, $\mu_2$, $\sigma_2$, $\mathbf{E}_2$, $\mathbf{B}_2$ respectively. The standard boundary conditions relating the field components across the interface $S$ may then be written as (Jackson, 1975, pp 19,20)

$$\hat{\mathbf{n}} \times (\mathbf{E}_2 - \mathbf{E}_1) = 0 \tag{1.34}$$

$$\hat{\mathbf{n}} \times (\frac{\mathbf{B}_2}{\mu_2} - \frac{\mathbf{B}_1}{\mu_1}) = \mathbf{J}_s \tag{1.35}$$

$$\hat{\mathbf{n}} \cdot (\epsilon_2 \mathbf{E}_2 - \epsilon_1 \mathbf{E}_1) = \rho_s \tag{1.36}$$

$$\hat{\mathbf{n}} \cdot (\mathbf{B}_2 - \mathbf{B}_1) = 0 \tag{1.37}$$

where $\rho_s$ and $\mathbf{J}_s$ are respectively the surface charge and current densities.

The third of these conditions serves only to provide the values of $\rho_s$, while the first and fourth indicate that the tangential electric fields and normal magnetic field are always continuous. We have discussed before why $\mu = \mu_0$ in most cases. Condition (1.35) can also be written as

$$\hat{\mathbf{n}} \times (\mathbf{B}_2 - \mathbf{B}_1) = \mu_0 \mathbf{J}_s, \tag{1.38}$$

indicating that the tangential magnetic field will be different if a surface current is present. However, surface currents only occur when one of the regions is

a perfect conductor or when a mathematically thin sheet of finite integrated conductivity occupies the boundary surface. At an ordinary interface boundary, where no surface currents can be supported, it holds that

$$\hat{\mathbf{n}} \times (\mathbf{B}_2 - \mathbf{B}_1) = 0. \tag{1.39}$$

This means that the tangential components of $\mathbf{B}$ are also continuous. Thus $\mathbf{B}$ itself is continuous across the boundary, i.e., $\mathbf{B}_2 = \mathbf{B}_1$, so are its tangential derivatives. Hence $\hat{\mathbf{n}} \cdot \nabla \times \mathbf{B}$, which involves only tangential derivatives, is also continuous. It follows therefore from (1.8) that

$$\hat{\mathbf{n}} \cdot (\sigma_2 \mathbf{E}_2 - \sigma_1 \mathbf{E}_1) = 0.$$

This condition states that the normal component of the conductive current is continuous across the boundary. This is peculiar to quasi-static fields. It does not apply when displacement currents are included.

If the boundary is the surface of the earth, and region 2 is the air layer above the earth which is regarded non-conductive, then the above equation reduces to

$$\hat{\mathbf{n}} \cdot \mathbf{E}_1 = 0 \tag{1.40}$$

i.e., the normal component of a quasi-static electric field vanishes at the surface of the earth.

## 1.5 The Thin Sheet Approximation

The geological structure of the first few kilometres of the earth is usually much more complicated than its deeper ones, so are electrical structures. Consider a thin surface covering layer of thickness $d$, as shown in Fig. 1.4a, it may contain terrestrial conductive variations such as that of ocean, continental slope, coast line, sediment and land, etc. These complicated structures can make the solution

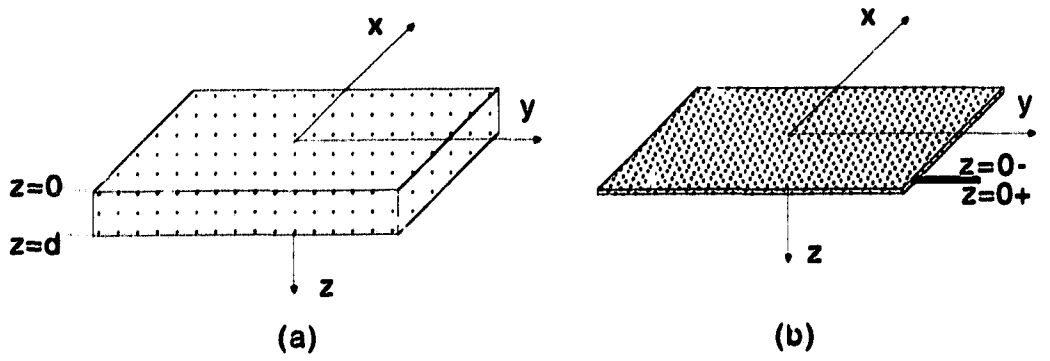


Figure 1.4: Thin sheet approximation reduces a layer of finite thickness into a double sided mathematically thin interface boundary.

of EM induction quite difficult. However, the problem can be greatly simplified by using the thin sheet method first developed by Price (1949).

Applying Ohm's law, i.e. equation (1.6), in the covering layer, we can write

$$\mathbf{J}(\mathbf{r}, z) = \sigma(\mathbf{r}, z)\mathbf{E}(\mathbf{r}, z) \tag{1.41}$$

where $\mathbf{r} = (x, y)$. An integration of (1.41) over the thickness $d$ of the covering layer leads to

$$\int_0^d \mathbf{J}(\mathbf{r}, z)\, dz = \int_0^d \sigma(\mathbf{r}, z)\mathbf{E}(\mathbf{r}, z)\, dz \tag{1.42}$$

where the integral on the right hand side may be approximated by

$$\int_0^d \sigma(\mathbf{r}, z)\mathbf{E}(\mathbf{r}, z)\, dz \approx \mathbf{E}(\mathbf{r}, 0) \int_0^d \sigma(\mathbf{r}, z)\, dz \tag{1.43}$$

to the first order of small quantities, when $d$ is small. The integrals

$$\int_0^d \mathbf{J}(\mathbf{r}, z)\, dz \quad \text{and} \quad \int_0^d \sigma(\mathbf{r}, z)\, dz$$

represent, respectively, the total sheet current intensity per unit length of surface at the point (surface current intensity) and the total conductivity per unit length (also called conductance); denoting the surface current intensity and conductance by $\mathbf{J}_s$ and $\tau(\mathbf{r})$ respectively, equation (1.42) can be written as

$$\mathbf{J}_s(\mathbf{r}) = \tau(\mathbf{r})\mathbf{E}(\mathbf{r}, 0), \tag{1.44}$$

which is independent of the $z$ variable. A layer of finite thickness is called 'thin sheet' if it satisfies this equation. Such a thin sheet layer of finite thickness thus may be approximated by a double sided mathematically thin interface, as shown in Fig. 1.4b, and consequently, the complexity of the problem is greatly reduced.

Schmucker (1970) studied the limits for this approximation. He used a plane 3 layer model which consists of a top layer of thickness $d$ (terrestrial surface layers), a poorly conducting intermediate layer of thickness $h$ (high resistivity zone of the crust and uppermost mantle), and a highly conducting substratum from $z = h + d$ downward to infinity. It was found that when the wavelength of the EM source is large enough, the ratio of electric field at top and bottom of the sheet was

$$\frac{\mathbf{E}(d)}{\mathbf{E}(0)} = 1 - \frac{d}{h+d} \tag{1.45}$$

as long as $\delta_1 > 3d$ where $\delta_1$ is the skin depth of the top layer. The conditions for (1.45) to hold were therefore set to be

$$d < \delta_1/3, \qquad h + d \gg d. \tag{1.46}$$

The physical significance of these conditions is quite clear. The first one requires that the top layer must be thin compared to its skin depth; otherwise, if the layer is too 'thick', skin effect attenuation of the electric field through the layer would be expected, whence $\mathbf{E}(z) \approx \mathbf{E}(0)$ for $0 \leq z \leq d$ would no longer be true and equation (1.43), and therefore (1.44), would no longer hold. The second condition requires that the underlying poor conductive layer be 'thick' compared with the top one. An opposite extreme case is when the top layer is underlain by a perfect conductor in the regfion $z \geq d$. It is well known that at the surface of the perfect conductor $z = d$, the condition $\mathbf{E}(d) \equiv 0$ holds, i.e. there is total attenuation of the electric field within the top layer. Thus equation (1.43) breaks down and consequently condition (1.44) is invalidated. Thus, a good conductor must be kept a distance away from the thin sheet layer.

Weaver (1994, p86) considered a more general problem and concluded that in a multi-layer model, the thin sheet boundary condition

$$\hat{\mathbf{z}} \times [(\mathbf{B})_{z=z_n+0} - (\mathbf{B})_{z=z_n-0}] = \mu_0 \tau_n (\mathbf{E})_{z=z_n} \tag{1.47}$$

can be applied to any layer which is sufficiently thin that three conditions

$$\nu \ll \alpha_n, \quad \alpha_n d_n \ll 1, \quad \sqrt{d_n} \ll |c(\nu, z_n + 0, \omega)|^{1/2} \tag{1.48}$$

are all satisfied, where $1/\alpha_n$, $d_n$ and $1/\nu$ are the skin-depth of the layer, the thickness of the layer and the horizontal wavelength of the elementray harmonic source field respectively and $c$ is the response function which, in the MT method, is in the form

$$c(\nu, \omega) = -\frac{i}{\omega}\left(\frac{E_x}{B_y}\right)_{z=0} = \frac{i}{\omega}\left(\frac{E_y}{B_x}\right)_{z=0}.$$

In other words, any layer may be regarded as a 'thin sheet' if its thickness is much less than the skin depth in the layer (2nd condition); the layer in turn should be much smaller than the horizontal wavelength of the field (1st condition); the layer's thickness also must be very much less than the modulus of the 'response' $c$ of underlying structures.

When the original sheet of finite thickness is compressed into a mathematically thin interface, the two separated surfaces, $z = 0$ and $z = d$, of the finite sheet become the two sides of a single interface, $z = 0-$ and $z = 0+$ respectively. According to (1.34) and (1.37) , the normal magnetic field and tangential electric fields are always continuous across the sheet, i.e.,

$$\hat{\mathbf{n}} \cdot (\mathbf{B}^+ - \mathbf{B}^-) = 0, \quad \hat{\mathbf{n}} \times (\mathbf{E}^+ - \mathbf{E}^-) = 0, \tag{1.49}$$

where $\mathbf{B}^+ = \mathbf{B}(\mathbf{r}, 0+)$, $\mathbf{B}^- = \mathbf{B}(\mathbf{r}, 0-)$, etc. The tangential magnetic field might be discontinuous, since the thin sheet interface can support surface currents. Combine (1.38) and (1.44), we have

$$\hat{\mathbf{n}} \times (\mathbf{B}^+ - \mathbf{B}^-) = \mu_0 \tau \mathbf{E}^T \tag{1.50}$$

where the superscript $T$ in $\mathbf{E}^T$ has been used to mark the tangential component of $\mathbf{E}$. At $z = 0+$, Maxwell equation (1.23) gives

$$(\nabla \times \mathbf{B})^+ = \mu_0 \sigma^+ \mathbf{E}^+, \quad (\mathbf{E}^+)^T = \mathbf{E}^T = \frac{\rho^+}{\mu_0}[(\nabla \times \mathbf{B})^+]^T. \tag{1.51}$$

Substitution of $\mathbf{E}^T$ in (1.50) by (1.51) yields the thin sheet boundary condition in terms of magnetic field,

$$\hat{\mathbf{n}} \times (\mathbf{B}^+ - \mathbf{B}^-) = \tau \rho^+ [(\nabla \times \mathbf{B})^+]^T, \tag{1.52}$$

or, in component form,

$$X^+ - X^- = \tau \rho^+ (X_z^+ - Z_x), \tag{1.53}$$

$$Y^+ - Y^- = \tau \rho^+ (Y_z^+ - Z_y), \tag{1.54}$$

where $\rho^+ = \rho(\mathbf{r}, 0+) = 1/\sigma^+$. Since the normal component of the magnetic field $Z$ and its tangential derivatives $Z_x$ and $Z_y$ are continuous, the superscripts of these terms in the above expressions have been dropped.

## 1.6 The Magnetic Source Field and Conductivity Model

The model under consideration is shown in Fig. 1.2. Since the aim of this thesis is to solve regional three-dimensional forward modelling problems, only local effects are under consideration. The earth's surface may be represented by a horizontal plane, taken to be the $xy$-plane of a right-handed Cartesian system with coordinates $(x, y, z)$ and unit vectors $(\hat{\mathbf{x}}, \hat{\mathbf{y}}, \hat{\mathbf{z}})$, where $\hat{\mathbf{x}}$ points into the paper representing the direction of North, and $\hat{\mathbf{z}}$ points downward into the earth.

The induction process is driven by a uniform magnetic source $\mathbf{B}^p$ located in the region $z < -h$. The primary field $\mathbf{B}^p$ then causes an induced current inside the earth ($z > 0$) which in turn gives a secondary induced magnetic field $\mathbf{B}^s$. It is understood that $\mathbf{B}^s = \mathbf{B}^n + \mathbf{B}^a$ where $\mathbf{B}^n$ is the normal induced field that

would exist in the region $z < 0$ if the earth were 1D and $\mathbf{B}^a$ is the anomalous induced field due to the anomalous conductivity structures, either 2D or 3D, inside the earth. It is well known that if the earth is taken as one-dimensional, then $\mathbf{B}^n = \mathbf{B}^p$ for $z \leq 0$, i.e. the induced normal field is a constant field and is identical to the primary field, no matter how the conductivity varies with depth. Even in 2-dimensional cases, $\mathbf{B}^n = \mathbf{B}^p$ still holds if it is a B-polarization mode. We therefore define the constant field

$$\mathbf{B}^p + \mathbf{B}^n = 2\mathbf{B}^p = \mathbf{B}_0$$

as the total normal magnetic field. Thus at the earth's surface, we have

$$\mathbf{B} = \mathbf{B}^p + \mathbf{B}^s = \mathbf{B}^p + \mathbf{B}^n + \mathbf{B}^a = \mathbf{B}_0 + \mathbf{B}^a. \tag{1.55}$$

In this thesis, we assume that $\mathbf{B}^p = \hat{\mathbf{x}}B^p$, that leads to $\mathbf{B}_0 = 2B^p\hat{\mathbf{x}} = B_0\hat{\mathbf{x}}$ and

$$\mathbf{B} = \mathbf{B}_0\hat{\mathbf{x}} + \mathbf{B}^a \tag{1.56}$$

where $\mathbf{B}$ is the total magnetic field on the surface of the earth, $B_0\hat{\mathbf{x}}$ is the total normal magnetic field and $\mathbf{B}^a$ is the anomalous magnetic field originating inside the earth. It is $\mathbf{B}^a$ that we are seeking.

The region $-h < z < 0$ representing the lower atmosphere is considered non-conductive, i.e. $\sigma \equiv 0$. From $z > 0$ downward is the conductive earth, where $0 \leq z \leq d$ can be occupied by three-dimensional inhomogeneities with arbitrary resistivity distribution $\rho(x, y, z)$, while from $z = d$ all the way to $z = +\infty$ is assumed to be a uniform half space with resistivity denoted by $\rho_0$. The resistivity structure is allowed to approach two-dimensional configurations at horizontal infinity $x = \pm\infty$ and $y = \pm\infty$. We define

$$\lim_{x\to\pm\infty} \rho(x, y, z) = \rho^{x\pm}(y, z), \quad \lim_{y\to\pm\infty} \rho(x, y, z) = \rho^{y\pm}(x, z) \tag{1.57}$$

At infinity $x = \pm\infty$, the total magnetic field tends to $\hat{\mathbf{x}}B_0$ which is parallel to the direction of the strike; therefore B-polarization problems in which the magnetic

fields are polarized along the strikes are present there. Correspondingly, E-polarization problems in which the electric fields are polarized along the strikes are reached at $y = \pm\infty$.

In this thesis, we are solving 3D EM equations in terms of the magnetic field **B**, it requires us to use the resistivity $\rho$ as the model parameter for describing the model's conductivity structure due to the reason given in Brewitt-Taylor and Weaver (1976); more discussion on this point will be given later in the introduction of Chapter 2. From now on, although we might still use the terms such as 'conductivity', 'conductivity structure' and the symbol $\sigma$ in the texts and equations, we shall use only the resistivity $\rho$ in the final equations that are ready for programming.

If the thin sheet conditions are satisfied, the near-surface conductivity structures can also be modeled by a thin sheet layer with conductance $\tau(x, y)$. The combination of a thin sheet layer at the surface, full three-dimensional structures (buried or outcropping) and two-dimensional limit configurations at horizontal infinity, all incorporated in this new algorithm, provides great flexibility and strong modelling power for solving the three-dimensional forward modelling problem.

## 1.7 2D and 3D grid meshs

The finite difference approach is used to solve the above modelling problem numerically. In order to apply this method, a conductivity model has to be divided into small grids. We consider a two-dimensional situation first. Let the $yz$-plane be covered by a mesh as shown by Fig. 1.5 whose nodes $(m, n)$, $1 \leq m \leq M$, $1 \leq n \leq N$, correspond to the points $(y = y_m, z = z_n)$. In this notation, the left and right side boundaries as well as the top and bottom boundaries are at $y = y_1$, $y = y_M$, $z = z_1 = 0$, $z = z_N > 0$ respectively. Variable

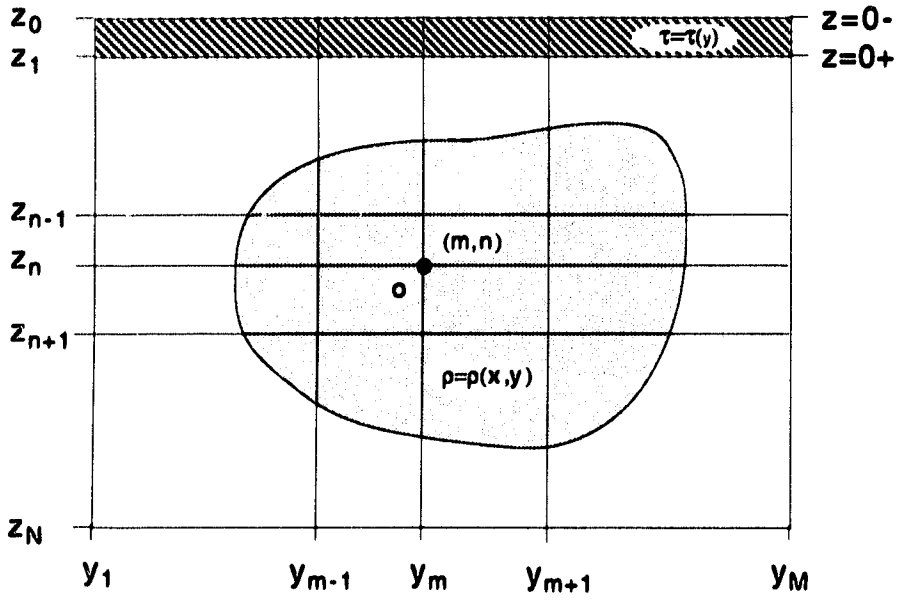


Figure 1.5: A 2D model covered by a numerical grid mesh.

nodal spacings (or grid steps) are introduced by the definitions

$$h_m = y_{m+1} - y_m,\ k_n = z_{n+1} - z_n\ (1 \le m \le M-1, 1 \le n \le N-1). \quad (1.58)$$

The resistivity values are not specified at the nodes themselves, but at the centres of the rectangular cells of the mesh. We define $\rho_{m+\frac{1}{2}n+\frac{1}{2}}$ $(1 \le m \le M-1, 1 \le n \le N-1)$ to be the given resistivity at $(m+\frac{1}{2}, n+\frac{1}{2})$, i.e., the point $y = y_m + \frac{1}{2}h_m$, $z = z_n + \frac{1}{2}k_n$.

Quite often, our concerns are only focused on a local problem which contains a central node and its immediate neighbouring ones. In this case, a less cumbersome subscript notation is applicable as shown in Fig. 1.6. We will name this notation as a local system to distinguish from the one defined previously which should be named as global system correspondingly.

In Fig. 1.6, assume that in the global system the central node is $(j,k)$, the neighbouring ones are $(m,n)$, $m = j-1, j, j+1$; $n = k-1, k, k+1$. Let $(p,q)$ denote the corresponding subscripts in the local system. If $F$ is any field

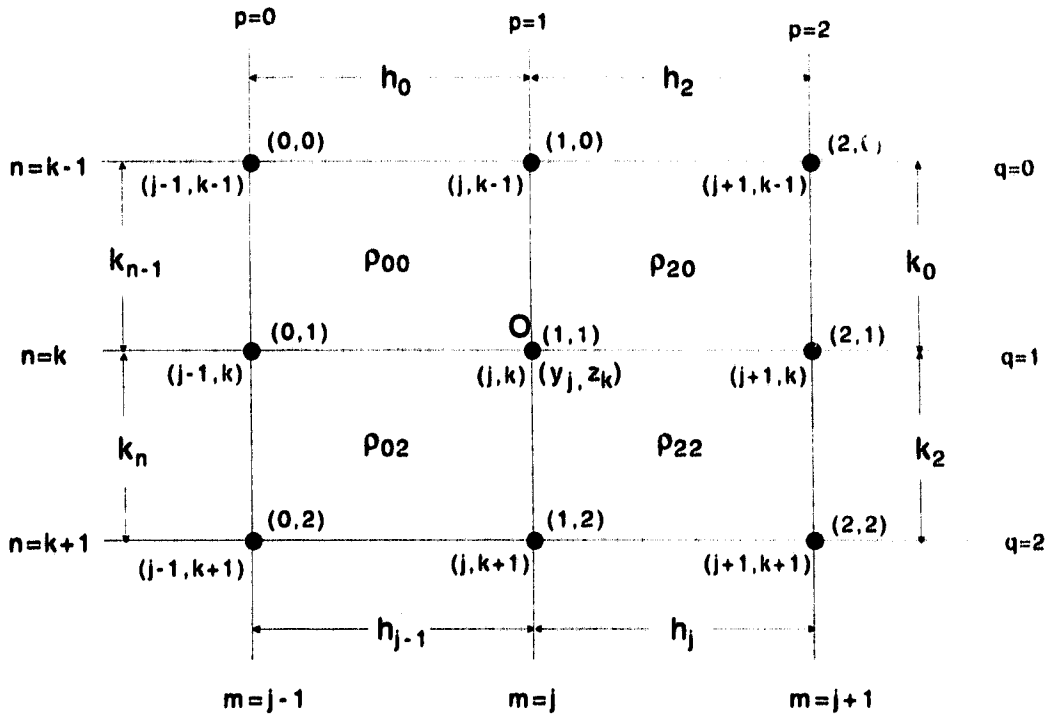


Figure 1.6: Global and local coordinate systems.

component, its values at any local node are defined as

$$F_{pq} := F_{m-j+1,n-k+1},\ m = j-1, j, j+1;\ n = k-1, k, k+1. \tag{1.59}$$

For example, we have $F_{pq} = F_{0q}$ for the nodes on the line $y = y_{j-1}$, $F_{1q}$ on $y = y_j$, and $F_{2q}$ on $y = y_{j+1}$. Similarly, $F_{pq} = F_{p0}$ for line $z = z_{k-1}$, $F_{p1}$ for $z = z_k$ and $F_{p2}$ for $z = z_{k+1}$. The central node is $F_{pq} = F_{11}$. The grid steps and resistivities are not quantities defined at nodes; they are related to the cells and are therefore assigned numerical subscripts of 0 or 2 depending on whether they belong to a cell on the positive or negative side of the central node in the dimension to which the subscript refers. For example, on the left side of $y = y_j$ (the negative side of the central point in $y$ dimension), we have $h_p = h_0 = y_m - y_{m-1}$ and $\rho_{pq} = \rho_{0q}$ while below the line $z = z_k$ (the positive side in $z$ dimension) $k_q = k_2 = z_{n+1} - z_n$

and $\rho_{pq} = \rho_{p2}$ , etc.

This notation was originally devised by C.R. Brewitt-Taylor, a former research associate with J.T. Weaver, and was recoded in a note. It has the advantage of leaving the subscript 1 available to denote the weighted average resistivity on the boundary between two cells. For example, the weighted average of resistivity on the boundary between the two cells with resistivities $\rho_{02}$ and $\rho_{22}$ can be written as

$$\rho_{12} = (h_0\rho_{02} + h_2\rho_{22})/(h_0 + h_2) = \sum_{p=0,2} h_p\rho_{p2}/h_s, \qquad (1.60)$$

where in this expression, as well as in the following parts of this thesis and in the computer program, $h_s = h_0 + h_2$, $h_{20} = h_2 - h_0$, $H_{02} = h_0h_2$, $H_{0s} = h_0h_s$ and $H_{2s} = h_2h_s$. Similar definitions apply to $k_s$, $k_{20}$, $K_{02}$, $K_{0s}$ and $K_{2s}$. By the same token, the weighted average of resistivity at the central node which is surrounded by the four cells $\rho_{00}$, $\rho_{02}$, $\rho_{20}$ and $\rho_{22}$ would be

$$\rho_{11} = (k_0\rho_{10} + k_2\rho_{12})/k_s = \sum_{q=0,2} k_q\rho_{1q}/k_s = \frac{1}{h_sk_s}\sum_{p=0,2}\sum_{q=0,2} h_pk_q\rho_{pq}. \qquad (1.61)$$

The notation for 3D problem can be generalized directly from the 2D notation by adding another set of symbols to describe the other horizontal axis, i.e. the $x$-axis. Let the grid nodes on the $x$-axis be $x_1$,...,$x_L$, we will index these nodes by $i$ or $l$, where $i$ teams up with $j$ for the $y$-axis and $k$ for the $z$-axis, while $l$ teams up with $m$ and $n$. The grid steps on the $x$-axis are denoted by $g$, and are defined similarly to (1.58), so that

$$g_l = x_{l+1} - x_l, \quad l = 1...L-1.$$

By including the $x$-axis in such a way, we have extended our 2D grid mesh into 3D. Its nodes are $(l, m, n)$, i.e. $(x_l, y_m, z_n)$ where $l = 1, ..., L$, $m = 1, ..., M$, and $n = 1, ..., N$. Similarly, we may use $(i, j, k)$ instead of $(l, m, n)$ as well. Quite often, we would like to distinguish the node in question, i.e. the central node,

from the surrounding ones. Although $(l,m,n)$ or $(i,j,k)$ might be used to index the central node sometimes, more frequently, a special set of indices will be used and only be used to mark the central node; we use $(\lambda,\mu,\nu)$ for the central node $(x_\lambda, y_\mu, z_\nu)$. For convenience, sometimes we also use notation $(\mathbf{r},z)$ to denote a point $(x,y,z)$. In fact, this notation has been used in equation (1.41) etc. Thus a central nodal point may be denoted by either $(x_\lambda, y_\mu, z_\nu)$ or $(\mathbf{r}_{\lambda\mu}, z_\nu)$ or $(\lambda,\mu,\nu)$ and the values of functions evaluated at this point would be $f(x_\lambda, y_\mu, z_\nu)$ or $f(\mathbf{r}_{\lambda\mu}, z_\nu)$ or $f_{\lambda\mu\nu}$ etc.

We also need to define the notation for the local system. The following symbols are adopted for the $x$-axis: $x_0 := x_{l-1}$, $x_1 := x_l$, $x_2 := x_{l+1}$, $g_0 := g_{l-1}$, $g_2 := g_l$, $g_s := g_0 + g_2$, $g_{20} := g_2 - g_0$, $G_{02} := g_0 g_2$, $G_{0s} := g_0 g_s$, $G_{2s} := g_2 g_s$; and a nodal point will be denoted by $(p,q,r) = (l-\lambda+1, m-\mu+1, n-\nu+1)$ where $l = \lambda-1, \lambda, \lambda+1$, $m = \mu-1, \mu, \mu+1$, $n = \nu-1, \nu, \nu+1$, and $p = 0,1,2$, $q = 0,1,2$ and $r = 0,1,2$. Naturally, the central node is (1,1,1). The function value at node $(p,q,r)$ will be denoted by $F_{pqr}$ The weighted average of resistivity are defined similarly to (1.60) and (1.61), i.e.

$$\rho_{pq1} = (k_0\rho_{pq0} + k_2\rho_{pq2})/k_s = \frac{1}{k_s}\sum_{r=0,2} k_r\rho_{pqr}, \qquad p=0,2,\ q=0,2,$$

$$\rho_{p11} = (h_0\rho_{p01} + h_2\rho_{p21})/h_s = \frac{1}{h_s}\sum_{q=0,2} h_q\rho_{pq1} = \frac{1}{h_s k_s}\sum_{q=0,2}\sum_{r=0,2}\rho_{pqr},\ p=0,2,$$

$$\rho_{111} = (g_0\rho_{011} + g_2\rho_{211})/g_s = \frac{1}{g_s}\sum_{p=0,2} g_p\rho_{p11} = \frac{1}{g_s h_s k_s}\sum_{p=0,2}\sum_{q=0,2}\sum_{r=0,2}\rho_{pqr}.$$

## 1.8 Some Useful Mathematical Expressions

Some mathematical expressions will be used in more than one place later in this thesis, we will derive them once and for all in this section.

When deriving the boundary conditions at $z = 0$ and $z = d$, we encounter some terms which can not be evaluated directly due to the absence of grid points in regions $z \le 0$ and $z \ge d$; these terms have to be related and expressed in the

terms defined in the region $0 \leq z \leq d$. We will look at the boundary $z = 0$ first. Within the region $0 < z < \frac{1}{2}k_1$, by definition we have

$$\rho(\mathbf{r}, z) := \rho(\mathbf{r}, \tfrac{1}{2}k_1),$$

i.e. $\rho(\mathbf{r}, z)$ is uniform along the $z$-direction. It follows that $\rho_z(\mathbf{r}, z) \equiv 0$. At any given point with $z = 0+$, the basic equation (1.28) thus gives

$$X_{xx} + X_{yy} + X'' + (X_y - Y_x)\bar{\rho}_y = i\alpha^2 X \tag{1.62}$$

$$Y_{xx} + Y_{yy} + Y'' + (Y_x - X_y)\bar{\rho}_x = i\alpha^2 Y \tag{1.63}$$

$$Z_{xx} + Z_{yy} + Z'' + (Z_y - Y')\bar{\rho}_y + (Z_x - X')\bar{\rho}_x = i\alpha^2 Z \tag{1.64}$$

with the understanding that all the values are estimated at $z = 0+$. The forward Taylor expression at $z = 0+$ gives

$$X_2 = X_1 + k_1 X_1' + \frac{1}{2}k_1^2 X_1'' \tag{1.65}$$

$$Y_2 = Y_1 + k_1 Y_1' + \frac{1}{2}k_1^2 Y_1'' \tag{1.66}$$

$$Z_2 = Z_1 + k_1 Z_1' + \frac{1}{2}k_1^2 Z_1'' \tag{1.67}$$

where $F_2$ and $F_1$ etc. represent $F_{z=k_1}$ and $F_{z=0+}$ respectively and $F$ stands for any field $X$, $Y$ or $Z$ and its derivatives with respect to $z$. Applying $Z' = -(X_x + Y_y)$ (i.e. $\nabla \cdot \mathbf{B} = 0$) to (1.67), we obtain

$$Z_1'' = 2(Z_2 - Z_1)/k_1^2 + 2(X_x + Y_y)/k_1. \tag{1.68}$$

Combining (1.62) and (1.65) to eliminate the $X''$ term, we obtain the expression for $X'$ at $z = 0+$ as

$$X_1' = \frac{X_2 - X_1}{k_1} + \frac{k_1}{2}\left[-i\alpha^2 X_1 + X_{xx} + X_{yy} + (X_y - Y_x)\bar{\rho}_y\right]. \tag{1.69}$$

Similarly, (1.63) and (1.66) yield

$$Y_1' = \frac{Y_2 - Y_1}{k_1} + \frac{k_1}{2}\left[-i\alpha^2 Y_1 + Y_{xx} + Y_{yy} + (Y_x - X_y)\bar{\rho}_x\right]. \tag{1.70}$$

Inserting (1.68), (1.69) and (1.70) into (1.64), we have

$$\begin{aligned} i\alpha^2 Z_1 &= Z_{xx} + Z_{yy} + Z_x\bar{\rho}_x + Z_y\bar{\rho}_y \\ &+\frac{2(Z_2 - Z_1)}{k_1^2} + \frac{2(X_x + Y_y)}{k_1} - \bar{\rho}_x\frac{(X_2 - X_1)}{k_1} - \rho_y\frac{(Y_2 - Y_1)}{k_1} \\ &-\frac{1}{2}k_1\bar{\rho}_x\left(-i\alpha^2 X_1 + X_{xx} + X_{yy} + (X_y - Y_x)\bar{\rho}_y\right) \\ &-\frac{1}{2}k_1\bar{\rho}_y\left(-i\alpha^2 Y_1 + Y_{xx} + Y_{yy} + (Y_x - X_y)\bar{\rho}_x\right). \end{aligned} \tag{1.71}$$

Taking a close look at the above equation, we find that if we multiply the equations with $k_1^2$ so that the coefficients of the $Z$ terms are $O(1)$, then the last two terms having $\frac{1}{2}k_1\bar{\rho}_x$ and $\frac{1}{2}k_1\bar{\rho}_y$, respectively, become of the order $O(k_1^3)$. Since we have neglected all the terms higher then $O(k_1^2)$ in the Taylor expansion (1.65) to (1.67), we may therefore drop them here as well. We then obtain the expression for the $z$-component at $z = 0+$ as

$$\begin{aligned} i\alpha^2 Z_1 &= Z_{xx} + Z_{yy} + Z_x\bar{\rho}_x + Z_y\bar{\rho}_y \\ &+\frac{2(Z_2 - Z_1)}{k_1^2} + \frac{2(X_x + Y_y)}{k_1} - \bar{\rho}_x\frac{(X_2 - X_1)}{k_1} - \bar{\rho}_y\frac{(Y_2 - Y_1)}{k_1} \end{aligned} \tag{1.72}$$

Next, we consider the bottom boundary at $z = d$. The vertical derivatives $X'$ and $Y'$ can also be derived similarly to (1.69) and (1.70), except backward Taylor expansions rather than forward ones have to be used here, e.g.

$$X_{N-1} = X_N - k_{N-1}X'(\mathbf{r}, d-) + \frac{1}{2}k_{N-1}^2 X''(\mathbf{r}, d-). \tag{1.73}$$

Comparing (1.73) with (1.65), we can write out the expression for $X'(\mathbf{r}, d-)$ by substituting $X_1$, $X_2$ and $k_1$ with $X_N$, $X_{N-1}$ and $-k_{N-1}$ in (1.69), e.g.

$$X'(\mathbf{r}, d-) = \frac{X_N - X_{N-1}}{k_{N-1}} - \frac{k_{N-1}}{2}\left[-i\alpha^2 X_N + X_{xx} + X_{yy} + (X_y - Y_x)\rho_y\right], \tag{1.74}$$

with the understanding that all the terms except $X_{N-1}$ are now evaluated at $z = d-$. Similarly, we have

$$Y'(\mathbf{r}, d-) = \frac{Y_N - Y_{N-1}}{k_{N-1}} - \frac{k_{N-1}}{2}\left[-i\alpha^2 Y_N + Y_{xx} + Y_{yy} + (Y_x - X_y)\bar{\rho}_x\right]. \tag{1.75}$$

For $Z'(\mathbf{r}, d-)$, we combine the basic equation (1.64), which is now estimated at $z = d-$, and the Taylor expansion

$$Z_{N-1} = Z_N - k_{N-1}Z'(\mathbf{r}, d-) + \frac{1}{2}k_{N-1}^2 Z''(\mathbf{r}, d-) \tag{1.76}$$

to eliminate $Z''$ term, giving

$$Z_{N-1} = Z_N - k_{N-1}Z'_N + \frac{1}{2}k_{N-1}^2(i\alpha^2 Z_N - Z_{xx} - Z_{yy} - Z_x\bar{\rho}_x - Z_y\bar{\rho}_y + X'\bar{\rho}_x + Y'\bar{\rho}_y). \tag{1.77}$$

We can then use the expressions for $X'$ and $Y'$ at $z = d-$ given by (1.74) and (1.75) to eliminate the $X'$ and $Y'$ terms in the above equation. When doing so, we can also neglect the terms involved with $k_{N-1}/2$ in expressions (1.74) and (1.75) for the same reasons that led to (1.72) from (1.71); thus, we see that

$$\begin{aligned} Z'(\mathbf{r}, d-) &= \frac{Z_N - Z_{N-1}}{k_{N-1}} + \frac{\bar{\rho}_x}{2}(X_N - X_{N-1}) + \frac{\bar{\rho}_y}{2}(Y_N - Y_{N-1}) \\ &\quad + \frac{k_{N-1}}{2}\left(i\alpha^2 Z_N - Z_{xx} - Z_{yy} - Z_x\bar{\rho}_x - Z_y\bar{\rho}_y\right). \end{aligned} \tag{1.78}$$

We have now obtained the expressions for $X'$, $Y'$ and $Z'$ at $z = d-$. Next, we will relate them with the corresponding terms at $z = d+$. As we have discussed before, when no surface current is present, the interface boundary conditions (1.34), (1.37) and (1.39) indicate that the tangential electrical components and all the magnetic components are continuous. Therefore at $z = d$, if a normal bottom boundary condition is used, we can write

$$\mathbf{B}(\mathbf{r}, d+) = \mathbf{B}(\mathbf{r}, d-) = \mathbf{B}(\mathbf{r}, d) \tag{1.79}$$

$$U(\mathbf{r}, d+) = U(\mathbf{r}, d-), \quad V(\mathbf{r}, d+) = V(\mathbf{r}, d-). \tag{1.80}$$

It is a consequence of $\nabla \cdot \mathbf{B} = 0$ and condition (1.79) that $Z'(\mathbf{r}, d)$ is also continuous, because it equals the sum of continuous horizontal derivatives $-(X_x + Y_y)$. We can thus write

$$Z'(\mathbf{r}, d+) = Z'(\mathbf{r}, d-) = Z'(\mathbf{r}, d). \tag{1.81}$$

$X'$ and $Y'$ may be discontinuous. Expressions for linking $X'(\mathbf{r}, d+)$ and $Y'(\mathbf{r}, d+)$ with $X'(\mathbf{r}, d-)$ and $Y'(\mathbf{r}, d-)$ have to be found. The Maxwell equation (1.23) gives

$$Z_y - Y' = \mu_0 \sigma U, \qquad X' - Z_x = \mu_0 \sigma V. \tag{1.82}$$

Combining the second expressions of both (1.80) and (1.82), we have

$$\rho_0 \left[X'(\mathbf{r}, d+) - Z_x(\mathbf{r}, d+)\right] = \rho(\mathbf{r}, d-) \left[X'(\mathbf{r}, d-) - Z_x(\mathbf{r}, d-)\right] \tag{1.83}$$

which leads to

$$X'(\mathbf{r}, d+) = R_\rho X'(\mathbf{r}, d-) + (1 - R_\rho) Z_x(\mathbf{r}, d) \tag{1.84}$$

where $R_\rho = \rho(\mathbf{r}, d-)/\rho_0$. Similarly, we can obtain

$$Y'(\mathbf{r}, d+) = R\ Y'(\mathbf{r}, d-) + (1 - R_\rho) Z_y(\mathbf{r}, d). \tag{1.85}$$

# Chapter 2

# TWO-DIMENSIONAL EM INDUCTION PROBLEMS

## 2.1 Introduction

Since our 3D model can approach 2D structures in the limit at infinity, forward problems for 2D models have to be solved in order to provide boundary conditions for the 3D computation. In this chapter, we will discuss the scheme for solving the 2D forward modelling problems, both B-polarization and E-polarization, in terms of the magnetic field only. Most of the content of the discussion on the E-polarization mode was also given in Pu, Agarwal and Weaver (1993b).

Numerical modelling of 2D problems can now be routinely undertaken by most research groups with the aid of any one of a number of two-dimensional (2D) computer programs based on finite difference, finite element, integral equation or other methods, that have been developed over the past two decades or so (e.g. Madden & Swift, 1969; Coggon, 1971; Hohmann, 1971; Jones, 1973; Kisak & Silvester, 1975; Brewitt-Taylor & Weaver, 1976; Kaikkonen, 1977; Wannamaker *et al.*, 1987; Travis & Chave, 1989). As is well-known, 2D problems separate into two distinct modes, generally called E-polarization and B-polarization, in which the electric ($E$) and magnetic ($B$) fields are respectively polarized along the 'direction of strike', i.e. parallel to the horizontal direction in which there is no variation in the earth's conductivity. The two modes are uncoupled and can be solved separately in terms of the single scalar component of the horizontally polarized field. Thus no advantage is gained by introducing potential functions — the two polarized components of the field, one in each mode, act as scalar

potentials from which the entire electromagnetic field can be derived.

In the finite difference method, the relevant equations can be obtained in a variety of ways — by the method of fictitious values, by straightforward Taylor expansions, or by integrating over rectangular domains surrounding each node, for example. All approaches lead to identical finite difference equations at each node, one for the electric field in E-polarization and the other for the magnetic field in B-polarization. They both have a simple interpretation as the discretization of the differential equation governing the relevant field component. In the equation satisfied by the electric field the conductivity at the node is assigned a value equal to the weighted (by cell area) average of the conductivities in the four cells surrounding it, while in the equation satisfied by the magnetic field it is the resistivity at the node that is given the weighted average value of the resistivities in the adjacent cells. In addition the resistivity gradients appearing in the differential equation for the magnetic field are defined by central difference formulae involving average resistivities on the grid lines passing through the node (Brewitt-Taylor and Weaver, 1976).

The generalization to three dimensions seems obvious enough. When solving for the electric field, the governing differential equation is discretized with the conductivity at the node equal to the average value of the conductivities, weighted by cell volume, in the eight cells surrounding the node in question; and when the differential equation for the magnetic field is discretized, a similarly weighted average value is used for the resistivity at the node while the resistivity gradients in the three coordinate directions are defined by central difference formulae analogous to those used in two dimensions. Certainly such a generalization of the equations would reduce to the correct 2D formulation when the given 3D model degenerates into a 2D structure, or on a boundary at infinity where the model tends to an E- or B-polarization configuration according as the problem is being solved in terms of the electric or magnetic fields (Figures

2.1a and 2.1b respectively). Consider, however, a general 3D structure of the type depicted schematically in Fig. 2.1c. Whichever field is used, there will always exist 2D configurations at infinity which are 'wrongly polarized' for the conventional 2D method of solution to apply. Suppose, for example, that we are solving for the magnetic field; then as $y \rightarrow \pm\infty$ the model tends to a B-polarization configuration expressed in terms of the only non-vanishing magnetic component at infinity (the $Y$-component) in the usual way, but as $x \rightarrow \pm\infty$ an E-polarization problem is approached which must be solved in terms of the $Y$- and $Z$-components of the magnetic field rather than the $x$-component of the electric field – $U$ which conventional practice in two-dimensions would require. While it is not difficult to write down separate discretizations of the differential equations satisfied by the two magnetic components, the question arises as to how the nodal values of the resistivity and its gradient should be defined. Normally the weighted average conductivities are used in E-polarization problems, but when solving for the magnetic field in the full 3D problem, we must use the weighted average resistivities if the equations on the boundaries at $y = \pm\infty$ are to reduce to the correct 2D form for B-polarization problems.

In fact there is really no choice at all. For the compelling reason stated above, weighted resistivities should be used when one is working with the magnetic rather than the electric field in an E-polarization problem, even though this means that a slightly modified model of the geo-electric structure at $x = \pm\infty$ will be treated (because the average resistivity values are not identical to the reciprocals of the average conductivities). It can be argued, however, that the end results will not be affected because one is merely adopting the different, but nevertheless appropriate, discrete representations of the same model that arise quite naturally when solving for the electric and magnetic fields in separate E- and B-polarization problems. Solving for the magnetic field with weighted resistivities does indeed give accurate solutions for most structures (e.g. the E-

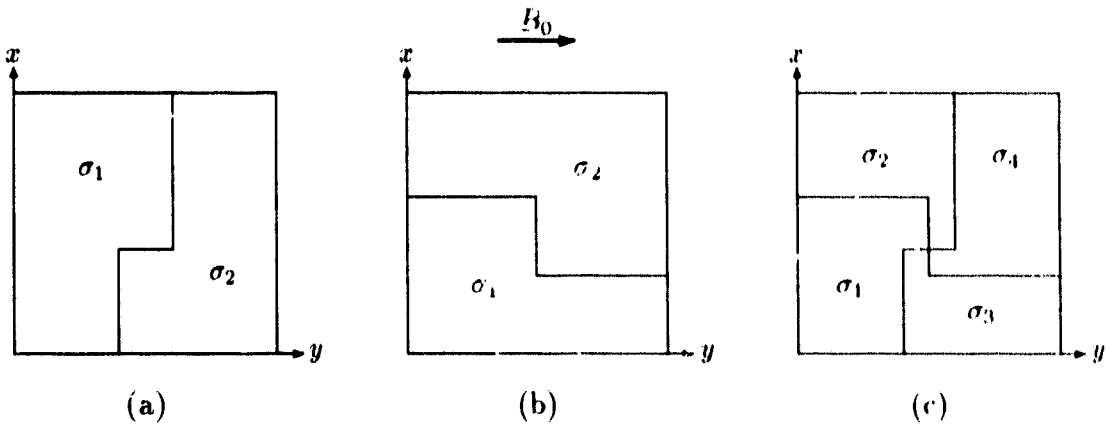


Figure 2.1: Plan view of a three-dimensional model which approaches (a) an E-polarization configuration, (b) a B-polarization configuration, and (c) both E- and B-polarization configurations on its boundaries at infinity. The downwards vertical $z$-axis is directed into the plane of the diagram.

polarization 'control model' of Weaver, LeQuang and Fischer, 1986), but for some others of a more extreme kind involving large conductivity gradients (as illustrated in Fig. 2.2 to be discussed later), it has been found that finer grids than would normally be used in a conventional E-polarization solution are required to maintain the desired accuracy. With a normal grid the discrepancy between the magnetic field solution and that obtained by the standard method is occasionally found to be quite significant — much greater, in fact, than the margin of error associated with the finite difference approximation.

In an attempt to overcome the problem of grid design with some of these extreme models we have chosen to solve the E-polarization equations for the magnetic field components by one of the other methods alluded to above, that which entails an integration over a rectangular domain covering the node. In the original formulation of E-polarization solutions in terms of the electric field, this method led directly to the standard finite difference equations which could then be interpreted in terms of averaged conductivity values assigned to the nodes. Therefore when the magnetic field is treated, the method will also by-pass the

question of how to average the resistivities and define their gradients at each node, and in fact yields completely different finite difference equations for the two components which have no simple interpretation in terms of either averaged resistivities or conductivities. The new equations also turn out to be numerically unstable 9-point equations rather than the usual 5-point ones.

According to the configuration shown by Fig. 2.1, the E-polarization mode occurs in the $yz$-plane and involves magnetic fields $\mathbf{B} = (0, Y, Z)$ as well as electric fields $\mathbf{E} = (U, 0, 0)$, while the B-polarization mode occurs in the $xz$-plane and involves $\mathbf{B} = (0, Y, 0)$ and $\mathbf{E} = (U, 0, W)$. Since we are solving the both modes by the magnetic fields only, at each nodal point we need one equation, $Y$-equation, for the B-polarization mode and two equations, $Y$- and $Z$-equation, for the E-polarization mode.

In this chapter, we shall first discuss the boundary conditions needed to complete the problem. Then we shall derive the 9-point finite difference equations for E-polarization and show how their solutions can be stabilized. After that, the complete sets of equations for both $E$- and B-polarization are laid out in the coordinate frame shown by Fig. 1.2, which is used in the other parts of this thesis and in the computer program as well. Finally the results of magnetic field calculations for some E-polarization test models will be presented and compared with the corresponding solutions obtained by conventional methods using the simpler equations satisfied by the electric field.

## 2.2 Boundary Conditions

The 9-point finite difference equations mentioned above apply to the region of $y_1 < y < y_M$, $z_1 < z < z_N$ and shall be called Governing Differential Equations, or GDE for short. Besides these GDE, we also need boundary conditions to complete the problem. We shall call those boundary conditions for $y = y_1$

and $y = y_M$ Side-Boundary-Conditions (SBC), those for $z = 0$ Top-boundary-Conditions (TBC), and those for $z = z_N = d$ Bottom-Boundary-Conditions (BBC).

For the SBC at $y = y_1$ and $y = y_M$, we use the values of the 1D solutions of the limiting 1D structures at infinity $y = -\infty$ and $y = +\infty$ respectively. In order for these 1D solutions to be reasonable approximations to the correct SBC values, the side boundary must be sufficiently far away (at least five skin-depths) from the nearest 2D conductive inhomogeneity, so that the corresponding distortion fields would be negligible at the sites of the side boundaries. TBC and BBC will be discussed separately in the following subsections.

### 2.2.1 Top Boundary Condition - TBC

When discussing TBC, we will assume that there is always a thin sheet layer, with the conductance $\tau = \tau(y)$ lying on the surface of the model. If such a thin sheet layer is not needed in the model under consideration, its effect can be easily removed by defining $\tau = 0$. The existence of the thin sheet layer makes the surface $z = 0$ double sided, i.e. the side of $z = 0+$ and the side of $z = 0-$ as shown in Fig. 1.4 and Fig. 1.5. The identities on the side of $z = 0-$ will be addressed as $f(y, 0-)$ or $f_{\lambda 0}$ when estimated at $y = y_\lambda$, and on the side of $z = 0+$ as $f(y, 0+)$ or $f_{\lambda 1}$, where $f$ stands for either electromagnetic fields or their derivatives.

At each node, there must be two separated equations for the two unknown variables, $Y$ and $Z$. These equations will be called the $Y$-equation and $Z$-equation respectively. On the side $z = 0-$, the $Y$-equation is given in the form of a Hilbert transform (Appendix B)

$$Y(y, 0-) = B_0 + \frac{1}{\pi} \int\!\!\!\!\!\!- _{-\infty}^{\infty} \frac{Z(u, 0-)}{y_\lambda - u} du, \tag{2.1}$$

while the fact that the $Z$ component is continuous across the thin sheet layer

serves as the $Z$-equation

$$Z(y,0-) = Z(y,0+). \tag{2.2}$$

The $Y$-equation on $z = 0+$ comes from the connection across the thin sheet layer given by (1.54), i.e.

$$Y(y,0+) - Y(y,0-) = \tau(y)\rho(y,0+)[Y'(y,0+) - Z_y(y,0+)], \tag{2.3}$$

where the derivative $Y'(y,0+)$ cannot be calculated directly by the central difference formula since there is no grid in the region of $z < 0$. It therefore has to be expressed by terms defined in the region of $z \geq 0$ only.

Within the region $0 < z < \frac{1}{2}k_1$, we have $\rho(y_\lambda, z) = \rho_{\lambda,1/2}$ which is uniform alor he $z$ direction, i.e. $\rho'(y_\lambda, 0+) = 0$. The basic equation (1.28),

$$\nabla^2\mathbf{B} - \frac{\nabla\rho}{\rho} \times (\nabla \times \mathbf{B}) = i\alpha^2\mathbf{B},$$

thus has its two components as

$$Y_{yy} + Y'' = i\alpha^2 Y, \tag{2.4}$$

$$Z_{yy} + Z'' + (Z_y - Y')\bar{\rho}_y = i\alpha^2 Z. \tag{2.5}$$

The Taylor expansion gives

$$Y_{\lambda 2} \approx Y_{\lambda 1} + k_1 Y'(y_\lambda, 0+) + \frac{k_1^2}{2} Y''(y_\lambda, 0+) \tag{2.6}$$

$$Z_{\lambda 2} \approx Z_{\lambda 1} + k_1 Z'(y_\lambda, 0+) + \frac{k_1^2}{2} Z''(y_\lambda, 0+). \tag{2.7}$$

With the help of (2.4), equation (2.6) gives the derivative $Y'$ as

$$Y'(y_\lambda, 0+) = Y'_{\lambda 1} = -(\frac{1}{k_1} + \frac{k_1}{2}i\alpha^2)Y_{\lambda 1} + \frac{1}{k_1}Y_{\lambda 2} + \frac{k_1}{2}(Y_{yy})_{\lambda 1}. \tag{2.8}$$

Putting (2.8) into (2.3), we obtain for the $Y$-equation on the side $z = 0+$ as

$$Y_{\lambda 1} = Y_{\lambda 0} + \tau_\lambda \rho_{\lambda \frac{1}{2}}[-(\frac{1}{k_1} + \frac{k_1}{2}i\alpha^2)Y_{\lambda 1} + \frac{1}{k_1}Y_{\lambda 2} + \frac{k_1}{2}(Y_{yy})_{\lambda 1} - (Z_y)_{\lambda 1}] \tag{2.9}$$

Note that when $\tau \equiv 0$, (2.9) becomes $Y_{\lambda 1} = Y_{\lambda 0}$, just what it should be when there is no thin sheet layer. Therefore, we can eliminate the effect of the thin sheet layer this way when it is not required. In the actual computation, we insert (2.1) into (2.9), i.e.

$$Y_{\lambda 1} = B_0 + \frac{1}{\pi} \int_{-\infty}^{\infty} \frac{Z(u,0-)}{y_\lambda - u}\, du$$
$$+\tau_\lambda \rho_{\lambda \frac{1}{2}} [-(\frac{1}{k_1} + \frac{k_1}{2} i\alpha^2) Y_{\lambda 1} + \frac{1}{k_1} Y_{\lambda 2} + \frac{k_1}{2} (Y_{yy})_{\lambda 1} - (Z_y)_{\lambda 1}] \quad (2.10)$$

so that the unknown variable $Y_{\lambda 0}$ can be removed which reduces the rank of the coefficient matrix.

For the $Z$-equation, we combine (2.5) and (2.7) to eliminate the $Z''$ terms and obtain

$$Z_{\lambda 2} - Z_{\lambda 1} = k_1 Z'_{\lambda 1}$$
$$+\frac{k_1^2}{2} \{i\alpha^2 Z_{\lambda 1} - (Z_{yy})_{\lambda 1} - [(Z_y)_{\lambda 1} - Y'_{\lambda 1}] \bar{\rho}_y\} \quad (2.11)$$

Multiplying (2.11) through by $2/k_1^2$, defining $A_y = -k_1 \bar{\rho}_y / 2$, and replacing both $Y'_{\lambda 1}$ and $Z'_{\lambda 1}$ in (2.11) by (2.8) and $Z' = -Y_y$ (2D form of $\nabla \cdot \mathbf{B} = 0$) respectively, we obtain for the $Z$-equation at $z = 0+$

$$A_y (Y_{yy})_{\lambda 1} + (Z_{yy})_{\lambda 1} + \frac{2}{k_1} (Y_y)_{\lambda 1} + \bar{\rho}_y (Z_y)_{\lambda 1}$$
$$= i\alpha^2 A_y Y_{\lambda 1} + \frac{\bar{\rho}_y}{k_1} (Y_{\lambda 2} - Y_{\lambda 1}) + i\alpha^2 Z_{\lambda 1} - \frac{2}{k_1^2} (Z_{\lambda 2} - Z_{\lambda 1}) \quad (2.12)$$

### 2.2.2 Bottom Boundary Condition – BBC

Several different forms of BBC have been studied. The simplest one is

$$Y(y, \infty) = 0, \quad Z(y, \infty) = 0. \quad (2.13)$$

In practice, however, we have used

$$Y(y, D) = 0, \quad Z(y, D) = 0, \quad (2.14)$$

where $D$, the depth of the bottom of the mesh, is large enough that $Y(y, D)$ and $Z(y, D)$ can be considered as being attenuated almost to zero.

Being more accurate, integral boundary conditions (Weaver, 1994) can be applied at $z = d$, where $d$ is chosen such that when $z > d$, $\rho(y, z) \equiv \rho_0$. In order to derive these integral equations, we adopt the following definitions of Fourier transform and convolution,

$$\hat{f}(\eta) = \frac{1}{\sqrt{2\pi}} \int_{-\infty}^{\infty} f(y) e^{i\eta y}\, dy, \qquad f(y) = \frac{1}{\sqrt{2\pi}} \int_{-\infty}^{\infty} \hat{f}(\eta) e^{-i\eta y}\, d\eta$$
$$f \star g(y) \equiv \frac{1}{\sqrt{2\pi}} \int_{-\infty}^{\infty} f(v) g(y - v)\, dv = \frac{1}{\sqrt{2\pi}} \int_{-\infty}^{\infty} \hat{f}(\eta) \hat{g}(\eta) e^{-i\eta y}\, d\eta \tag{2.15}$$

In $z > d$, since $\rho(y, z) \equiv \rho_0$, the basic equation becomes

$$\nabla^2 \mathbf{B} = i\alpha_0^2 \mathbf{B}$$

or

$$\frac{\partial^2 F}{\partial y^2} + \frac{\partial^2 F}{\partial z^2} = i\alpha_0^2 F \tag{2.16}$$

where $F$ can be either $Y(y, z)$ or $Z(y, z)$ and $\alpha_0^2 = i\omega\mu_0/\rho_0$ is a constant. The Fourier transform of (2.16) is

$$\hat{F}''(\eta, z) = (\eta^2 + i\alpha_0^2)\hat{F}(\eta, z). \tag{2.17}$$

The solution of (2.17) in $z > 0$ that satisfies the condition $F(y, \infty) = 0$ is

$$\hat{F}(\eta, z) = \hat{F}(\eta, d+) \exp[-(z - d)\gamma_0(\eta)] \tag{2.18}$$

where $\gamma_0(\eta) = (\eta^2 + i\alpha_0^2)^{1/2}$.

A tabulated Fourier transform (Erdélyi, 1954, §1.4(26)) gives

$$\frac{1}{\sqrt{2\pi}} \int_{-\infty}^{\infty} P(y, z) \exp(i\eta y)\, dy = \sqrt{\frac{\pi}{2}} \frac{\exp[-z\gamma_0(\eta)]}{z\alpha_0\sqrt{i}} \tag{2.19}$$

where $P(y, z)$ is defined as

$$P(y, z) = \frac{K_1[(y^2 + z^2)^{\frac{1}{2}} \alpha_0 \sqrt{i}]}{(y^2 + z^2)^{\frac{1}{2}}}, \tag{2.20}$$

and $K_1$ is the modified Bessel function of order 1. Applying the convolution theorem to (2.18), we have

$$F(y,z) = \frac{(z-d)\alpha_0\sqrt{i}}{\pi}\int_{-\infty}^{\infty} F(v,d+)P(y-v,z-d)\,dv. \qquad (2.21)$$

Although it is a solution to the differential equation (2.16), it is not convenient to use, since the integral does not converge by itself at $z = d+$. A better form can be found as follows: with $\eta = 0$ and with $y$ and $z$ being replaced by $y - v$ and $z - d$ respectively, (2.19) becomes

$$\exp[-(z-d)\alpha_0\sqrt{i}] = \frac{(z-d)\alpha_0\sqrt{i}}{\pi}\int_{-\infty}^{\infty} F(v,d+)P(y-v,z-d)\,dv. \qquad (2.22)$$

Multiplying (2.22) by $F(y,d+)$ and subtracting it from (2.21), we have

$$F(y,z) - F(y,d+)\exp[-(z-d)\alpha_0\sqrt{i}] = \frac{(z-d)\alpha_0\sqrt{i}}{\pi}\int_{-\infty}^{\infty}[F(v,d+) - F(y,d+)]P(y-v,z-d)\,dv. \qquad (2.23)$$

Differentiate (2.23) and evaluate it at $z = d$. Then the new form of the solution to (2.16) is

$$F'(y,d+) + \alpha_0\sqrt{i}F(y,d+) = \frac{\alpha_0\sqrt{i}}{\pi}\int_{-\infty}^{\infty}[F(v,d+) - F(y,d+)]\frac{K_1(|y-v|\alpha_0\sqrt{i})}{|y-v|}\,dv \qquad (2.24)$$

where $F$ can be either $Y$ or $Z$. When $F$ is replaced by $Y$, (2.24) serves as the integral BBC $Y$-equation, and when it is replaced by $Z$, it serves as the integral BBC $Z$-equation.

There is a second integral $Z$-equation. Replacing $\hat{F}$ by $\hat{Z}$ in (2.18) and differentiating it with respect to $z$, it gives

$$\hat{Z}(\eta,z) = -\hat{Z}'(\eta,z)/\gamma_0(\eta) \qquad (2.25)$$

The inverse Fourier transform of $1/\gamma_0(\eta)$ is $(2/\pi)^{1/2}K_0(y)$ where $K_0$ is the modified Bessel function of 2nd kind and of order zero (Erdélyi, 1954, §1.2(17)).

With the help of the convolution theorem, the inversion of the above equation is

$$Z(y,z) = -\frac{1}{\pi}\int_{-\infty}^{\infty} Z'(y,z)K_0(|y-v|\alpha_0\sqrt{i}\,)\,dv. \tag{2.26}$$

Replace $Z'$ by $Z' = -\partial Y/\partial y$ in (2.26) and evaluate it at $z = d+$. Then

$$Z(y,d+) = \frac{1}{\pi}\int_{-\infty}^{\infty} \frac{\partial Y}{\partial y}(y,d+)K_0(|y-v|\alpha_0\sqrt{i})\,dv. \tag{2.27}$$

By partial integration, it follows that

$$Z(y,d) = \frac{\alpha_0}{\sqrt{i}}\int_{-\infty}^{\infty} \operatorname{sgn}(v-y)Y(v,d)K_1(\alpha_0\sqrt{i}|v-y|)\,dv. \tag{2.28}$$

Since it calculates the $Z$ component from the $Y$ component, (2.28) provides a strong connection between the two components, and is therefore a better integral BBC $Z$-equation.

Besides the integral equations mentioned above, a differential form of the $Z$-equation is also useful sometimes. In the region $z_N - \frac{1}{2}k_{N-1} < z < d$, for the same reason as in the TBC, we have $\rho'(y,d-) = 0$ and the basic equations (2.4), (2.5)

$$Y_{yy} + Y'' = i\alpha^2 Y, \tag{2.29}$$

$$Z_{yy} + Z'' + (Z_y - Y')\bar{\rho}_y = i\alpha^2 Z, \tag{2.30}$$

still apply, only now

$$\alpha^2 = \omega\mu_0/\rho^-,\ \ \rho^- = \rho(y, d - \tfrac{1}{2}k_{N-1}), \text{ and } \bar{\rho}_y = (\partial\rho^-/\partial y)/\rho^-.$$

The backward Taylor expansions give

$$Y_{N-1} = Y_N - k_{N-1}Y'_N + \frac{k_{N-1}^2}{2}Y''_N \tag{2.31}$$

$$Z_{N-1} = Z_N - k_{N-1}Z'_N + \frac{k_{N-1}^2}{2}Z''_N. \tag{2.32}$$

All the terms except $Y_{N-1}$ and $Z_{N-1}$ are evaluated on $Z = d-$. Combining (2.29) to (2.32), and with the help of $Z' = -\partial Y/\partial y$, eliminating $Y'_N, Z'_N, Y''_N, Z''_N$, we arrive at the differential BBC $Z$-equation:

$$Z_{yy} + \bar{\rho}_y(Z_y - Y') - \frac{2}{k_{N-1}}Y_y = \left(\frac{2}{k_{N-1}^2} + i\alpha^2\right) Z_N - \frac{2}{k_{N-1}^2}Z_{N-1} \qquad (2.33)$$

## 2.3 Governing Differential Equations–GDE

The natural differential equation applied to the region of $0 < z < d$ is the basic equation

$$\nabla^2\mathbf{B} - \frac{\nabla\rho}{\rho} \times (\nabla \times \mathbf{B}) = \frac{i\omega\mu_0}{\rho}\mathbf{B} \qquad (2.34)$$

or, in component form

$$Y_{yy} + Y_{zz} + (Y_z - Z_y)\frac{\rho_z}{\rho} = \frac{i\omega\mu_0}{\rho}Y, \qquad (2.35)$$

$$Z_{yy} + Z_{zz} + (Z_y - Y_z)\frac{\rho_y}{\rho} = \frac{i\omega\mu_0}{\rho}Z. \qquad (2.36)$$

These equations can be discretized straightforwardly by substituting the partial derivatives with the corresponding central difference formulae. But when defining the values of $\rho$, $\rho_y$ and $\rho_z$ at nodal points, a difficulty arises.

It has been shown (Brewitt-Taylor and Weaver, 1976) that for solving 2D E-polarization problems, one should solve the equation for the single component of electric field $U$ (i.e. $E_x$)

$$\nabla^2 U = i\omega\mu_0\sigma U,$$

and use the conductivity $\sigma$ as the model parameter. The value of $\sigma$ at a node point is defined as the weighted average of conductivities of all the four cells surrounding the given node point;

$$\bar{\sigma} = \frac{h_0k_0\sigma_{00} + h_2k_0\sigma_{20} + h_0k_2\sigma_{02} + h_2k_2\sigma_{22}}{(h_0 + h_2)(k_0 + k_2)}. \qquad (2.37)$$

In a special case of $\sigma_{00} = \sigma_{20} = \sigma_0$, $\sigma_{02} = \sigma_{22} = \sigma_2$, it is simplified to

$$\bar{\sigma} = \frac{k_0\sigma_0 + k_2\sigma_2}{k_0 + k_2}. \qquad (2.38)$$

But our situation is different; we not only have to solve E-polarization problems by two magnetic fields rather than one single electric field, but also have to employ the resistivity $\rho$ and its derivatives rather than conductivity $\sigma$ (without derivatives) as the model parameter in order to maintain consistency with the 3D calculation. When using $\rho$ as the model parameter, its value at a node point is naturaliy the weighted resistivity. The counterpart of (2.38) is

$$\bar{\rho} = \frac{k_0\rho_0 + k_2\rho_2}{k_0 + k_2}. \tag{2.39}$$

It is easy to see that, although $\rho = 1/\sigma$,

$$\bar{\rho} = \frac{k_0\rho_0 + k_2\rho_2}{k_0 + k_2} = \frac{k_0\frac{1}{\sigma_0} + k_2\frac{1}{\sigma_2}}{k_0 + k_2} = \frac{k_0\sigma_2 + k_2\sigma_0}{(k_0 + k_2)\sigma_0\sigma_2} \neq \frac{1}{\bar{\sigma}},$$

and therefore,

$$\frac{i\omega\mu_0}{\bar{\rho}} \neq i\omega\mu_0\bar{\sigma}.$$

This simply means that the same model is described differently in our equations which use weighted resistivity $\bar{\rho}$ from those which use the weighted conductivity $\bar{\sigma}$. Of course, we can compensate for this difference by employing a finer grid at the cost of entailing more grid points and therefore more memory and computation, but for the 3D modelling problems where the memory and CPU time might be constantly under stress, this price might just be too high to pay. On the other hand, if we ignore this difference and use the same grid as would normally be used in a conventional E-polarization solution, then for some extreme models, such as the one shown in Fig. 2.2 in which a highly conducting surface layer and a resistive crust overlie a deep conducting vertical fault, an unacceptable discrepancy (Fig. 2.7) between results generated by the program of Brewitt-Taylor and Weaver (1976) based on traditional E-polarization modelling with the electric field and weighted average *conductivities* (broken line) and those obtained by solving directly for the magnetic field components on the

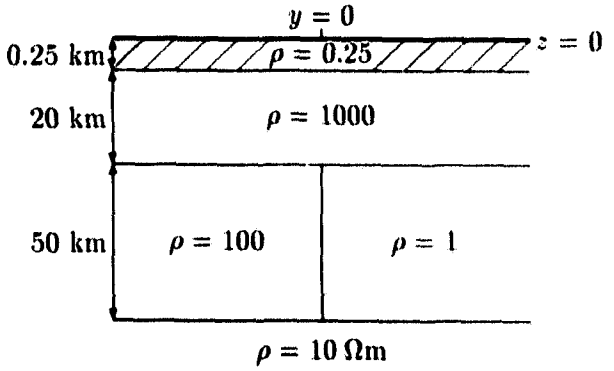


Figure 2.2: Model 2D-a, two-dimensional model used for test calculations.

same grid using weighted average *resistivities* at the nodes (solid line), would be produced.

In order to overcome this difficulty, it is our desire to avoid defining the values of model parameter $\rho$ at the nodes. One alternative approach is to convert the differential equations applied to a node point into equations obtained by integrating along a path enclosing that point. Starting with the Maxwell equations (1.23) and (1.22), i.e.

$$\nabla \times \mathbf{B} = \mu_0 \sigma \mathbf{E}, \tag{2.40}$$

$$\nabla \times \mathbf{E} = -i\omega \mathbf{B}, \tag{2.41}$$

instead of taking the curl of (2.40) directly to obtain the basic equation (1.28) or (2.34), we first write $\sigma$ as $1/\rho$ and move it to the other side of the equation, so that

$$\rho \nabla \times \mathbf{B} = \mu_0 \mathbf{E}. \tag{2.42}$$

Then we take the curl and integrate the result over the area $\mathcal{A}$ which is enclosed by the path $\mathcal{C}$ shown in Fig. 2.3, where the four corners $P, Q, R, S$ of $\mathcal{C}$ are the centres of the four cells adjacent to node O. This procedure gives

$$\int\int_{\mathcal{A}} d\mathbf{S} \times \nabla \times (\rho \nabla \times \mathbf{B}) = -i\omega\mu_0 \int\int_{\mathcal{A}} d\mathbf{S} \times \mathbf{B}. \tag{2.43}$$

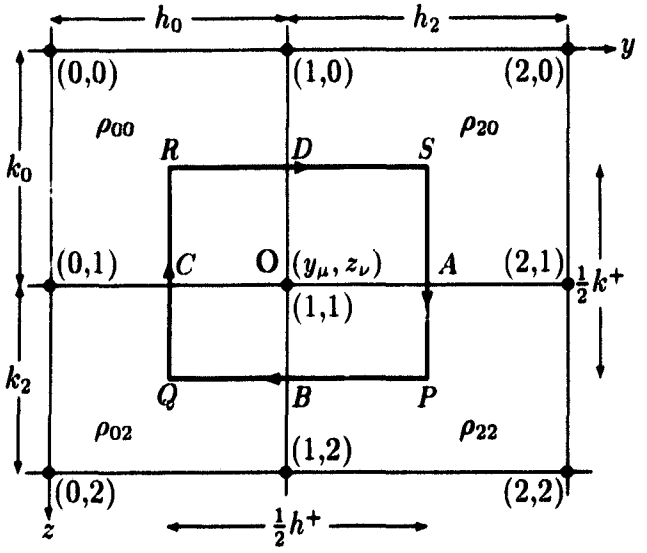


Figure 2.3: Integration around a node.

Applying the vector relation ((36), p115, D.S. Jones, 1964) to the left hand side of (2.43), we have

$$\int\int_A d\mathbf{S} \times \nabla \times (\rho\nabla \times \mathbf{B}) = \oint_C d\mathbf{l} \times (\rho\nabla \times \mathbf{B}) + \int\int_A \nabla \cdot (\rho\nabla \times \mathbf{B}) d\mathbf{S} - \int\int_A (\hat{\mathbf{x}} \cdot \nabla)(\rho\nabla \times \mathbf{B})\, dS, \tag{2.44}$$

where $d\mathbf{S} = \hat{\mathbf{x}} dS = \hat{\mathbf{x}}\, dy\, dz$ and $d\mathbf{l} = \hat{\mathbf{y}} dy + \hat{\mathbf{z}} dz$ . Since

$$\nabla \cdot (\rho\nabla \times \mathbf{B}) = \nabla\rho \cdot (\nabla \times \mathbf{B}) + \rho\nabla \cdot (\nabla \times \mathbf{B})$$

and $\nabla \cdot (\nabla \times \mathbf{B}) \equiv 0$, and since in the 2D case $\nabla\rho \perp (\nabla \times \mathbf{B} \parallel \mathbf{E})$, so that $\nabla\rho \cdot (\nabla \times \mathbf{B}) \equiv 0$, it follows that $\nabla \cdot (\rho\nabla \times \mathbf{B}) \equiv 0$. Also because $\hat{\mathbf{x}}$ is the strike direction of our 2D models, the identity

$$(\hat{\mathbf{x}} \cdot \nabla)(\rho\nabla \times \mathbf{B}) = \frac{\partial}{\partial x}(\rho\nabla \times \mathbf{B}) \equiv 0$$

always holds. Thus

$$\int\int_A d\mathbf{S} \times \nabla \times (\rho\nabla \times \mathbf{B}) = \oint_C d\mathbf{l} \times (\rho\nabla \times \mathbf{B}) = -\oint_C (\rho\nabla \times \mathbf{B}) \times d\mathbf{l} \tag{2.45}$$

and (2.43) becomes

$$\oint_C (\rho \nabla \times \mathbf{B}) \times d\mathbf{l} = i\omega\mu_0 \int\int_A (\hat{\mathbf{x}} \times \mathbf{B})\, dS, \tag{2.46}$$

In the component form, this result is expressed by the two integrals

$$\oint_C \rho(Y_z - Z_y)\, dy = -i\omega\mu_0 \int\int_A Y\, dy\, dz, \tag{2.47}$$

$$\oint_C \rho(Y_z - Z_y)\, dz = -i\omega\mu_0 \int\int_A Z\, dy\, dz \tag{2.48}$$

which can be written in the form

$$\begin{aligned} &\int_{RD} \rho_{00}(Y_z - Z_y)\, dy + \int_{DS} \rho_{20}(Y_z - Z_y)\, dy \qquad (2.49)\\ &+ \int_{PB} \rho_{22}(Y_z - Z_y)\, dy + \int_{BQ} \rho_{02}(Y_z - Z_y)\, dy \;=\; -i\omega\mu_0 \int\int_A Y\, dy\, dz,\\ &\int_{QC} \rho_{02}(Y_z - Z_y)\, dz + \int_{CR} \rho_{00}(Y_z - Z_y)\, dz \qquad (2.50)\\ &+ \int_{SA} \rho_{20}(Y_z - Z_y)\, dz + \int_{AP} \rho_{22}(Y_z - Z_y)\, dz \;=\; -i\omega\mu_0 \int\int_A Z\, dy\, dz. \end{aligned}$$

## 2.4 Cell-integral Equations

We call equation (2.46) a cell-integral equation because its L.H.S. is an integral along the curve $C$ that encloses the nodal point O by running through the surrounding cells along the trace of their centre lines, and its R.H.S. is an integral over those parts of the adjacent cells that are enclosed by the curve $C$. Equations (2.47) and (2.48) clearly show that the model parameter $\rho$ only appears in the integrals along $C$, so that no values of $\rho$ or its derivatives at the nodal points are involved; equations (2.49) and (2.50) indicate that all the values of $\rho$ are well defined. The difficulty encountered by the conventional equations (2.35) and (2.36) has been successfully avoided.

In the process of discretization, (2.49) will be taken as a working example. For the right-hand side, the magnetic field $Y$ within the area $A$ will be approx-

imated by its value at the nodal point O, and the integral then will be

$$i\omega\mu_0 \int\int_A Y\, dy\, dz = i\omega\mu_0 \frac{(h_0+h_2)}{2}\frac{(k_0+k_2)}{2} Y_{11}. \tag{2.51}$$

The derivatives $Y_z$ and $Z_y$ are slightly more complicated. For $Y_z$, the derivative normal to the line segment $RS$, a single value (estimated at point $D$) will be used on both $RD$ and $DS$, i.e.

$$(Y_z)_{RD} = (Y_z)_{DS} = (Y_z)_D = \frac{Y_{11}-Y_{10}}{k_0}. \tag{2.52}$$

For $Z_y$, the derivative tangential to the line segmets $RD$ and $DS$, two values (estimated at points $R$ and $S$) will be used respectively in the two segments, i.e.

$$(Z_y)_{RD} = (Z_y)_R = \frac{1}{2}\left(\frac{Z_{11}-Z_{01}}{h_0} + \frac{Z_{10}-Z_{00}}{h_0}\right) = \frac{Z_{11}-Z_{01}+Z_{10}-Z_{00}}{2h_0},$$

$$(Z_y)_{DS} = (Z_y)_S = \frac{1}{2}\left(\frac{Z_{21}-Z_{11}}{h_2} + \frac{Z_{20}-Z_{10}}{h_2}\right) = \frac{Z_{21}-Z_{11}+Z_{20}-Z_{10}}{2h_2}. \tag{2.53}$$

Similarly, in the segments $PB$ and $BQ$ we have

$$(Y_z)_{PB} = (Y_z)_{BQ} = (Y_z)_B = \frac{Y_{12}-Y_{11}}{k_2}, \tag{2.54}$$

$$(Z_y)_{PB} = (Z_y)_P = \frac{1}{2}\left(\frac{Z_{21}-Z_{11}}{h_2} + \frac{Z_{22}-Z_{12}}{h_2}\right) = \frac{Z_{21}-Z_{11}+Z_{22}-Z_{12}}{2h_2},$$

$$(Z_y)_{BQ} = (Z_y)_Q = \frac{1}{2}\left(\frac{Z_{11}-Z_{01}}{h_0} + \frac{Z_{12}-Z_{02}}{h_0}\right) = \frac{Z_{11}-Z_{01}+Z_{12}-Z_{02}}{2h_0}. \tag{2.55}$$

On inserting expressions from (2.52) to (2.55) into the equation (2.49) and dividing it through by the weighted average of resistivity $\bar{\rho}$ to make the coefficients dimensionless, we find that the integral equation is expressed in the form

$$\begin{aligned}(ic_0 + c_{10} + c_{12})Y_{11} = {} & c_{10}Y_{10} + c_{12}Y_{12} + (\bar{\rho}_{00} - \bar{\rho}_{20} - \bar{\rho}_{02} + \bar{\rho}_{22})Z_{11} \\ & + (\bar{\rho}_{02} - \bar{\rho}_{00})Z_{01} - (\bar{\rho}_{22} - \bar{\rho}_{20})Z_{21} - (\bar{\rho}_{20} - \bar{\rho}_{00})Z_{10} + (\bar{\rho}_{22} - \bar{\rho}_{02})Z_{12} \\ & - \bar{\rho}_{00}Z_{00} + \bar{\rho}_{20}Z_{20} + \bar{\rho}_{02}Z_{02} - \bar{\rho}_{22}Z_{22},\end{aligned} \tag{2.56}$$

where

$$\bar{\rho}_{l,m} = \rho_{l,m}/\bar{\rho},\ (l = 0, 2;\ m = 0, 2),$$
$$\bar{\rho} = \frac{h_0 k_0 \rho_{00} + h_2 k_0 \rho_{20} + h_0 k_2 \rho_{02} + h_2 k_2 \rho_{22}}{(h_0 + h_2)(k_0 + k_2)}, \tag{2.57}$$

and

$$c_0 = \frac{\omega \mu_0}{\bar{\rho}}(h_0 + h_2)(k_0 + k_2) = \alpha^2 h_s k_s, \tag{2.58}$$

$$c_{10} = \frac{2}{k_0}(\bar{\rho}_{00} h_0 + \bar{\rho}_{20} h_2) := \frac{2h_s}{k_0}\bar{\rho}_{10},\ \ c_{12} = \frac{2}{k_2}(\bar{\rho}_{02} h_0 + \rho_{22} h_2) := \frac{2h_s}{k_2}\rho_{12}. \tag{2.59}$$

A similar procedure brings (2.50) into the form

$$\begin{aligned}(ic_0 + c_{01} + c_{21})Z_{11} = {} & c_{01}Z_{01} + c_{21}Z_{21} + (\bar{\rho}_{00} - \rho_{20} - \rho_{02} + \rho_{22})Y_{11} \\ & -(\bar{\rho}_{02} - \bar{\rho}_{00})Y_{01} + (\bar{\rho}_{22} - \bar{\rho}_{20})Y_{21} + (\bar{\rho}_{20} - \bar{\rho}_{00})Y_{10} - (\rho_{22} - \rho_{02})Y_{12} \\ & -\bar{\rho}_{00}Y_{00} + \bar{\rho}_{20}Y_{20} + \rho_{02}Y_{02} - \rho_{22}Y_{22},\end{aligned} \tag{2.60}$$

where $c_0$ is the same as above, and

$$c_{01} = \frac{2}{h_0}(\bar{\rho}_{00} k_0 + \bar{\rho}_{02} k_2) := \frac{2k_s}{h_0}\bar{\rho}_{01},\ \ c_{21} = \frac{2}{h_2}(\bar{\rho}_{20} k_0 + \bar{\rho}_{22} k_2) := \frac{2k_s}{h_2}\rho_{21}. \tag{2.61}$$

Equations (2.56) and (2.60) are the finite difference forms of the $Y$ and $Z$ cell-integral equations applied to the region of $y_1 < y < y_M$, $0 < z < d$, or to the corresponding grid points $2 \le j \le M-1$, $2 \le k \le N-1$. Note that they involve the field values from all the 9 grid points around the node point, while the conventional ones only involve 5 points.

## 2.5 The Convergency of the Cell-integral Equations

Although the cell-integral equations we have derived offered some advantages over the conventional ones mathematically, it was found they had a fatal weak point; they are numerically unstable. When the attempt was made to solve these equations by an iterative method, the iteration process was successful for a small test model, M777, which has a uniform conductivity structure with only

7 grid points in both horizontal and vertical directions. The result was excellent for this simple model. But when the model was enlarged a little, the process started to diverge.

In order to understand why this is happening, let us simplify the equation (2.60) by assuming $h_0 = h_2 = h$, $k_0 = k_2 = k$, and $\rho_{00} = \rho_{02} = \rho_{20} = \rho_{22} = \rho$, and dividing it throughout by $\rho$. The simplified form of (2.60) is

$$\left(\frac{i\omega\mu_0}{\rho}4hk + 8\frac{k}{h}\right) Z_{11} = 4\frac{k}{h}Z_{01} + 4\frac{k}{h}Z_{21} - Y_{00} + Y_{20} + Y_{02} - Y_{22} \qquad (2.62)$$

where the L.H.S. term $Z_{11}$ is the diagonal element of the linear equation set to be solved. In the coefficient of this diagonal element, the ratio of the amplitudes of the first and second terms is

$$R = \frac{\omega\mu_0 4hk/\rho}{8k/h} = \frac{\omega\mu_0}{2\rho}h^2 = \left(\frac{h}{\delta}\right)^2 \qquad (2.63)$$

where $\delta = \sqrt{2\rho/\omega\mu_0}$ is the skin depth. When we design a mesh, it is a common practice to keep the grid steps no larger than $\delta/3$ within $3\delta$ from a conductivity contrast boundary. So, for some points, we have $(\frac{h}{\delta})^2 < \frac{1}{9}$, i.e., the 2nd term $(8k/h)$ is dominant in magnitude.

The cause of the instability can now be clearly seen. The dominant term $(8k/h)$ may easily be less then 1, so long as $h > 8k$, and which is almost inevitable in our grid design. This means that at some grid points, where the surrounding cells take the shape of a long strip, the modulus of the diagonal coefficient, $|i\omega\mu_0 4hk/\rho + 8k/h|$, may be smaller than 1. But the coefficients of $Y_{00}$,$Y_{20}$,$Y_{02}$ and $Y_{22}$, the 4 terms involved with the 4 corners ($Q$, $R$, $S$, $P$) of the integral path $C$ in Fig. 2.3, are always exactly 1 in this special case, i.e. larger than some of the diagonal ones. In other words, the non-diagonal corner terms exert more influence than those diagonal ones, thus violating the necessary condition for the convergence of the iteration and thereby causing it to diverge.

A great deal of effort, both mathematical, and numerical, has been spent attempting to circumvent this divergency problem. Among them were derivation of a set of 5-point cell-integral formulae, an application of the method of shifting the spectrum, use of direct solution methods and adding $\mathrm{div}\,\mathbf{B} = 0$ to the 9 points cell-integral formulae, just to name a few. The 5-point cell-integral formulae were also derived from equations (2.40) and (2.41), but with different approximations for the derivatives of $Y$ and $Z$. This new set of formulae involved only 5 grid points and had stronger diagonal coefficients. The convergence problem was solved. But unfortunately it converged to the wrong solution! The method of shifting the spectrum was originally derived by Hutson, Kendal and Malin (1972). This technique did make the 9-point (cell-integral) equations converge, but the speed of convergence was so slow that it was hardly tolerable even for a 2D problem, not to mention what it would be like with 3D models.

A result of the direct solution given by the 9-point equations (2.56) and (2.60) for model 2D-a (Fig. 2.2) is presented in Fig. 2.8. The result was obtained by using a subroutine which solves a banded complex double precision matrix via Gauss-elimination; the subroutine was obtained from a FTP site for many mathematical softwares, at Internet address "netlib@research.att.com" which refers to a gateway machine, 192.20.225.2, at AT & T Bell Labs in Murray Hill, New Jersey. Although the direct solution in Fig. 2.8 still differs from the solution given by Brewitt-Taylor and Weaver (1976), it was an important step towards our later success; it enabled us to see what the results delivered by equations (2.56) and (2.60) were like. By comparing them with those generated by the programs of Brewitt-Taylor and Weaver (1976), and Poll (1994), we could see that our result was basically following the correct trend. Only if we could eliminate the spikes, presumably caused by the poor condition of the coefficient matrix, could we hope to get a reasonable agreement.

It was interesting to notice that when we used the iteration process with

the help of shifting the spectrum for convergence and started with the correct solution from Brewitt-Taylor and Weaver as the initial value, the iterative results marched away from the good solution and finally converged towards that of the direct method. This clearly indicated that our result from the direct method was the true solution to equations (2.56) and (2.60), even though it was not the right answer to the problem. So, we had to modify our equations mathematically to improve the condition of their coefficient matrix.

The source of the poor conditioning for that particular model was identified to be the $Z$-equation where the $k/h$ ratio was too small. We had to strengthen the diagonal coefficients. Obviously, if $k/h$ is too small, then $h/k$ must be large. Thus, it should be possible to solve the problem by including an extra term with $h/k$ into the diagonal coefficient of the $Z$-equation where $k/h$ was the dominant term. Such a term was found in $\nabla \cdot \mathbf{B} = 0$.

Applying $\nabla \cdot \mathbf{B} = 0$ at point $(1, \frac{3}{2})$ in Fig. 2.4, we obtain

$$\left(\frac{\partial Z}{\partial z}\right)_{(1,\frac{3}{2})} = \frac{Z_{12} - Z_{11}}{k_2} = -\left(\frac{\partial Y}{\partial y}\right)_{(1,\frac{3}{2})} = -\frac{1}{2}\left[\left(\frac{\partial Y}{\partial y}\right)_{(1,1)} + \left(\frac{\partial Y}{\partial y}\right)_{(1,2)}\right],$$

or,

$$Z_{11} = Z_{12} + \frac{k_2}{2}\left[\frac{h_0}{h_2 h_s}(Y_{21} + Y_{22}) + \frac{h_{20}}{h_0 h_2}(Y_{11} + Y_{12}) - \frac{h_2}{h_0 h_s}(Y_{01} + Y_{02})\right]. \quad (2.64)$$

When $h_0 = h_2 = h$, the above equation shows that

$$\frac{h}{k} Z_{11} = \frac{h}{k} Z_{12} + \frac{1}{4}(Y_{21} + Y_{22} - Y_{01} - Y_{02}), \quad (2.65)$$

the coefficient of $Z_{11}$ being just what we wanted. Multiplying (2.64) by a factor $f$ and adding it to the $Z$-equation (2.60), we obtained the result showed in Fig. 2.9. Although there was still some small vibration, it was a milestone for us. Very soon, it was found that by applying $\nabla \cdot \mathbf{B} = 0$ at point $(1, \frac{1}{2})$, so that

$$Z_{11} = Z_{10} - \frac{k_0}{2}\left[\frac{h_0}{h_2 h_s}(Y_{20} + Y_{21}) + \frac{h_{20}}{h_0 h_2}(Y_{10} + Y_{11}) - \frac{h_2}{h_0 h_s}(Y_{00} + Y_{01})\right], \quad (2.66)$$

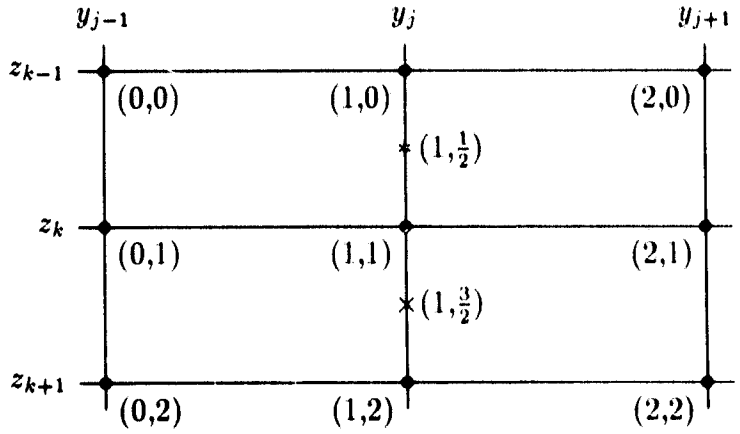


Figure 2.4: the symbols $\times$ and $*$ respectively denote the points where equations (2.64) and (2.66) are obtained by applying div $\mathbf{B} = 0$.

and by adding this equation instead of (2.64) to the $Z$-equation (2.60), we could remove the unwanted vibration in Fig. 2.9. The new result is presented in Fig. 2.10.

## 2.6 Auxiliary Equations for the Cell-integral Equations

Generally, the weak diagonal coefficient can be caused by either or both of the $Y$ and $Z$- equations (2.56) and (2.60). For example, we tried another model, 2D-b as shown in Fig. 2.5; and we found that no matter which equation, (2.64) or (2.66), was used to modify the $Z$-equation (2.60), it failed to bring good results. It was identified that the problematic equation is the $Y$-equation for this model. Therefore, we need another formula for the $Y$-equation which will modify this equation as formula (2.66) modifies the $Z$-equation (2.60). Though (2.66) is good for the $Z$-equation (2.60), it is not symmetrical about the $z$-direction and cannot be readily extended to the $Y$-equation. However, a new set of such equations can be found in the following way. First, take the gradient of the scalar equation $\nabla \cdot \mathbf{B} = 0$ to produce a vector equation

$$\nabla(\nabla \cdot \mathbf{B}) = 0. \tag{2.67}$$

Then, integrate it in the same way as (2.43). This leads to

$$\int\int_A d\mathbf{S} \times \nabla(\nabla \cdot \mathbf{B}) = 0. \tag{2.68}$$

By formula (35) ( p114, D.S. Jones, 1964), we have

$$\int\int_A d\mathbf{S} \times \nabla(\nabla \cdot \mathbf{B}) = \oint_C (\nabla \cdot \mathbf{B})\, d\mathbf{l} = 0, \tag{2.69}$$

or,

$$\oint_C (\frac{\partial Y}{\partial y} + \frac{\partial Z}{\partial z})\, dy = 0 \tag{2.70}$$

$$\oint_C (\frac{\partial Y}{\partial y} + \frac{\partial Z}{\partial z})\, dz = 0. \tag{2.71}$$

Equation (2.70) leads to

$$\int_R^S (\frac{\partial Y}{\partial y}\, dy + \frac{\partial Z}{\partial z}\, dy) + \int_P^Q (\frac{\partial Y}{\partial y}\, dy + \frac{\partial Z}{\partial z}\, dy) = 0, \tag{2.72}$$

where

$$\begin{aligned} \int_R^S \frac{\partial Y}{\partial y}\, dy &= (Y)_S - (Y)_R \\ &= \frac{1}{4}(Y_{10} + Y_{20} + Y_{11} + Y_{21}) - \frac{1}{4}(Y_{00} + Y_{10} + Y_{01} + Y_{11}) \\ &= \frac{1}{4}(Y_{20} + Y_{21} - Y_{00} - Y_{01}), \end{aligned} \tag{2.73}$$

and following the approximation to the normal derivatives in (2.52), we may write

$$\int_R^S \frac{\partial Z}{\partial z}\, dy = \left(\frac{\partial Z}{\partial z}\right)_D \frac{(h_0 + h_2)}{2} = \frac{(Z_{11} - Z_{10})}{k_0} \frac{h_s}{2}. \tag{2.74}$$

Similarly,

$$\int_P^Q \frac{\partial Y}{\partial y}\, dy = (Y)_Q - (Y)_P = \frac{1}{4}(Y_{01} + Y_{02} - Y_{21} - Y_{22}), \tag{2.75}$$

$$\int_P^Q \frac{\partial Z}{\partial z}\, dy = \frac{(Z_{12} - Z_{11})}{k_2} \left(-\frac{h_s}{2}\right). \tag{2.76}$$

By substituting expressions from (2.73) to (2.76) into (2.72), we obtain

$$\frac{2h_s k_s}{k_0 k_2} Z_{11} = \frac{2h_s}{k_2} Z_{12} + \frac{2h_s}{k_0} Z_{10} + (Y_{00} - Y_{20} - Y_{02} + Y_{22}). \tag{2.77}$$

Similarly, (2.71) gives

$$\frac{2h_s k_s}{h_0 h_2} Y_{11} = \frac{2k_s}{h_2} Y_{21} + \frac{2k_s}{h_0} Y_{01} + (Z_{00} - Z_{20} - Z_{02} + Z_{22}). \tag{2.78}$$

(2.77) and (2.78) are our new pair of equations for augmenting the diagonal terms of the cell-integral equation (2.56) and (2.60). The final equations we have used in the computer code are in the form of

Equation (2.56) + Equation (2.78)

Equation (2.60) + Equation (2.77)

which can be expressed explicitly as

$$\begin{aligned}
&(ic_0 + c_{10} + c_{12} + \frac{2h_s k_s}{h_0 h_2}) Y_{11} - (\bar{\rho}_{00} - \bar{\rho}_{20} - \bar{\rho}_{02} + \bar{\rho}_{22}) Z_{11} = \\
&\quad c_{10} Y_{10} + c_{12} Y_{12} + \frac{2k_s}{h_2} Y_{21} + \frac{2k_s}{h_0} Y_{01} \\
&+(1 - \bar{\rho}_{00}) Z_{00} - (1 - \bar{\rho}_{20}) Z_{20} - (1 - \bar{\rho}_{02}) Z_{02} + (1 - \bar{\rho}_{22}) Z_{22} \\
&+(\bar{\rho}_{02} - \bar{\rho}_{00}) Z_{01} - (\bar{\rho}_{22} - \bar{\rho}_{20}) Z_{21} - (\bar{\rho}_{20} - \bar{\rho}_{00}) Z_{10} + (\rho_{22} - \rho_{02}) Z_{12},
\end{aligned} \tag{2.79}$$

$$\begin{aligned}
&(ic_0 + c_{01} + c_{21} + \frac{2h_s k_s}{k_0 k_2}) Z_{11} - (\bar{\rho}_{00} - \bar{\rho}_{20} - \bar{\rho}_{02} + \bar{\rho}_{22}) Y_{11} = \\
&\quad c_{01} Z_{01} + c_{21} Z_{21} + \frac{2h_s}{k_2} Z_{12} + \frac{2h_s}{k_0} Z_{10} \\
&+(1 - \bar{\rho}_{00}) Y_{00} - (1 - \bar{\rho}_{20}) Y_{20} - (1 - \bar{\rho}_{02}) Y_{02} + (1 - \bar{\rho}_{22}) Y_{22} \\
&-(\bar{\rho}_{02} - \bar{\rho}_{00}) Y_{01} + (\bar{\rho}_{22} - \bar{\rho}_{20}) Y_{21} + (\bar{\rho}_{20} - \bar{\rho}_{00}) Y_{10} - (\bar{\rho}_{22} - \bar{\rho}_{02}) Y_{12}.
\end{aligned} \tag{2.80}$$

For model 2D-a, Fig. 2.11 shows that the new set of equations (2.79) and (2.80) give almost the same result as do (2.56) together with (2.60) modified by (2.66)

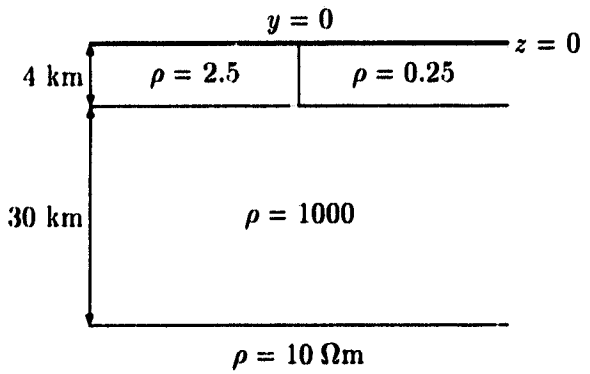


Figure 2.5: Model 2D-b, a two-dimensional model used for test calculations.

(Fig. 2.10). As a further check on the accuracy of our solution we have also computed the magnetic field inside the earth across the bottom surface of the vertically faulted slab at a depth of 70.25 km (see Fig. 2.2). The results are compared with those given by the program of Brewitt-Taylor and Weaver (1976) in Fig. 2.12, and once again excellent agreement is obtained.

For model 2D-b, although the combination of (2.56) with modified (2.60) failed to deliver an acceptable solution, the new pair of the equations (2.79) and (2.80) do bring good results as shown in Fig. 2.13. The graphs indicate that the solutions given by (2.79) and (2.80) (solid line) not only are stable but also are closer to those of Brewitt-Taylor and Weaver (broken line) compared with those calculated by using weighted average resistivities at the nodes (dotted line).

Finally, to confirm that the new formulae remain accurate even for those models that were not problematical when weighted resistivities were used, we have computed the magnetic response of the three-segment 'control model' shown in Fig. 2.6 for which a quasi-analytic solution is available (Weaver, LeQuang and Fischer, 1986). The perfectly conducting basement in the model was simulated in the finite difference program by assigning a sufficiently small numerical value for the resistivity in the region $z > d$. The variations of the two components across the surface $z = 0$ are seen to agree extremely well, for the

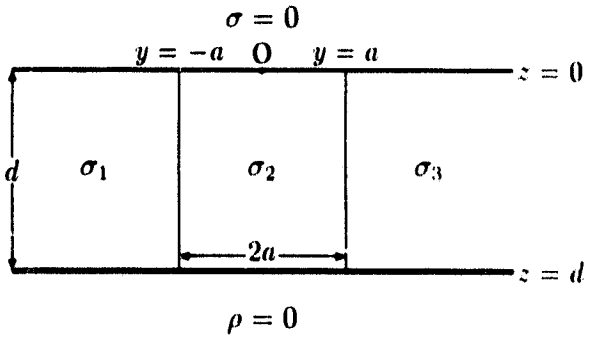


Figure 2.6: The three-segment control model of Weaver, LeQuang and Fischer (1986). The parameter values used in the numerical calculations were $\sigma_1 = 0.1$ S/m, $\sigma_2 = 1.0$ S/m, $\sigma_3 = 0.5$ S/m, $a = 10$ km and $d = 50$ km.

chosen period of 300 s, with the analytic solutions depicted by the broken line in Fig. 2.14.

To see why these two auxiliary equations (2.77) and (2.78) have successfully modified equations (2.56) and (2.60), let us take a close look at (2.80) which is the combination of (2.77) and (2.60). If we assume that the resistivity is uniform at node point O in Fig. 2.3, i.e. $\rho_{00} = \rho_{02} = \rho_{20} = \rho_{22} = \rho = \bar{\rho}$ in equation (2.80), then we obtain

$$(\frac{i\omega\mu_0 h_s k_s}{\rho} + \frac{2h_s k_s}{h_0 h_2} + \frac{2h_s k_s}{k_0 k_2})Z_{11} = \frac{2k_s}{h_0}Z_{01} + \frac{2k_s}{h_2}Z_{21} + \frac{2h_s}{k_2}Z_{12} + \frac{2h_s}{k_0}Z_{10}. \quad (2.81)$$

The effect of adding (2.77) to (2.60) is obvious, it not only strengthens the diagonal coefficient by $2h_s k_s/k_0 k_2$, but also weakens the influence exerted by the terms from the corner nodes, $Y_{00}, Y_{20}, Y_{02}$ and $Y_{22}$; in this special case when $\rho$ is uniform, the corner terms are completely cancelled out, while in general, these terms will be greatly reduced in importance.

If we divide (2.81) by $h_s k_s$ and rearrange its terms, then we have

$$\Big(\frac{2}{h_2 h_s}Z_{21} - \frac{2}{h_0 h_2}Z_{11} + \frac{2}{h_0 h_s}Z_{01}\Big) + \Big(\frac{2}{k_2 k_s}Z_{12} - \frac{2}{k_0 k_2}Z_{11} + \frac{2}{k_0 k_s}Z_{10}\Big) = \frac{i\omega\mu_0}{\rho}Z_{11}. \quad (2.82)$$

This is nothing else but the finite difference form of

$$\nabla^2 Z = \frac{i\omega\mu_0}{\rho} Z. \tag{2.83}$$

In the same way, (2.79) simplifies to the finite difference representation of

$$\nabla^2 Y = \frac{i\omega\mu_0}{\rho} Y. \tag{2.84}$$

Thus, at a node point in a uniform region, (2.83) and (2.84) merely state that

$$\nabla^2 \mathbf{B} = \frac{i\omega\mu_0}{\rho}\mathbf{B}, \quad \text{or} \quad \left(\frac{i\omega\mu_0}{\rho} - \nabla^2\right)\mathbf{B} = 0, \tag{2.85}$$

in accordance with what is required at a node point of uniform resistivity.

In fact, if we go back to equation (2.43), divide it by the averaged resistivity $\bar{\rho}$ and rewrite it as

$$\frac{1}{\bar{\rho}} \int\int_{\mathcal{A}} d\mathbf{S} \times [i\omega\mu_0\mathbf{B} + \boldsymbol{\nabla} \times (\rho \boldsymbol{\nabla} \times \mathbf{B})] = 0, \tag{2.86}$$

a well-known vector relation leads to

$$\frac{1}{\bar{\rho}} \int\int_{\mathcal{A}} d\mathbf{S} \times [i\omega\mu_0\mathbf{B} + (\boldsymbol{\nabla}\rho) \times (\boldsymbol{\nabla} \times \mathbf{B}) + \rho\boldsymbol{\nabla}(\boldsymbol{\nabla} \cdot \mathbf{B}) - \rho\nabla^2\mathbf{B}] = 0. \tag{2.87}$$

When the resistivity is uniform within $\mathcal{A}$, i.e. $\bar{\rho} = \rho$ and $\boldsymbol{\nabla}\rho = 0$, then the $(\boldsymbol{\nabla}\rho) \times (\boldsymbol{\nabla} \times \mathbf{B})$ term drops out, and the above equation becomes

$$\int\int_{\mathcal{A}} d\mathbf{S} \times [\frac{i\omega\mu_0}{\rho}\mathbf{B} - \nabla^2\mathbf{B}] + \int\int_{\mathcal{A}} d\mathbf{S} \times \boldsymbol{\nabla}(\boldsymbol{\nabla} \cdot \mathbf{B}) = 0. \tag{2.88}$$

Note that the integrand of the first integral on the L.H.S. of the above equation is the same as (2.85), and the second integral is the same as (2.68), i.e. the extra term we included to stabilize the cell-integral equations. Mathematically, the second integral is zero; it makes no difference if we keep or drop it. But when transforming (2.43) into (2.46), we have converted

$$\int\int_{\mathcal{A}} d\mathbf{S} \times \boldsymbol{\nabla} \times (\rho \boldsymbol{\nabla} \times \mathbf{B})$$

into

$$\oint_C d\mathbf{l} \times (\rho \boldsymbol{\nabla} \times \mathbf{B})$$

by (2.45); and the second integral in (2.88), i.e.

$$\int\int_A d\mathbf{S} \times \boldsymbol{\nabla}(\boldsymbol{\nabla} \cdot \mathbf{B})$$

has been implicitly included. It seems that the numerical effect of this term in the $\oint d\mathbf{l}$ form of equation (2.46) is to weaken the diagonal coefficients and increment some of the non-diagonal ones. We need to compensate its effect by applying its negative term to the equations. This is the significance of obtaining equation (2.80) by adding equation (2.77) into (2.60); it reduces (at grid points in a non-uniform region) or removes (at grid points in a uniform region) the relative influence of the term

$$\int\int_A d\mathbf{S} \times \boldsymbol{\nabla}(\boldsymbol{\nabla} \cdot \mathbf{B})$$

in equation (2.88).

The instability could also have been anticipated on physical grounds. The magnetic field $\mathbf{B} + \boldsymbol{\nabla}\phi$, where $\phi(\mathbf{r}, z)$ is an arbitrary scalar function, identically satisfies (2.46) when $\omega = 0$. Thus for small frequencies, the approximate solution for the magnetic field will be indeterminate (i.e. unstable) to the extent of the gradient of a scalar function $\phi$ which vanishes together with its derivatives on the surface $z = 0$ and at infinity in the region $z > 0$. Only by invoking condition $\boldsymbol{\nabla} \cdot \mathbf{B} = 0$ explicitly can we ensure that $\phi \equiv 0$, hence $\mathbf{B}$ determinate and stable.

## 2.7 E-polarization Problems

Since our 3D model can approach limiting 2D structures on the boundaries at infinity, both 2D E-polarization and B-polarization will be encountered. In Chapter 1, as shown in Fig. 1.2, we have assumed that the external stimulating

magnetic source field is in the $x$-direction only. Therefore, the E-polarization problems occur at $y = y_1$ and $y = y_M$ respectively. They are both in the $xz$-plane. However, in order to be consistent with the conventional coordinate frame for the E-polarization mode, in this chapter we have assumed the source field to be in the $y$-direction as shown in Fig. 2.1, so that the E-polarization would occur in the $yz$-plane and involve the fields already familiar to us, $E\hat{\mathbf{x}}$, $Y\hat{\mathbf{y}}$ and $Z\hat{\mathbf{z}}$. The equations obtained so far, therefore, have all been derived in the $yz$-plane with fields components $\mathbf{E} = (U, 0, 0)$ and $\mathbf{B} = (0, Y, Z)$. Now, in order to be consistent with the other parts of this thesis and the computer program, these equations have to be converted according to the configuration given by Fig. 1.2, i.e. they have to be transformed into the $xz$-plane with field components $\mathbf{E} = (0, V, 0)$ and $\mathbf{B} = (X, 0, Z)$. This can be done by rotating the coordinate frame for 90° clockwise about the $z$-axis. Consequently, $x$ and $X$ in the equations written in the old frame should be replaced by $-y$ and $-Y$ respectively in the new frame, while the old $y$ and $Y$ should be replaced by the new $x$ and $X$ repectively. The two equations needed for each node point are now the $X$-equation for the $x$-component and the $Z$-equation for the $z$-component. Above the thin sheet at $z = 0-$, equations (2.1) and (2.2) become

$$X(x,0-) = B_0 + \frac{1}{\pi} \int_{-\infty}^{\infty} \frac{Z(u,0-)}{x_\lambda - u}\, du, \tag{2.89}$$

$$Z(x,0-) = Z(x,0+); \tag{2.90}$$

Beneath the thin sheet at $z = 0+$, (2.10) and (2.12) give

$$X_{\lambda 1} = B_0 + \frac{1}{\pi} \int_{-\infty}^{\infty} \frac{Z(u,0--)}{x_\lambda - u}\, du + \tau_\lambda \rho_{\lambda \frac{1}{2}} [-(\frac{1}{k_1} + \frac{k_1}{2} i\alpha^2) X_{\lambda 1} + \frac{1}{k_1} X_{\lambda 2} + \frac{k_1}{2} (X_{xx})_{\lambda 1} - (Z_x)_{\lambda 1}] \tag{2.91}$$

and

$$A_x (X_{xx})_{\lambda 1} + (Z_{xx})_{\lambda 1} + \frac{2}{k_1} (X_x)_{\lambda 1} + \bar{\rho}_x (Z_x)_{\lambda 1}$$

$$= i\alpha^2 A_x X_{\lambda 1} + \frac{\bar{\rho}_x}{k_1}(X_{\lambda 2} - X_{\lambda 1}) + i\alpha^2 Z_{\lambda 1} - \frac{2}{k_1^2}(Z_{\lambda 2} - Z_{\lambda 1}) \qquad (2.92)$$

where $A_x = -\frac{1}{2}k_1\bar{\rho}_x$, $\bar{\rho}_x = [(\partial\rho/\partial x)/\rho]_{\lambda\frac{1}{2}}$, $\alpha^2 = \omega\mu_0/\rho_{\lambda\frac{1}{2}}$.

The equations applied to region $0+ \leq z \leq z_N$, i.e. GDE, will be directly obtained from of the finite difference form of cell-integral equations given by (2.79) and (2.80).

For the bottom boundary condition at $z = z_N = d$, the counterpart of (2.24) in the $xz$-plane is

$$F'(x,d+) + \alpha_0\sqrt{i}F(x,d+) = \frac{\alpha_0\sqrt{i}}{\pi}\int_{-\infty}^{\infty}[F(u,d+) - F(x,d+)]\frac{k_1(|x-u|\alpha_0\sqrt{i})}{|x-u|}du. \qquad (2.93)$$

Both $X$- and $Z$-equations are to be obtained from this equation by substituting $F$ with $X$ and $Z$ respectively. But the equations will be given at $z = d+$, they have to be related to be at $z = d-$. With $Y \equiv 0$, $\partial/\partial y \equiv 0$ and $\mathbf{r} = x\hat{\mathbf{x}}$, equations (1.79) and (1.81) yield

$$X(x,d+) = X(x,d-) = X(x,d),\ Z(x,d+) = Z(x,d-) = Z(x,d), \qquad (2.94)$$

$$Z'(x,d+) = Z'(x,d-) = Z'(x,d); \qquad (2.95)$$

equation (1.84) provides the relation between $X'(x,d+)$ and $X'(x,d-)$ as follows:

$$X'(x,d+) = R_\rho X'(x,d-) + (1 - R_\rho)Z_x(x,d),\ R_\rho = \rho(x,d-)/\rho_0; \qquad (2.96)$$

and from (1.74) and (1.78), we have $X'(x,d-)$ and $Z'(x,d)$ respectively as

$$X'(x,d-) = \frac{X_N - X_{N-1}}{k_{N-1}} - \frac{k_{N-1}}{2}(-i\alpha^2 X_N + X_{xx}), \qquad (2.97)$$

$$Z'(x,d) = \frac{Z_N - Z_{N-1}}{k_{N-1}} - \frac{k_{N-1}}{2}(-i\alpha^2 Z_N + Z_{xx} + \rho_x Z_x) + \frac{\bar{\rho}_x}{2}(X_N - X_{N-1}). \qquad (2.98)$$

Thus, we have the equations of the bottom boundary condition for the 2D E-polarization mode at $z = d-$ as

$$R_\rho X'(x,d-) + (1-R_\rho)Z_x(x,d) + \alpha_0\sqrt{i}X(x,d) = \frac{\alpha_0\sqrt{i}}{\pi}\int_{-\infty}^{\infty}[X(u,d)-X(x,d)]\frac{K_1(|x-u|\alpha_0\sqrt{i})}{|x-u|}\,du \qquad (2.99)$$

and

$$Z'(x,d) + \alpha_0\sqrt{i}Z(x,d) = \frac{\alpha_0\sqrt{i}}{\pi}\int_{-\infty}^{\infty}[Z(u,d)-Z(x,d)]\frac{K_1(|x-u|\alpha_0\sqrt{i})}{|x-u|}\,du. \qquad (2.100)$$

The other two alternative $Z$-equations for the bottom boundary conditions at $z = d$, given by (2.28) and (2.33), are converted as follows:

$$Z(x,d) = \frac{\alpha_0}{\sqrt{i}}\int_{-\infty}^{\infty}\mathrm{sgn}\,(u-x)X(u,d)K_1(\alpha_0\sqrt{i}|u-x|)\,du \qquad (2.101)$$

and

$$Z_{xx} + \bar{\rho}_x(Z_x - X') - \frac{2}{k_{N-1}}X_x = \left(\frac{2}{k_{N-1}^2} + i\alpha^2\right)Z_N - \frac{2}{k_{N-1}^2}Z_{N-1} \qquad (2.102)$$

where $X' = X'(x,d-)$ and is given by (2.97).

## 2.8 Finite Difference Equations for E-polarization

The equations listed above for the 2D E-polarization problems are now cast into finite difference form. At $z = 0-$, where $k = 0$, equations (2.89) and (2.90) yield

$$X_{\lambda 0} = B_0 - \frac{1}{\pi}\sum_{l=1}^{L}H_{\lambda l}Z_{l0} \qquad (2.103)$$

$$Z_{\lambda 0} = Z_{\lambda 1} \qquad \lambda = 2,...,L-1 \qquad (2.104)$$

where $H_{\lambda l}$ are the coefficients of the Hilbert transform and are derived in Appendix B.

At $z = 0+$, where $k = 1$, $\lambda = 2...L-1$, equations (2.91) and (2.92) become

$$\left[\left(\frac{1}{g_{\lambda-1}g_\lambda}+\frac{1}{k_1^2}+\frac{1}{2}i\alpha^2\right)k_1\tau_\lambda\rho_{\lambda\frac{1}{2}}+1\right]X_{\lambda 1}=B_0-\frac{1}{\pi}\sum_{l=1}^{L}H_{\lambda l}Z_{l1}$$
$$+\tau_\lambda\rho_{\lambda\frac{1}{2}}\left(\frac{k_1}{g_\lambda g_\lambda^+}X_{\lambda+1\,1}+\frac{k_1}{g_{\lambda-1}g_\lambda^+}X_{\lambda-1\,1}+\frac{1}{k_1}X_{\lambda 2}\right)$$
$$-\tau_\lambda\rho_{\lambda\frac{1}{2}}\left(\frac{g_{\lambda-1}}{g_\lambda g_\lambda^+}Z_{\lambda+1\,1}+\frac{g_\lambda^-}{g_{\lambda-1}g_\lambda}Z_{\lambda 1}-\frac{g_\lambda}{g_{\lambda-1}g_\lambda^+}Z_{\lambda-1\,1}\right)$$
$$\lambda=2...L-1. \qquad (2.105)$$

and

$$\left(\frac{2-\bar\rho_x g_\lambda^-}{g_{\lambda-1}g_\lambda}+\frac{2}{k_1^2}+i\alpha^2\right)Z_{\lambda 1}=\frac{2+\rho_x g_{\lambda-1}}{g_\lambda g_\lambda^+}Z_{\lambda+1\,1}+\frac{2-\rho_x g_\lambda}{g_{\lambda-1}g_\lambda^+}Z_{\lambda-1\,1}+\frac{2}{k_1^2}Z_{\lambda 2}$$
$$+\frac{2}{g_\lambda g_\lambda^+}\left(A_x+\frac{g_{\lambda-1}}{k_1}\right)X_{\lambda+1\,1}+\frac{2}{g_{\lambda-1}g_\lambda^+}\left(A_x-\frac{g_\lambda}{k_1}\right)X_{\lambda-1\,1}-\frac{\rho_x}{k_1}X_{\lambda 2}$$
$$+\left[\frac{2}{g_{\lambda-1}g_\lambda}\left(A_x-\frac{g_\lambda^-}{k_1}\right)-\frac{\bar\rho_x}{k_1}+i\alpha^2A_x\right]X_{\lambda 1}$$
$$\lambda=2...L-1. \qquad (2.106)$$

where $\alpha^2=\omega\mu_0/\rho_{\lambda,\frac{1}{2}}$, $A_x=-\frac{1}{2}k_1(\bar\rho_x)_{\lambda\frac{1}{2}}$, $g_\lambda^-=g_\lambda-g_{\lambda-1}$, $g_\lambda^+=g_\lambda+g_{\lambda-1}$.

In the region $k_1\le z\le Z_{N-1}$, where $\lambda=2,...,L-1$, $\mu=2,...,N-1$, equations (2.79) and (2.80) are both in the local coordinate system and can be converted into the $xz$-plane as follows:

$$(ic_0+c_{10}+c_{12}+\frac{2g_sk_s}{g_0g_2})X_{11}-(\bar\rho_{00}-\rho_{20}-\rho_{02}+\rho_{22})Z_{11}=$$
$$c_{10}X_{10}+c_{12}X_{12}+\frac{2k_s}{g_2}X_{21}+\frac{2k_s}{g_0}X_{01}$$
$$+(1-\bar\rho_{00})Z_{00}-(1-\bar\rho_{20})Z_{20}-(1-\rho_{02})Z_{02}+(1-\rho_{22})Z_{22}$$
$$+(\bar\rho_{02}-\bar\rho_{00})Z_{01}-(\bar\rho_{22}-\bar\rho_{20})Z_{21}-(\bar\rho_{20}-\rho_{00})Z_{10}+(\rho_{22}-\rho_{02})Z_{12}, \qquad (2.107)$$

and

$$(ic_0+c_{01}+c_{21}+\frac{2g_sk_s}{k_0k_2})Z_{11}-(\bar\rho_{00}-\rho_{20}-\rho_{02}+\rho_{22})X_{11}=$$

$$
\begin{aligned}
&c_{01}Z_{01} + c_{21}Z_{21} + \frac{2g_s}{k_2}Z_{12} + \frac{2g_s}{k_0}Z_{10} \\
&+(1-\bar{\rho}_{00})X_{00} - (1-\bar{\rho}_{20})X_{20} - (1-\bar{\rho}_{02})X_{02} + (1-\bar{\rho}_{22})X_{22} \\
&-(\bar{\rho}_{02}-\bar{\rho}_{00})X_{01} + (\bar{\rho}_{22}-\bar{\rho}_{20})X_{21} + (\bar{\rho}_{20}-\bar{\rho}_{00})X_{10} - (\bar{\rho}_{22}-\bar{\rho}_{02})X_{12},
\end{aligned}
\tag{2.108}
$$

where

$$
\begin{aligned}
\bar{\rho}_{p,q} &= \rho_{p,q}/\bar{\rho},\ (p=0,2;\ q=0,2), \\
\bar{\rho} &= \frac{g_0k_0\rho_{00} + g_2k_0\rho_{20} + g_0k_2\rho_{02} + g_2k_2\rho_{22}}{(g_0+h_2)(k_0+k_2)},
\end{aligned}
\tag{2.109}
$$

and

$$
c_0 = \frac{\omega\mu_0}{\bar{\rho}}(g_0+g_2)(k_0+k_2) = \alpha^2 g_s k_s, \tag{2.110}
$$

$$
c_{10} = \frac{2}{k_0}(\bar{\rho}_{00}g_0 + \bar{\rho}_{20}g_2) = \frac{2g_s}{k_0}\bar{\rho}_{10},\ c_{12} = \frac{2}{k_2}(\bar{\rho}_{02}g_0 + \bar{\rho}_{22}g_2) = \frac{2g_s}{k_2}\bar{\rho}_{12}, \tag{2.111}
$$

$$
g_0 = g_{\lambda-1},\ g_2 = g_\lambda,\ g_s = g_0+g_2,\ k_0 = k_{\mu-1},\ k_2 = k_\mu,\ k_s = k_0+k_2.
$$

At $z = z_N = d$, the finite difference forms of (2.99) and (2.100) are

$$
\begin{aligned}
&\left[R_\rho k_{N-1}\left(\frac{1}{{k_{N-1}}^2} + i\alpha^2 + \frac{1}{g_{\lambda-1}g_\lambda}\right) + \alpha_0\sqrt{i} + S\right]X_{\lambda N} = \sum_{l=1}^{L} C_{\lambda l}X_{lN} \\
&\quad + R_\rho k_{N-1}\left(\frac{1}{g_\lambda g_\lambda^+}X_{\lambda+1N} + \frac{1}{g_{\lambda-1}g_\lambda^+}X_{\lambda-1N} + \frac{1}{{k_{N-1}}^2}X_{\lambda N-1}\right) \\
&\quad -(1-R_\rho)\left(\frac{g_{\lambda-1}}{g_\lambda g_\lambda^+}Z_{\lambda+1N} + \frac{g_\lambda^-}{g_{\lambda-1}g_\lambda}Z_{\lambda N} - \frac{g_{\lambda+1}}{g_{\lambda-1}g_\lambda^+}Z_{\lambda-1N}\right)
\end{aligned}
\tag{2.112}
$$

and

$$
\begin{aligned}
&\left[k_{N-1}\left(\frac{1}{{k_{N-1}}^2} + \frac{1}{2}\left(i\alpha^2 + \frac{2-\bar{\rho}_x g_\lambda^-}{g_{\lambda-1}g_\lambda}\right)\right) + \alpha_0\sqrt{i} + S\right]Z_{\lambda N} = \sum_{l=1}^{L} C_{\lambda l}Z_{lN} \\
&\quad + \frac{k_{N-1}}{2}\left(\frac{2+\bar{\rho}_x g_{\lambda-1}}{g_\lambda g_\lambda^+}Z_{\lambda+1N} + \frac{2-\bar{\rho}_x g_\lambda}{g_{\lambda-1}g_\lambda^+}Z_{\lambda-1N} + \frac{2}{{k_{N-1}}^2}Z_{\lambda N-1}\right) \\
&\quad -\frac{1}{2}\bar{\rho}_x(X_{\lambda N} - X_{\lambda N-1}) \\
&\qquad\qquad \lambda = 2 \ldots L-1.
\end{aligned}
\tag{2.113}
$$

where $\alpha^2 = \omega\mu_0/\rho_{\lambda N-\frac{1}{2}}$, $\bar{\rho}_x = [(\partial\rho/\partial x)/\rho]_{\lambda N-\frac{1}{2}}$, $\alpha_0^2 = \omega\mu_0/\rho_0$, $g_\lambda^- = g_\lambda - g_{\lambda-1}$ and $g_\lambda^+ = g_\lambda + g_{\lambda-1}$, while $C_{\lambda l}$ and $S$ are given by (B.44) and (B.47) respectively in Appendix B.

The alternative $Z$-equations (2.101) and (2.102) lead to

$$Z_{\lambda N} = \frac{\alpha_0}{\sqrt{i}} \sum_{l=1}^{L} D_{\lambda l} X_{l N} \tag{2.114}$$

and

$$\begin{aligned}
&\left[\frac{2}{k_{N-1}} + k_{N-1}\left(i\alpha^2 + \frac{2-\bar{\rho}_x g_\lambda^-}{g_{\lambda-1}g_\lambda}\right)\right] = \\
&\quad k_{N-1}\left[\frac{2+\bar{\rho}_x g_{\lambda-1}}{g_\lambda g_\lambda^+} Z_{\lambda+1\,N} + \frac{2-\bar{\rho}_x g_\lambda}{g_{\lambda-1}g_\lambda^+} Z_{\lambda-1\,N}\right] + \frac{2}{k_{N-1}} Z_{\lambda\,N-1} \\
&\quad + \frac{\bar{\rho}_x k_{N-1}^2 - 2g_{\lambda-1}}{g_\lambda g_\lambda^+} X_{\lambda+1\,N} + \frac{\bar{\rho}_x k_{N-1}^2 + 2g_\lambda}{g_{\lambda-1}g_\lambda^+} X_{\lambda-1\,N} + \bar{\rho}_x X_{\lambda\,N-1} \\
&\quad - \left[\left(\bar{\rho}_x + \frac{2g_\lambda^-}{g_{\lambda-1}g_\lambda}\right) + \bar{\rho}_x k_{N-1}^2\left(\frac{1}{g_{\lambda-1}g_\lambda} + i\alpha^2\right)\right] X_{\lambda N}
\end{aligned} \tag{2.115}$$

where $D_{\lambda l}$ can be derived similarly to $C_{\lambda l}$.

## 2.9 B-polarization Problems

According to Fig. 1.2, the B-polarization problems occur at $x = x_1$ and $x = x_L$ respectively. They are both in the $yz$-plane. The conductivity structure is uniform in the $x$-direction; therefore the derivatives with respect to $x$ are all zero. The only non-vanishing magnetic component in B-polarization is $X(y, z)$.

The upper surface, $z = 0-$, of the thin sheet is the boundary between the conductive earth and the non-conductive air layer. It is well known that on this boundary, for the B-polarization problem, the magnetic field is constant; its intensity is the same as that above a 1D structure for the same source, and it is called normal field. It is denoted by $B_0$ in this thesis. Therefore, we have

$$X_0 = B_0, \tag{2.116}$$

where we have defined $X_0 := X(y, 0-)$. Similarly, we also define $X_1 := X(y, 0+)$, $X_1' := X'(y, 0+)$ and $X_2 := X(y, k_1)$. Keeping in mind that $Y \equiv 0$, $Z \equiv 0$, $\partial/\partial x \equiv 0$ and $\partial^2/\partial x^2 \equiv 0$, we see that beneath the thin sheet at $z = 0+$, equation (1.53) links the component across the thin sheet according to the relation

$$X_1 - X_0 = \tau\rho^+ X_1'. \tag{2.117}$$

The expression of the derivative $X_1'$ has been derived in Chapter 1 for a gereral 3D case given by (1.69); the 2D form of $X_1'$ can be obtained by simplifing from (1.69), so that

$$X_1' = \frac{X_2 - X_1}{k_1} + \frac{k_1}{2}[-i\alpha^2 X_1 + X_{yy} + X_y\bar{\rho}_y]. \tag{2.118}$$

We therefore obtain for the equation at $z = 0+$

$$\left[1 + \frac{\tau\rho^+}{k_1} + \frac{1}{2}i\alpha^2\tau\rho^+ k_1\right] X_1 = B_0 + \frac{\tau\rho^+}{k_1}X_2 + \frac{\tau\rho^+ k_1}{2}[X_{yy} + \bar{\rho}_y X_y]. \tag{2.119}$$

In the region $z_1 \le z \le z_{N-1}$ , i.e. at nodes $k = 2, ..., N-1$, the ordinary equation for a standard B-polarization problem is used. It is the basic equation for magnetic field which comes from (1.29) as

$$X_{yy} + X_{zz} + X_z\bar{\rho}_z + X_y\bar{\rho}_y = i\alpha^2 X. \tag{2.120}$$

On the bottom boundary, at $z = d$, equation (2.24) provides the $X$-equation with $F$ substituted by $X$, i.e.

$$X'(y, d+) + \alpha_0\sqrt{i}X(y, d+) =$$
$$\frac{\alpha_0\sqrt{i}}{\pi}\int_{-\infty}^{\infty}[X(v, d+) - X(y, d+)]\frac{k_1(|y - v|\alpha_0\sqrt{i})}{|y - v|}\,dv. \tag{2.121}$$

Since we have $Z_x \equiv 0$, equation (1.84) yield $X'(y, d+) = R_\rho X'(y, d-)$. Take into consideration that $X$ is continuous across the boundary, we can also write the above equation as

$$R_\rho X'(y, d-) + \alpha_0\sqrt{i}X(y, d) =$$
$$\frac{\alpha_0\sqrt{i}}{\pi}\int_{-\infty}^{\infty}[X(v, d) - X(y, d)]\frac{k_1(|y - v|\alpha_0\sqrt{i})}{|y - v|}\,dv, \tag{2.122}$$

where $X'(y,d-)$ can be obtained by simplifing from its 3D form (1.74) as

$$X'(y,d-) = \frac{X_N - X_{N-1}}{k_{N-1}} - \frac{k_{N-1}}{2}[-i\alpha^2 X_N + X_{yy} + X_y\bar{\rho}_y]. \qquad (2.123)$$

## 2.10 Finite Difference Equations for B-polarization

The corresponding finite difference forms of the equations of the previous section are as follows:

at $z = 0-$,

$$X_{m0} = B_0 \qquad m = 1,...,M, \quad n = 0; \qquad (2.124)$$

at $z = 0+$,

$$\left[1 + T\left(\frac{2}{k_1^2} + \frac{2 - \bar{\rho}_y h_m^-}{h_{m-1}h_m^+} + i\alpha^2_{m\frac{1}{2}}\right)\right] X_{m1} =$$
$$B_0 + T\left(\frac{2 + \bar{\rho}_y h_{m-1}}{h_m h_m^+} X_{m+11} + \frac{2 - \bar{\rho}_y h_m}{h_{m-1}h_m^+} X_{m-11} + \frac{2}{k_1^2} X_{m2}\right),$$
$$m = 2...M-1, \; n = 1 \qquad (2.125)$$

where

$$T = \frac{1}{2}\tau_m \rho_{m\frac{1}{2}} k_1, \; \bar{\rho}_y = [(\partial\rho/\partial y)/\rho]_{m\frac{1}{2}}, \alpha^2_{m\frac{1}{2}} = \omega\mu_0/\rho_{m\frac{1}{2}},$$
$$h_m^- = h_m - h_{m-1}, \; h_m^+ = h_m + h_{m-1};$$

in the region $z_1 \le z \le z_{N-1}$,

$$\left(i\alpha^2_{mn} + \frac{2 - \bar{\rho}_y h_m^-}{h_{m-1}h_m} + \frac{2 - \bar{\rho}_z k_n^-}{k_{n-1}k_n}\right) X_{mn} = \frac{2 + \bar{\rho}_y h_{m-1}}{h_m h_m^+} X_{m+1n}$$
$$+ \frac{2 - \bar{\rho}_y h_m}{h_{m-1}h_m^+} X_{m-1n} + \frac{2 + \bar{\rho}_z k_{n-1}}{k_n k_n^+} X_{mn+1} + \frac{2 - \bar{\rho}_z k_n}{k_{n-1}k_n^+} X_{mn-1},$$
$$m = 2...M-1, \; n = 2...N-1 \qquad (2.126)$$

where

$$\alpha^2_{mn} = \omega\mu_0/\rho_{mn};$$

at $z = d$,

$$\left[\frac{R_\rho k_{N-1}}{2}\left(\frac{2}{{k_{N-1}}^2} + i\alpha_{mN-\frac{1}{2}} + \frac{2-\bar{\rho}_y h_m^-}{h_{m-1}h_m}\right) + \alpha_0\sqrt{i}(1+S/\pi)\right] X_{mN} =$$
$$\frac{R_\rho k_{N-1}}{2}\frac{(2+\bar{\rho}_y h_{m-1})}{h_m h_m^+} X_{m+1N} + \frac{R_\rho k_{N-1}}{2}\frac{(2-\bar{o}_y h_m)}{h_{m-1}h_m^+} X_{m-1N}$$
$$+\frac{R_\rho}{k_{N-1}} X_{mN-1} + \sum_{j=1}^{M} C_{mj} X_{jN}$$
$$m = 2...M-1,\ n = N \qquad (2.127)$$

where

$$R_\rho = \rho_{mN-\frac{1}{2}}/\rho_0$$

and $C_{mj}$, $S$ are given in Appendix B.

## 2.11 Numerical Results of the 2D EM Modelling

Graphs of 2D E-polarization numerical results of the models 2D-a (Fig. 2.2), 2D-b (Fig. 2.5) and the three-segments control model (Fig. 2.6) are presented here. Fig. 2.7 to 2.12 are for model 2D-a; Fig. 2.13 is for model 2D-b; and Fig. 2.14 is for the control model.

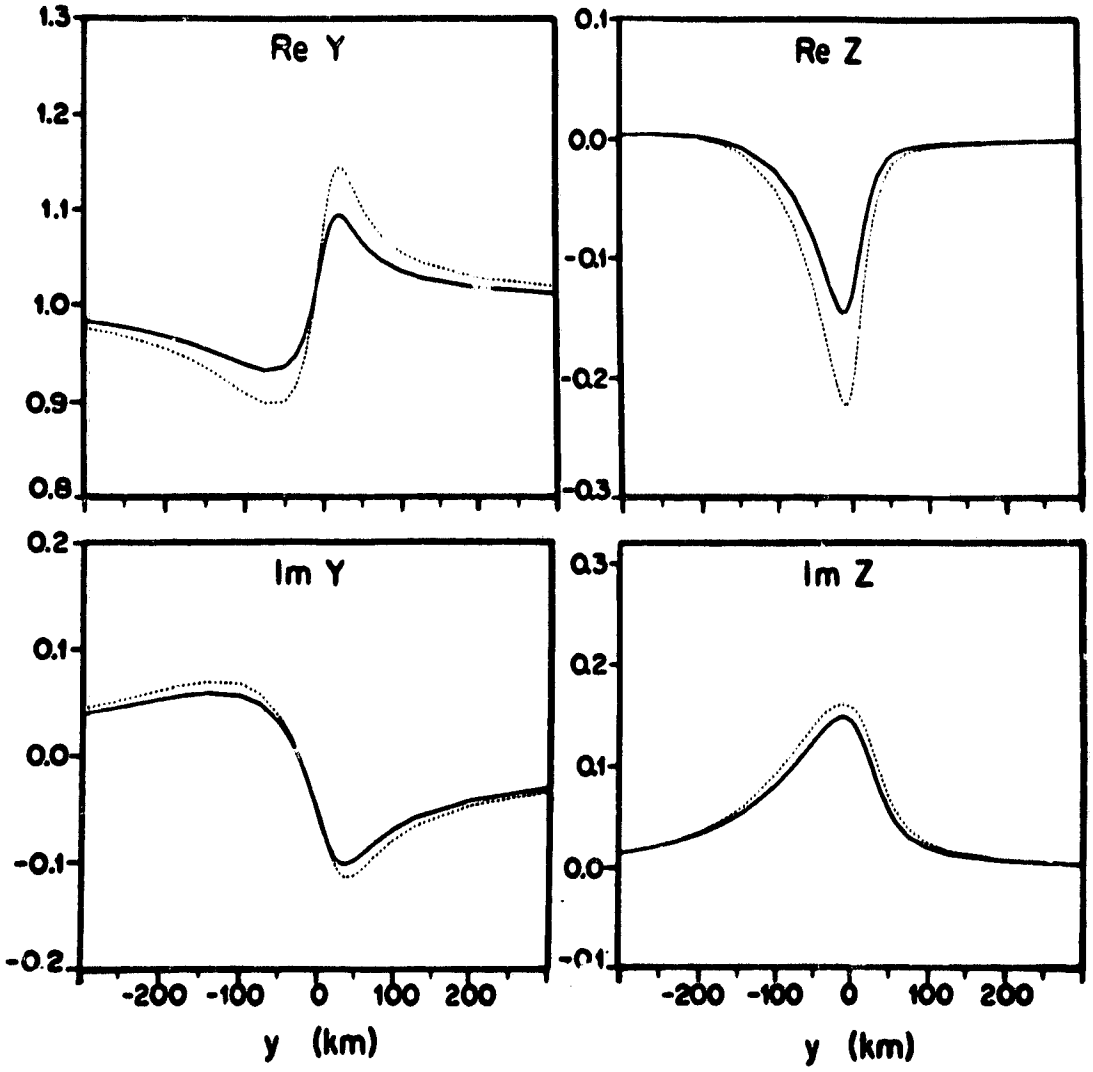


Figure 2.7: Real and imaginary parts of the magnetic components $Y$ and $Z$ on the surface $z = 0$ of the model shown in Fig. 2.2. The solid line graphs represent the variation of the magnetic field calculated directly by the finite difference method using weighted average *resistivities* at the nodes; the broken line graphs depict the same variations as obtained by numerical differentiation of the electric field calculated with the finite difference program of Brewitt-Taylor and Weaver (1976) in which weighted average *conductivities* are assigned to the nodes. The period of the source field is 1000 s. Both $Y$ and $Z$ are normalized by $B_0$.

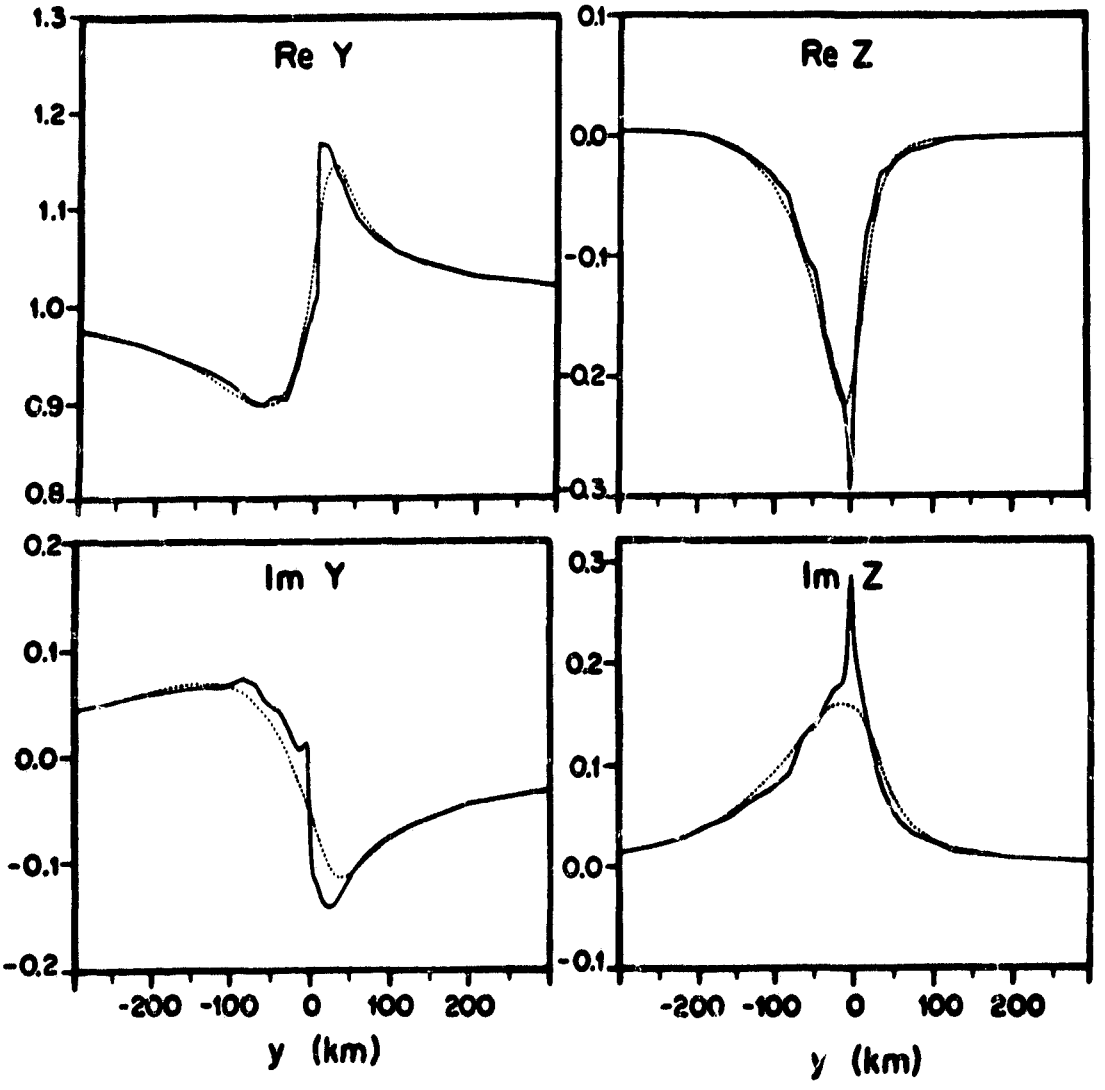


Figure 2.8: The same variations as in Fig. 2.7 but with the solid line now depicting the (numerically unstable) field variations generated by formulae (2.56) and (2.60) via the method of direct solution. Both $Y$ and $Z$ are normalized by $B_0$.

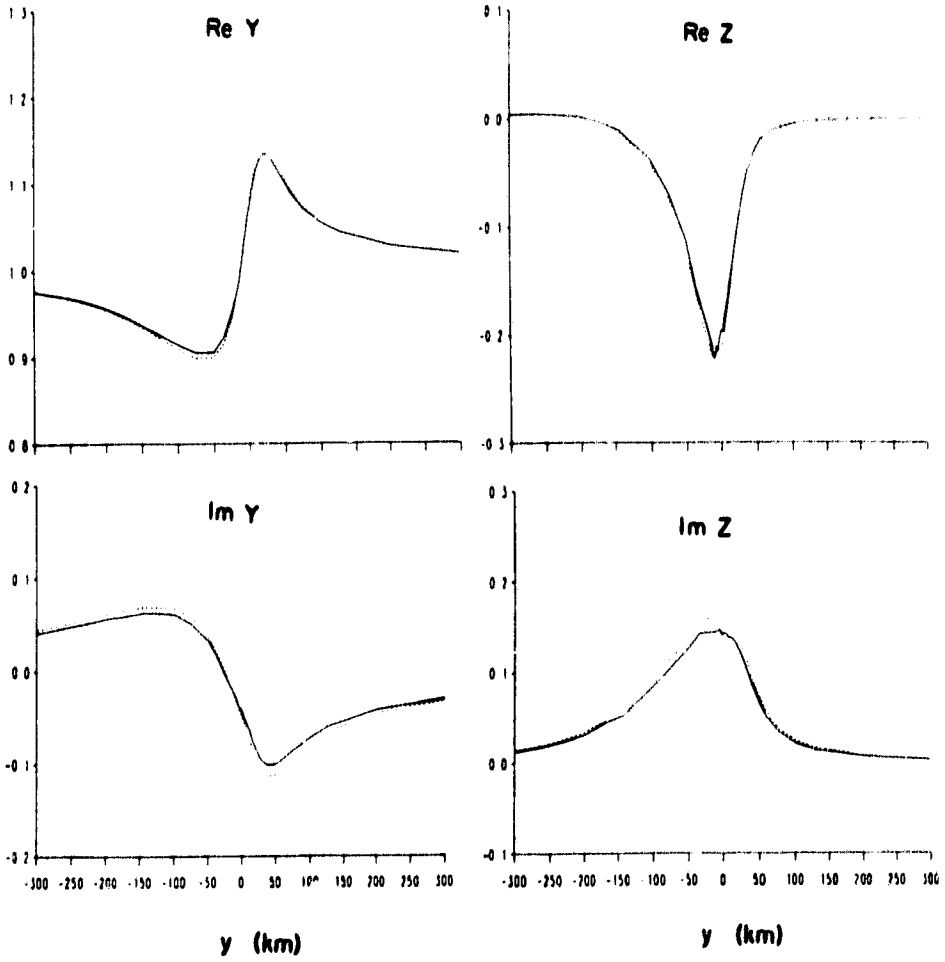


Figure 2.9: The same as Fig. 2.8 but with the solid line now depicting the improved field variations generated by formulae (2.56) and modified (2.60), where (2.60) is modified by including (2.64) so that the diagonal terms can be strengthened. Both $Y$ and $Z$ are normalized by $B_0$.

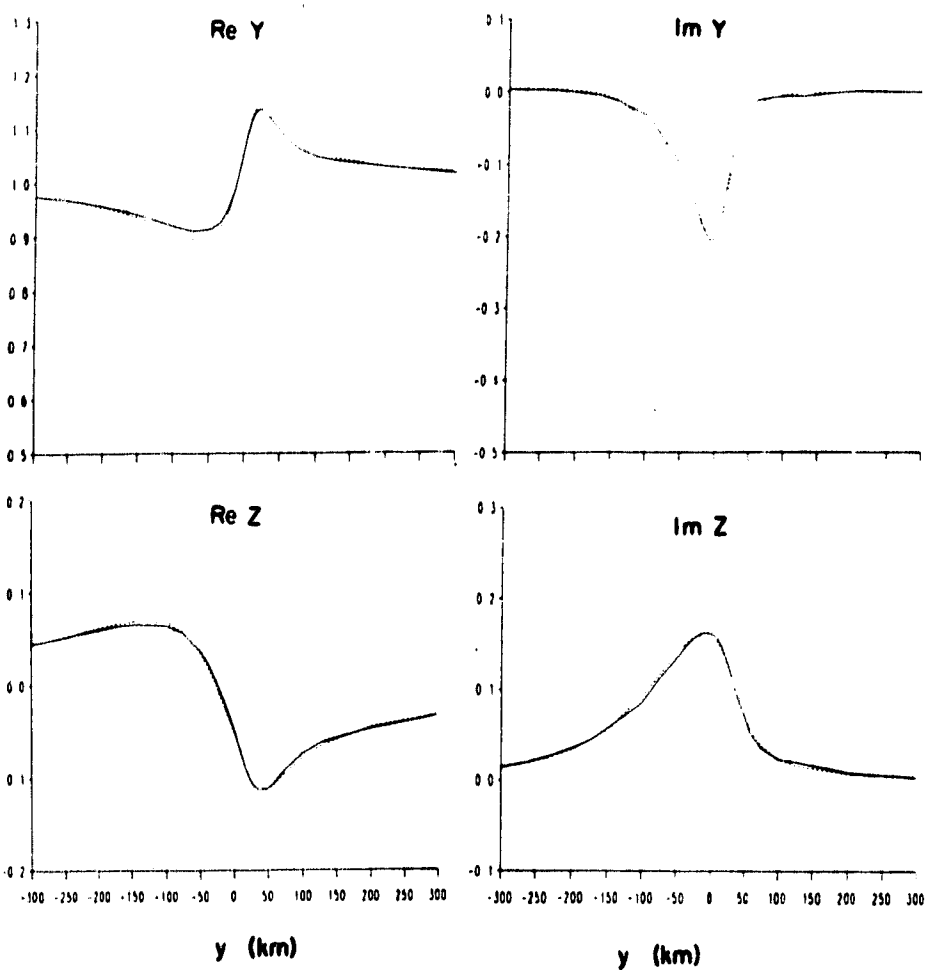


Figure 2.10: Same as Fig. 2.9 but formula (2.60) is now modified by including (2.66) rather than (2.64). Both $Y$ and $Z$ are normalized by $B_0$.

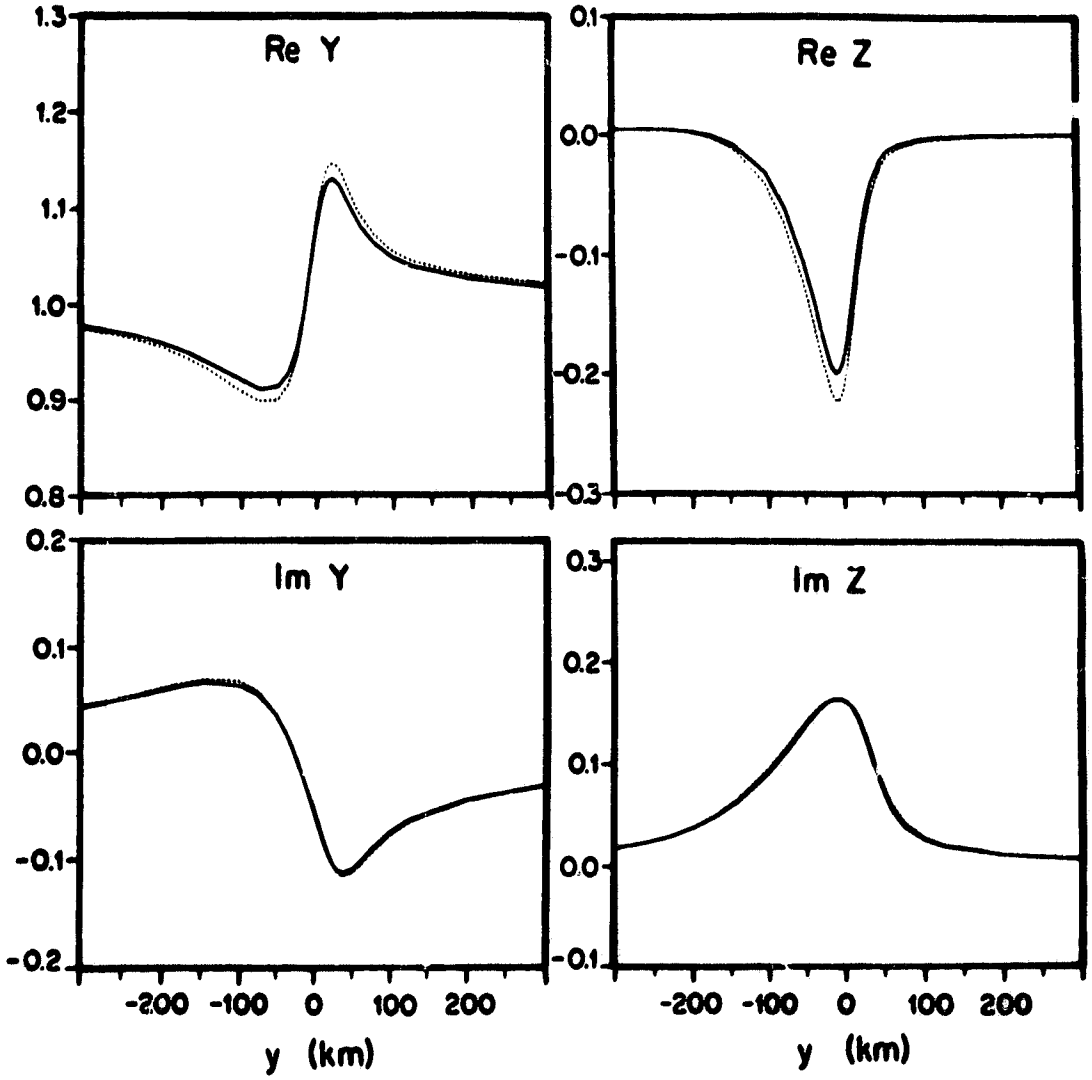


Figure 2.11: The same as Figures 2.7 to 2.9 except that the solid line now represents the magnetic field components generated by the new finite difference formulae (2.79) and (2.80). Both $Y$ and $Z$ are normalized by $B_0$.

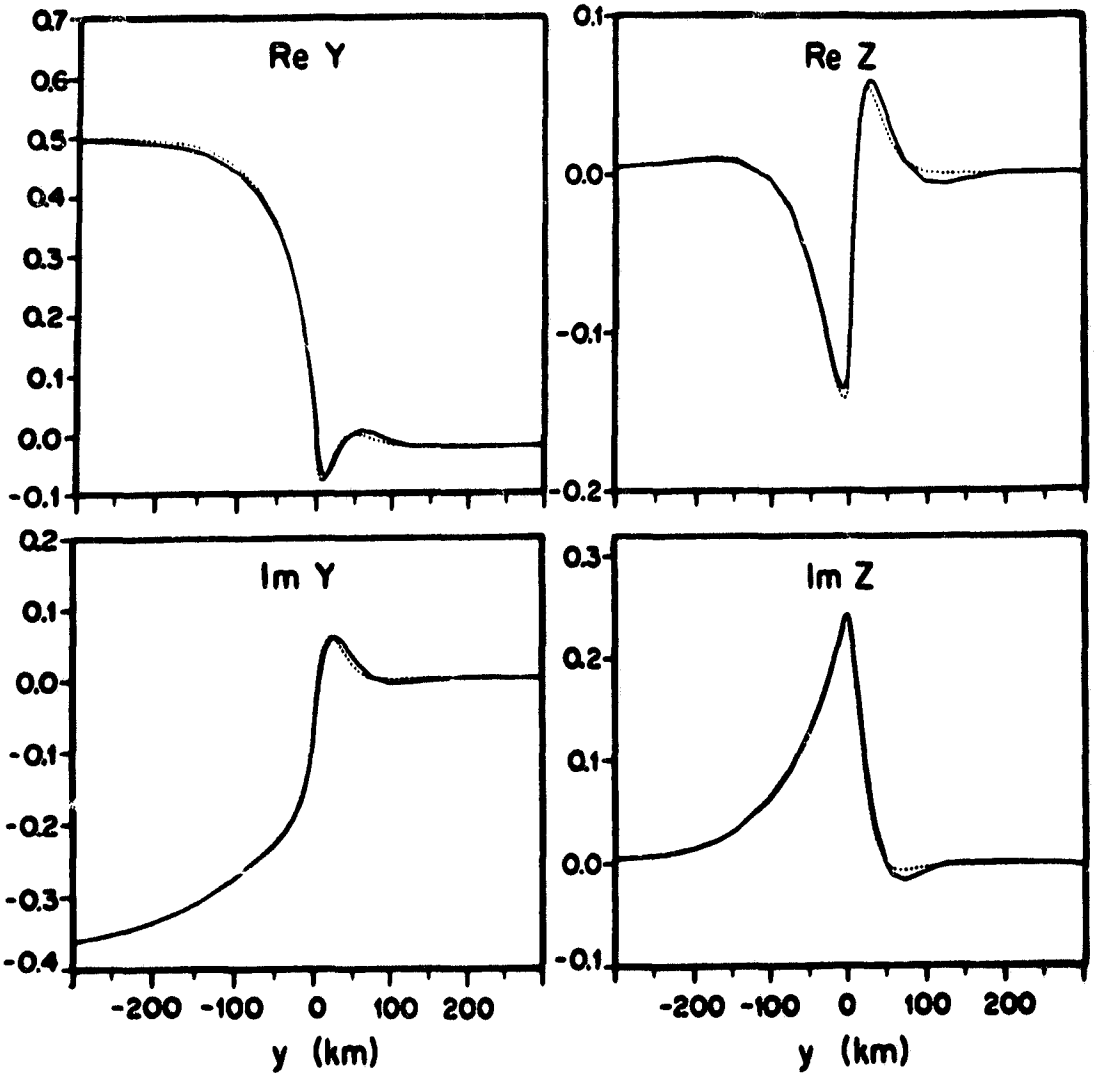


Figure 2.12: As in Fig. 2.11 but for the magnetic field on the bottom surface of the anomalous slab at depth 70.25 km in Fig. 2.2. Both $Y$ and $Z$ are normalized by $B_0$.

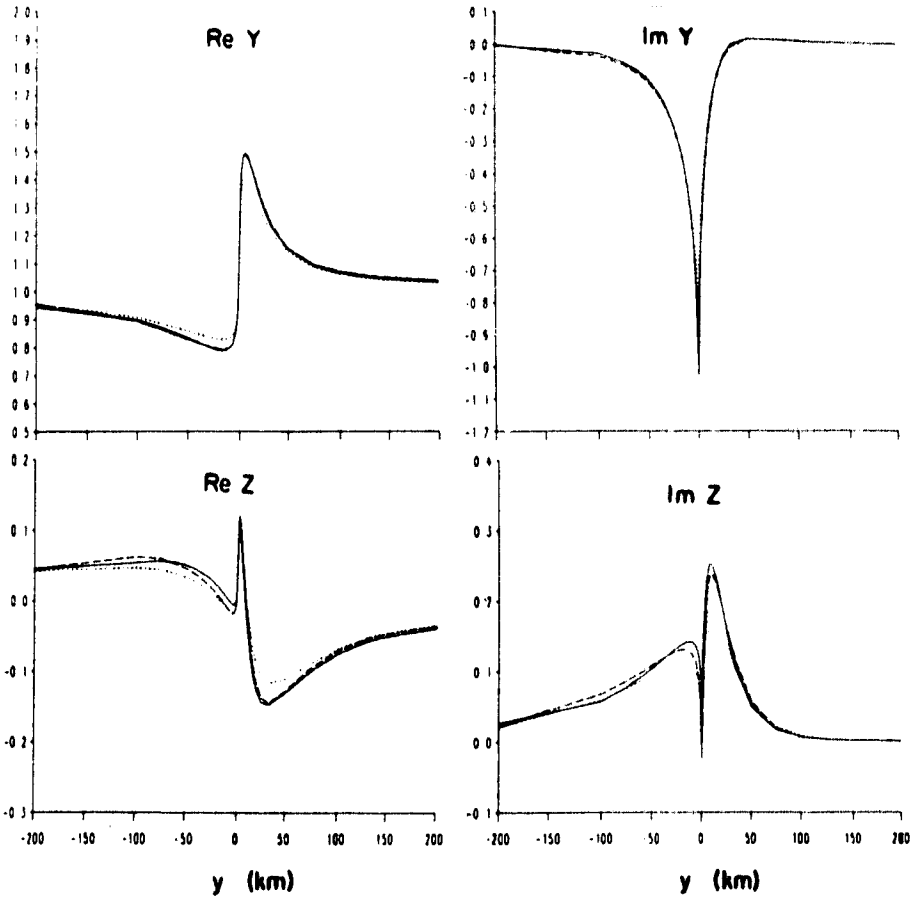


Figure 2.13: All the three lines (solid, broken and dotted) depict the same variations of $Y$ and $Z$ (normalized by $B_0$) on the surface $z = 0$ of test model, 2D-b, as shown in Fig. 2.5. The solid line graphs are given by (2.79) and (2.80), the new finite difference equations obtained via cell-integral approach; the dotted line graphs are calculated directly by the finite difference method using weighted average *resistivities* at the nodes; the broken line graphs are calculated by the program of Brewitt-Taylor and Weaver (1976) in which weighted average *conductivities* are assigned to the nodes. The period of the source field is 1000 s.

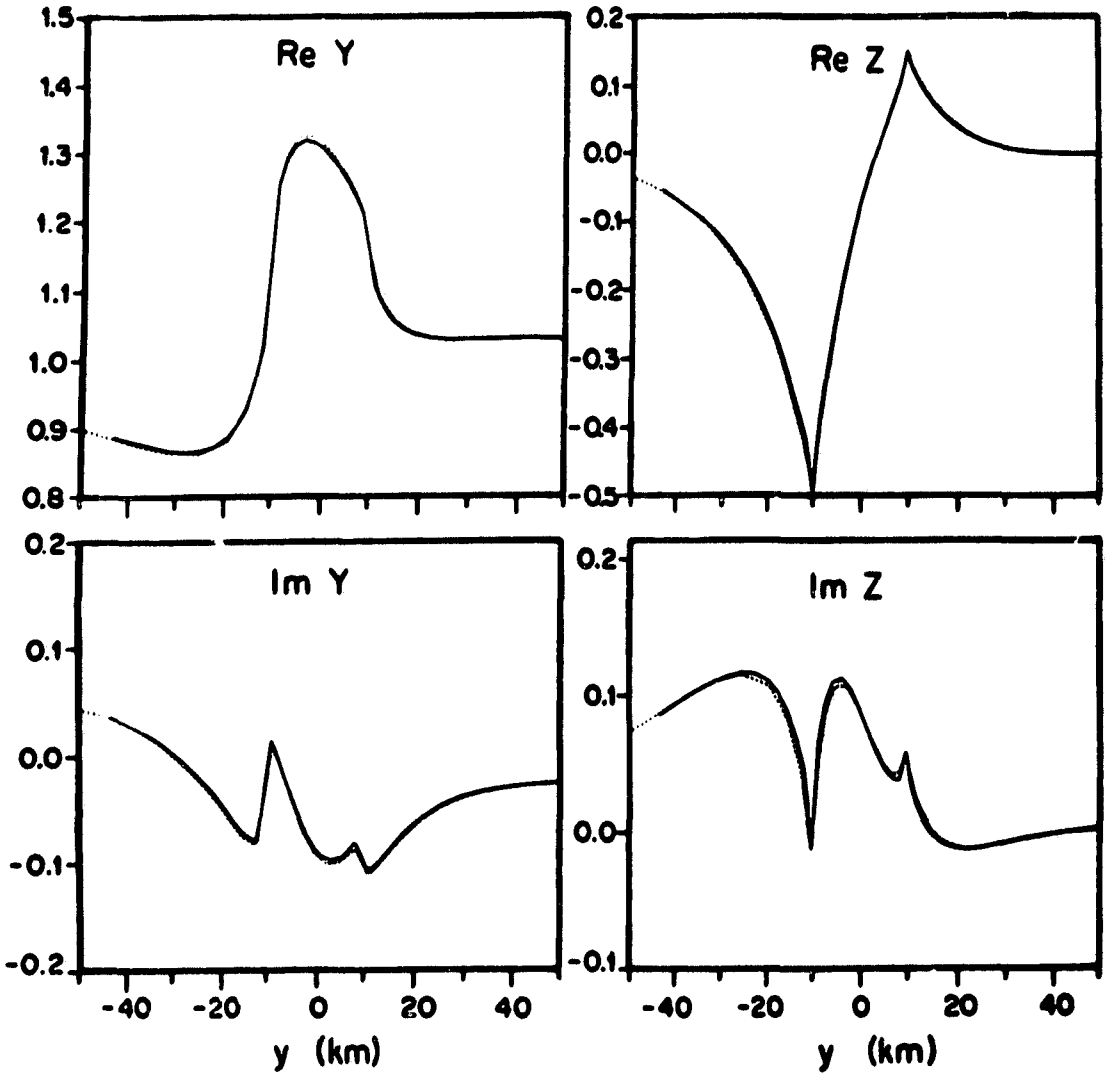


Figure 2.14: Variations of the real and imaginary parts of the magnetic components $Y$ and $Z$ (in units of $B_0$) across the surface $z = 0$ of the control model shown in Fig. 2.6. The solid line is given by the new finite difference formulae (2.79) and (2.80) and the broken line is the quasi-analytic solution of Weaver, LeQuang and Fischer (1986) (broken line). The period of the source field is 300 s.

# Chapter 3

# THREE-DIMENSIONAL EM INDUCTION PROBLEMS

---

In this chapter we discuss the boundary conditions and the governing differential equations in the 3D situation. The Governing Differential Equations, or GDE as we call them in abbreviation, consist of one set of equations that apply in the region of $x_2 \leq x \leq x_{L-1}$, $y_2 \leq y \leq y_{M-1}$, $z_2 \leq z \leq z_{N-1}$. The boundary conditions, on the other hand, consist of TBC, BBC and SBC. TBC stands for Top-Boundary-Conditions, but since we have included a thin sheet layer at the top of the model, TBC may as well stand for the Thin sheet-Boundary-Conditions. TBC in turn have two groups of equations, of which one set applies above the thin sheet at $z = 0-$, and the other beneath the thin sheet at $z = 0+$. BBC stands for the Bottom-Boundary-Conditions applying at the bottom of the model, $z = d$. SBC means Side-Boundary-Condition. It falls into two groups, as can be seen from Fig. 1.2. One is for the E-polarization and is applied at $y = y_1$ and $y = y_M$. The other is for the B-polarization and is applied at $x = x_1$ and $x = x_L$. In the same way that 1D solutions are used to serve as the side boundary conditions in a 2D problem, 2D solutions are used to serve as the side boundary conditions in a 3D problem. In order for these 2D SBC to apply, the side boundaries must be far enough away from the nearest conductivity contrast, so that the distortion field due to the 3D inhomogeneity can be neglected at the locations of the boundaries. Then the pre-calculated solutions of the limit 2D conductivity structures of both B-polarization and E-polarization can be applied as the values of the Side-Boundary-Conditions. The 2D problems for SBC have

been discussed in Chapter 2. In this chapter, we will only have to check TBC, BBC and GDE. We will start with TBC first.

## 3.1 Top Boundary Conditions - TBC

In this section, we discuss two sets of boundary conditions applied at the top of the model; one set is applied above the thin sheet layer at $z = 0-$, the other is applied beneath the thin sheet layer at $z = 0+$.

### 3.1.1 Boundary Conditions Above Thin Sheet at $z = 0-$

Above the thin sheet, at $z = 0-$, the component forms of equation (1.56) are

$$X = B_0 + X^a, \quad Y = Y^a, \quad Z = Z^a. \tag{3.1}$$

The second and third equations indicate that the $Y$ and $Z$-components of the total field and the anomalous field are identical due to the absence of the corresponding components in the source field. So $Y$ and $Y^a$, $Z$ and $Z^a$ are interchangeable.

$X^a$, $Y^a$ and $Z^a$ are not independent. In fact, both $X^a$ and $Y^a$ can be determined from $Z^a$ alone. The relations have been presented by Weaver (1964) and will also be derived after the discussion of the bottom boundary conditions in a later section. The equations (22) and (23) of Weaver (1964) give

$$X^a = -M_1 Z^a, \quad Y^a = -M_2 Z^a \tag{3.2}$$

where $M_1$ and $M_2$ are defined as

$$\begin{aligned} M_1 Z^a &:= \frac{1}{2\pi} \int_{-\infty}^{\infty} \int_{-\infty}^{\infty} Z^a(u,v) \frac{x-u}{[(x-u)^2 + (y-v)^2]} \, du \, dy \\ M_2 Z^a &:= \frac{1}{2\pi} \int_{-\infty}^{\infty} \int_{-\infty}^{\infty} Z^a(u,v) \frac{y-v}{[(x-u)^2 + (y-v)^2]} \, du \, dy. \end{aligned} \tag{3.3}$$

Combine (3.1) and (3.2) and drop the superscript of the $Z$ component. Then $X$ and $Y$ can be expressed in terms of $Z$ (i.e. $Z^a$) by

$$X(\mathbf{r},0-) = B_0 - M_1 Z(\mathbf{r},0-), \quad Y(\mathbf{r},0-) = -M_2 Z(\mathbf{r},0-). \tag{3.4}$$

These two integral equations can serve as the $X$- and $Y$-equations of surface boundary conditions for the $X$- and $Y$-components at $z = 0-$. The equation for the $Z$-component comes from the fact that the normal magnetic field $Z$ is continuous across the thin sheet, i.e.

$$Z(\mathbf{r},0-) = Z(\mathbf{r},0+). \tag{3.5}$$

This equation provides the link between the field values of surface nodes and interior ones.

### 3.1.2 Boundary Conditions Beneath Thin Sheet at $z = 0+$

Equations for the $X$- and $Y$-components come from the thin sheet conditions (1.53) and (1.54). If we denote $X(\mathbf{r},0-)$, $X(\mathbf{r},0+)$, $X'(\mathbf{r},0+)$ and $\rho(\mathbf{r},0+)$ as $X_0$, $X_1$, $X_1'$ and $\rho^+$ respectively, these two equations can be written as

$$X_1 - X_0 = \tau\rho^+(X_1' - Z_x) \tag{3.6}$$

$$Y_1 - Y_0 = \tau\rho^+(Y_1' - Z_y). \tag{3.7}$$

The derivatives, $X_1'$ and $Y_1'$, are given by (1.69) and (1.70) respectively; inserting them into the above equations, we have

$$\begin{aligned} X_1 &= X_0 + \tau\rho^+\left[(X_2 - X_1)/k_1 - Z_x\right] \\ &\quad + \frac{\tau\rho^+ k_1}{2}\left[-i\alpha^2 X_1 + X_{xx} + X_{yy} + (X_y - Y_x)\bar{\rho}_y\right]_{0+} \end{aligned} \tag{3.8}$$

$$\begin{aligned} Y_1 &= Y_0 + \tau\rho_+\left[(Y_2 - Y_1)/k_1 - Z_y\right] \\ &\quad + \frac{\tau\rho_+ k_1}{2}\left[-i\alpha^2 Y_1 + Y_{xx} + Y_{yy} + (Y_x - X_y)\bar{\rho}_x\right]_{0+} \end{aligned} \tag{3.9}$$

as the boundary conditions for the $X$- and $Y$-components beneath the thin sheet layer at $z = 0+$. The equation for $Z$-component is given in Chapter 1 by (1.72).

## 3.2 Bottom Boundary Conditions-BBC

Most of the mathematical development shown in this section can also be found in the work of Weaver (1994). In the region $z > d$, the conductivity $\sigma(x, y, z) = \sigma_0$ is a constant. The basic equation (1.28) becomes

$$\nabla^2 \mathbf{B} = i\alpha_0^2 \mathbf{B}, \text{ or } \nabla^2 \Phi = i\alpha_0^2 \Phi \tag{3.10}$$

where $\alpha_0^2 = \omega\mu_0\sigma_0 = \omega\mu_0/\rho_0$ and $\Phi$ stands for any component $X$, $Y$ or $Z$. We adopt the following definitions of double Fourier transform and convolution,

$$\hat{f}(\boldsymbol{\varrho}) = \frac{1}{2\pi}\int_{-\infty}^{\infty} f(\mathbf{r})\exp(i\mathbf{r}\cdot\boldsymbol{\varrho})\,d\mathbf{r} \qquad f(\mathbf{r}) = \frac{1}{2\pi}\int_{-\infty}^{\infty} \hat{f}(\boldsymbol{\varrho})\exp(-i\mathbf{r}\cdot\boldsymbol{\varrho})\,d\boldsymbol{\varrho} \tag{3.11}$$

$$f\star g(\mathbf{r}) \equiv \frac{1}{2\pi}\int_{-\infty}^{\infty} f(\mathbf{s})g(\mathbf{r}-\mathbf{s})\,d\mathbf{s} = \frac{1}{2\pi}\int_{-\infty}^{\infty} \hat{f}(\boldsymbol{\varrho})\hat{g}(\boldsymbol{\varrho})\exp(-i\mathbf{r}\cdot\boldsymbol{\varrho})\,d\boldsymbol{\varrho}$$

where

$$\mathbf{r} = (x, y),\ \boldsymbol{\varrho} = (\xi, \eta),\ \mathbf{s} = (u, v),\ \mathbf{r}\cdot\boldsymbol{\varrho} = (x\xi + y\eta),$$
$$\mathbf{r} - \mathbf{s} = (x-u, y-v),\ d\mathbf{r} = dx\,dy,\ d\boldsymbol{\varrho} = d\xi\,d\eta,\ d\mathbf{s} = du\,dv.$$

According to this definition, the Fourier transform of (3.10) is

$$\hat{\Phi}''(\boldsymbol{\varrho}, z) = [\gamma_0(\varrho)]^2\hat{\Phi}(\boldsymbol{\varrho}, z) \tag{3.12}$$

where $\gamma_0(\varrho) = [\varrho^2 + i\alpha_0^2]^{1/2}$, $\varrho^2 = \xi^2 + \eta^2$. The general solution to this equation is

$$\hat{\Phi}(\boldsymbol{\varrho}, z) = c_1\exp[\gamma_0(\varrho)z] + c_2\exp[-\gamma_0(\varrho)z].$$

Where the main branch of $\gamma_0(\varrho)$ is understood, i.e. $\mathrm{Re}\,\gamma_0(\varrho) \geq 0$. The solution that satisfies the boundary condition $\hat{\Phi}(\boldsymbol{\varrho}, +\infty) = 0$ and $\hat{\Phi}(\boldsymbol{\varrho}, z)_{z=d+} = F(\boldsymbol{\varrho}, d+)$ can be written as

$$\hat{\Phi}(\boldsymbol{\varrho}, z) = F(\boldsymbol{\varrho}, d+)\exp[-(z-d)\gamma_0(\varrho)] \tag{3.13}$$

$$= \frac{F'(\boldsymbol{\varrho}, d+)}{\gamma_0(\varrho)}\exp[-(z-d)\gamma_0(\varrho)]. \tag{3.14}$$

Defining

$$\hat{f}_1(\varrho, z) := -\exp[-(z-d)\gamma_0(\varrho)], \quad \hat{f}_2(\varrho, z) := \exp[-(z-d)\gamma_0(\varrho)]/\gamma_0(\varrho), \tag{3.15}$$

we can write the inverse Fourier transform of $\hat{f}_2$ as

$$\begin{aligned} f_2(\mathbf{r}, z) &= \frac{1}{2\pi}\int_{-\infty}^{\infty} \exp[-z\gamma_0(\varrho)]/\gamma_0(\varrho)\exp[-i\mathbf{r}\cdot\boldsymbol{\varrho}]\, d\boldsymbol{\varrho} \\ &= \frac{1}{2\pi}\int_{-\infty}^{\infty} \exp[-z\gamma_0(\varrho)]/\gamma_0(\varrho)\varrho\, d\varrho \int_0^{2\pi} \exp[-ir\varrho\cos(\theta-\theta_0)]\, d\theta \end{aligned} \tag{3.16}$$

where $\theta_0$ is the polar angle of $\mathbf{r}$. According to Olver (1964, 9.1.18),

$$\frac{1}{2\pi}\int_0^{2\pi} \exp[-ir\varrho\cos(\theta-\theta_0)]\, d\theta = \frac{1}{\pi}\int_0^{\pi} \cos[r\varrho\cos(\theta)]\, d\theta = J_0(r\varrho). \tag{3.17}$$

That leads (3.15) to

$$f_2(\mathbf{r}, z) = r^{-\frac{1}{2}}\int_0^{\infty} \varrho^{\frac{1}{2}} \frac{\exp[-z(\varrho^2+\beta^2)^{\frac{1}{2}}]}{(r^2+\beta^2)^{\frac{1}{2}}} J_0(r\varrho)(r\varrho)^{\frac{1}{2}}\, d\varrho \tag{3.18}$$

where $\beta^2 = i\alpha_0^2$. Making use of the Hankel transform defined as

$$g(y) = \int_0^{\infty} f(x)J_0(yx)(yx)^{1/2}\, dx, \quad y > 0 \tag{3.19}$$

and tabulated by Erdélyi (1954, §8.2(24)), we obtain the expression for $f_2(\mathbf{r}, z)$ and denote it by $S(\mathbf{r}, z)$ from now on, so that

$$S(\mathbf{r}, z) := f_2(\mathbf{r}, z) = \exp(-R\alpha_0\sqrt{i})/R, \quad R^2 = r^2 + z^2. \tag{3.20}$$

Similarly, with the help of Erdélyi (1954, §8.2(23)), we get

$$f_1(\mathbf{r}, z) = -z(1 + R\alpha_0\sqrt{i})S(\mathbf{r}, z)/R^2 = S'(\mathbf{r}, z). \tag{3.21}$$

Actually, from (3.15) we can see that

$$\hat{f}_1(\varrho, z) = \hat{f}_2'(\varrho, z),$$

therefore a straight-forward differentiation in $z$ could also have given us

$$f_1(\mathbf{r}, z) = f_1'(\mathbf{r}, z) = S'(\mathbf{r}, z).$$

Applying the convolution theorem (3.11) to (3.13) and (3.14), we get the solution to (3.10) as

$$\Phi(\mathbf{r}, z) = -\frac{1}{2\pi}\int_{-\infty}^{\infty} \Phi(\mathbf{s}, d+) S'(\mathbf{r}-\mathbf{s}, z-d)\, d\mathbf{s} \tag{3.22}$$

$$= -\frac{1}{2\pi}\int_{-\infty}^{\infty} \Phi'(\mathbf{s}, d+) S(\mathbf{r}-\mathbf{s}, z-d)\, d\mathbf{s} \tag{3.23}$$

If we further define

$$Q(\mathbf{r}, z) := -S'(\mathbf{r}, z)/z = (1 + R\alpha_0\sqrt{i})S(\mathbf{r}, z)/R^2, \tag{3.24}$$

and note that

$$S'(\mathbf{r}, z) = \frac{dS}{dR}\frac{\partial R}{\partial z} = \frac{z}{R}\frac{dS}{dR}, \qquad \frac{\partial S}{\partial r} = \frac{r}{R}\frac{dS}{dR}, \tag{3.25}$$

a simple integration by parts in polar coordinates gives

$$\frac{z}{2\pi}\int_{-\infty}^{\infty} Q(\mathbf{r}, z)\, d\mathbf{r} = -\frac{1}{2\pi}\int_0^{2\pi}\int_0^{\infty}\left(\frac{dS}{dR}\frac{z}{R}\right) r\, dr\, d\theta$$

$$= -z\int_0^{\infty}\frac{dS}{dR}\frac{\partial R}{\partial r}\, dr = -zS|_{r=0}^{\infty} = z\exp\left(-|z|\alpha_0\sqrt{i}]/|z|\right) \tag{3.26}$$

i.e.

$$\frac{z}{2\pi}\int_{-\infty}^{\infty} Q(\mathbf{r}, z)\, d\mathbf{r} = \exp(-z\alpha_0\sqrt{i}), \quad z > 0 \tag{3.27}$$

which can also be written as

$$\Phi(\mathbf{r}, d+)\exp\left[-(z-d)\alpha_0\sqrt{i}\right] = \frac{z-d}{2\pi}\int_{-\infty}^{\infty}\Phi(\mathbf{r}, d+)Q(\mathbf{r}-\mathbf{s}, z-d)\, d\mathbf{s} \tag{3.28}$$

by multiplying $\Phi(\mathbf{r}, d+)$ onto each side and substituting $z-d$ for $z$. Subtracting (3.28) from (3.22), we have

$$\Phi(\mathbf{r}, z) - \Phi(\mathbf{r}, d+)\exp[-(z-d)\alpha_0\sqrt{i}] =$$

$$\frac{z-d}{2\pi}\int_{-\infty}^{\infty}[\Phi(\mathbf{s}, d+) - \Phi(\mathbf{r}, d+)]\, Q(\mathbf{r}-\mathbf{s}, z-d)\, d\mathbf{s}. \tag{3.29}$$

Then differentiating this equation with respect to $z$ at $z = d+$, we obtain

$$\Phi'(\mathbf{r}, d+) + \alpha_0\sqrt{i}\Phi(\mathbf{r}, d+) = \frac{1}{2\pi}\int_{-\infty}^{\infty}[\Phi(\mathbf{s}, d+) - \Phi(\mathbf{r}, d+)]\, Q(|\mathbf{r}-\mathbf{s}|)\, d\mathbf{s} \quad (3.30)$$

where, for convenience, we have written

$$Q(r) \equiv Q(\mathbf{r}, 0) = r^{-3}(1 + r\alpha_0\sqrt{i})\exp(-r\alpha_0\sqrt{i}) \quad (3.31)$$

Replacing $\Phi$ by $X$,$Y$ and $Z$ in turn, (3.30) would give all the three equations needed for the bottom boundary conditions. There is one problem, though; all the values in the equations are evaluated at $z = d+$ and some of them, e.g. $X'(\mathbf{r}, d+)$ and $Y'(\mathbf{r}, d+)$, cannot be evaluated directly due to the absence of grid points in the region of $z > 0$. These terms have to be converted into the ones defined in $z < 0$ with the help of (1.84) and (1.85). Then we can write the bottom boundary conditions as

$$R_\rho X'(\mathbf{r}, d-) + (1 - R_\rho)Z_x(\mathbf{r}, d) + \alpha_0\sqrt{i}X(\mathbf{r}, d) = M_d X(\mathbf{r}, d) \quad (3.32)$$

$$R_\rho Y'(\mathbf{r}, d-) + (1 - R_\rho)Z_y(\mathbf{r}, d) + \alpha_0\sqrt{i}Y(\mathbf{r}, d) = M_d Y(\mathbf{r}, d) \quad (3.33)$$

$$Z'(\mathbf{r}, d) + \alpha_0\sqrt{i}Z(\mathbf{r}, d) = M_d Z(\mathbf{r}, d) \quad (3.34)$$

where

$$M_d\Phi(\mathbf{r}, d) = \frac{1}{2\pi}\int_{-\infty}^{\infty}[\Phi(\mathbf{s}, d) - \Phi(\mathbf{r}, d)]\, Q(|\mathbf{r}-\mathbf{s}|)\, d\mathbf{s} \quad (3.35)$$

and $\Phi$ stands for any magnetic component( $X$, $Y$ or $Z$ ).

The other $Z$-equation, corresponding to (2.33) of the 2D problem, can be obtained by substituting $Z'$ with $-(X_x + Y_y)$ in equation (1.77). It gives

$$Z_{xx} + Z_{yy} + \bar{\rho}_x(Z_x - X') + \bar{\rho}_y(Z_y - Y') - \frac{2}{k_{N-1}}(X_x + Y_y) = \left(\frac{2}{k_{N-1}^2} + i\alpha^2\right)Z_N - \frac{2}{k_{N-1}^2}Z_{N-1}. \quad (3.36)$$

where $X'$ and $Y'$ stand for $X'(\mathbf{r}, d-)$ and $Y'(\mathbf{r}, d-)$ and are given by (1.74) and (1.75 ) respectively.

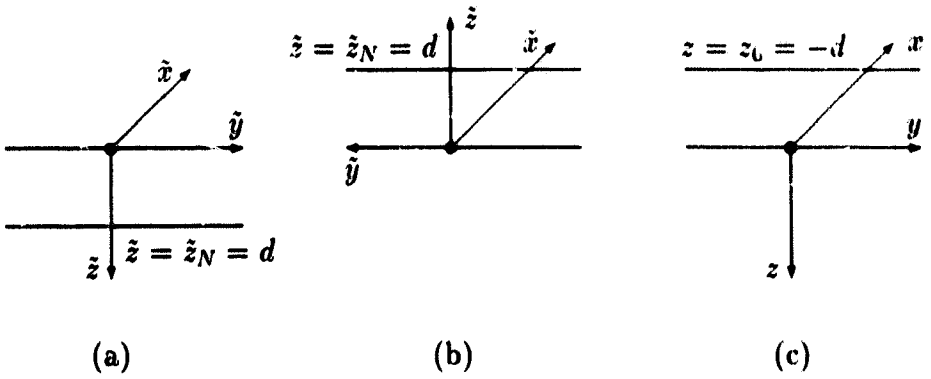


Figure 3.1: Transformation of coordinate frame. (a) The original set up of the coordinate frame and the conductivity structure. (b) Rotating the frame and the structure together about the $\tilde{x}$-axis through 180°. (c) Rotating the frame alone about the $\tilde{x}$-axis through 180°.

## 3.3 Proof of the TBC-Equations in (3.2)

The equations for the surface boundary condition in (3.2) can be derived from (3.23). First, let us denote the current coordinate frame as $\tilde{x}$, $\tilde{y}$ and $\tilde{z}$ as shown in fig (3.1a), where $\tilde{z} = \tilde{z}_N = d$ is the bottom boundary. Equation (3.10) and its solution (3.23) apply in the region $\tilde{z} \geq d$. We first rotate the conductivity structure and the coordinate frame together through 180° about the $\tilde{x}$ axis as shown by fig (3.1b), then rotate the coordinate frame alone through 180° about $\tilde{x}$, and denote the new coordinate system as $x$, $y$ and $z$. The coordinate transformation is

$$x = \tilde{x}, \quad y = -\tilde{y}, \quad z = -\tilde{z}. \tag{3.37}$$

Accordingly, the derivative in (3.23) becomes $\Phi' = \partial\Phi/\partial\tilde{z} = -\partial\Phi/\partial z$, and the integral equation (3.23), which is now evaluated at $z = -d$, can be written in the new system as

$$\Phi(\mathbf{r}, z) = \frac{1}{2\pi}\int_{-\infty}^{\infty} \frac{\partial\Phi(\mathbf{s}, -d-0)}{\partial z} S(\mathbf{r}-\mathbf{s}, z+d)\, d\mathbf{s}, \; z \leq -d. \tag{3.38}$$

The above equation defines the magnetic fields in the region $z \leq -d$ which originate from region $z \geq -d$ and satisfy the condition $\lim_{z\to-\infty} \Phi(\mathbf{r}, z) = 0$. If we regard region $z < -d$ as an air layer, i.e.

$$\sigma_0 = 0, \quad \alpha_0^2 = \omega\mu_0\sigma_0 = 0, \quad z < -d,$$

it follows from the basic equation (1.33) that, we can write the magnetic field in this region as the gradient of a scalar protential function such as

$$\mathbf{B}(\mathbf{r}, z) = -\nabla\Omega(\mathbf{r}, z), \quad z \leq -d. \tag{3.39}$$

where the scalar potential function $\Omega$ satisfies

$$\nabla^2\Omega(\mathbf{r}, z) = 0, \quad z \leq -d. \tag{3.40}$$

Since (3.23) is the solution of the second equation of (3.10) and integral (3.38) is the same as (3.23) but cast into the new coordinate frame, it follows that the integral (3.38) still satisfies the same equation as (3.10) in the new frame, i.e.

$$\nabla^2\Phi = i\alpha_0^2\Phi. \tag{3.41}$$

Comparing (3.41) and (3.40), we can obtain equation (3.40) from (3.41) with $\alpha_0 = 0$, and we therefore assume that the solution to (3.40) can also be obtained from that of (3.41) with $\alpha_0 = 0$, i.e.

$$\Omega(x, y, z) = \frac{1}{2\pi}\int_{-\infty}^{\infty} -Z(u, v, -d)S(x-u, y-v, z+d)\,du\,dv, \quad z \leq -d, \tag{3.42}$$

where we have used relation $Z = -\partial\Omega/\partial z$, given by (3.39), and the fact that $Z$ is continuous, i.e. $Z(\mathbf{r}, -d+) = Z(\mathbf{r}, -d-) = Z(\mathbf{r}, -d)$. Therefore, the $X$-component is given by

$$X(x, y, z) = -\frac{\partial\Omega}{\partial x} = \frac{1}{2\pi}\int_{-\infty}^{\infty} Z(u, v, -d)\frac{\partial}{\partial x}S(x-u, y-v, z+d)\,du\,dv.$$

With $\alpha_0 = 0$, (3.20) leads to

$$S(x,y,z) = \frac{1}{R} = \frac{1}{[x^2+y^2+z^2]^{1/2}} \quad \text{and}$$

$$\frac{\partial}{\partial x}S(x-u,y-v,z+d) = -\frac{x-u}{[(x-u)^2+(y-v)^2+(z+d)^2]^{3/2}};$$

so that we have

$$X(x,y,z) = -\frac{1}{2\pi}\int_{-\infty}^{\infty} Z(u,v,-d)\frac{x-u}{[(x-u)^2+(y-v)^2+(z+d)^2]^{3/2}}\,du\,dv. \tag{3.43}$$

This means that $X$ component at any point with $z \leq -d$ can be determined by the values of $Z$ at the $z = -d$ plane. When $d = 0-$ and $z \to 0$, (3.43) yields

$$X(x,y,0) = -\frac{1}{2\pi}\int_{-\infty}^{\infty} Z(u,v,0)\frac{x-u}{[(x-u)^2+(y-v)^2]^{3/2}}\,du\,dv. \tag{3.44}$$

It is the same as the first equation of (3.2), except that we have used $X$ and $Z$ for the anomalous field instead of $X^a$ and $Z^a$. Similar conclusions can be drawn for the second equation in (3.2), i.e., the equation for the $Y$-component. Hence, equations in (3.2) are proved.

## 3.4 Finite Difference Equations at $z = 0-,\ 0+,\ d$

In the previous sections, we have discussed the analytic forms of the boundary conditions. Above the thin sheet, at $z = 0-$, the $X$- and $Y$-equations are given by (3.4) while $Z$-equations by (3.5); beneath the thin sheet, at $z = 0+$, the $X$-, $Y$- and $Z$-equations are respectively given by (3.6), (3.7) and (1.72); at the bottom boundary $z = d$, the three equations are (3.32), (3.33) and (3.34) where equation (3.34) can also be replaced by (3.36). In this section, we are going to write these equations in finite difference form so that they are ready for programming.

### 3.4.1 Finite Difference Equations at $z = 0-$

The integral operators $M_1$, $M_2$ and $M_d$ defined by (3.3) and (3.35) are discussed in Appendix A; the boundary condition above the thin sheet at $z = 0-$, equations (3.4) and (3.5), can be written as

$$X_{\lambda\mu 0} = B_0 + \sum_{l=1}^{L}\sum_{m=1}^{M} A_{\lambda\mu}^{lm} Z_{\lambda\mu 0}, \tag{3.45}$$

$$Y_{\lambda\mu 0} = \sum_{l=1}^{L}\sum_{m=1}^{M} B_{\lambda\mu}^{lm} Z_{\lambda\mu 0}, \tag{3.46}$$

$$Z_{\lambda\mu 0} = Z_{\lambda\mu 1}, \tag{3.47}$$

$$\lambda = 2...L-1, \quad \mu = 2...M-1, \quad \nu = 0$$

where $A_{\lambda\mu}^{lm}$ and $B_{\lambda\mu}^{lm}$ are given by (A.130) and (A.131) respectively in Appendix A.

### 3.4.2 Finite Difference Equations at $z = 0+$

In equations (3.6), (3.7) and (1.72), let us define $R := \tau\rho^+$, $T := Rk_1/2$; substitute $F_0$, $F_1$, and $F_2$ by their corresponding full notations in the 3D mesh in local system, e.g. $F_0 = F(\mathbf{r}, 0-) = F_{110}$, $F_1 = F(\mathbf{r}, 0+) = F_{111}$ and $F_2 = F(\mathbf{r}, k_1) = F_{112}$ etc.. The equations of surface boundary conditions beneath the thin sheet at $z = 0+$ then become respectively

$$\begin{aligned}
X_{111} &= X_{110} + R[(X_{112} - X_{111})/k_1 - Z_x] \\
&\quad + T\left[-i\alpha^2 X_{111} + X_{xx} + X_{yy} + (X_y - Y_x)\bar{\rho}_y\right] \\
Y_{111} &= Y_{110} + R[(Y_{112} - Y_{111})/k_1 - Z_y] \\
&\quad + T\left[-i\alpha^2 Y_{111} + Y_{xx} + Y_{yy} + (Y_x - X_y)\bar{\rho}_x\right] \\
i\alpha^2 Z_{111} &= Z_{xx} + Z_{yy} + Z_x\bar{\rho}_x + Z_y\bar{\rho}_y + 2(X_x + Y_y)/k_1 \\
&\quad - \bar{\rho}_x\frac{(X_{113} - X_{111})}{k_1} - \bar{\rho}_y\frac{(Y_{112} - Y_{111})}{k_1} + \frac{2(Z_{112} - Z_{111})}{k_1^2}.
\end{aligned} \tag{3.48}$$

Inserting the corresponding central difference expressions of the derivatives, we have the final finite difference form of these equations as

$$\left[1+\frac{R}{k_1}+i\alpha^2T+\frac{2T}{G_{02}}+\frac{T(2-\bar{\rho}_y h_{20})}{H_{02}}\right]X_{111}=X_{110}+\frac{R}{T}X_{112}$$
$$+\frac{2T}{G_{2s}}X_{211}+\frac{2T}{G_{0s}}X_{011}+\frac{T(2+\bar{\rho}_y h_0)}{H_{2s}}X_{121}+\frac{T(2-\bar{\rho}_y h_2)}{H_{0s}}X_{101}$$
$$-\frac{T\bar{\rho}_y g_0}{G_{2s}}Y_{211}-\frac{T\bar{\rho}_y g_{20}}{G_{02}}Y_{111}+\frac{T\bar{\rho}_y g_2}{G_{0s}}Y_{011}$$
$$-\frac{Rg_0}{G_{2s}}Z_{211}-\frac{Rg_{20}}{G_{02}}Z_{111}+\frac{Rg_2}{G_{0s}}Z_{011},$$
$$\lambda=2\ldots L-1\quad \mu=2\ldots M-1,\quad \nu=1; \tag{3.49}$$

$$\left[1+\frac{R}{k_1}+i\alpha^2T+\frac{2T}{H_{02}}+\frac{T(2-\bar{\rho}_x g_{20})}{G_{02}}\right]Y_{111}=Y_{110}+\frac{R}{T}Y_{112}$$
$$+\frac{2T}{H_{2s}}Y_{121}+\frac{2T}{H_{0s}}Y_{101}+\frac{T(2+\bar{\rho}_x g_0)}{G_{2s}}Y_{211}+\frac{T(2-\bar{\rho}_x g_2)}{G_{0s}}Y_{011}$$
$$-\frac{T\bar{\rho}_x h_0}{H_{2s}}X_{121}-\frac{T\bar{\rho}_x h_{20}}{H_{02}}X_{111}+\frac{T\bar{\rho}_x h_2}{H_{0s}}X_{101}$$
$$-\frac{Rh_0}{H_{2s}}Z_{121}-\frac{Rh_{20}}{H_{02}}Z_{111}+\frac{Rh_2}{H_{0s}}Z_{101},$$
$$\lambda=2\ldots L-1\quad \mu=2\ldots M-1,\quad \nu=1; \tag{3.50}$$

$$\left(i\alpha^2+\frac{2}{k_1^2}+\frac{2-\bar{\rho}_x g_{20}}{G_{02}}+\frac{2-\bar{\rho}_y h_{20}}{H_{02}}\right)Z_{111}=+\frac{2}{k_1^2}Z_{112}$$
$$\frac{2g_0}{k_1G_{2s}}X_{211}+\left(\frac{\bar{\rho}_x}{k_1}+\frac{2g_{20}}{k_1G_{02}}\right)X_{111}-\frac{2g_2}{k_1G_{0s}}X_{011}-\frac{\bar{\rho}_x}{k_1}X_{112}$$
$$+\frac{2h_0}{k_1H_{2s}}Y_{121}+\left(\frac{\bar{\rho}_y}{k_1}+\frac{2h_{20}}{k_1H_{02}}\right)Y_{111}-\frac{2h_2}{k_1H_{0s}}Y_{101}-\frac{\bar{\rho}_y}{k_1}Y_{112}$$
$$+\frac{2+\bar{\rho}_x g_0}{G_{2s}}Z_{211}+\frac{2-\bar{\rho}_x g_2}{G_{0s}}Z_{011}+\frac{2+\bar{\rho}_y h_0}{H_{2s}}Z_{121}+\frac{2-\bar{\rho}_y h_2}{H_{0s}}Z_{101}$$
$$\lambda=2\ldots L-1\quad \mu=2\ldots M-1,\quad \nu=1 \tag{3.51}$$

where $R=\tau\rho^+$, $T=\tau\rho^+k_1/2$, $\alpha^2=\omega\mu_0/\rho^+$ and $\rho^+=\rho(\mathbf{r},0+)=\rho(\mathbf{r},\frac{1}{2}k_1)$.

### 3.4.3 Finite Difference Equations at $z = d$

The equations of the bottom boundary condition (BBC) are (3.32), (3.33) and (3.34). The integral operator $M_d$ that is involved with all the three equations is discussed in Appendix A. The finite difference forms of (3.32), (3.33) and (3.34) are respectively

$$\begin{aligned}
&\left\{\alpha_0\sqrt{i}\left(1+\frac{k_{N-1}}{2}\alpha_0\sqrt{i}\right)+R_\rho\left[\frac{1}{k_{N-1}}+\frac{k_{N-1}}{2}\left(\frac{2}{G_{02}}+\frac{2-h_{20}\bar{\rho}_y}{H_{02}}\right)\right]+S\right\}X_{111}\\
&= \frac{\alpha_0}{2\pi}\sum_{l=1}^{L}\sum_{m=1}^{M}C^{lm}_{\lambda\mu}X_{lmN}+\frac{R_\rho k_{N-1}}{G_{2s}}X_{211}+\frac{R_\rho k_{N-1}}{G_{0s}}X_{011}+\frac{R_\rho}{k_{N-1}}X_{110}\\
&\quad+\frac{R_\rho k_{N-1}(2+h_0\bar{\rho}_y)}{2H_{2s}}X_{121}+\frac{R_\rho k_{N-1}(2-h_2\bar{\rho}_y)}{2H_{0s}}X_{101}\\
&\quad-\frac{R_\rho k_{N-1}g_0\bar{\rho}_y}{2G_{2s}}Y_{211}-\frac{R_\rho k_{N-1}g_{20}\bar{\rho}_y}{2G_{02}}Y_{111}+\frac{R_\rho k_{N-1}g_2\bar{\rho}_y}{2G_{0s}}Y_{011}\\
&\quad-\frac{(1-R_\rho)g_0}{G_{2s}}Z_{211}-\frac{(1-R_\rho)g_{20}}{G_{02}}Z_{111}+\frac{(1-R_\rho)g_2}{G_{0s}}Z_{011},\\
&\qquad\qquad \lambda = 2...L-1,\quad \mu = 2...M-1,\quad \nu = N, \qquad (3.52)
\end{aligned}$$

$$\begin{aligned}
&\left\{\alpha_0\sqrt{i}\left(1+\frac{k_{N-1}}{2}\alpha_0\sqrt{i}\right)+R_\rho\left[\frac{1}{k_{N-1}}+\frac{k_{N-1}}{2}\left(\frac{2}{H_{02}}+\frac{2-g_{20}\bar{\rho}_x}{G_{02}}\right)\right]+S\right\}Y_{111}\\
&= \frac{\alpha_0}{2\pi}\sum_{l=1}^{L}\sum_{m=1}^{M}C^{lm}_{\lambda\mu}Y_{lmN}+\frac{R_\rho k_{N-1}}{H_{2s}}Y_{121}+\frac{R_\rho k_{N-1}}{H_{0s}}Y_{101}+\frac{R_\rho}{k_{N-1}}Y_{110}\\
&\quad+\frac{R_\rho k_{N-1}(2+g_0\bar{\rho}_x)}{2G_{2s}}Y_{211}+\frac{R_\rho k_{N-1}(2-g_2\bar{\rho}_x)}{2G_{0s}}Y_{011}\\
&\quad-\frac{R_\rho k_{N-1}h_0\bar{\rho}_x}{2H_{2s}}X_{121}-\frac{R_\rho k_{N-1}h_{20}\bar{\rho}_x}{2H_{02}}X_{111}+\frac{R_\rho k_{N-1}h_2\bar{\rho}_x}{2H_{0s}}X_{101}\\
&\quad-\frac{(1-R_\rho)h_0}{H_{2s}}Z_{121}-\frac{(1-R_\rho)h_{20}}{H_{02}}Z_{111}+\frac{(1-R_\rho)h_2}{H_{0s}}Z_{101}\\
&\qquad\qquad \lambda = 2...L-1,\quad \mu = 2...M-1,\quad \nu = N, \qquad (3.53)
\end{aligned}$$

$$\begin{aligned}
&\left\{\alpha_0\sqrt{i}\left(1+\frac{k_{N-1}}{2}\alpha_0\sqrt{i}\right)+\frac{1}{k_{N-1}}+\frac{k_{N-1}}{2}\left(\frac{2-g_{20}\bar{\rho}_x}{G_{02}}+\frac{2-h_{20}\bar{\rho}_y}{H_{02}}\right)+S\right\}Z_{111}\\
&= \frac{\alpha_0}{2\pi}\sum_{l=1}^{L}\sum_{m=1}^{M}C^{lm}_{\lambda\mu}Z_{lmN}-\frac{Z_{110}}{k_{N-1}}+\frac{\bar{\rho}_x}{2}(X_{111}-X_{110})+\frac{\bar{\rho}_y}{2}(Y_{111}-Y_{110})
\end{aligned}$$

$$-\frac{k_{N-1}}{2}\left(\frac{2+g_0\bar{\rho}_x}{G_{2s}}Z_{211}+\frac{2-g_2\bar{\rho}_x}{G_{0s}}Z_{011}+\frac{2+h_0\bar{\rho}_y}{H_{2s}}Z_{121}+\frac{2-h_2\bar{\rho}_y}{H_{0s}}Z_{101}\right)$$
$$\lambda = 2...L-1,\quad \mu = 2...M-1,\quad \nu = N, \tag{3.54}$$

where $S = (\alpha_0/2\pi)\sum_{l=0}^{L}\sum_{m=0}^{M} I_{00}^{lm}$, $I_{00}^{lm}$ and $C_{\lambda\mu}^{lm}$ are given by (A.148), (A.149) and (A.143) in appendix A, $R_o = \rho(\mathbf{r}, d-)/\rho_0 = \rho_{\lambda\mu N-\frac{1}{2}}/\rho_0$ and $\alpha_0^2 = \omega\mu_0/\rho_0$. The finite difference form of equation (3.36) is

$$\left[\frac{2}{k_{N-1}}+k_{N-1}\left(i\alpha^2+\frac{2-\bar{\rho}_x g_{20}}{G_{02}}+\frac{2-\bar{\rho}_y h_{20}}{H_{02}}\right)\right]Z_{111} =$$
$$\frac{k_{N-1}^2\bar{\rho}_x-2g_0}{G_{2s}}X_{211}+\frac{k_{N-1}^2\bar{\rho}_x+2g_2}{G_{0s}}X_{011}+\frac{k_{N-1}^2\bar{\rho}_x}{H_{2s}}X_{121}+\frac{k_{N-1}^2\bar{\rho}_x}{H_{0s}}X_{101}$$
$$-\left[\left(\bar{\rho}_x+\frac{2g_{20}}{G_{02}}\right)+\bar{\rho}_x k_{N-1}^2\left(i\alpha^2+\frac{1}{G_{02}}+\frac{1}{H_{02}}\right)\right]X_{111}+\bar{\rho}_x X_{110}$$
$$+\frac{k_{N-1}^2\bar{\rho}_y-2h_0}{H_{2s}}Y_{121}+\frac{k_{N-1}^2\bar{\rho}_y+2h_2}{H_{0s}}Y_{101}+\frac{k_{N-1}^2\bar{\rho}_y}{G_{2s}}Y_{211}+\frac{k_{N-1}^2\bar{\rho}_y}{G_{0s}}Y_{01}$$
$$-\left[\left(\bar{\rho}_y+\frac{2h_{20}}{H_{02}}\right)+\bar{\rho}_y k_{N-1}^2\left(i\alpha^2+\frac{1}{G_{02}}+\frac{1}{H_{02}}\right)\right]Y_{111}+\bar{\rho}_y Y_{110}$$
$$+k_{N-1}\left[\frac{2+\bar{\rho}_x g_0}{G_{2s}}Z_{211}+\frac{2-\bar{\rho}_x g_2}{G_{0s}}Z_{011}+\frac{2+\bar{\rho}_y h_0}{H_{2s}}Z_{121}+\frac{2-\bar{\rho}_y h_2}{H_{0s}}Z_{101}\right]$$
$$+\frac{2}{k_{N-1}}Z_{110},$$
$$\lambda = 2...L-1,\quad \mu = 2...M-1,\quad \nu = N, \tag{3.55}$$

where $\alpha^2 = \omega\mu_0/\rho(\mathbf{r}, d-) = \omega\mu_0/\rho_{\lambda\mu N-\frac{1}{2}}$.

It is worth mentioning that most of the algebra manipulation in the previous sections can be done by using the MAPLE system installed on the University of Victoria IBM3090 main frame computer. MAPLE is a symbolic computation language system developed at the University of Waterloo. Several other symbolic computation systems also exist, such as ALTRAN, CAMAL, REDUCE, MACSYMA and MATHEMATICA.

## 3.5 Governing Differential Equations-GDE

The 3D counterpart of the 2D equation (2.46) comes from applying volume integration to Maxwell's equations and using the vector relation

$$\int_V (\nabla \times \mathbf{A})\, dv = \oint_S d\mathbf{S} \times \mathbf{A} \tag{3.56}$$

where $V$ is a volume bounded by a closed surface $S$, with $d\mathbf{S}$ positive outward from the enclosed volume. This relation is given by Jones (1964, p113, eq. 29) and can also be derived from the well-known Gauss divergence theorem

$$\int_V (\nabla \cdot \mathbf{A}) dv = \oint_S \mathbf{A} \cdot d\mathbf{S}. \tag{3.57}$$

Assume $\mathbf{a}$ is an arbitrary but constant vector, so that $\nabla \cdot (\mathbf{a} \times \mathbf{A}) = \mathbf{A} \cdot (\nabla \times \mathbf{a}) - \mathbf{a} \cdot (\nabla \times \mathbf{A}) = -\mathbf{a} \cdot (\nabla \times \mathbf{A})$. If we replace $\mathbf{A}$ by $\mathbf{a} \times \mathbf{A}$ in the Gauss theorem, its L.H.S. then becomes

$$\int_V \nabla \cdot (\mathbf{a} \times \mathbf{A}) dv = \int_V -\mathbf{a} \cdot (\nabla \times \mathbf{A}) dv = -\mathbf{a} \cdot \int_V (\nabla \times \mathbf{A}) dv, \tag{3.58}$$

while its R.H.S. is

$$\oint_S (\mathbf{a} \times \mathbf{A}) \cdot d\mathbf{S} = \oint_S \mathbf{a} \cdot (\mathbf{A} \times d\mathbf{S}) = -\mathbf{a} \cdot \oint d\mathbf{S} \times \mathbf{A} \tag{3.59}$$

Since $\mathbf{a}$ is arbitrary, we can conclude from (3.57), (3.58) and (3.59) that equation (3.56) is true.

A volume integration of the Maxwell equation (1.22) gives

$$\int_V \nabla \times \mathbf{E}\, dv = -i\omega \int_V \mathbf{B}\, dv \tag{3.60}$$

which can be further transformed by (3.56) and Maxwell equation (1.23) into

$$\int_V \nabla \times \mathbf{E}\, dv = \oint d\mathbf{S} \times \mathbf{E} = -\frac{1}{\mu_0} \oint \rho(\nabla \times \mathbf{B}) \times d\mathbf{S}. \tag{3.61}$$

Equation (3.60) then becomes

$$\oint_S \rho(\nabla \times \mathbf{B}) \times d\mathbf{S} = i\omega\mu_0 \int_V \mathbf{B}\, dv. \tag{3.62}$$

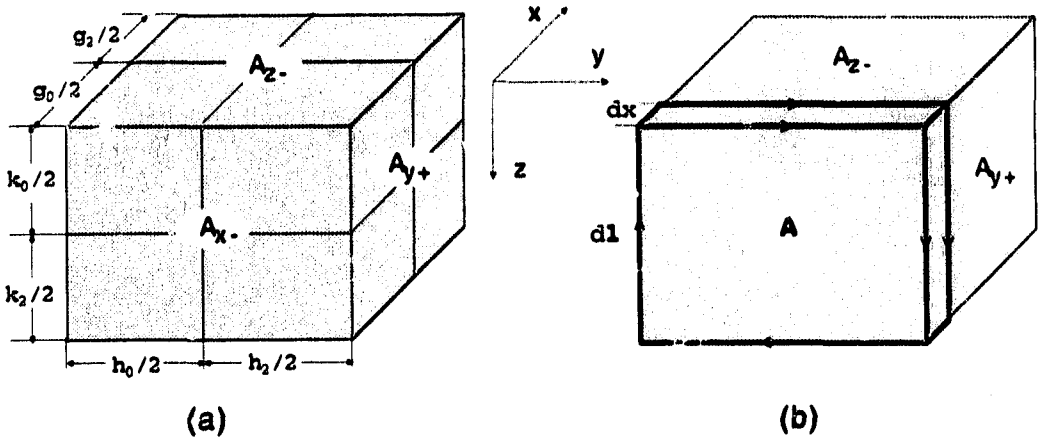


Figure 3.2: (a) 3D cubic integral cell. (b) The surface of the integral cell when the model is uniform along the $x$-direction.

This is our vector integral equation for general 3D cases where $V$ is the cubic volume containing the node in question $(x_\lambda, y_\mu, z_\nu)$, defined by $(-g_0/2 \leq x - x_\lambda \leq g_2/2, -h_0/2 \leq y - y_\mu \leq h_2/2, -k_0/2 \leq z - z_\nu \leq k_2/2)$, while $S$ is the outward surface enclosing $V$ (Fig. 3.2a) with

$$\mathbf{S} = \hat{\mathbf{x}}A_{x+} - \hat{\mathbf{x}}A_{x-} + \hat{\mathbf{y}}A_{y+} - \hat{\mathbf{y}}A_{y-} + \hat{\mathbf{z}}A_{z+} - \hat{\mathbf{z}}A_{z-}.$$

When the given 3D model degenerates into a 2D conductive structure, the 3D equation (3.62) should reduce to the correct 2D formula given by (2.46). Assume that the model is uniform in the $x$-direction, i.e. $\partial\rho/\partial x \equiv 0$, $\partial\mathbf{B}/\partial x \equiv 0$. As shown by Fig. 3.2b, let $A$ be the positive surface of any cross section of the volume $V$ with the $yz$-plane, i.e. $\mathbf{A} = \frac{1}{4}(h_0 + h_2)(k_0 + k_2)\hat{\mathbf{x}}$, and let $C$ be the path enclosing the surface with $d\mathbf{l}$ be the vector segment of $C$. We can write

$$d\mathbf{S} = \hat{\mathbf{x}}dy\,dz + \hat{\mathbf{y}}dx\,dz + \hat{\mathbf{z}}dx\,dy = \hat{\mathbf{x}}dy\,dz + d\mathbf{l} \times d\mathbf{x} \tag{3.63}$$

and

$$d\mathbf{S} \times \hat{\mathbf{x}} = -\hat{\mathbf{x}} \times (d\mathbf{l} \times d\mathbf{x}) = -d\mathbf{l}\,dx. \tag{3.64}$$

Take a cross product of equation (3.62) by $\hat{\mathbf{x}}$; its L.H.S. and R.H.S. become respectively

$$\begin{aligned} \oint_A \rho(\nabla \times \mathbf{B}) \times d\mathbf{S} \times \hat{\mathbf{x}} &= -\oint_A \rho(\nabla \times \mathbf{B}) \times d\mathbf{l}\, dx \\ = -\int_{x_\lambda - h_0/2}^{x_\lambda + h_2/2} dx \oint_C \rho(\nabla \times \mathbf{B}) \times d\mathbf{l} &= -\frac{h_0 + h_2}{2} \oint_C \rho(\nabla \times \mathbf{B}) \times d\mathbf{l}, \end{aligned} \tag{3.65}$$

and

$$\int_V \mathbf{B}\, dv \times \hat{\mathbf{x}} = \int_{x_\lambda - h_0/2}^{x_\lambda + h_2/2} dx \int_A \mathbf{B} \times \hat{\mathbf{x}} dS = -\frac{h_0 + h_2}{2} \int_A \hat{\mathbf{x}} \times \mathbf{B}\, dS. \tag{3.66}$$

Whence equation (3.62) reduces to

$$\oint_C \rho(\nabla \times \mathbf{B}) \times d\mathbf{l} = i\omega\mu_0 \int_A \hat{\mathbf{x}} \times \mathbf{B} d\mathbf{S},$$

which is the same as (2.46). Therefore, our 3D equation (3.62) does indeed degenerate into the correct 2D formula (2.46) when the given model is a 2D structure.

## 3.6 Finite Difference Forms of 3D GDE

For better performance in numerical computation, we first normalize equation (3.62) to make its coefficients dimensionless by dividing it through with $\alpha^2 \bar{\rho} V = (\omega\mu_0/\bar{\rho})\bar{\rho}(g_s h_s k_s/8)$. Hence the equation becomes

$$\frac{8i}{g_s h_s k_s} \int_V \mathbf{B}\, dv = \frac{1}{\alpha^2 \bar{\rho} V} \oint_S \rho(\nabla \times \mathbf{B}) \times d\mathbf{S}. \tag{3.67}$$

The finite difference representation of the L.H.S. of this equation is obtained by approximating $\mathbf{B}(x, y, z) = \mathbf{B}_{111}$ for $(x, y, z) \in V$ in the local system. Thus we have

$$\frac{8i}{g_s h_s k_s} \int_V \mathbf{B}\, dv = \frac{8i}{g_s h_s k_s} \mathbf{B}_{111} \frac{g_s h_s k_s}{8} = i(X_{111}\hat{\mathbf{x}} + Y_{111}\hat{\mathbf{y}} + Z_{111}\hat{\mathbf{z}}). \tag{3.68}$$

Inserting expression $\nabla \times \mathbf{B} = (Z_y - Y_z)\hat{\mathbf{x}} + (X_z - Z_x)\hat{\mathbf{y}} + (Y_x - X_y)\hat{\mathbf{z}}$ into the R.H.S. of the dimensionless 3D GDE (3.67), we can express the integral as follows:

$$\begin{aligned}
&\oint_S \rho(\nabla \times \mathbf{B}) \times ds = \oint_S \rho(\nabla \times \mathbf{B}) \times (\hat{\mathbf{x}}\,dydz + \hat{\mathbf{y}}\,dxdz + \hat{\mathbf{z}}\,dxdy) \\
&= \int_{A_{x-}} \rho(\nabla \times \mathbf{B}) \times (-\hat{\mathbf{x}})\,dydz + \int_{A_{x+}} \rho(\nabla \times \mathbf{B}) \times \hat{\mathbf{x}}\,dydz \\
&+ \int_{A_{y-}} \rho(\nabla \times \mathbf{B}) \times (-\hat{\mathbf{y}})\,dxdz + \int_{A_{y+}} \rho(\nabla \times \mathbf{B}) \times \hat{\mathbf{y}}\,dxdz \\
&+ \int_{A_{z-}} \rho(\nabla \times \mathbf{B}) \times (-\hat{\mathbf{z}})\,dxdy + \int_{A_{z+}} \rho(\nabla \times \mathbf{B}) \times \hat{\mathbf{z}}\,dxdy \\
&= \left[\int_{A_{x+}} - \int_{A_{x-}}\right] \rho[(Z_x - X_z)\hat{\mathbf{z}} + (Y_x - X_y)\hat{\mathbf{y}}]\,dydz \\
&+ \left[\int_{A_{y+}} - \int_{A_{y-}}\right] \rho[(Z_y - Y_z)\hat{\mathbf{z}} + (X_y - Y_x)\hat{\mathbf{x}}]\,dxdz \\
&+ \left[\int_{A_{z+}} - \int_{A_{z-}}\right] \rho[(Y_z - Z_y)\hat{\mathbf{y}} + (X_z - Z_x)\hat{\mathbf{x}}]\,dxdy \qquad (3.69)
\end{aligned}$$

Thus, the three components of equation (3.67) are

$$\begin{aligned}
iX_{111} &= \frac{1}{\alpha^2\bar{\rho}V}\left[\int_{A_{y+}} - \int_{A_{y-}}\right] \rho X_y\,dxdz + \frac{1}{\alpha^2\bar{\rho}V}\left[\int_{A_{z+}} - \int_{A_{z-}}\right] \rho X_z\,dxdy \\
&+ \frac{1}{\alpha^2\bar{\rho}V}\left[\int_{A_{y-}} - \int_{A_{y+}}\right] \rho Y_x\,dxdz + \frac{1}{\alpha^2\bar{\rho}V}\left[\int_{A_{z-}} - \int_{A_{z+}}\right] \rho Z_x\,dxdy \qquad (3.70)
\end{aligned}$$

$$\begin{aligned}
iY_{111} &= \frac{1}{\alpha^2\bar{\rho}V}\left[\int_{A_{x+}} - \int_{A_{x-}}\right] \rho Y_x\,dydz + \frac{1}{\alpha^2\bar{\rho}V}\left[\int_{A_{z+}} - \int_{A_{z-}}\right] \rho Y_z\,dxdy \\
&+ \frac{1}{\alpha^2\bar{\rho}V}\left[\int_{A_{x-}} - \int_{A_{x+}}\right] \rho X_y\,dydz + \frac{1}{\alpha^2\bar{\rho}V}\left[\int_{A_{z-}} - \int_{A_{z+}}\right] \rho Z_y\,dxdy \qquad (3.71)
\end{aligned}$$

$$\begin{aligned}
iZ_{111} &= \frac{1}{\alpha^2\bar{\rho}V}\left[\int_{A_{x+}} - \int_{A_{x-}}\right] \rho Z_x\,dydz + \frac{1}{\alpha^2\bar{\rho}V}\left[\int_{A_{y+}} - \int_{A_{y-}}\right] \rho Z_y\,dxdz \\
&+ \frac{1}{\alpha^2\bar{\rho}V}\left[\int_{A_{x-}} - \int_{A_{x+}}\right] \rho X_z\,dydz + \frac{1}{\alpha^2\bar{\rho}V}\left[\int_{A_{y-}} - \int_{A_{y+}}\right] \rho Y_z\,dxdz \qquad (3.72)
\end{aligned}$$

### 3.6.1 Integrals with Normal Derivatives

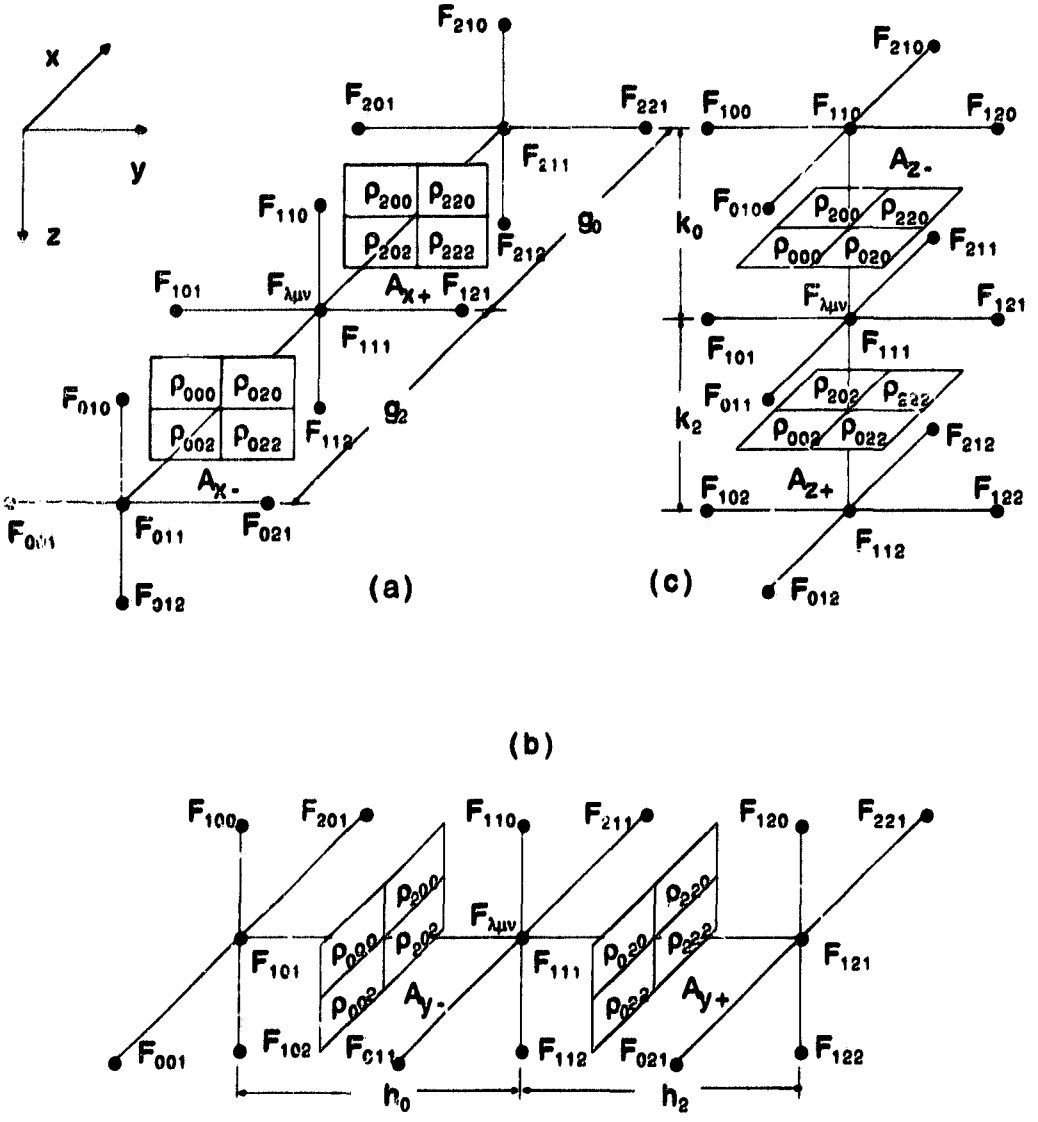


Figure 3.3: Perspective views of the grid nodes and the integration surfaces. (a) The view of the nodes and the integration surface related to the $x$-axis. (b) The view of the nodes and the integration surface related to the $y$-axis. (c) The view of the nodes and the integration surface related to the $z$-axis. F stands for any magnetic component, $X$, $Y$ or $Z$. $A_{y-}$ is the integral surface located at $y = y_{\mu-1/2} = y_\mu - \frac{1}{2}h_0$, defined by $g_s k_s/4$ and $A_{y+}$ is also defined by $g_s k_s/4$, but located at $y = y_{\mu+1/2} = y_\mu + \frac{1}{2}h_2$.

On each surface, there are both normal and tangential derivatives. The normal derivatives are approximated at the center of the surface. For instance, on $A_{y-}$ (Fig. 3.2a and Fig. 3.3b), it is assumed that

$$X_y|_{y-} = (X_{111} - X_{101})/h_0, \tag{3.73}$$

whence

$$\int_{A_{y-}} \rho X_y dxdz = \frac{(X_{111} - X_{101})}{4h_0}(\rho_{000}g_0k_0 + \rho_{002}g_0k_2 + \rho_{200}g_2k_0 + \rho_{202}g_2k_2)$$

and

$$\frac{1}{\alpha^2\bar{\rho}V}\int_{A_{y-}} \rho X_y\, dxdz = (X_{111} - X_{101})\frac{2\bar{\rho}_{101}}{\alpha^2 h_0 h_s} \tag{3.74}$$

where

$$\bar{\rho}_{101} := \rho_{101}/\bar{\rho} := (\rho_{000}g_0k_0 + \rho_{002}g_0k_2 + \rho_{200}g_2k_0 + \rho_{202}g_2k_2)/g_sk_s\bar{\rho} \tag{3.75}$$

Similarly, we have $X_y|_{y+} = (X_{121} - X_{111})/h_2$ (Fig. 3.3b) and

$$\frac{1}{\alpha^2\bar{\rho}V}\int_{A_{y-}} \rho X_y\, dxdz = (X_{121} - X_{111})\frac{2\bar{\rho}_{121}}{\alpha^2 h_2 h_s} \tag{3.76}$$

where

$$\bar{\rho}_{121} = \rho_{121}/\bar{\rho} = (\rho_{020}g_0k_0 + \rho_{022}g_0k_2 + \rho_{220}g_2k_0 + \rho_{222}g_2k_2)/g_sk_s\bar{\rho}. \tag{3.77}$$

The four other integrals involved with normal derivatives, $\int_{A_{z-}} \rho Y_z\, dxdy$, $\int_{A_{z+}} \rho Y_z\, dxdy$, $\int_{A_{x-}} \rho F_x\, dxdz$ and $\int_{A_{x+}} \rho F_x\, dxdz$ can also be written out similarly. If we define

$$\begin{aligned}(c_{011}, c_{101}, c_{110}) &= (2/\alpha^2)(\bar{\rho}_{011}/g_0g_s, \bar{\rho}_{101}/h_0h_s, \bar{\rho}_{110}/k_0k_s),\\ (c_{211}, c_{121}, c_{112}) &= (2/\alpha^2)(\bar{\rho}_{211}/g_2g_s, \bar{\rho}_{121}/h_2h_s, \bar{\rho}_{112}/k_2k_s),\end{aligned} \tag{3.78}$$

then we can write all the integrals involving normal derivatives as

$$\begin{aligned}&\frac{1}{\alpha^2\bar{\rho}V}\int_{A_{x-}}\rho F_x\, dydz = (F_{111} - F_{011})c_{011}, \quad \frac{1}{\alpha^2\bar{\rho}V}\int_{A_{x+}}\rho F_x\, dydz = (F_{211} - F_{111})c_{211},\\ &\frac{1}{\alpha^2\bar{\rho}V}\int_{A_{y-}}\rho F_y\, dxdz = (F_{111} - F_{101})c_{101}, \quad \frac{1}{\alpha^2\bar{\rho}V}\int_{A_{y+}}\rho F_y\, dxdz = (F_{121} - F_{111})\,c_{121},\\ &\frac{1}{\alpha^2\bar{\rho}V}\int_{A_{z-}}\rho F_z\, dxdy = (F_{111} - F_{110})c_{110}, \quad \frac{1}{\alpha^2\bar{\rho}V}\int_{A_{z+}}\rho F_z\, dxdy = (F_{112} - F_{111})\,c_{112},\end{aligned} \tag{3.79}$$

### 3.6.2 Integrals with Tangential Derivatives

The tangential derivatives are more complicated than the normal ones. For instance, in integral $\int_{A_{z-}} \rho F_y \, dxdy$ (Fig. 3.2a and Fig. 3.3c), we adopt the notation

$$\begin{aligned} F_y|_{z-} &= F_y|_{(1,?,1-\frac{1}{2})} = \frac{1}{2}(F_y|_{(1,?,0)} + F_y|_{(1,?,1)}) \\ &= \begin{cases} \frac{1}{2}(F_y|_{(1,1-\frac{1}{2},0)} + F_y|_{(1,1-\frac{1}{2},1)}), & y < y_1; \\ \frac{1}{2}(F_y|_{(1,1+\frac{1}{2},0)} + F_y|_{(1,1+\frac{1}{2},1)}), & y > y_1; \end{cases} \\ &= \begin{cases} \frac{1}{2}(F_{110} - F_{100} + F_{111} - F_{101})/h_0, & y < y_1; \\ \frac{1}{2}(F_{120} - F_{110} + F_{121} - F_{111})/h_2, & y > y_1; \end{cases} \end{aligned} \tag{3.80}$$

where the first term, $F_y|_{z-}$, is the tangential derivative on the plane $A_{z-}$, i.e. $z = z_n - \frac{1}{2}k_{n-1}$ in the global system or $z = z_{1-\frac{1}{2}}$ in the local system; the second term, $F_y|_{(1,?,1-\frac{1}{2})}$, shows that this derivative is estimated on the $x$-axis ($x = x_1$ in the local system) and half-way between planes $z = z_0$ and $z = z_1$ (also in the local system), while the question mark in the place of the second subscript indicates that the position on the $y$-axis is yet to be determined. The third expression is the average of the corresponding derivatives on the two planes, $z = z_0$ and $z = z_1$. The fourth expression says that the derivatives are estimated differently in the $y$-direction; they are estimated at $y = y_{1-\frac{1}{2}}$ when $y < y_1$ and $y = y_{1+\frac{1}{2}}$ when $y > y_1$ which are approximated by the central difference formulae in the last step. The corresponding integral then can be estimated as

$$\begin{aligned} \int_{A_{z-}} \rho F_y \, dxdy &= \frac{1}{2h_0}(F_{110} - F_{100} + F_{111} - F_{101}) \left( \rho_{000} \frac{g_0}{2} \frac{h_0}{2} + \rho_{200} \frac{g_2}{2} \frac{h_0}{2} \right) \\ &+ \frac{1}{2h_2}(F_{120} - F_{110} + F_{121} - F_{111}) \left( \rho_{020} \frac{g_0}{2} \frac{h_2}{2} + \rho_{220} \frac{g_2}{2} \frac{h_2}{2} \right). \end{aligned} \tag{3.81}$$

Therefore,

$$\frac{1}{\alpha^2 \bar{\rho} V} \int_{A_{z-}} \rho F_y \, dxdy = (F_{110} - F_{100} + F_{111} - F_{101}) \frac{(\rho_{000} g_0 + \rho_{200} g_2)}{\alpha^2 \bar{\rho} g_s h_s k_s}$$

$$
\begin{aligned}
&+ \quad (F_{120} - F_{110} + F_{121} - F_{111}) \frac{(\rho_{020} g_0 + \rho_{220} g_2)}{\alpha^2 \bar{\rho} g_s h_s k_s} \\
&:= \quad (F_{110} - F_{100} + F_{111} - F_{101}) c_{100} \\
&+ \quad (F_{120} - F_{110} + F_{121} - F_{111}) c_{120}. \qquad (3.82)
\end{aligned}
$$

Similarly, for integral $\frac{1}{\alpha^2 \bar{\rho} V} \int_{A_{z+}} \rho F_y \, dxdy$, we have

$$
\begin{aligned}
F_y|_{z+} &= F_y|_{(1,?,1+\frac{1}{2})} = \frac{1}{2}(F_y|_{(1,?,1)} + F_y|_{(1,?,2)}) \\
&= \begin{cases} \frac{1}{2}(F_y|_{(1,1-\frac{1}{2},1)} + F_y|_{(1,1-\frac{1}{2},2)}), & y < y_1; \\ \frac{1}{2}(F_y|_{(1,1+\frac{1}{2},1)} + F_y|_{(1,1+\frac{1}{2},2)}), & y > y_1; \end{cases} \\
&= \begin{cases} \frac{1}{2}(F_{111} - F_{101} + F_{112} - F_{102}), & y < y_1; \\ \frac{1}{2}(F_{121} - F_{111} + F_{122} - F_{112}), & y > y_1; \end{cases} \qquad (3.83)
\end{aligned}
$$

and

$$
\begin{aligned}
\frac{1}{\alpha^2 \bar{\rho} V} \int_{A_{z+}} \rho F_y \, dxdy &= (F_{111} - F_{101} + F_{112} - F_{102}) \frac{(\rho_{002} g_0 + \rho_{202} g_2)}{\alpha^2 \bar{\rho} g_s h_s k_s} \\
&+ (F_{121} - F_{111} + F_{122} - F_{112}) \frac{(\rho_{022} g_0 + \rho_{222} g_2)}{\alpha^2 \bar{\rho} g_s h_s k_s}. \\
&:= (F_{111} - F_{101} + F_{112} - F_{102}) c_{102} \\
&+ (F_{121} - F_{111} + F_{122} - F_{112}) c_{122}. \qquad (3.84)
\end{aligned}
$$

Following the procedure that takes (3.80) to (3.82), all the integrals on $A_{x-}$, $A_{y-}$ and $A_{z-}$ can be worked out and written as

$$
\begin{aligned}
\frac{1}{\alpha^2 \bar{\rho} V} \int_{A_{x-}} \rho F_y \, dydz &= (F_{111} - F_{101} + F_{011} - F_{001}) \, c_{001} \\
&+ (F_{121} - F_{111} + F_{021} - F_{011}) \, c_{021} \\
\frac{1}{\alpha^2 \bar{\rho} V} \int_{A_{x-}} \rho F_z \, dydz &= (F_{111} - F_{110} + F_{011} - F_{010}) \, c_{010} \\
&+ (F_{112} - F_{111} + F_{012} - F_{011}) \, c_{012} \\
\frac{1}{\alpha^2 \bar{\rho} V} \int_{A_{y-}} \rho F_x \, dxdz &= (F_{111} - F_{011} + F_{101} - F_{001}) \, c_{001} \\
&+ (F_{211} - F_{111} + F_{201} - F_{101}) \, c_{201} \\
\frac{1}{\alpha^2 \bar{\rho} V} \int_{A_{y-}} \rho F_z \, dxdz &= (F_{111} - F_{110} + F_{101} - F_{100}) \, c_{100}
\end{aligned}
$$

$$
\begin{aligned}
& + (F_{112} - F_{111} + F_{102} - F_{101})\, c_{102} \\
\frac{1}{\alpha^2 \bar{\rho} V} \int_{A_{z-}} \rho F_x \, dxdy &= (F_{111} - F_{011} + F_{110} - F_{010})\, c_{010} \\
& + (F_{211} - F_{111} + F_{210} - F_{110})\, c_{210} \\
\frac{1}{\alpha^2 \bar{\rho} V} \int_{A_{z-}} \rho F_y \, dxdy &= (F_{111} - F_{101} + F_{110} - F_{100})\, c_{100} \\
& + (F_{121} - F_{111} + F_{120} - F_{110})\, c_{120}
\end{aligned} \tag{3.85}
$$

where we have defined

$$
c_{1pq} = \frac{\bar{\rho}_{1pq}}{\alpha^2 h_s k_s},\ c_{p1q} = \frac{\bar{\rho}_{p1q}}{\alpha^2 g_s k_s},\ c_{pq1} = \frac{\bar{\rho}_{pq1}}{\alpha^2 g_s h_s},\ p = 0,2,\ q = 0,2. \tag{3.86}
$$

Comparing (3.82) and (3.84), the former is the finite difference expression of an integral over the surface $A_{z-}$ which is located at $z = z_{1-\frac{1}{2}}$ while the latter is over $A_{z+}$ located at $z = z_{1+\frac{1}{2}}$. The only difference between the integrals is in the locations of the integration surfaces on the $z$-axis, which results in their respective finite difference expressions differing only in the 3rd subscript which is the one related to the $z$-coordinate. It is easy to see by comparing the finite difference expression for the integral over $A_{z-}$ with that over $A_{z+}$, that the 3rd subscript is incremented by 1 for $F_{pq?}$ and by 2 for $c_{pq?}$. By analogy, we can obtain the finite difference expressions for the integrals over $A_{x+}$ from those over $A_{x-}$ at once, simply by incrementing the 1st subscript by 1 for $F_{?pq}$ and by 2 for $c_{?pq}$. For the integrals over $A_{y-}$ and $A_{y+}$, the 2nd subscript should be similarly incremented.

### 3.6.3 3D Cell-integral Equations

Inserting all the integrals into equations (3.70), (3.71) and (3.72), we have

$$
\begin{aligned}
iX_{111} &= (X_{121} - X_{111})c_{121} - (X_{111} - X_{101})c_{101} \\
&+ (X_{112} - X_{111})c_{112} - (X_{111} - X_{110})c_{110} \\
&+ (Y_{111} - Y_{011} + Y_{101} - Y_{001})c_{001} + (Y_{211} - Y_{111} + Y_{201} - Y_{101})c_{201}
\end{aligned}
$$

$$
\begin{aligned}
&- (Y_{121} - Y_{021} + Y_{111} - Y_{011})c_{021} - (Y_{221} - Y_{121} + Y_{211} - Y_{111})c_{221} \\
&+ (Z_{111} - Z_{011} + Z_{110} - Z_{010})c_{010} + (Z_{211} - Z_{111} + Z_{210} - Z_{110})c_{210} \\
&- (Z_{112} - Z_{012} + Z_{111} - Z_{011})c_{012} - (Z_{212} - Z_{112} + Z_{211} - Z_{111})c_{212}
\end{aligned}
\tag{3.87}
$$

$$
\begin{aligned}
iY_{111} &= (Y_{211} - Y_{111})c_{211} - (Y_{111} - Y_{011})c_{011} \\
&+ (Y_{112} - Y_{111})c_{112} - (Y_{111} - Y_{110})c_{110} \\
&+ (X_{111} - X_{101} + X_{011} - X_{001})c_{001} + (X_{121} - X_{111} + X_{021} - X_{011})c_{021} \\
&- (X_{211} - X_{201} + X_{111} - X_{101})c_{201} - (X_{221} - X_{211} + X_{121} - X_{111})c_{221} \\
&+ (Z_{111} - Z_{101} + Z_{110} - Z_{100})c_{100} + (Z_{121} - Z_{111} + Z_{120} - Z_{110})c_{120} \\
&- (Z_{112} - Z_{102} + Z_{111} - Z_{101})c_{102} - (Z_{122} - Z_{112} + Z_{121} - Z_{111})c_{122}
\end{aligned}
\tag{3.88}
$$

$$
\begin{aligned}
iZ_{111} &= (Z_{211} - Z_{111})c_{211} - (Z_{111} - Z_{011})c_{011} \\
&+ (Z_{121} - Z_{111})c_{121} - (Z_{111} - Z_{101})c_{101} \\
&+ (X_{111} - X_{110} + X_{011} - X_{010})c_{010} + (X_{112} - X_{111} + X_{012} - X_{011})c_{012} \\
&- (X_{211} - X_{210} + X_{111} - X_{110})c_{210} - (X_{212} - X_{211} + X_{112} - X_{111})c_{212} \\
&+ (Y_{111} - Y_{110} + Y_{101} - Y_{100})c_{100} + (Y_{112} - Y_{111} + Y_{102} - Y_{101})c_{102} \\
&- (Y_{121} - Y_{120} + Y_{111} - Y_{110})c_{120} - (Y_{122} - Y_{121} + Y_{112} - Y_{111})c_{122}
\end{aligned}
\tag{3.89}
$$

By re-arranging the terms in these three equations, we have

$$
\begin{aligned}
(i + c_{101} + c_{121} + c_{110} + c_{112})X_{111} &= c_{101}X_{101} + c_{121}X_{121} + c_{110}X_{110} + c_{112}X_{112} \\
&+(c_{221} - c_{201} + c_{001} - c_{021})Y_{111} + c_{201}Y_{201} - c_{221}Y_{221} - c_{001}Y_{001} + c_{021}Y_{021} \\
&+(c_{021} - c_{001})Y_{011} - (c_{221} - c_{201})Y_{211} - (c_{201} - c_{001})Y_{101} + (c_{221} - c_{021})Y_{121} \\
&+(c_{212} - c_{210} + c_{010} - c_{012})Z_{111} + c_{012}Z_{012} - c_{212}Z_{212} - c_{010}Z_{010} + c_{210}Z_{210} \\
&+(c_{012} - c_{010})Z_{011} - (c_{212} - c_{210})Z_{211} - (c_{210} - c_{010})Z_{110} + (c_{212} - c_{012})Z_{112}
\end{aligned}
$$

(3.90)

$$
\begin{aligned}
(i + c_{011} + c_{211} + c_{110} + c_{112})Y_{111} &= c_{011}Y_{011} + c_{211}Y_{211} + c_{110}Y_{110} + c_{112}Y_{112} \\
&+(c_{221} - c_{201} + c_{001} - c_{021})X_{111} + c_{201}X_{201} - c_{221}X_{221} - c_{001}X_{001} + c_{021}X_{021} \\
&+(c_{201} - c_{001})X_{101} - (c_{221} - c_{021})X_{121} - (c_{021} - c_{001})X_{011} + (c_{221} - c_{201})X_{211} \\
&+(c_{122} - c_{102} + c_{100} - c_{120})Z_{111} + c_{120}Z_{120} - c_{122}Z_{122} - c_{100}Z_{100} + c_{102}Z_{102} \\
&+(c_{102} - c_{100})Z_{101} - (c_{122} - c_{120})Z_{121} - (c_{120} - c_{100})Z_{110} + (c_{122} - c_{102})Z_{112}
\end{aligned}
\tag{3.91}
$$

$$
\begin{aligned}
(i + c_{011} + c_{211} + c_{101} + c_{121})Z_{111} &= c_{011}Z_{011} + c_{211}Z_{211} + c_{101}Z_{101} + c_{121}Z_{121} \\
&+(c_{212} - c_{210} + c_{010} - c_{012})X_{111} + c_{012}X_{012} - c_{212}X_{212} - c_{010}X_{010} + c_{210}X_{210} \\
&+(c_{210} - c_{010})X_{110} - (c_{212} - c_{012})X_{112} - (c_{012} - c_{010})X_{011} + (c_{212} - c_{210})X_{211} \\
&+(c_{122} - c_{120} + c_{100} - c_{102})Y_{111} + c_{102}Y_{102} - c_{122}Y_{122} - c_{100}Y_{100} + c_{120}Y_{120} \\
&+(c_{120} - c_{100})Y_{110} - (c_{122} - c_{102})Y_{112} - (c_{102} - c_{100})Y_{101} + (c_{122} - c_{120})Y_{121}
\end{aligned}
\tag{3.92}
$$

In fact, if we make a transformation

$$X \to Y \to Z \to X, \quad x \to y \to z \to x, \tag{3.93}$$

in the analytical form of the $X$, $Y$ and $Z$ equations given by (3.70), (3.71) and (3.72), the equations also transfer in the same order, i.e.

$X$-equation $\to$ $Y$-equation $\to$ $Z$-equation $\to$ $X$-equation.

It can be confirmed by (3.79), (3.82), (3.85) and (3.86) that the corresponding transformations of the finite difference expressions for the integrals would be

$$
\begin{array}{llll}
X_{ijk} & \to Y_{kij} & \to Z_{jki} & \to X_{ijk} \\
c_{lmn} & \to c_{nlm} & \to c_{mnl} & \to c_{lmn}.
\end{array}
\tag{3.94}
$$

By this means, we can also obtain the $Y$- and $Z$-equations from the $X$-equation alone. It serves as a simple check on the correctness of the final expressions.

### 3.6.4 3D Auxiliary Equations

In the 2D case, besides the cell-integral form of basic equation (2.46), we also needed an auxiliary equation similar to (2.69) to help with the convergence problem. The 3D auxiliary equation corresponding to (2.69) can be obtained from the vector integral relation given by Jones (1964, p113, eq. 23) in the form

$$\int_V \nabla(\nabla \cdot \mathbf{B})\, dv = \oint_S (\nabla \cdot \mathbf{B})\, d\mathbf{S} = 0. \tag{3.95}$$

In scaled component form this is:

$$\frac{1}{\alpha^2 V}\left[\int_{A_{x+}} - \int_{A_{x-}}\right](X_x + Y_y + Z_z)\, dydz = 0 \tag{3.96}$$

$$\frac{1}{\alpha^2 V}\left[\int_{A_{y+}} - \int_{A_{y-}}\right](X_x + Y_y + Z_z)\, dxdz = 0 \tag{3.97}$$

$$\frac{1}{\alpha^2 V}\left[\int_{A_{z+}} - \int_{A_{z-}}\right](X_x + Y_y + Z_z)\, dxdy = 0 \tag{3.98}$$

Once again, we see that the transformation (3.93) connects these equations as follows: Eq. (3.96) → Eq. (3.97) → Eq. (3.98) → Eq. (3.96). The integrals that involve normal or tangential derivatives can be obtained from (3.79) or (3.85) respectively, by assuming that $\rho/\bar{\rho} \equiv 1$ which leads to the following new definitions:

$$\begin{aligned} c_{011} &= \frac{2\bar{\rho}_{011}}{\alpha^2 g_0 g_s} = \frac{2}{\alpha^2 g_0 g_s} =: d_{011}, \quad c_{211} = \frac{2\bar{\rho}_{211}}{\alpha^2 g_2 g_s} = \frac{2}{\alpha^2 g_2 g_s} =: d_{211} \\ c_{1pq} &= \frac{1}{\alpha^2 h_s k_s} =: d_1,\ c_{p1q} = \frac{1}{\alpha^2 g_s k_s} =: d_2,\ c_{pq1} = \frac{1}{\alpha^2 g_s h_s} =: d_3 \end{aligned} \tag{3.99}$$

as well as the following expressions for the integrals:

$$\begin{aligned} \frac{1}{\alpha^2 V}\int_{A_{x-}} X_x\, dydz &= (X_{111} - X_{011})d_{011}, \\ \frac{1}{\alpha^2 V}\int_{A_{x-}} Y_y\, dydz &= (Y_{121} - Y_{101} + Y_{021} - Y_{001})d_3, \end{aligned}$$

$$\begin{aligned}
\frac{1}{\alpha^2 V}\int_{A_{z-}} Z_z\,dydz &= (Z_{112}-Z_{110}+Z_{021}-Z_{001})d_2,\\
\frac{1}{\alpha^2 V}\int_{A_{x+}} X_x\,dydz &= (X_{211}-X_{111})d_{211},\\
\frac{1}{\alpha^2 V}\int_{A_{x+}} Y_y\,dydz &= (Y_{221}-Y_{201}+Y_{121}-Y_{101})d_3,\\
\frac{1}{\alpha^2 V}\int_{A_{z+}} Z_z\,dydz &= (Z_{211}-Z_{211}+Z_{112}-Z_{110})d_2. \qquad (3.100)
\end{aligned}$$

Substituting all the above integral expressions into (3.96), we obtain

$$\begin{aligned}
(d_{211}+d_{011})X_{111} &= d_{211}X_{211}+d_{011}X_{011} \qquad (3.101)\\
&+d_3(Y_{221}-Y_{201}-Y_{021}+Y_{001})+d_2(Z_{212}-Z_{210}-Z_{012}+Z_{010})
\end{aligned}$$

Applying the transformation of (3.93) and (3.94) to (3.99), we can see that $d_1 \rightarrow d_2 \rightarrow d_3 \rightarrow d_1$. The same transformations take (3.101) into

$$\begin{aligned}
(d_{121}+d_{101})Y_{111} &= d_{121}Y_{121}+d_{101}Y_{101} \qquad (3.102)\\
&+d_1(Z_{122}-Z_{120}-Z_{102}+Z_{100})+d_3(X_{221}-X_{021}-X_{201}+X_{001}),\\
(d_{112}+d_{110})Z_{111} &= d_{112}Z_{112}+d_{110}Z_{110} \qquad (3.103)\\
&+d_2(X_{212}-X_{012}-X_{210}+X_{010})+d_1(Y_{122}-Y_{102}-Y_{120}+Y_{100}.
\end{aligned}$$

Thus we have obtained all three auxiliary equations required to aid convergence of the three cell-integral equations.

### 3.6.5 3D Finite Difference Equations

By adding (3.101), (3.102) and (3.103) to (3.90), (3.91) and (3.92) respectively, we obtain the finite difference equations applied in the region $0 < z < z_N$ as:

$$\begin{aligned}
&(i+d_{011}+d_{211}+c_{101}+c_{121}+c_{110}+c_{112})X_{111} =\\
&\quad d_{011}X_{011}+d_{211}X_{211}+c_{101}X_{101}+c_{121}X_{121}+c_{110}X_{110}+c_{112}X_{112}\\
&\quad +(c_{221}-c_{021}+c_{001}-c_{201})Y_{111}+(c_{212}-c_{012}+c_{010}-c_{210})Z_{111}
\end{aligned}$$

$$+(d_3 - c_{001})Y_{013} - (d_3 - c_{021})Y_{021} + (d_3 - c_{221})Y_{221} - (d_3 - c_{201})Y_{201}$$
$$+(c_{021} - c_{001})Y_{001} - (c_{221} - c_{201})Y_{211} - (c_{201} - c_{001})Y_{101} + (c_{221} - c_{021})Y_{121}$$
$$+(d_2 - c_{010})Z_{010} - (d_2 - c_{210})Z_{210} + (d_2 - c_{212})Z_{212} - (d_2 - c_{012})Z_{012}$$
$$+(c_{012} - c_{010})Z_{011} - (c_{212} - c_{210})Z_{211} - (c_{210} - c_{010})Z_{110} + (c_{212} - c_{012})Z_{112} \tag{3.104}$$

$$(i + c_{011} + c_{211} + d_{101} + d_{121} + c_{110} + c_{112})Y_{111} =$$
$$c_{011}Y_{011} + c_{211}Y_{211} + d_{101}Y_{101} + d_{121}Y_{121} + c_{110}Y_{110} + c_{112}Y_{112}$$
$$+(c_{221} - c_{201} + c_{001} - c_{021})X_{111} + (c_{122} - c_{102} + c_{100} - c_{120})Z_{111}$$
$$+(d_3 - c_{001})X_{001} - (d_3 - c_{021})X_{021} + (d_3 - c_{221})X_{221} - (d_3 - c_{201})X_{201}$$
$$+(c_{201} - c_{001})X_{101} - (c_{221} - c_{021})X_{121} - (c_{021} - c_{001})X_{011} + (c_{221} - c_{201})X_{211}$$
$$+(d_1 - c_{100})Z_{100} - (d_1 - c_{102})Z_{102} + (d_1 - c_{122})Z_{122} - (d_1 - c_{120})Z_{120}$$
$$+(c_{102} - c_{100})Z_{101} - (c_{122} - c_{120})Z_{121} - (c_{120} - c_{100})Z_{110} + (c_{122} - c_{102})Z_{112} \tag{3.105}$$

$$(i + c_{011} + c_{211} + c_{101} + c_{121} + d_{110} + d_{112})Z_{111} =$$
$$c_{011}Z_{011} + c_{211}Z_{211} + c_{101}Z_{101} + c_{121}Z_{121} + d_{110}Z_{110} + d_{112}Z_{112}$$
$$+(c_{212} - c_{210} + c_{010} - c_{012})X_{111} + (c_{122} - c_{120} + c_{100} - c_{102})Y_{111}$$
$$+(d_2 - c_{010})X_{010} - (d_2 - c_{210})X_{210} + (d_2 - c_{212})X_{212} - (d_2 - c_{012})X_{012}$$
$$+(c_{210} - c_{010})X_{110} - (c_{212} - c_{012})X_{112} - (c_{012} - c_{010})X_{011} + (c_{212} - c_{210})Y_{211}$$
$$+(d_1 - c_{100})Y_{100} - (d_1 - c_{120})Y_{120} + (d_1 - c_{122})Y_{122} - (d_1 - c_{102})Y_{102}$$
$$+(c_{120} - c_{100})Y_{110} - (c_{122} - c_{102})Y_{112} - (c_{102} - c_{100})Y_{101} + (c_{122} - c_{120})Y_{121}$$
$$\lambda = 2...L-1, \quad \mu = 2...M-1, \quad \nu = 2...N-1 \tag{3.106}$$

where $c_{pqr}$ are given by (3.78), (3.86) and $d_{pqr}$ by (3.99) respectively.

It can be easily verified that at a node where $\nabla\rho = 0$, we have

$$\begin{array}{rcll} (c_{pi1}, c_{1p1}, c_{11p}) & = & (d_{p11}, d_{1p1}, d_{11p}), & p = 0,2 \\ (c_{1pq}, c_{p1q}, c_{pq1}) & = & (d_1, d_2, d_3), & p = 0,2,\ q = 0,2 \end{array} \tag{3.107}$$

and the above equations degenerate into

$$(i + d_{011} + d_{211} + d_{101} + d_{121} + d_{110} + d_{112})F_{111} =$$
$$d_{011}X_{011} + d_{211}F_{211} + d_{101}X_{101} + d_{121}F_{121} + d_{110}X_{110} + d_{112}F_{112}$$

which can be re-written as

$$\begin{aligned} i\alpha^2 F_{111} &= \frac{2}{g_2 g_s}F_{211} - \frac{2}{g_0 g_2}F_{111} + \frac{2}{g_0 g_s}F_{011} \\ &+ \frac{2}{h_2 h_s}F_{121} - \frac{2}{h_2 h_2}F_{111} + \frac{2}{h_0 h_s}F_{101} \\ &+ \frac{2}{k_2 k_s}F_{112} - \frac{2}{k_0 k_2}F_{111} + \frac{2}{k_0 k_s}F_{110} \end{aligned} \tag{3.108}$$

where $F$ stands for $X$, $Y$ or $Z$. Obviously, this represents the correct finite difference expression of the differential equation of magnetic field $\mathbf{B}$ applied to a uniform region, i.e.

$$\nabla^2\mathbf{B} = i\alpha^2\mathbf{B}, \qquad \alpha^2 = \omega\mu_0/\rho.$$

It can also be verified that when the conductivity structure is two-dimensional, the 3D equations (3.104), (3.105) and (3.106) reduce to those for the 2D case. Thus, if the strike is in the $y$-direction, then (3.104) and (3.106) degenerate to the 2D E-polarization equations (2.107) and (2.108) respectively, while (3.105) vanishes. If the strike is in the $x$-direction, then (3.104) degenerates to the 2D B-polarization equation (2.126), while (3.105) and (3.106) vanish.

# Chapter 4

# THREE-DIMENSIONAL NUMERICAL MODELLING RESULTS

Computer programs (in FORTRAN 77) have been developed to solve 3D forward modelling problems by using the finite difference equations obtained in the previous chapters. These programs are EM2DBD, EM2DED and EM3D. EM2DBD solves 2D B-polarization problems in order to provide boundary conditions at the side boundaries $x = x_1$ and $x = x_L$ of the model shown in Fig. 1.2. EM2DED provides the E-polarization solutions for the boundaries at $y = y_1$ and $y = y_M$. EM3D solves the 3D problem by using the boundary conditions prepared by EM2DBD and EM2DED. More detailed descriptions on the programs and the instruction on how to use them are given separately in EM3D PROGRAM GUIDE. Some of the numerical results obtained during the process of the development of the programs and the progress report can be found in the following publication and presentations: Pu, Agarwal and Weaver (1988); Weaver and Pu (1988); Pu, Agarwal and Weaver (1991, 1992a, 1992b, 1993a, 1993b).

In this chapter, we will show a few representative numerical results calculated by the algorithm developed in this thesis; some of these results are used for checking the accuracy of the computer program, others are applications for investigating the properties of the EM induction phenomena. Since our algorithm solves directly for the three magnetic components, it is convenient to use induction vectors, which depend only on the magnetic fields, to display the calculated results in the applications, thereby avoiding the numerical differentiation

required to calculate electric fields.

## 4.1 A Check of Accuracy

In order to check the computer program, some models have been calculated and compared with respect to the results given by existing programs. First, we compare against 2D programs. In the previous chapter, when deriving the 3D equations, we have shown that our 3D equations can degenerate into correct 2D forms when the given 3D model has a 2D conductivity distribution, i.e. the conductivity structure is uniform along one horizontal direction (the strike direction). For such a model, if we have programmed our formulae correctly and the 3D numerical computation is stable and converges, then we should obtain the solution with 2D configuration as well, i.e. the solution should be uniform along the direction of the strike. The values of this 3D solution in a cross-sectional plane that is normal to the strike should be the correct 2D solution for the 2D cross-sectional structure.

These 2D values can be compared against the solutions for the same 2D structure given by established 2D forward modeling programs, such as Brewitt-Taylor and Weaver (1976), Green and Weaver (1978) etc. Several such models have been computed and compared, some of them are for B-polarization, but most of them are for E-polarization and among them are the two test models used in Chapter 2, i.e. the model shown by Fig. 2.2 and Fig. 2.5. They all produce very satisfactory results when compared with the solutions given by the 2D programs by Poll (1994) and by Brewitt-Taylor and Weaver (1976). In order to see if the 3D results are uniform along the strike direction for 2D conductivity distribution, two 3D models with 2D structures same as the left-half and the front-half of the model shown in Fig. 4.8 for E- and B-polarizations respectively have been studied. The results were so uniform that when the 2D

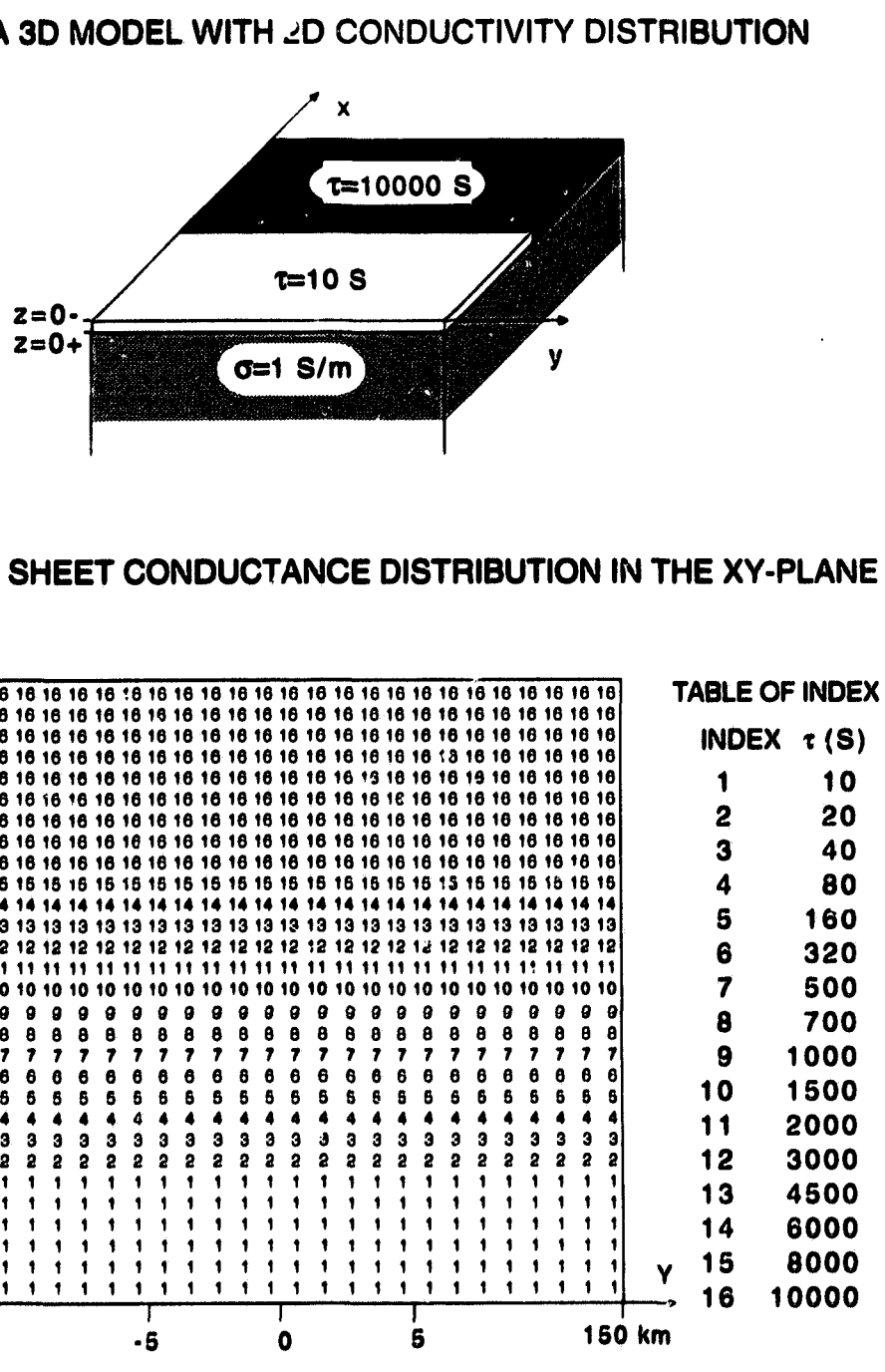


Figure 4.1: A 3D thin sheet model with coastline-like 2D conductivity structure.

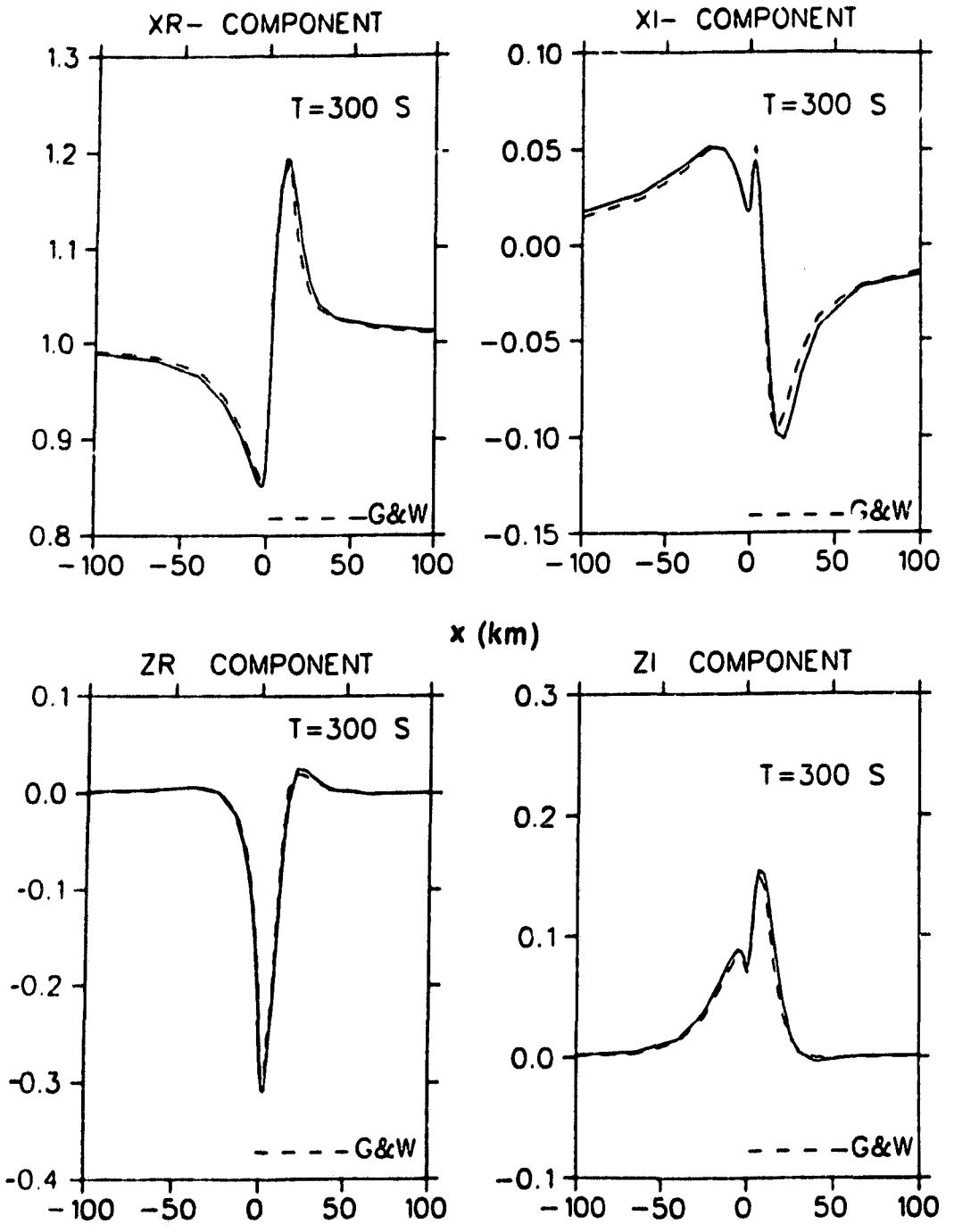


Figure 4.2: Variations of the real and imaginary parts of the E-polarization magnetic fields ($X$ and $Z$, normalized by $B_0$) above the thin sheet in the $xz$-plane for the model shown in Fig. 4.1 with the period of the source field T=300 s. The solid and broken lines depict the results given by the 3D program of this thesis and Green and Weaver (1978) respectively.

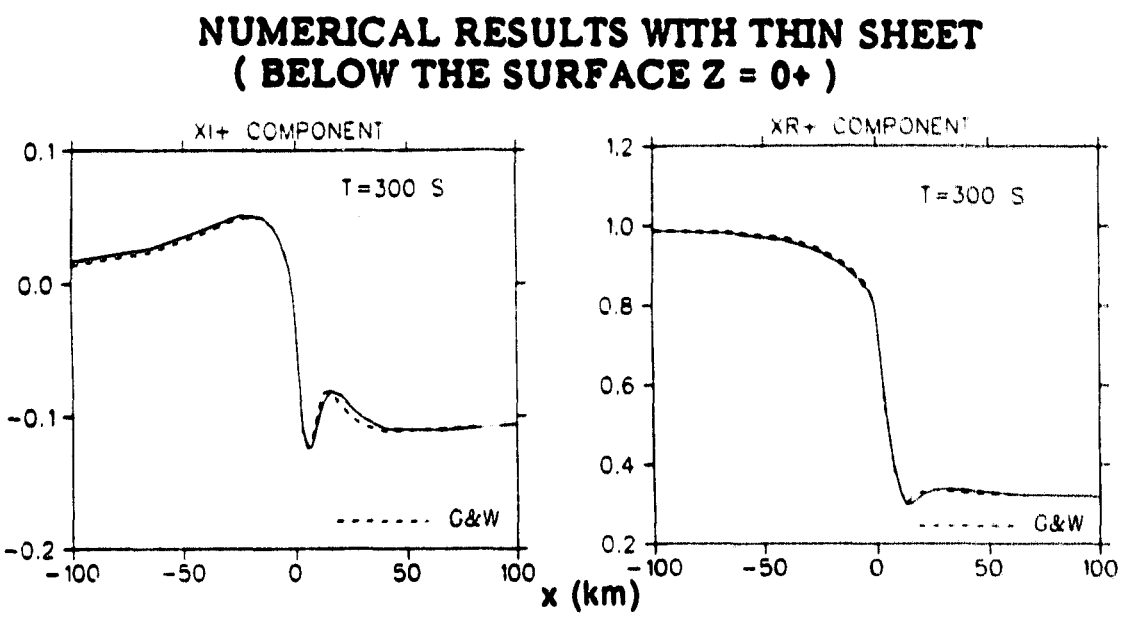


Figure 4.3: Same as in Fig. 4.2, but only the results for the $X$-component (normalized by $B_0$) beneath the thin sheet are ploted, those for the $Z$-component are the same as above the thin sheet.

variations of the magnetic fields in several different cross-sections normal to the strike were plotted together, they are practically indistinguishable from one another.

The comparisons between the 3D and 2D results for a thin sheet model are presented here. The model, as shown in Fig. 4.1, has a coastline-like lateral conductivity contrast at the top with the strike lying in the $y$-direction. Beneath this conductivity contrast is the uniform half space with the resistivity $\rho \equiv 1$ $\Omega$m. The conductivity contrast at the top is simulated by a thin sheet layer. The conductance of the thin sheet layer increases from 10 S to 10000 S in the $x$-direction within a 20 km wide transition zone. Fig. 4.1 shows the model and the thin sheet conductance distribution in the grid cells in the $xy$-plane, note that since variable grid steps are used, the scales in the $x$ and $y$ directions are not linear. Fig. 4.1 also shows the table for the index numbers and the corresponding conductance values they represent. The results are compared against those given by the 2D thin sheet program developed by Green and Weaver (1978), as shown

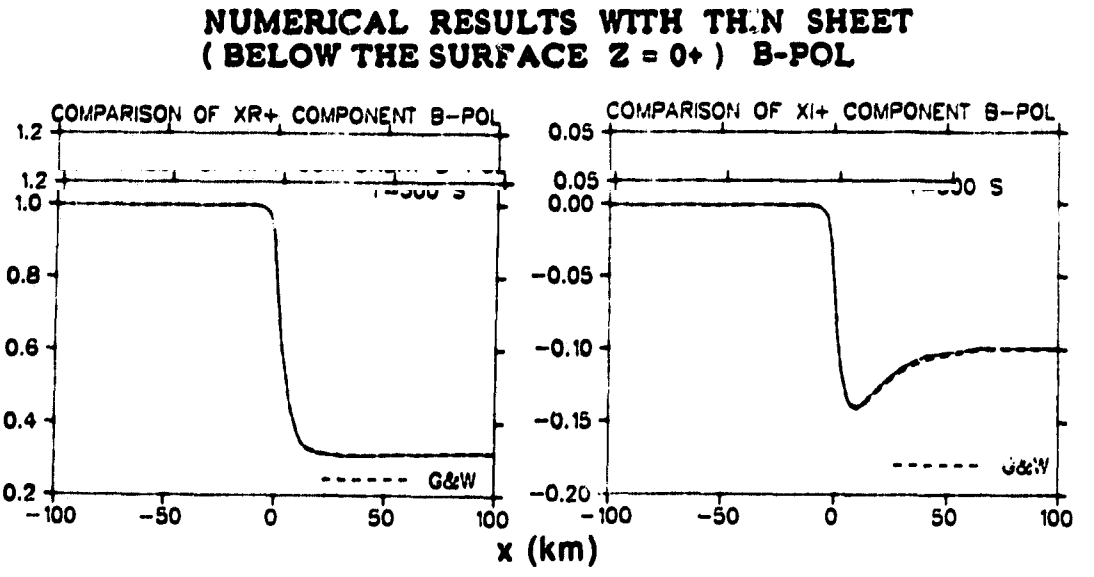


Figure 4.4: Variations of the real and imaginary parts of the B-polarization magnetic fields ($X$, normalized by $B_0$) beneath the thin sheet in the $yz$-plane for a model which is obtained by rotating the model shown in Fig. 4.1 90° clockwise through the $z$-axis.

in Fig. 4.2, 4.3 and 4.4, where the solid lines depict the results computed by our new program and the broken lines are by Green and Weaver. Both Fig. 4.2 and 4.3 are the results for the E-polarization problem. Fig. 4.2 are the results above the thin sheet layer and Fig. 4.3 are the results beneath the thin sheet layer. We see that in both locations, above and beneath the thin sheet, our solution matches that of Green and Weaver. In order to compute the B-polarization magnetic variations for the 2D structure shown in Fig. 4.1, we have to rotate the model through 90° clockwise about the $z$-axis (viewing from above the Earth). Since the magnetic field is constant above the thin sheet, only the results beneath the thin sheet at $z = 0+$ are plotted (Fig. 4.4). We see that our 3D results match almost exactly the 2D results obtained by Green and Weaver (1978).

A 3D thin sheet model, as shown in Fig. 4.5, was also calculated. The results were compared with those given by McKirdy, Weaver and Dawson (1985), which is a well accepted 3D thin-sheet program. Fig. 4.6 shows the results

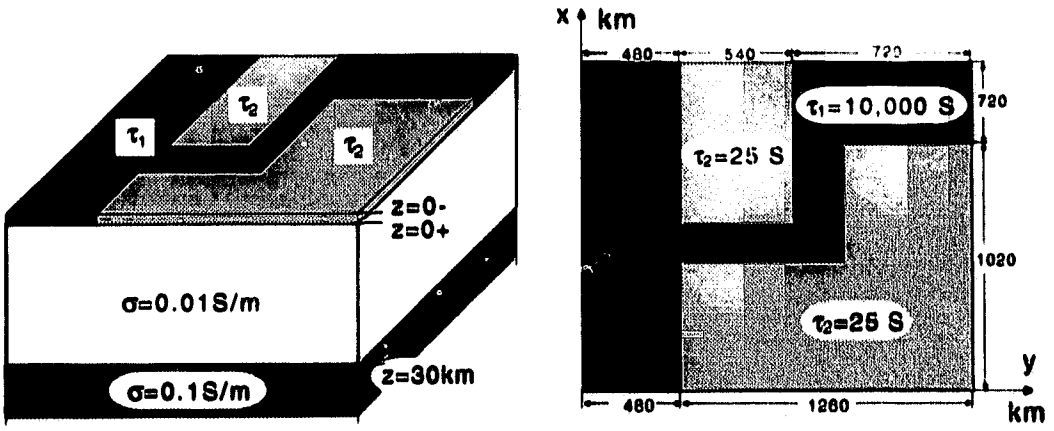


Figure 4.5: A 3D thin sheet model. $\tau_1$ and $\tau_2$ represent the conductances of the ocean and the land respectively. The rectangle in the top part simulates penisular.

computed by our new 3D program and Fig. 4.7 shows the results given by McKirdy, Weaver and Dawson. The two results show very similar features in all the three components $X$, $Y$ and $Z$. This gives us confidence that our new program is giving a sensible 3D result. There are also some differences. For example, in the plot of the $X$-component for the results of McKirdy, Weaver and Dawson (1985), variations occur along the edges $x = x_0$ and $x = x_L$ where 2D B-polarization results apply, that is where the $X$-component (which is normal to the plane) should be constant on the surface boundary. The reason that the results given by the program of McKirdy, Weaver and Dawson vary along 2D B-polarization boundaries might be that the boundary condition in the program is based on the assumption that the normal derivatives tend to zero at horizontal infinity. There is a difficulty with this boundary condition; the program uses equal grid steps and only allowed 30 by 30 grid points at the time when this model was calculated. If a smaller grid step were used, then the side boundary would not be far enough from the nearest conductivity contrast, or if a larger grid step were used, then the grid would not be fine enough near the conductivity contrast. In our new algorithm, not only are the correct 2D solutions used for

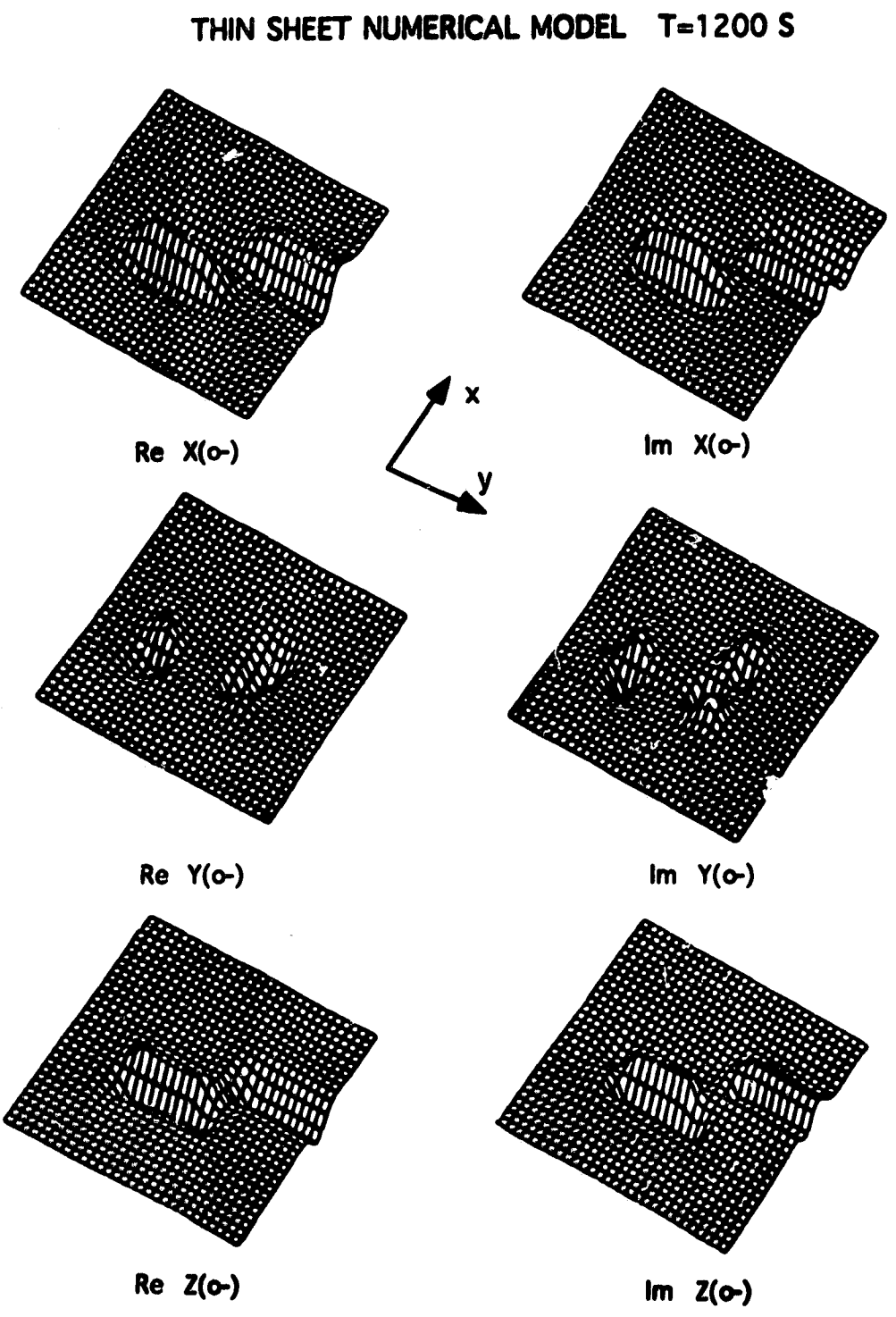


Figure 4.6: Perspective plots of the real and imaginary parts of the magnetic field components (X,Y,Z) for a regional magnetic field in the $x$-direction, calculated by the 3D program developed in this thesis.

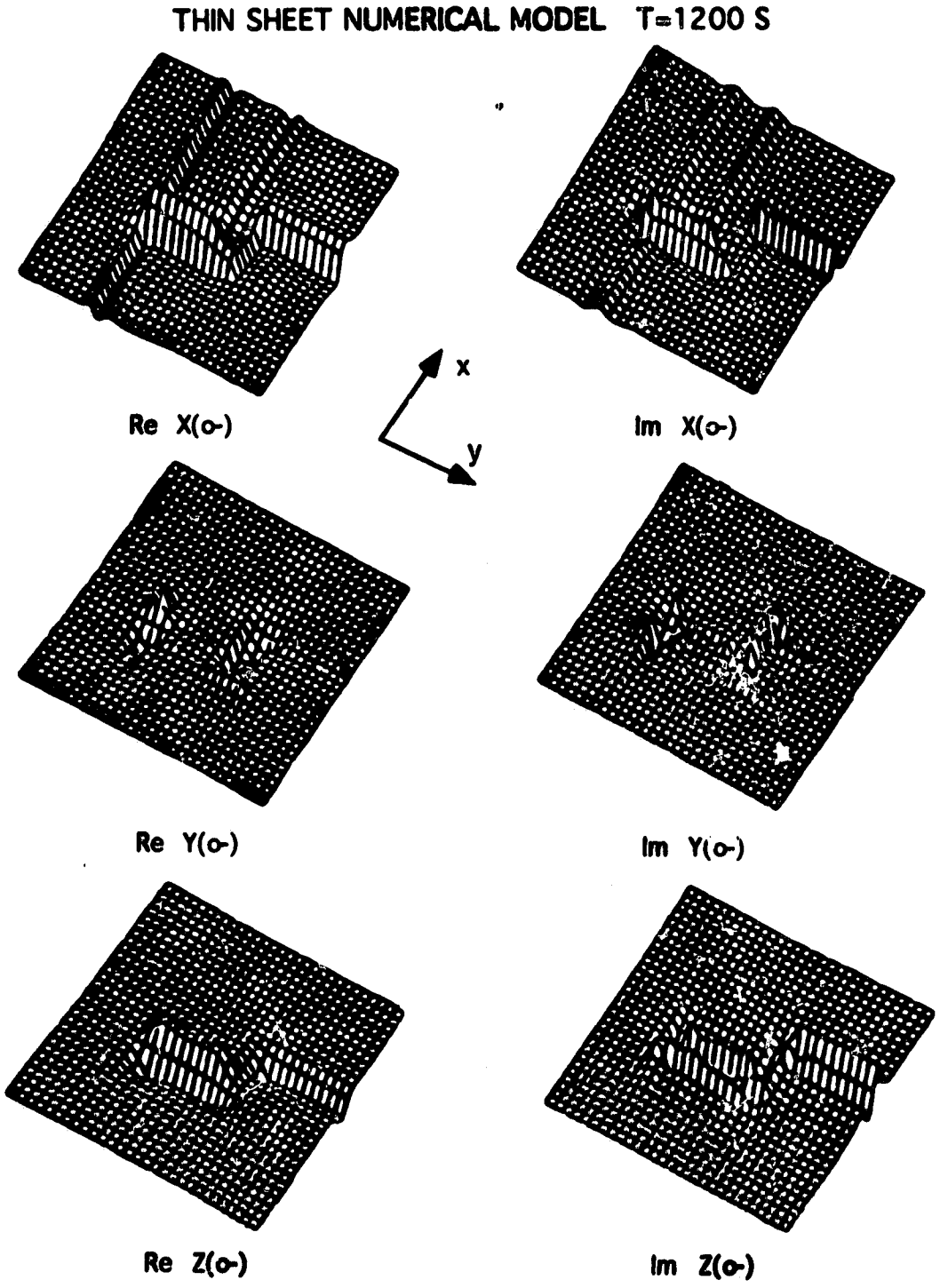


Figure 4.7: Perspective plots of the real and imaginary parts of the magnetic field components (X,Y,Z) for a regional magnetic field in the $x$-direction, calculated by McKirdy, Weaver and Daswon (1985).

the side boundary conditions, but also variable grid steps on a more than 40 by 40 grid can be handled comfortably by the IBM 3090 main frame computer at the University of Victoria. Therefore, our results are believed to be better than those of McKirdy, Weaver and Dawson (1985).

## 4.2 A Model with Crossed Lateral Conductivity Contrasts

The model, as shown in Fig. 4.8, consists of two different lateral variations in conductivity in perpendicular directions: a near surface 2D structure with a S-N strike and a deep buried 2D structure with a W-E strike. The former structure

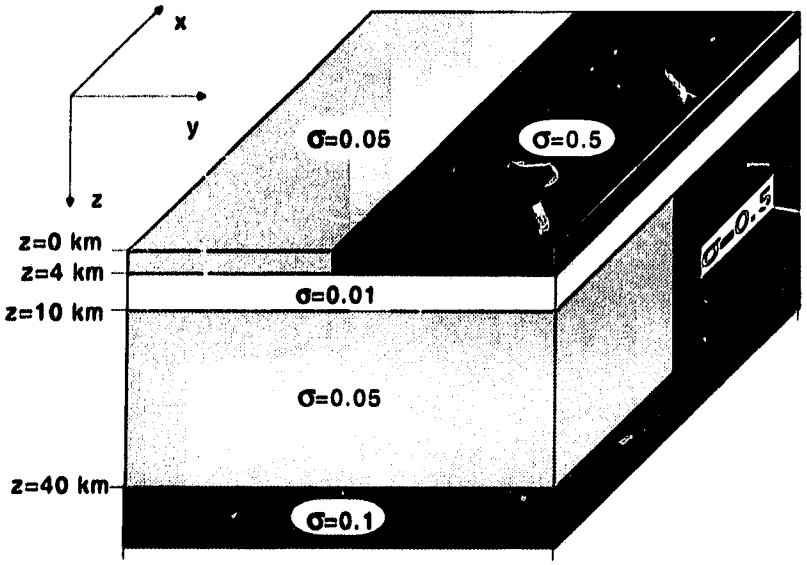


Figure 4.8: A model with crossed lateral conductivity contrasts.

can be represented either by a thin sheet layer of conductance of $\tau = 200$ S and $\tau = 2000$ S respectively or by a layer of 4 km thick with $\sigma = 0.05$ S/m and $\sigma = 0.5$ S/m respectively, and the latter structure is 30 km thick with $\sigma = 0.05$ S/m and $\sigma = 0.5$ S/m respectively. The two conductivity contrasts are separated by a 6 km thick of uniform resistive layer with $\sigma = 0.01$ S/m. Underlying the W-E strike of the deep buried structure is uniform half space with $\sigma = 0.1$ S/m.

A similar model with the same structure but different parameters has also been studied where the surface lateral conductivity contrast has been simulated by a thin sheet layer. The results were presented at the 10th IUGG meeting in Vienna in 1991 (Pu, Agarwal and Weaver, 1990). In the study presented in this thesis, however, we have chosen to represent the top structure by a layer with finite thickness of 4 km.

Calculations have been done for a range of periods, although only six of them (10, 100, 500, 1000, 2000, 10000 s) are presented here in Fig. 4.9. The same results are also included in Weaver (1994, p284). The results clearly show that the induction vectors (with the directions reversed in all the six plots) rotate 90° from E-W to N-S as the period increases from 10 s to 10000 s. At short periods induction vectors point towards the good conductor in the surface anomaly. At very long periods the effect of the deep anomaly is dominant and the directions of induction vectors reveal its perpendicular strike.

At intermediate periods the directions of the induction vectors reflect the combined effect of the surface and deep seated anomalies. Directions can vary from site to site. The standard interpretation that there is a good conductor in the direction indicated by the induction vector should be used with caution.

## 4.3 Small Conductive Block Over Buried Dividing Regions

The results of this model were presented at the Canadian Geophysical Union Annual Meeting held in Banff, May 9-11, 1993 (Pu, Agarwal and Weaver, 1993). In this study, distortion effects in electromagnetic induction due to the presence of near surface inhomogeneities have been investigated for a series of simple synthetic models. The study was conducted primarily as a preliminary to an intended investigation of various decompositions of the impedance tensor.

The basic model, as shown in Fig. 4.10, consists of a small conductive block of

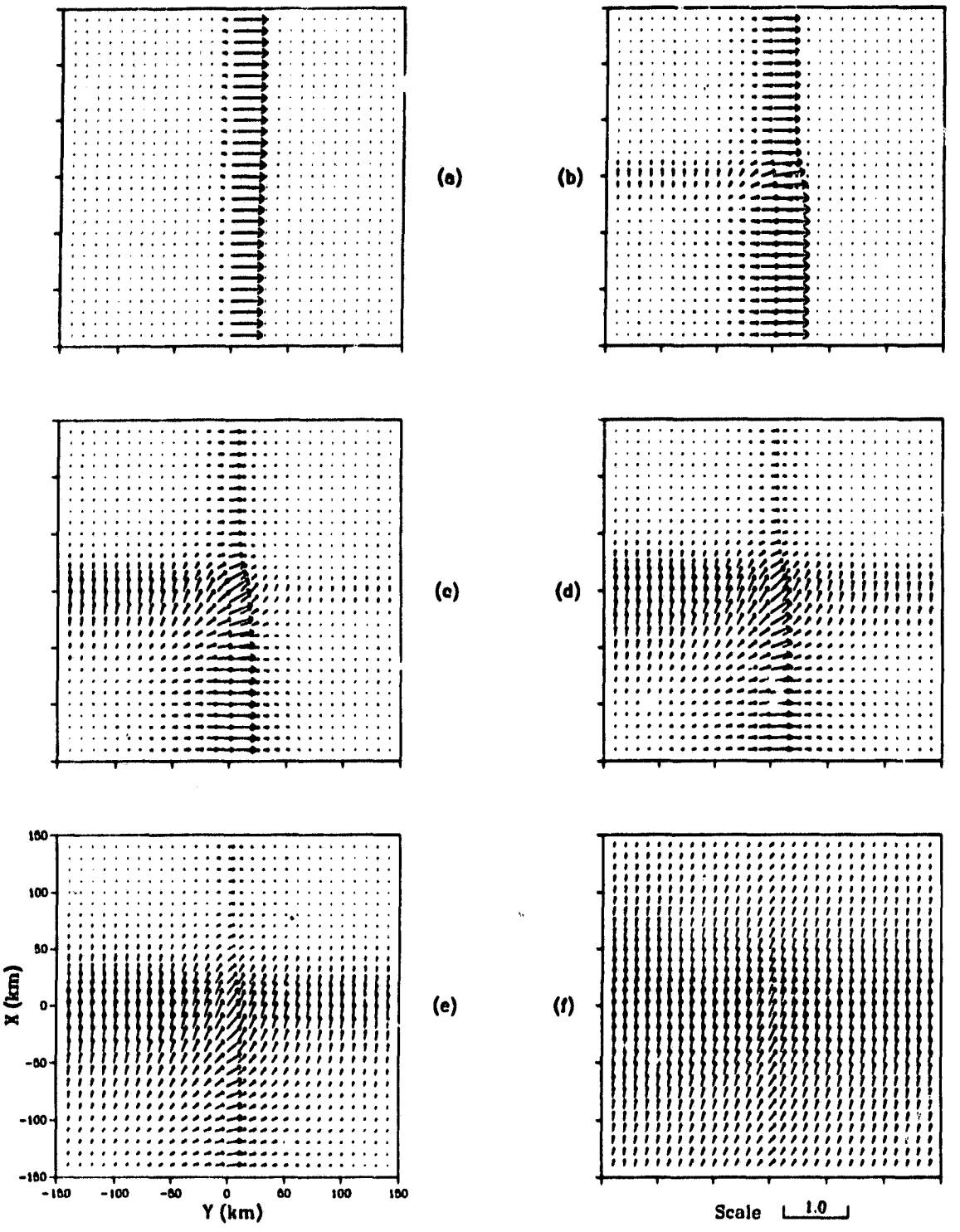


Figure 4.9: The real induction vectors (with the direction reversed) at the top of the model shown in Fig. 4.8. Graphs (a), (b), (c), (d), (e), (f) are for the periods 10, 100, 500, 1000, 2000, 10000 seconds respectively.

dimensions 5km by 5km by 1km, with resistivity $\rho = 1$ Ωm, which is embedded at the top of a uniform layer of 3 km thickness and resistivity 100 Ωm, and underlain by two half-slabs, 30 km thick and of resistivities 2 Ωm and 20 Ωm. The region below 33 km is a uniform half-space of resistivity $\rho = 10$ Ωm. The numerical results are calculated for a period of 5 s and three configurations, (a) surface anomaly alone, (b) 2D deep structure alone, (c) surface anomaly and deep-seated structure together. The corresponding skin depths at this period for resistivities 2, 10, 20 and 100 Ωm are 1.59, 3.56, 5.03 and 11.25 km respectively. A comparison of induction vectors calculated for configurations (a), (b) and (c) are presented. The difference vectors (c)−(a), (c)−(b) and the coupling vectors (c)−(a)−(b) are also shown to indicate the mutual coupling between the near-surface and deep-seated anomalies. The difference vectors have been used in investigations of the geoelectric structures of the Earth by many authors (e.g. Hebert *et al.*, 1983; Meng and Dosso, 1990; Chen, Dosso and Ingham, 1993; Kang, Dosso and Ogunade, 1993; Bapat *et al.*, 1993). The validity of the difference vector method was studied by Weaver and Agarwal (1990) and Dosso and Meng (1992). The directions of both real and imaginary vectors have been reversed so that the real vectors will point to the more conductive region.

A group of models which varied from the basic model were also investigated. The variations are on three parameters; the horizontal displacement of the near surface block, the vertical displacement of the deep buried 2D structure and the frequency. As shown in Fig. 4.10, we name the basic model with 5-sec period as CASE-0, and name the models in which horizontal displacements of the small block are to the left and right as CASE-1 and CASE-2 respectively. The vertical displacements of the deep buried 2D structure are called CASE-3 and CASE-4, in which the gaps between the bottom of the near surface block and the top of the buried 2D structure are increased from 2 km to 4 km and 10 km respectively. In CASE-5 and CASE-6, the spatial configuration of the basic

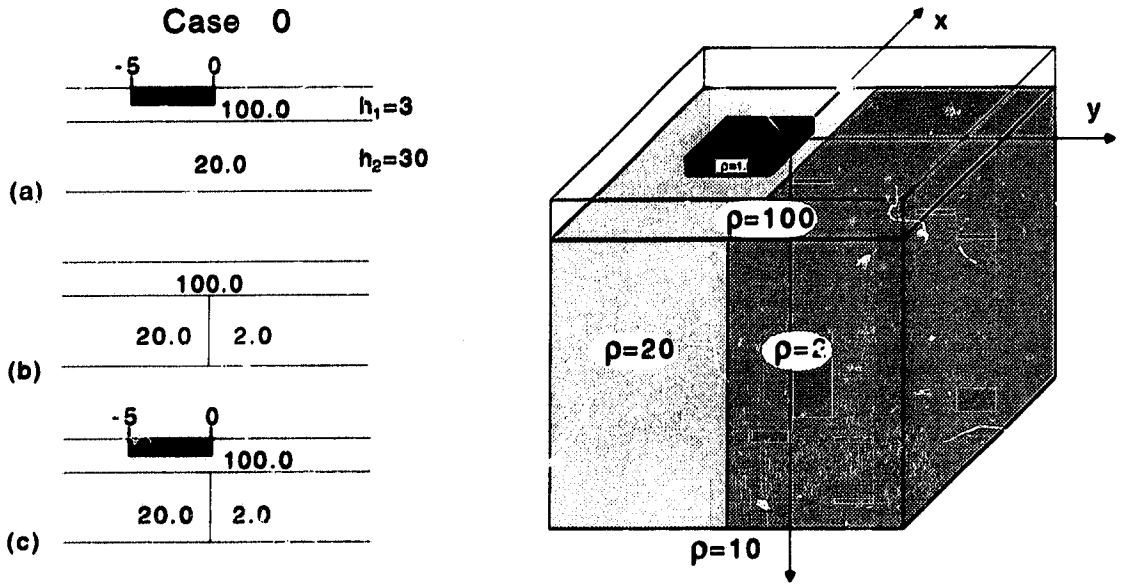


**The Basic Model**

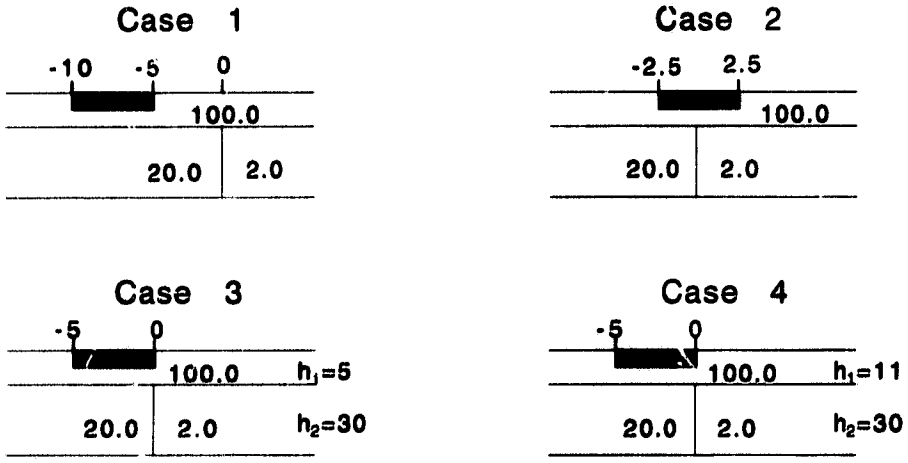


**Case 5**
**Basic Model (T=10 s)**

**Case 6**
**Basic Model (T=50 s)**

Figure 4.10: An investigation of the EM induction between a near surface small conductive block (5 by 5 by 1 with $\rho = 1$) over a buried lateral resistivity contrast (20 vs 2). The units of the values of resistivity and distance are $\Omega$m and km respectively.

model is kept fixed, but instead of using the period of 5 sec, we used 10 sec and 50 sec respectively.

Fig. 4.11 shows induction vectors obtained from CASE-0. Plot (a) is due to the near surface conductive block only. Both real and imaginary vectors point toward the conductive block. Plot (b) is due to the 2D deep seated structure only. We see that real induction vectors point toward the more conductive region while imaginary vectors do just the opposite. Plot (c) is the result of both near surface block and deep buried 2D structure together. The distortion due to the surface block is clearly seen. Fig. 4.12 shows the difference and coupling induction vectors obtained from CASE-0. In (c)−(b), the transfer functions of structure (b) are subtracted from those of (c), in order to remove the contribution of structure (b) in structure (c). The induction vectors of the difference transfer functions (c)−(b) are then plotted. If the total induction effect in structure (c) is the linear combination of the effects in the substructures (a) and (b), then (c)−(b) should reveal the true picture of (a). We see that this is no quite true. The induction vectors in (c)−(b) represent a distorted picture of (a), indicating that the linear addition of induction vectors is not quite valid. In (c)−(a) in which the contribution of (a) is removed from (c), again we see a distortion of the true picture of 2D induction vectors depicted in plot (b). In (c)−(a)−(b), we have subtracted the contributions of both (a) and (b) from (c), which would yield null vectors if induction vectors could be linearly superposed. What remains is due to the mutual coupling between the two substructures and is consequently called 'coupling vectors' (suggested by J.T. Weaver in private discussion). The smaller these vectors, the weaker the mutual coupling effect is. When these vectors are small enough so that they can be neglected, then the linear addition of induction vector can be considered valid. Here we see that the imaginary coupling vectors are much smaller than the real ones.

Both Figs. 4.13 and 4.14 are obtained from CASE-1, in which the near sur-

face block is displaced 5 km to the left, so its center is further away from the conductive boundary of the buried 2D structure. Its relative position with respect to the boundary can be seen clearly in plot (c). Compared with CASE-0, the imaginary coupling vectors in (c)−(a)−(b) increased a little. But the real coupling vectors of (c)−(a)−(b) decreased even more. On the whole, this indicates that the mutual coupling effect is less in CASE-1 than in CASE-0. The next two figures, Fig. 4.15 and 4.16 are from CASE-2. In this configuration, the surface block is moved 2.5 km to right and the center of the block is now sitting directly above the conductivity boundary of the buried 2D structure. Although plot (c) changes accordingly to reflect the new position of the block, the mutual coupling effect remains approximately the same as in CASE-0. Perhaps in this case, the displacement is not large enough to make much difference.

Figs. 4.17 and 4.18 show the results from CASE-3. The only difference between this model and CASE-0 is that the gap between the bottom of the surface block and the top of the buried 2D structure is increased to 4 km from 2 km (the resistive uniform layer is now 5 km thick). The consequence of this variation is that the induction vectors become larger in plot (a) and smaller in (b). In fact, the change of relative strengths of the induction vectors of the block and the 2D structure can also be seen in plot (c). Here the influence of the block has become locally dominant. In some regions the total induction vectors have been reversed opposite to the directions of the 2D background ones. The mutual coupling effect shown in plot (c)−(a)−(b) did not change much.

Figs. 4.19 and 4.20 are from CASE-4 in which the gap is further increased to 10 km (the resistive uniform layer is now 11 km thick). Induction vectors in plot (a) are further increased and (b) further decreased. The influence of the near surface block is totally dominant in plot (c) now. The mutual coupling is much weaker than in previous cases.

Figs. 4.21 and 4.22 are for CASE-5 where the spatial configurations are kept

the same as in CASE-0, but the period of the source field is 10 sec rather than 5 sec. The corresponding skin depths associated with resistivities 1, 2, 10, 20 and 100 Ωm are 1.59, 2.25, 5.03, 7.11 and 15.9 km. Compared with the results for 5-sec period in CASE-0, the induction vectors for the surface block in plot (a) are smaller while the ones of 2D structure in plot (b) are larger. In plot (c)−(a)−(b), however, the real coupling vectors are weaker while the imaginary ones are stronger. The strength of mutual coupling has not changed significantly. The next figure, Fig. 4.23, shows the results of CASE-6, where the period is further increased to 50 sec. The corresponding skin depths are now 3.56, 5.03, 11.3, 15.9 and 35.6 km. The induction vectors due to the surface block can hardly be seen now, while the 2D induction vectors are much stronger. There is hardly any distortion in plot (c) due to the existence of the surface block; therefore, no difference vectors and mutual coupling effects are plotted for this case.

In this application of our versatile three-dimensional modelling program, we have investigated the distortion, caused by a small surface anomaly, of induction vectors associated with a two-dimensional buried anomaly. The surface anomaly exerts a strong influence on the induction vectors and there is evidence of mutual coupling in a certain region. It seems that the strength of the mutual coupling effect depends on two factors. One is the relative strengths of the induction caused by the surface anomaly and the deep seated 2D structure. The other one is the displacement of the surface anomaly from the strike of the buried structure. If the induction caused by the surface anomaly and the buried structure are well balanced, mutual coupling is enhanced. Otherwise if one part is much weaker than the other, mutual coupling is reduced. Even when the induction intensities are well balanced, however, the mutual coupling may still become weaker when the displacement of the surface anomaly from the strike of the buried structure increases, as can be seen in CASE-1.

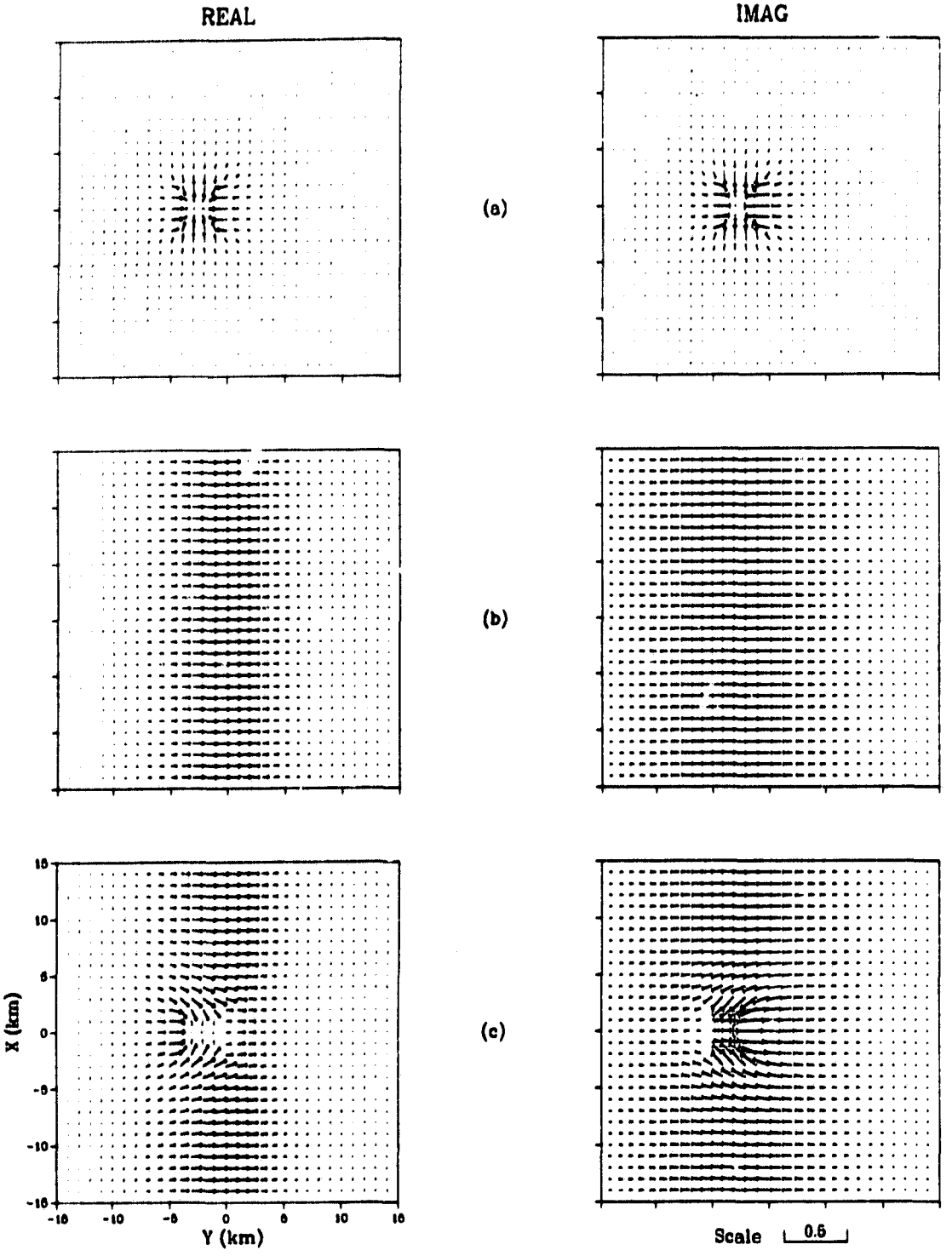


Figure 4.11: Reversed induction vectors for the basic model, Case 0 in Fig. 4.10, with the period of the source field T=5 s. (a) the surface anomaly only; (b) the buried 2D structure only; (c) the surface anomaly and buried structure together.

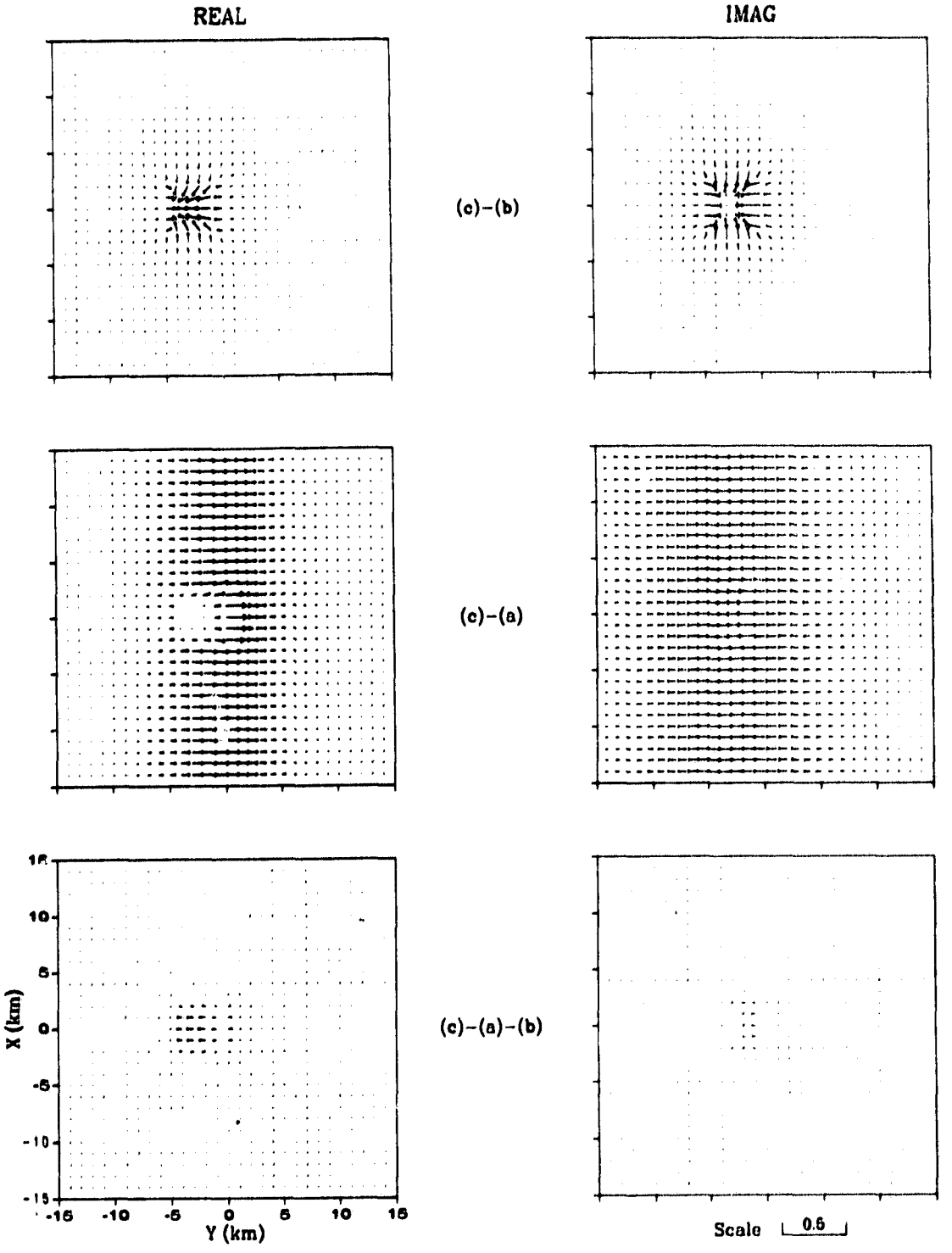


Figure 4.12: Difference and coupling vectors for the basic model, Case 0 in Fig. 4.10., with T=5 s.

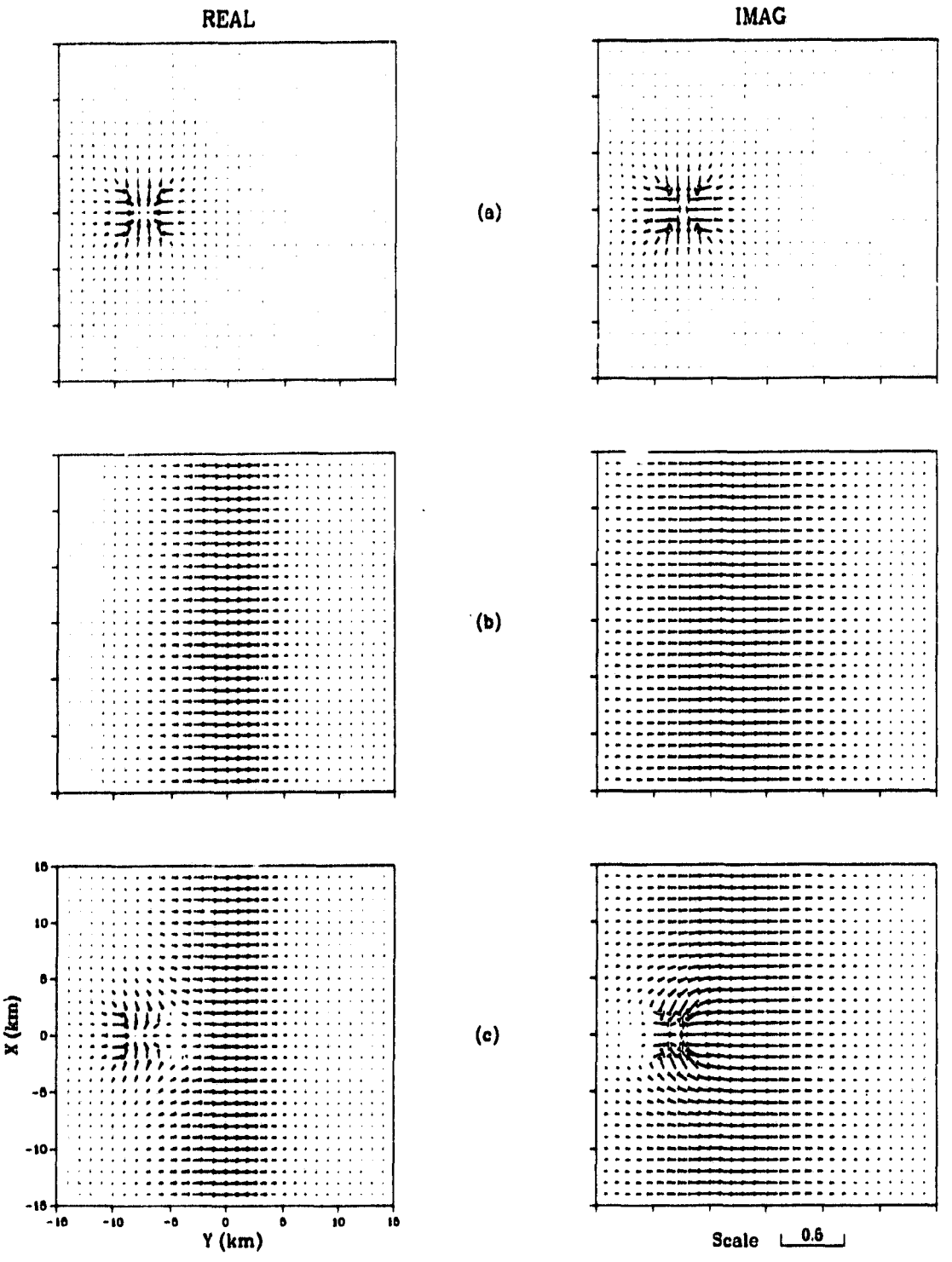


Figure 4.13: Reversed induction vectors for Case 1 in Fig. 4.10 with T= 5 s. (a) the surface anomaly only; (b) the buried 2D structure only; (c) the surface anomaly and buried structure together.

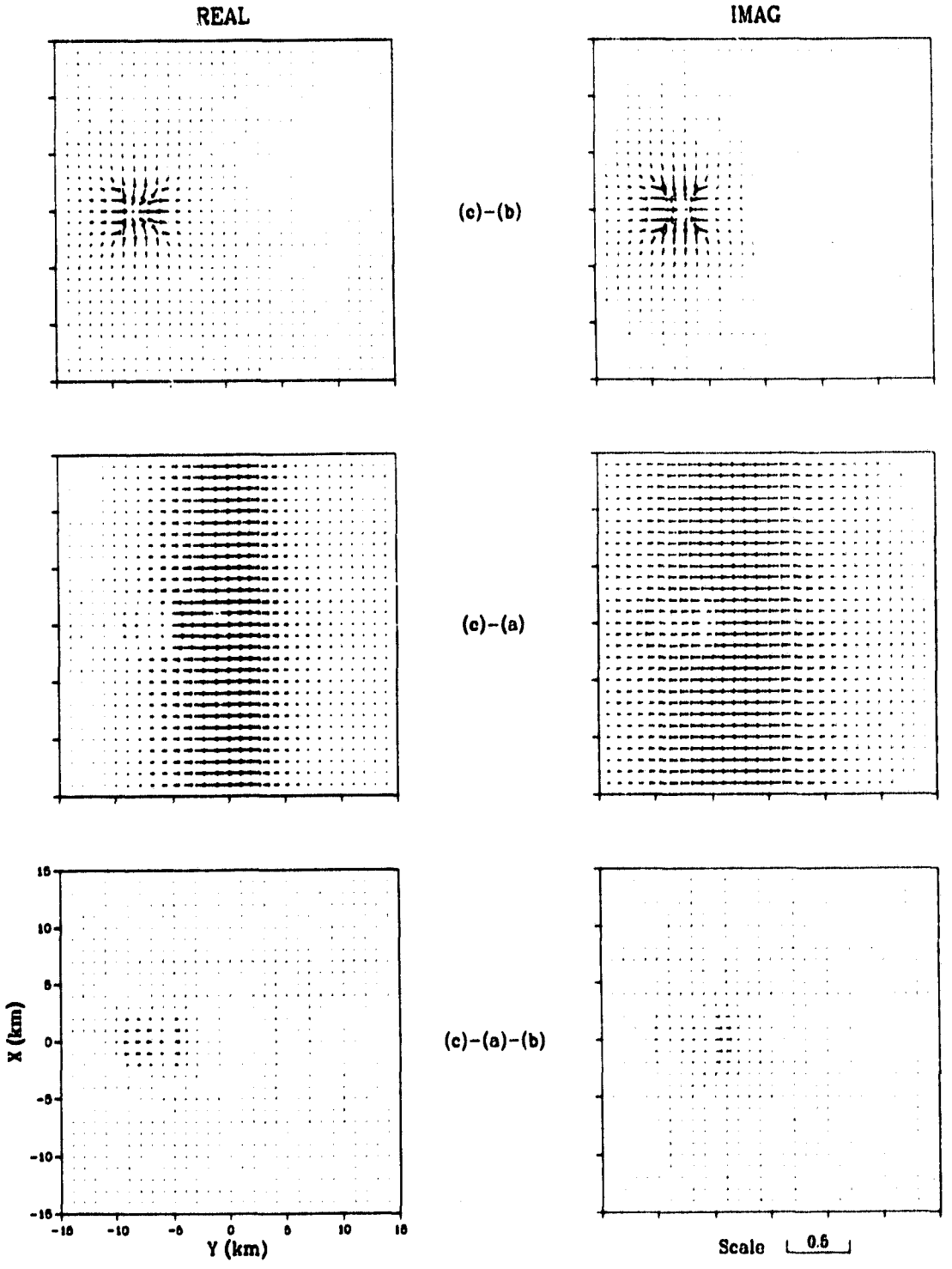


Figure 4.14: Difference and coupling vectors for Case 1 in Fig. 4.10 with T=5 s.

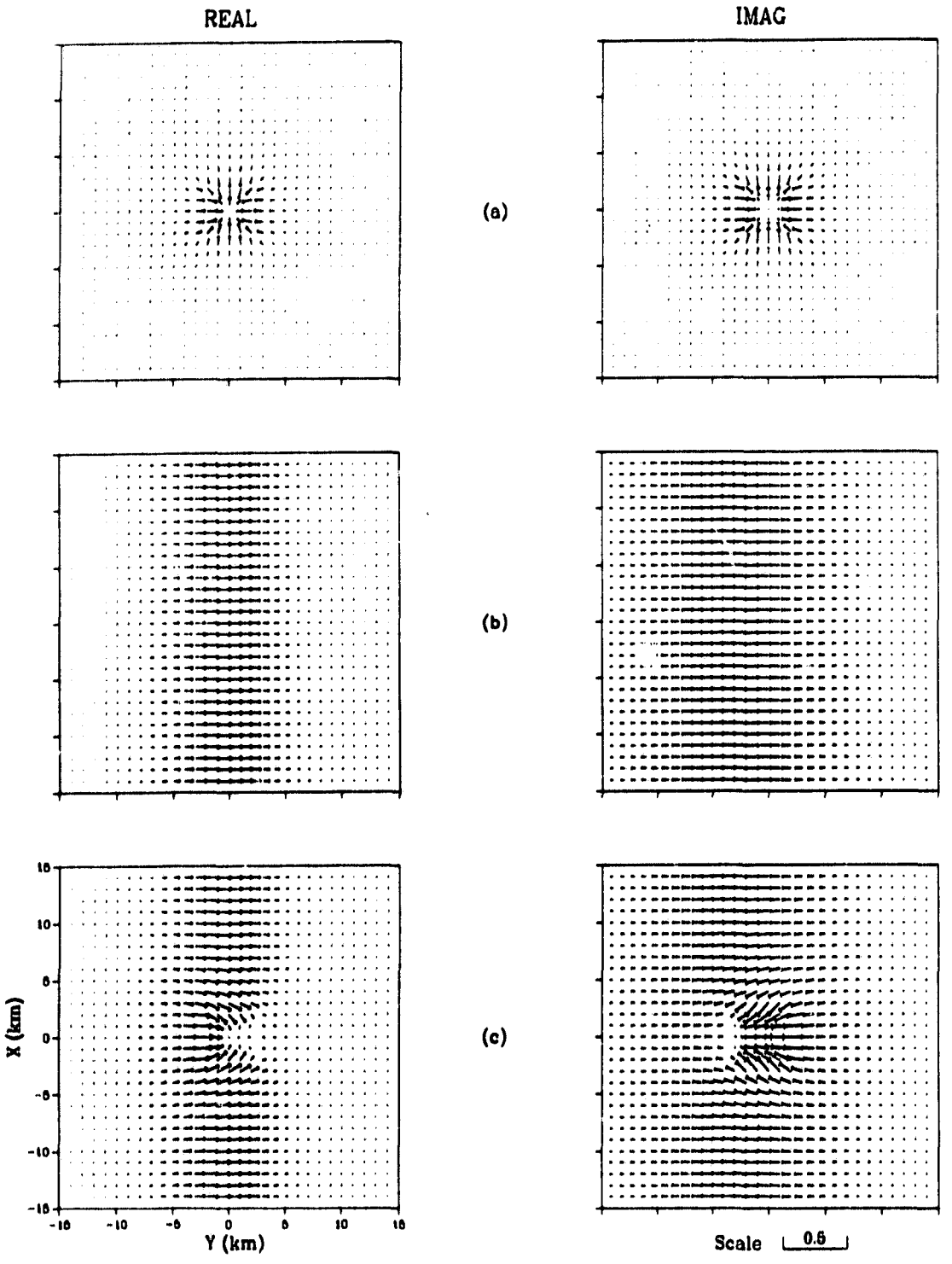


Figure 4.15: Reversed induction vectors for Case 2 in Fig. 4.10 with T=5 s. (a) the surface anomaly only; (b) the buried 2D structure only; (c) the surface anomaly and buried structure together.

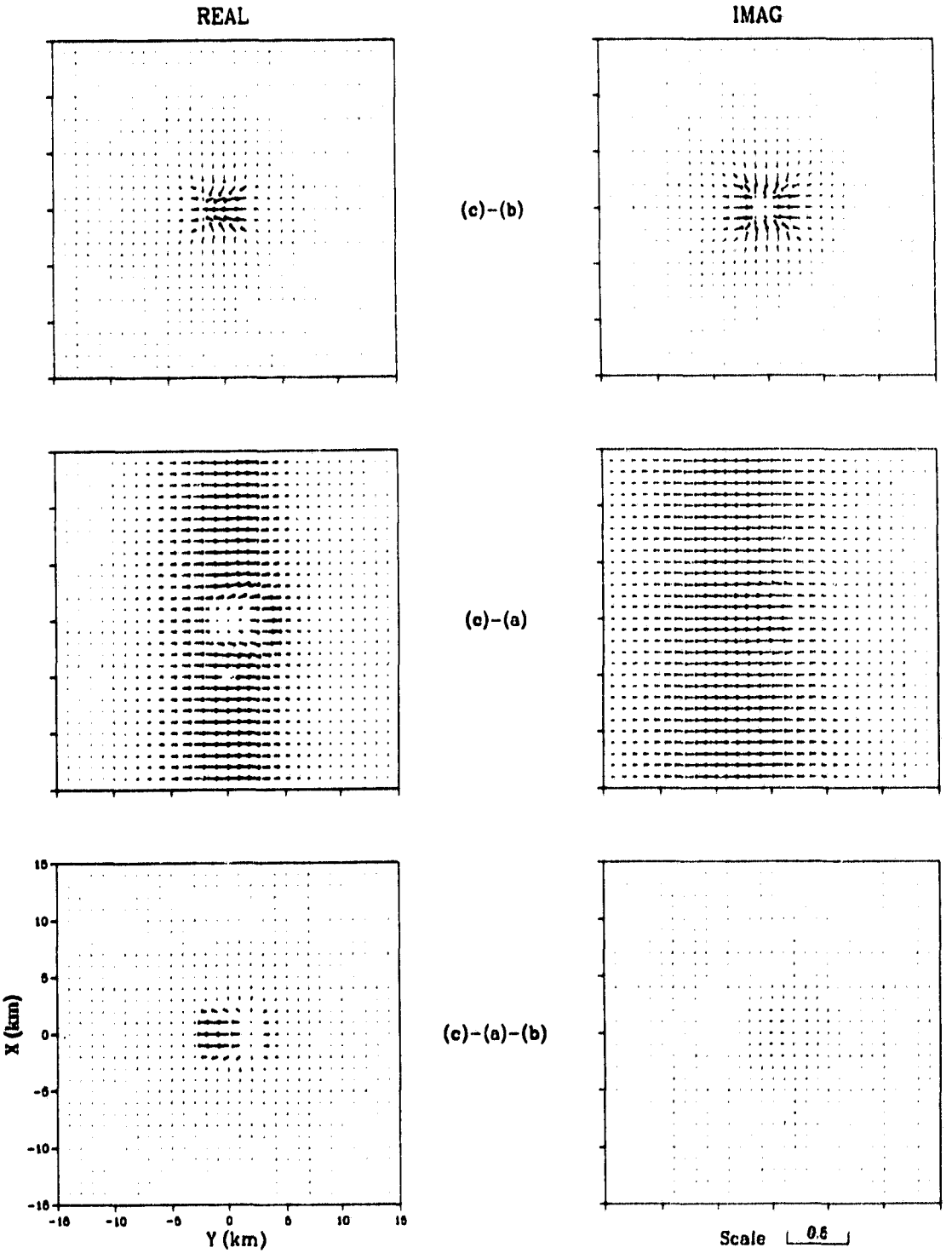


Figure 4.16: Difference and coupling vectors for Case 2 in Fig. 4.10 with T=5 s.

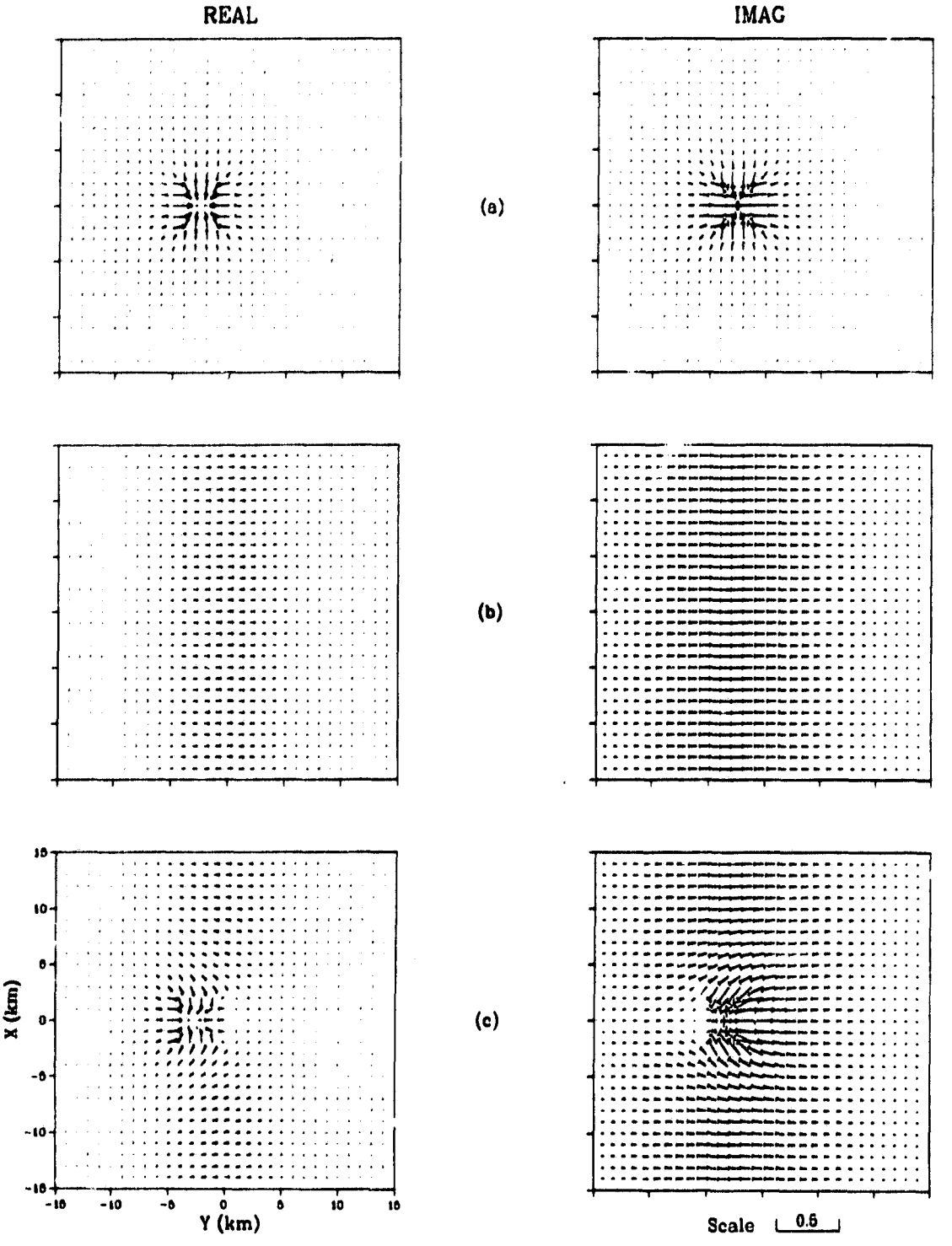


Figure 4.17: Reversed induction vectors for Case 3 in Fig. 4.10 with T=5 s. (a) the surface anomaly only; (b) the buried 2D structure only; (c) the surface anomaly and buried structure together.

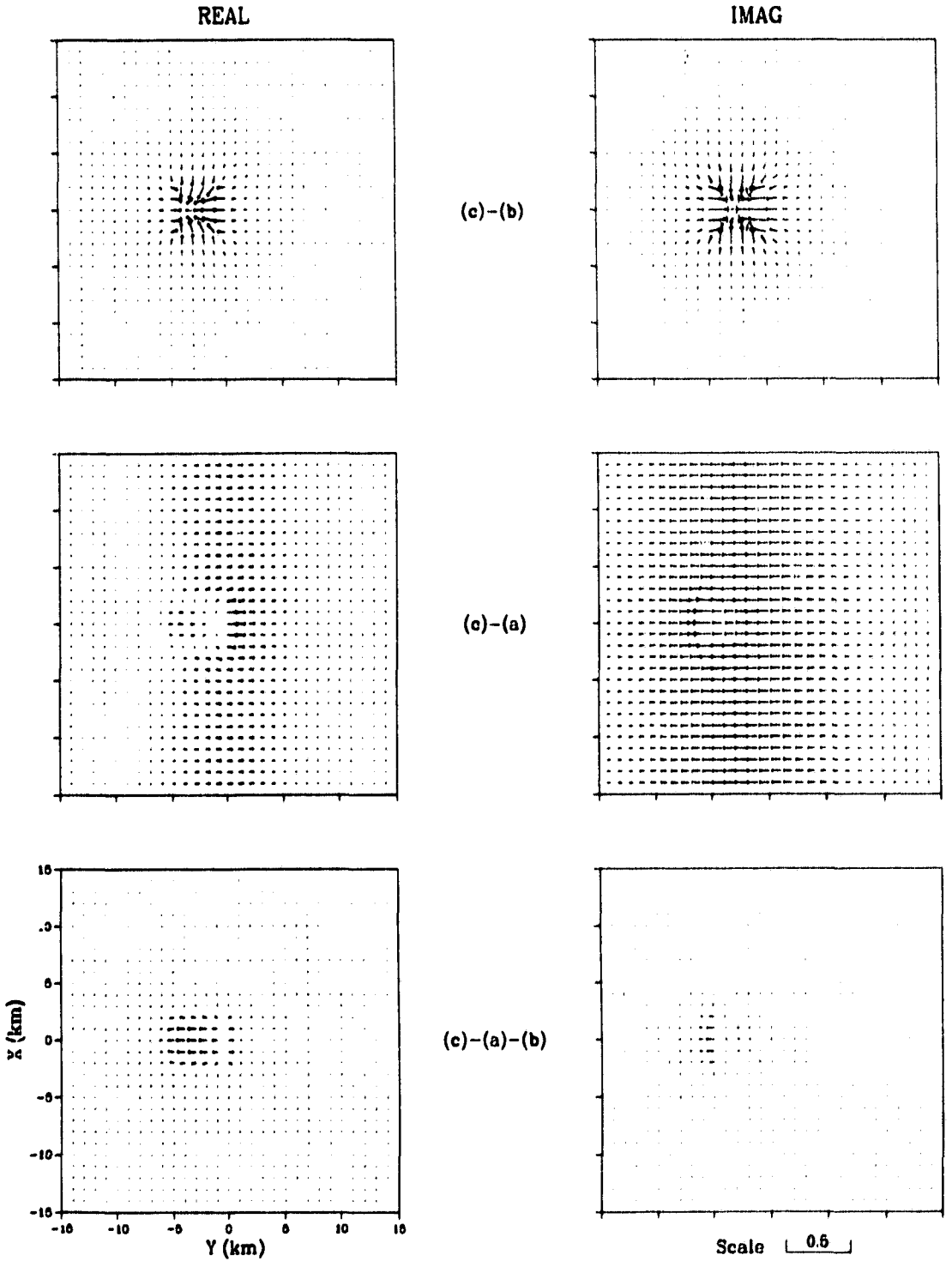


Figure 4.18: Difference and coupling vectors for Case 3 in Fig. 4.10 with T=5 s.

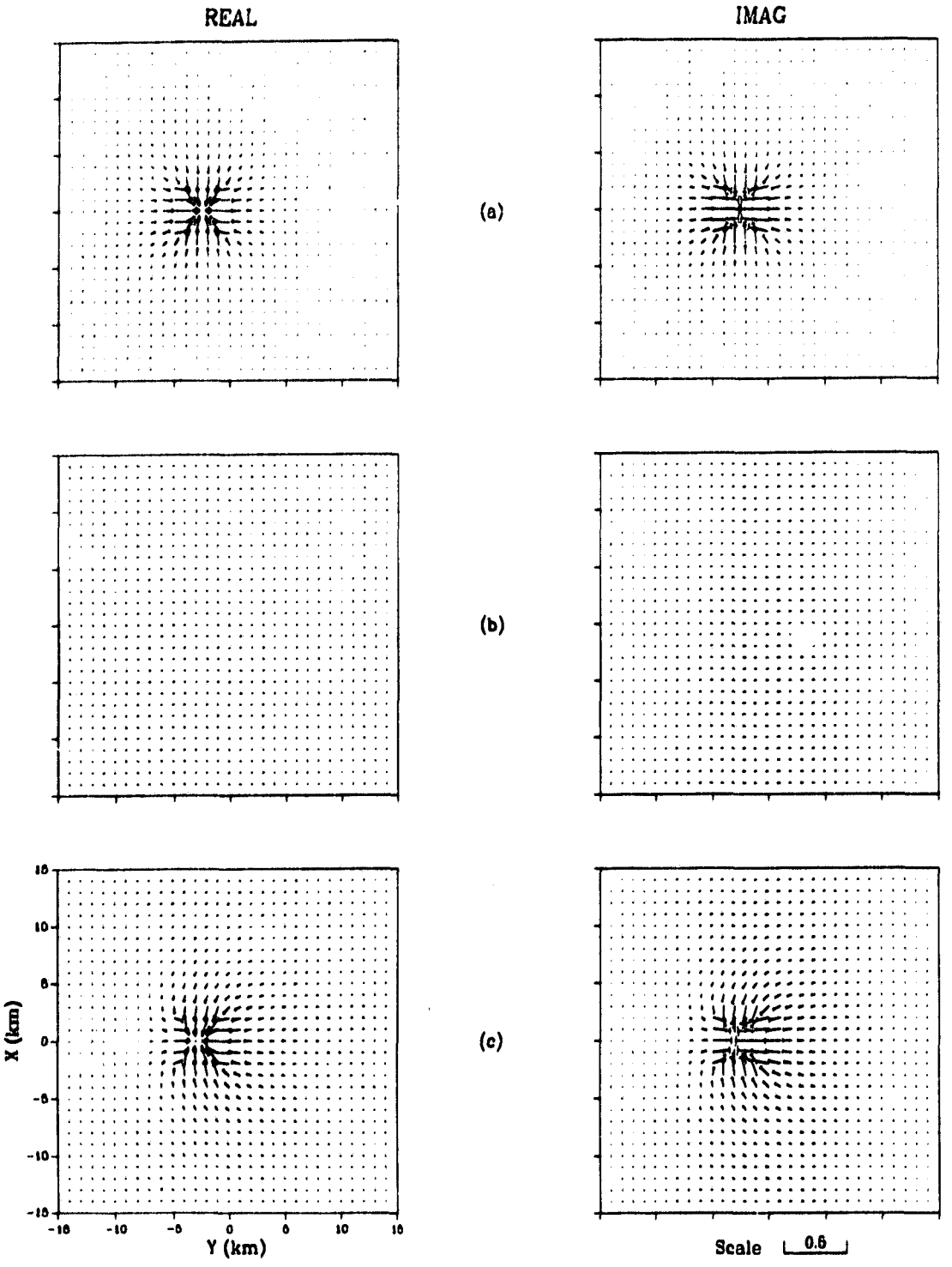


Figure 4.19: Reversed induction vectors for Case 4 in Fig. 4.10 with T=5 s. (a) the surface anomaly only; (b) the buried 2D structure only; (c) the surface anomaly and buried structure together.

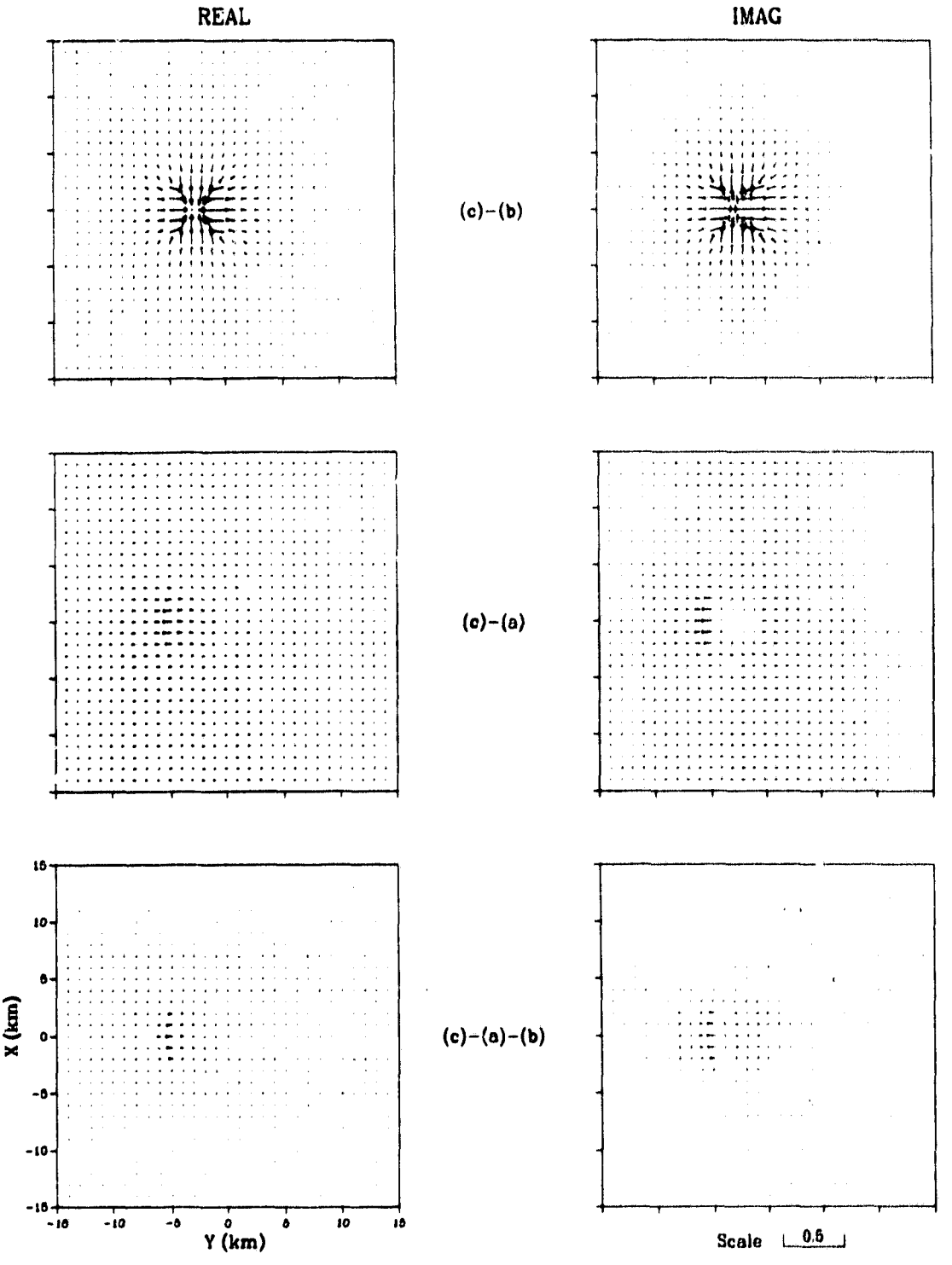


Figure 4.20: Difference and coupling vectors for [illegible] 4 in Fig. 4.10 with T=5 s.

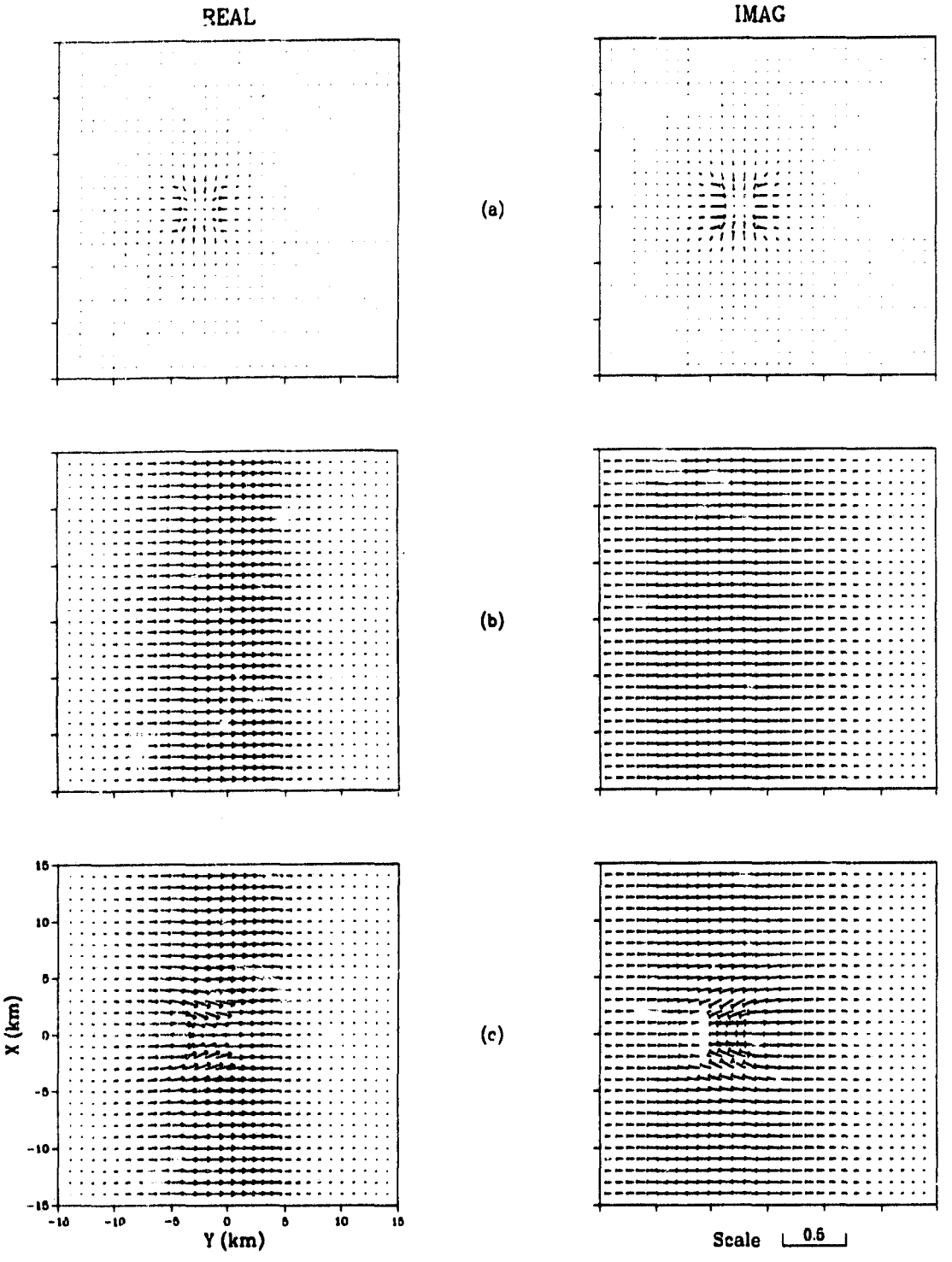


Figure 4.21: Reversed induction vectors for Case 5 in Fig. 4.10, the basic model but for T=10 s. (a) the surface anomaly only; (b) the buried 2D structure only; (c) the surface anomaly and buried structure together.

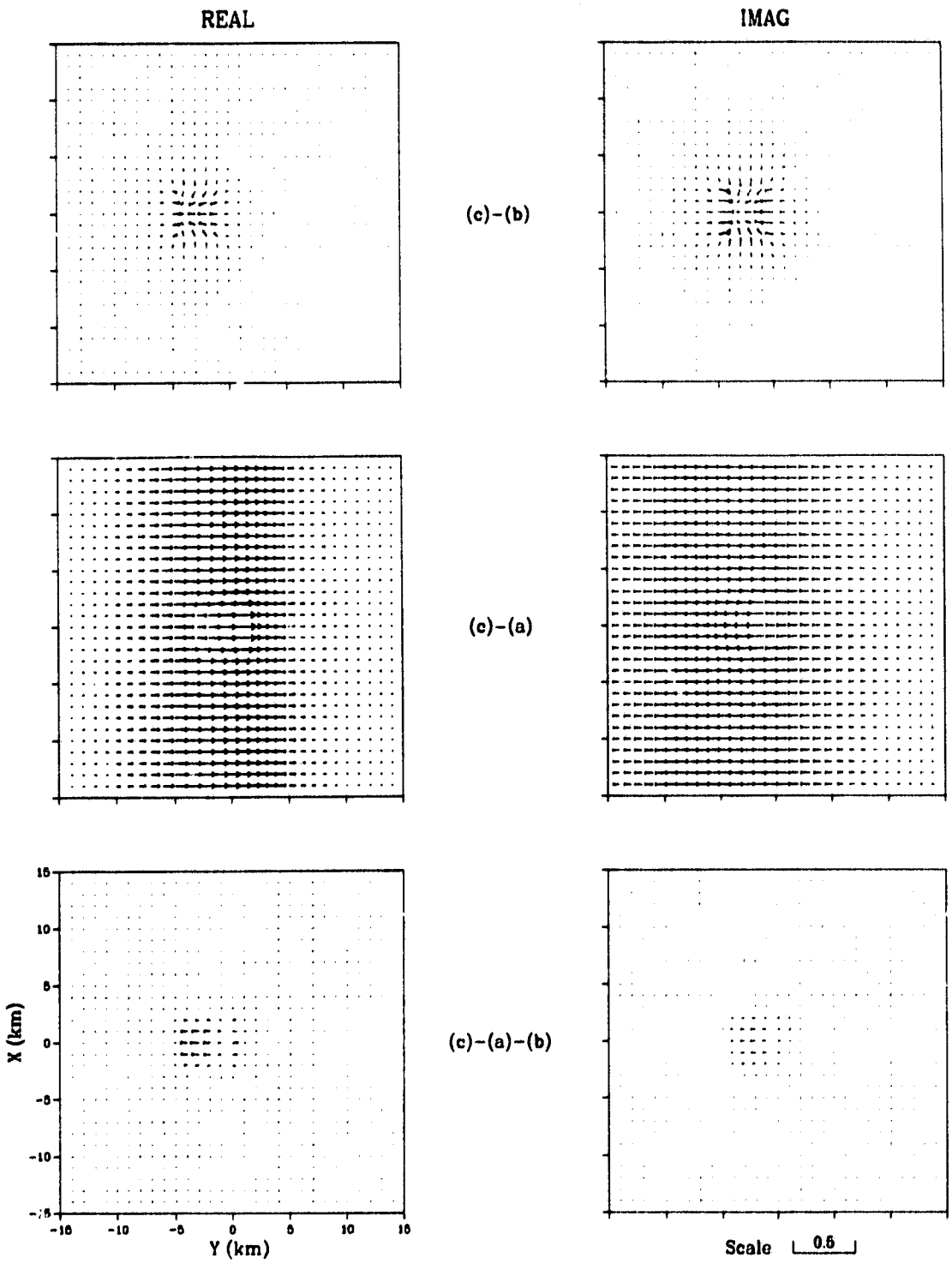


Figure 4.22: Difference and coupling vectors for Case 5 in Fig. 4.10, the basic model but for T=10 s.

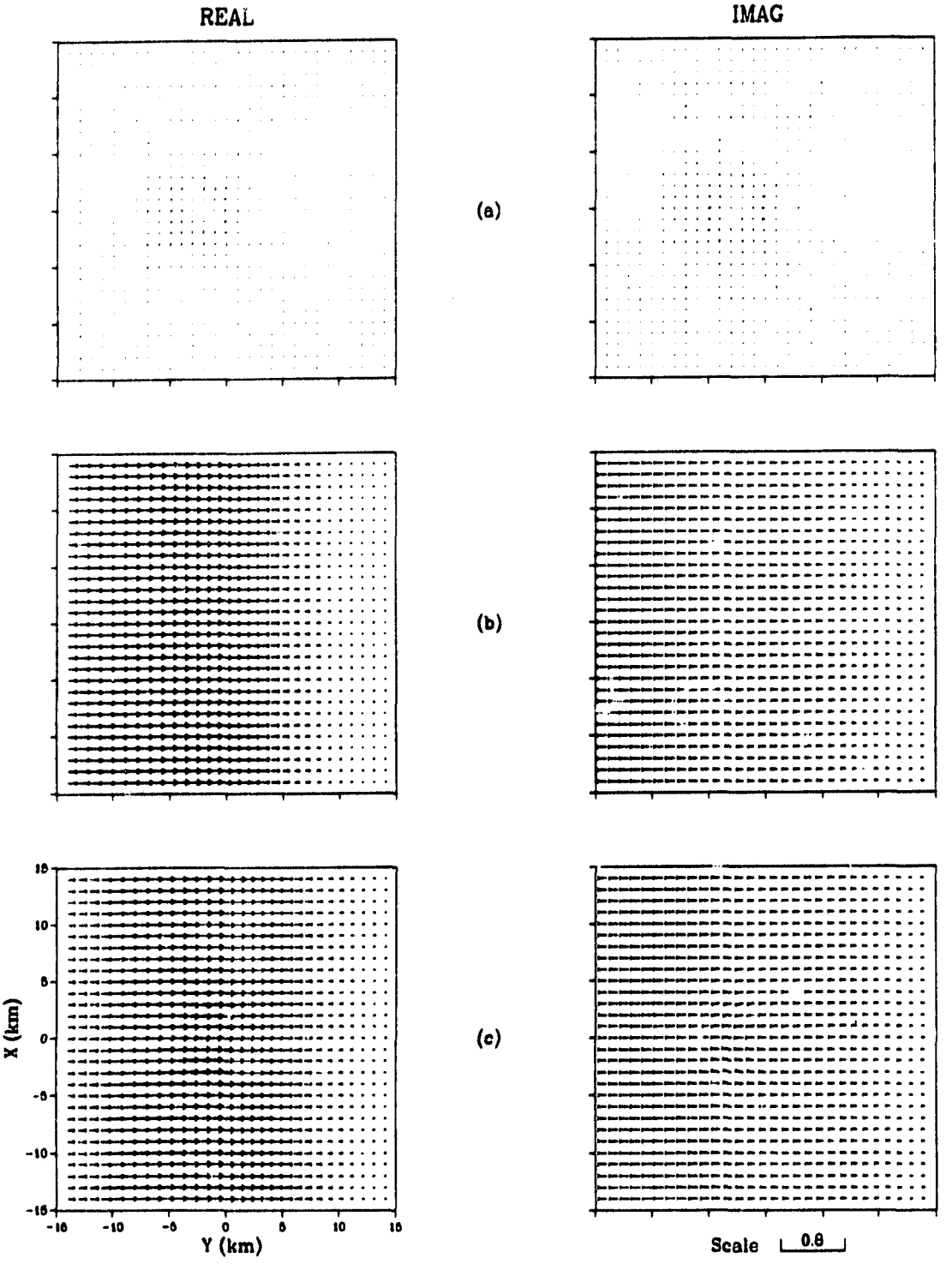


Figure 4.23: Reversed induction vectors for Case 6 in Fig. 4.10, the basic model but for T=50 s. (a) the surface anomaly only; (b) the buried 2D structure only; (c) the surface anomaly and buried structure together.

# Chapter 5

# CONCLUSIONS AND FUTURE WORK

## 5.1 Conclusions

The 3D forward modelling problem has interested many researchers in the EM induction community in the past few years. Much work has been done in developing 3D programs, but it is still rather a challenging field. In this thesis, we have developed an algorithm for solving the 3D forward modelling problems. The algorithm offers the following novel features:

1) It incorporates an anomalous thin sheet at the surface of a conventional 3D structure. It offers, therefore, the advantage of other thin sheet programs, such as those of Vasseur and Weidelt (1977) and McKirdy, Weaver and Dawson (1985), in which the modelling of a near surface conductivity anomaly can be much simplified, together with the usual capability of modelling buried structures of finite thickness.

2) Both the thin sheet and the underlying 3D geoelectric structures may approach 2D configurations at infinity. This feature plus the incorporation of the thin sheet enable us to model quite general geophysical structures.

3) It uses integral boundary conditions on the surface and at the bottom, and hence reduces the size of the mesh by removing the air layer above the surface and a uniform half-space beneath the anomalous structures. The height of the air layer is normally difficult to determine. By eliminating this layer, the model design becomes much easier and the solution becomes more accurate.

4) It employs cell-integral finite difference equations in the region $z > 0$ which

we have found requires fewer grid points than the conventional finite difference equations, for the same accuracy, especially in the models involving extreme conductivity contrasts. This is quite appreciable for the 3D problem, since it can significantly reduce the number of grid points, and hence the computer storage and computation.

5) The solutions are obtained in terms of the magnetic field, which is of primary interest in many of the EM methods used to investigate the structure of the earth. In most previous programs, solutions were obtained in terms of the electric field, so that an extra step of numerical differentiation is required to obtain the magnetic fields. By obtaining the solution for the magnetic field directly, we have removed this extra source of numerical error in the magnetic field, although numerical differentiation is still required, of course, to obtain the electric field.

The accuracy of our computer program has been checked against some established programs. In Chapter 2, we have compared the solutions of our 2D program for a model with rather extreme conductivity contrasts (Fig. 2.2) with respect to the solutions obtained by Brewitt-Taylor and Weaver (1976). Our results were found to be reasonably accurate (Fig. 2.11 and 2.12) with the usage of the cell-integral finite equations. For a model with moderate contrasts, e.g. the control model in Fig. 2.6, for which a quasi-analytic solution is available (Weaver, LeQuang and Fischer, 1986), the accuracy of our solution was superb (Fig. 2.14).

The accuracy of the 3D part of the program was checked first by using the 3D models with 2D conductivity structures. The solutions for a model with a thin sheet (Fig. 4.1) were checked against those of Green and Weaver (1978). The comparison was made for the results both above and beneath the thin sheet layer in Fig. 4.2 and 4.3 for E-polarization, and beneath the thin sheet in Fig. 4.4 for B-polarization. The E-polarization solutions match quite well and the B-

polarization solutions are even better; they match almost exactly with those of Green and Weaver. The solutions without the thin sheet compared satisfactorily with those of Brewitt-Taylor and Weaver (1976).

The results of the 3D part of the program were also checked against those of McKirdy, Weaver and Dawson (1985) by a 3D thin sheet model and the solution delivered by our program was found to be more physically meaningful.

Based on all these checks and comparisons, we are confident that our program is working well and can provide very accurate solutions for general 3D models with moderate conductivity contrasts. Even for the models with rather extreme conductivity contrasts, it yields very reasonable results. A number of applications of the program to various synthetic models has demonstrated its usefulness. In particular, the application to the model of a small near surface conductive block over a buried conductivity contrast in Fig. 4.10 shows that our program is capable of picking up fine details in the magnetic variations of 3D models with delicate structures.

## 5.2 Future Work

An important application of our program can be the test of the validity of various tensor decomposition schemes used in magnetotelluric (MT) studies. The (MT) method is one of the most useful ways of studying the large scale properties and deep structure of the earth. In the MT method, the data are normally presented in the frequency domain by an impedance tensor $\mathbf{Z}(\mathbf{r}, \omega)$ which maps the measured horizontal conponents of the magnetic field $\mathbf{H}(\mathbf{r}, \omega)$ at the earth's surface to the horizontal electric field by $\mathbf{E}(\mathbf{r},\omega) = \mathbf{Z}(\mathbf{r},\omega)\mathbf{H}(\mathbf{r},\omega)$ where $\mathbf{Z}(\mathbf{r}, \omega)$ is a rank 2, complex tensor,

$$\mathbf{Z} = \begin{pmatrix} Z_{11} & Z_{12} \\ Z_{21} & Z_{22} \end{pmatrix}.$$

When the coordinate axes correspond to the principal axes (i.e. natural axes), the impedance tensor has the form

$$\mathbf{Z}_2 = \begin{pmatrix} 0 & a \\ -b & 0 \end{pmatrix}.$$

Otherwise the measured impedance tensor can be derived from $\mathbf{Z}_2$ via the standard rotation transformation $\mathbf{Z} = \mathbf{R}\mathbf{Z}_2\mathbf{R}^T$ where $\mathbf{R}$ is a rotation operator

$$\mathbf{R} = \begin{pmatrix} cos\theta & sin\theta \\ -sin\theta & cos\theta \end{pmatrix}$$

and $\theta$ is the angle between the measurement frame and the natural frame.

There is no such simple decomposition when $\mathbf{Z}$ is produced from an arbitrary 3D conductivity distribution. Following the lead of Schmucker (1970) and Larsen (1977), the distorted field $\mathbf{E}^D$ and undistorted field $\mathbf{E}^U$ are related to a distortion tensor $\mathbf{D}$ by the expression $\mathbf{E}^D = \mathbf{D}\mathbf{E}^U$, i.e.

$$\mathbf{E}^D = \mathbf{D}\mathbf{E}^U = \mathbf{D}\mathbf{Z}\mathbf{H} = \mathbf{Z}_m\mathbf{H}$$

where $\mathbf{Z}$ is the impedance tensor for a 1D or 2D normal region while $\mathbf{Z}_m$ is the actually measured, distorted impedance tensor.

Attempts have been made to decompose the distortion tensor parameters. It is desirable to separate those parts of the data due to the large-scale structure which need to be fitted to a model from those due to the small-scale features which are usually not of interest. Various tensor decompositions have been proposed (e.g. Eggers, 1982; Spitz, 1985; Yee, 1985; Latorraca, Madden and Korringa, 1986; Cevallos, 1986; Yee and Paulson, 1987; Bahr, 1988; Groom and Bailey, 1989, 1991). Among them, the one by Groom and Bailey (1989) appears to have considerable merit. They considered a model of 1D or 2D regional background with a weak 3D structure. By 'weak' they mean the anomalies are near-surface and in small scale. They pointed out that even for a small structure, the distortion can be large if the conductivity contrast is great. It is

usual, however, in current practice to regard the distortion arising from small anomalies as being insignificant. Groom and Bailey write the distortion tensor as $\mathbf{C}$ and factor it as

$$\mathbf{C} = g\mathbf{TSA}$$

where $\mathbf{T}$, $\mathbf{S}$ and $\mathbf{A}$ have the physical interpretation as the twist, shear and anisotropy operators respectively.

Although some of these schemes (e.g. Groom and Bailey, 1989) are in general usage, a thorough test of their validity has not yet been made. Such a test requires the availability of a versatile and efficient three-dimensional program which has the capability of modelling small near-surface anomalies embedded in a large two-dimensional structure. The program developed in this thesis is ideally suited to this problem, because of the features of incorporating an anomalous thin sheet at the surface of an otherwise quite general three-dimensional structure, plus its ability to handle the high conductivity contrasts and to detect the fine magnetic variations. In fact, the study of a small surface conductive block over buried dividing regions in this chapter has been conducted primarily as a preliminary to this intended test. Of course, the calculation of the electric field has to be implemented in order to do this task. The procedure to carry out the test would be:

1. For a given 1D or 2D model with some small scale, near-surface 3D structures present, calculate the magnetic and electric fields for a given frequency. Then calculate the corresponding impedance tensor $\mathbf{Z}_m(\mathbf{r},\omega)$ at different positions from these fields.

2. For the same model, but with the 3D structures removed, calculate the EM fields and the corresponding normal impedance tensor $\mathbf{Z}(\mathbf{r}, \omega)$

3. Obtain the distortion tensor $\mathbf{D}(\mathbf{r},\omega) = \mathbf{Z}_m(\mathbf{r},\omega)\mathbf{Z}^{-1}(\mathbf{r},\omega)$

4. Decompose the impedance tensor obtained in step 1 according to the

decomposition proposal to be tested and compare th' corresponding distortion tensor with that obtained in step 3.

If Groom and Bailey's method or any other decomposition proposals are found to be satisfactory in removing EM distortions, it will be a great help to the interpretation of MT data.

# Bibliography

Agarwal, A.K., Poll, H.E. and Weaver, J.T. (1993). One- and two-dimensional inversion of magnetotelluric data in continental regions. Phys. Earth Planet. Inter. **81**, 155–176.

Agarwal, A.K. and Weaver, J.T. (1993). Inversion of the COPROD2 data by a method of modelling. J. Geomag. Geoelectr. **45**, 969–983.

Ashour, A.A. and Chapman, S. (1965). The magnetic field of electric currents in an unbounded plane sheet, uniform except for a circular area of different uniform conductivity. Geophys. J. R. astr. Soc. **48**, 385–392.

Bahr, K. (1988). Interpretation of the magnetotelluric impedance tensor: regional induction and local telluric distortion. J. Geophys. **62**, 119–127.

Bapat, V.J., Segawa, J., Honkura, Y. and Tarits, P. (1993). Numerical estimation of the sea effect on the distribution of induction arrows in the Japanese island arc. Phys. Earth Planet. Inter. **81**, 215–229.

Brewitt-Taylor, C.R. and Weaver, J.T. (1976). On the finite difference solution of two-dimensional induction problems. Geophys. J. R. astr. Soc. **47**, 375–396.

Cagniard, L. (1953). Basic theory of the magnetotelluric method of geophysical prospecting. Geophysics **18**, 605–635.

Cevallos, C. (1986). Magnetotelluric interpretation - another approach: Ph.D thesis, Macquarie University, Sydney, Australia.

Červ, V and Pek, J. (1990). Modelling and analysis of electromagnetic fields in 3D inhomogeneous media. Surveys in Geophysics. **11** 205-229.

Chan, E., Dosso, H.W., and Law, L.K. (1981). An analogue model study of electromagnetic induction for cape and bay coastlines. Phys. Earth Planet. Inter. **25**, 167–176.

Chen, J., Dosso, H.W. and Nienaber, W. (1989). Laboratory Electromagnetic Model Results for the EMSLAB Region. Journal of Geophysical Research, **94**, 14167-14172.

Chen, J., Dosso, H.W. and Ingham, M. (1990). Electromagnetic Induction in New Zealand : Analogue Model and Field Results. Phys. Earth Planet. Inter. **62**, 257–270.

Chen, J., Dosso, H.W. and Ingham, M. (1993). Electromagnetic Induction in New Zealand South Island. Phys. Earth Planet. Inter. **81**, 253–260.

Coggon, J.H. (1971). Electromagnetic and electrical modeling by the finite-element method. Geophysics **36**, 132–155.

Das, U.C. and Verma, S.K. (1981). Numerical considerations on computing the EM response of three-dimensional inhomogeneities in a layerd earth. Geophys. J. R. astr. Soc. **66**, 733–740.

Das, U.C. and Verma, S.K. (1982). Electromagnetic response of an arbitrarily shaped three-dimensional conductor in a layered earth-numerical results. Geophys. J. R. astr. Soc. **68**, 55–66.

Dawson, T.W. (1979). Three-dimensional electromagnetic induction in thin sheets. Ph.D. thesis, Dept. of Physics, Univ. of Victoria, 409 pp.W. (1979).

deGroot-Hedlin, C.D. and Constable, S.C. (1990). Occam's inversion to generate smooth, two-dimensional models from magnetotelluric data. Geophysics **55**, 1613–1624.

d'Erceville, I. and Kunetz, G. (1962). The effect of a fault on the Earth's natural electromagnetic field. Geophysics **27**, 651–665.

Dosso, H.W. (1966). A plane-wave analogue model for studying electromagnetic variations. Can. J. Phys. **44**, 67–80.

Dosso, H.W. (1973). A review of analogue model studies of the coast effect. Phys. Earth Planet. Inter. **7**, 294–302.

Dosso, H.W., Agarwal, A.K. and Chen, J. (1992). EM induction in the Vancouver Island region: 3D numerical, Analogue model, and field site results. PAGEOPH, **138**, 193–206.

Dosso, H.W. and Meng, Z.M. (1992). The coast effect response in geomagnetic field measurements. Plate. Phys. Earth Planet. Inter. **70**, 39–56.

Dosso, H.W., Nienaber, W. and Chen, J. (1989). Laboratory electromagnetic modelling of the subducting Juan de Fuca Plate. Phys. Earth Planet. Inter. **53**, 221–227.

Dosso, H.W., Nienaber, W., and Hutton, V.R.S. (1980). An analogue model study of electromagnetic induction in the British Island region. Phys. Earth Planet. Inter. **22**, 68–85.

Dosso, H.W., Nienaber, W., and Parkinson, W.D. (1985). An analogue model study of electromagnetic induction in the Tasmania region. Phys. Earth Planet. Inter. **39**, 118–133.

Dosso, H.W., Ramaswamy, V., Jones, F.W., and Thomson, D.J. (1974). On the comparison of laboratory electromagnetic analogue model measurements and finite-difference numerical calculations. Phys. Earth Planet. Inter. **9**, 108–110.

Dosso, H.W., Weaver, J.T. (1983). The collective review papers presented at the 6th IAGA Workshop on Electromagnetic Induction in Earth and Moon-Preface. Geophys. Surv. **6**, 103.

Eggers, D.E. (1982). An eigenstate formulation of the magnetotelluric impedance tensor. Geophysics **47**, 1204–1214.

Erdélyi, A. (ed.) (1954). *Tables of Integral Transforms* Vols. I and II. McGraw-Hill, New York.

Everett, M.E. and Schultz, A. (1993). Two-dimensional nonlinear magnetotelluric inversion using a Genetic algorithm. J. Geomag. Geoelectr. **45**, 1013–1026.

Gordon, A.N. (1951). Electromagnetic induction in a uniform semi-infinite conductor. Q. J. Mech. Appl. Math. **4**, 116–128.

Green, V.R. and Weaver, J.T. (1978). Two-dimensional induction in a thin sheet of variable integrated conductivity at the surface of a uniformly conducting earth. Geophys. J. R. astr. Soc. **55**, 721–736.

Groom, R.W. and Bailey, R.C. (1989). Decomposition of magnetotelluric impedance tensors in the presence of a local three-dimensional galvanic distortion. J. Geophys. Res. **94**, 1913–1925.

Groom, R.W. and Bailey, R.C. (1991). Analytic investigations of the effects of near-surface three-dimensional galvanic scatterers on MT tensor decompositions. Geophysics **56**, 496–518.

Hebert, D., Dosso, H.W., Nienaber, W., & Wright, J.A. (1983). Analogue model study of electromagnetic induction in the Newfoundland region. Phys. Earth Planet. Inter. **36**, 101–131.

Hohmann, G.W. (1971). Electromagnetic scattering by conductors in the earth near a line source of current. Geophysics **36**, 101–131.

Hohmann, G.W. (1975). Three-dimensional induced polarization and electromagnetic modeling. Geophysics **40**, 309–324.

Hohmann, G.W. (1983). Three-dimensional EM modelling. Geophysical Surveys **6**, 27–53.

Hu, W.B., Dosso, H.W., and Nienaber, W. (1984). Analogue model magnetic field responses of an ocean channel, an island and a seamount in the Hainan Island region. J. Geophys. **55**, 222–227.

Hutson, V.C.L., Kendall, P.C. and Malin, S.R.C. (1972). Computation of the solution of geomagnetic induction problems: a general method, with applications. Geophys. J. R. astr. Soc. **28**, 489–498.

Jackson, J.D. (1975). Classical electrodynamics, 2nd ed. John Wiley and Sons, Inc., New York.

Jones, A.G. (1983). The problem of current channelling: a critical review. Geophysical Surveys **6**, 79–122.

Jones, D.S. (1964). *The Theory of Electromagnetism.* Pergamon Press, Oxford.

Jones, F. W. (1973). Induction in laterally non-uniform conductors: theory and numerical models. Phys. Earth Planet. Inter. **7**, 282–293.

Jones, F.W. (1974a). The perturbations of slowly varying electromagnetic fields by three-dimensional conducting bodies. Can. J. Phys. **52**, 1195–1202.

Jones, F.W. (1974b). The perturbations of geomagnetic fields by two-dimensional and three-dimensional conductivity inhomogeneities. Pure and Appl. Geophys. **112**, 793–800.

Jones, F.W. (1974c). The effect of an island and bay structure on alternating geomagnetic fields at three periods. Geophys. J. R. astr. Soc. **36**, 627–639.

Jones, F W. and Pascoe, L.J. (1971). A general computer program to determine the perturbation of alternating electric currents in a two-dimensional model. Geophys. J. R. astr. Soc. **23**, 3–30.

Jones, F.W. and Pascoe, L.J. (1972). The perturbation of alternating geomagnetic fields by three-dimensional conductivity inhomogeneities. Geophys. J. R. astr. Soc. **27**, 479–484.

Jones, F.W. and Price, A.T. (1970). The perturbations of alternating geomagnetic fields by conductivity anomalies. Geophys. J. R. astr. Soc. **20**, 317–334.

Jones, F.W. and Vozoff, K. (1978). The calculation of magnetotelluric quantities for three-dimensional conductivity inhomogeneities. Geophysics **43**, 1167-1175.

Jupp, D.L.B and Vozoff, K. (1977). Two-dimensional magnetotelluric inversion. Geophys. J. R. astr. Soc. **50**, 333–352.

Kaikkonen, P. (1977). A finite element package for electromagnetic modelling. J. Geophys. **43**, 179–192.

Kaikkonen, P. (1980). Numerical finite element modeling in geophysical applications of electromagnetic fields. Ph.D thesis, Acta Univ. Oul. A 93, 1980 Phys. 18, 135 pp.

Kaikkonen, P. (1986). Numerical electromagnetic modelling including studies of characteristic dimensions: a review. Surveys in Geophysics. **8**, 301–337.

Kang, S., Dosso, H.W. and Ogunade, S.O. (1993). Electromagnetic induction in south-west Nigeria: Analogue model and field results. J. Geomag. Geoelectr. **45**, 805–816.

Kisak, E. and Silvester, P. (1975). A finite element package for magnetotelluric modelling. Comp. Phys. Comm. **10**, 421–433.

Larsen, J.C. (1977). Removal of local surface conductivity effects from low frquency mantle response curves. Acta Geodaet. Geophys. et Montanist. Acad. Sci. Hung. **12**, 183–186.

LaTorraca, G.A., Madden, T.R. and Korringa, J. (1986). An analysis of the magnetotelluric impedance for three-dimensional conductivity structures. Geophysics **51**, 1819–1829.

Lines, L.R. and Jones, F.W. (1973a). The perturbation of alternating geomagnetic fields by three-dimensional island structures. Geophys. J. R. astr. Soc. **32**, 133–154.

Lines, L.R. and Jones, F.W. (1973b). The perturbation of alternating geomagnetic fields by an island near a coastline. Can. J. Earth Sci. **10**, 510–518.

Madden, T.R. and Swift, C.M. (1969). Magnetotelluric studies of the electrical conductivity structure of the crust and upper mantle, in *The Earth's Crust and Upper Mantle.* (Edited by P.J. Hart.) A.G.U. Monograph **13**, 469–479.

McKirdy, D.McA. and Weaver, J.T. (1984). Induction in a thin sheet of variable conductance at the surface of a stratified earth — I: Two-dimensional theory. Geophys. J. R. astr. Soc. **78**, 93–103.

McKirdy, D.McA., Weaver, J.T. and Dawson, T.W. (1985). Induction in a thin sheet of variable conductance at the surface of a stratified earth — II: Three-dimensional theory. Geophys. J. R. astr. Soc. **80**, 177–194.

Meng, Z. (1991). Analogue, numerical and field site studies of EM induction in the China-Korea-Japan region. Ph.D. thesis, Dept. of Phys. and Astro. University of Victoria, Victoria BC Canada.

Meng, Z. and Dosso, H.W. (1990). An analogue model study of EM induction in the Japan – Korea – China region. Phys. Earth Planet. Inter. **62**, 246–256.

Meng, Z., Dosso, H.W. and Nienaber, W. (1990). An analogue model study of EM induction in the North China – Korea coastal region. Phys. Earth Planet. Inter. **60**, 25–39.

Menvielle, M. (1988). Effects of crustal conductivity heterogeneities on the electromagnetic field. Surveys in Geophysics **9**, 319–348.

Neves, V.S. (1957). The magneto-telluric method in two-dimensional structures. Ph.D. thesis, Dept. of Geology and Geophysics, MIT, 186 pp.

Nienaber, W., Dosso, H.W., Law, L.K., Jones, F.W., and Ramaswamy, V. (1977). Studies of electromagnetic induction for island-continent ocean channels with applications to Vancouver Island. Acta Geodaet., Geophys. et Montanist. Acad. Sci. Hung. **12**, 187–190.

Nienaber, W., Dosso, H.W., Law, L.K., Jones, F.W., and Ramaswamy, V. (1979). An analogue model study of electromagnetic induction in the Vancouver Island region. J. Geomagn. Geoelectr. **3**, 115–132.

Oldenburg, D.W. and Ellis, R.G. (1991). Inversion og geophysical data mapping using an approximate inverse mapping. Geophys. J. Int. **105**, 325–353.

Olver, F.W.J. (1964). Bessel functions of integral order, Chapter 9 in *Handbook of Mathematical Functions.* (Edited by M. Abramowitz and I.A. Stegun.) U.S. Dept. Commerce, Nat. Bur. Stand., Washington, D.C.

Poll, H.E. (1994). Ph.D. thesis in prepariration, Dept. of Phys. and Astro. University of Victoria, Victoria BC Canada.

Price, A.T. (1949). The induction of electric currents in non-uniform thin sheets and shells. Q. J. Mech. Appl. Math. **2**, 283–310.

Price, A.T. (1950). Electromagnetic induction in a semi-infinite conductor with a plane boundary. Q. J. Mech. Appl. Math. **3**, 385–410.

Price, A.T. (1962). The theory of magnetotelluric methods when the source field is considered. J. Geophys. Res. **67**, 1907–1918.

Price, A.T. (1964). A note on the interpretation of magnetic variations and magnetitelluric data. J. Geomag. Geoelec. **15**, 241–248.

Pridmore, D.F., Hohmann, G.W., Ward, S.H., and Sill, W.R. (1981). An investigation of finite element modeling for electrical and electromagnetic data in three dimensions. Geophysics **46**, 1009–1024.

Pu, X.H. (1993). Integrals for boundary conditions in three-dimensional electromagnetic modelling. CEOR Report 93-11, University of Victoria, British Columbia, Canada.

Pu, X.H., Agarwal, A.K. and Weaver, J.T. (1988). A new three-dimensional electromagnetic modelling algorithm. Proceedings of the 35th Annual Meet-

ing of Pacific Northwest Region Americal Geophysical Union. 23-30 Sep., 1988. Royal Roads Millitary College, Victoria, BC Canada.

Pu, X.H., Agarwal, A.K. and Weaver, J.T. (1991). A theoretical investigation of anisotropic geoelectric structures using three-dimensional numerical models. Unpublished poster presentation, IAGA Abstract GAM 1.6, International Union of Geodesy and Geophysics, Vienna.

Pu, X.H., Agarwal, A.K. and Weaver, J.T. (1992a). Numerical solution of two-dimensional E-polarization problems using the magnetical field. 11th Workshop on Electromagnetic Induction in the Earth. 26 Aug.-2 Sep., 1992. Victoria University of Wellington, Wellington, New Zealand.

Pu, X.H., Agarwal, A.K. and Weaver, J.T. (1992b). Numerical solution of two and three-dimenstional problems using the magnetic fields. Proceedings of the 39th Annual Meeting of Pacific Northwest Region Americal Geophysical Union. 23-25 Sep., 1992. Victoria, BC Canada.

Pu, X.H., Agarwal, A.K. and Weaver, J.T. (1993a). Distortion effects due to small surface inhomogeneities in geo-electromagnetic induction. Scientific meeting of the Canadian Geophysical Union (CGU), May 9-11, 93, Banff Alberta, Canada. Program and abstracts, No 118.

Pu, X.H., Agarwal, A.K. and Weaver, J.T. (1993b). Magnetic field solutions of E-polarization induction problems. J. Geomag. Geoelectr. **45**, 859–872.

Raiche, A.P. (1974). An integral equation approach to three-dimensional modelling. Geophys. J. R. astr. Soc. **36**, 363–376.

Rankin, D. (1962). The magnetotelluric effect of a Dike. Geophysics **27**, 666–676.

Reddy, I.K. and Rankin, D. (1973). Magnetotelluric response of a two-dimensional sloping contact by the finite element method. Pure and Appl. Geophys. **105**, 847–857.

Reddy, I.K., Rankin, D. and Phillips, R.J. (1977). Three-dimensional modeling in magnetotelluric and magnetic variational sounding. Geophys. J. R. astr. Soc. **51**, 313–326.

Rikitake, T. (1973). Global electrical conductivity of the earth. Phys. Earth Planet. Inter. **7**, 245–250.

Rodi, W.L. (1976). A technique for improving the accuracy of finite element solutions for magnetotelluric data. Geophys. J. R. astr. Soc. **44**, 483–506.

Schmucker, U. (1970). Anomalies of geomagnetic variations in the southwestern United States. Bull. Scripps Inst. Oceanog. **13**, Univ. Calif. Press.

Schmucker, U. (1993). 2D modelling with linearized integral equations, J. Geomag. Geoelectr. **45**, 1045–1062.

Schnegg, P.A. (1993). An automatic scheme for 2-D magnetotelluric modelling, based on low-order polynomial fitting. J. Geomag. Geoelectr. **45**, 1039–1043.

Silvester, P. and Haslam, C.R.S. (1972). Magnetotelluric modeling by the finite element method. Geophys. Prospecting **20**, 872–891.

Smith, J.T. and Booker, J.R. (1991). The rapid relaxation inverse for two- and three-dimensional magnetotelluric data, J. Geophys. Res. **96**, 3905–3922.

Spitz, S. (1985). The magnetotelluric impedance tensor properties with respect to rotations. Geophysics **50**, 1610–1617.

Summers, D.M. and Weaver, J.T. (1973). Electromagnetic induction in a stratified conducting half-space by an arbitary periodic source. Can. J. Phys. **41**, 484–495.

Ting, S.C. and Hohmann, G.W. (1981). Integral equation modeling of three-dimensional magnetolelluric response. Geophysics **46**, 182–197.

Travis, B.J. and Chave, A.D. (1989). A moving finite element method for magnetotelluric modeling. Phys. Earth Planet. Inter. **53**, 432–443.

Uchida, T. (1993). Smooth 2-D inversion for magnetotelluric data based on statistical criterion ABIC. J. Geomag. Geoelectr. **45**, 841–858.

Vasseur, G. and Weidelt, P. (1977). Bimodal electromagnetic induction in non-uniform thin sheets with an application to the northern Pyrenean induction anomaly. Geophys. J. R. astr. Soc. **51**, 669–690.

Verentsov, Iv. M. (1983). Modern trends in the solution of forward and inverse 3D electromagnetic induction problems. Geophysical Surveys **6**55–78.

Wait, J.R. (1954). On the relation between telluric currents and the Earth's magnetic field. Geophysics **19**, 281–289.

Wannamaker, P.E., Stodt, J.A. and Rijo, L. (1987). A stable finite element solution for two-dimensional magnetotelluric modelling. Geophys. J. R. astr. Soc. **88**, 277–296.

Weaver, J.T. (1963). The electromagnetic field within a discontinuous conductor with reference to geomagnetic micropulsations near a coastline. Can. J. Phys. **41**, 484–495.

Weaver, J.T. (1964). On the separation of local geomagnetic fields into external and internal parts. Z. Geophys. **30**, 29–36.

Weaver, J.T. (1971). The general theory of electromagnetic induction in a conducting half-space. Geophys. J. R. astr. Soc. **22**, 83–100. **7**, 245–250.

Weaver, J.T. (1973). Induction in a layered plane Earth by uniform and non-uniform source fields. Phys. Earth Planet. Inter. **7**, 266–281.

Weaver, J.T. (1994). *Mathematical methods for geo-electromagnetic induction.* John Wiley and Sons, Inc., New York.

Weaver, J.T. and Agarwal, A.K. (1991). Is addition of induction vectors meaningful? Phys. Earth Planet. Inter. **65**, 267–275.

Weaver, J.T. and Agarwal, A.K. (1993). Automatic one-dimensional inversion of magnetotelluric data by the method of modelling. Geophys. J. Int. **112**, 115–123.

Weaver, J.T., LeQuang, B.V. and Fischer, G. (1985). A comparison of analytical and numerical results for a two-dimensional control model in electromagnetic induction–I. B-polarization calculations. Geophys. J. R. astr. Soc. **82**, 263–278.

Weaver, J.T., LeQuang, B.V. and Fischer, G. (1986). A comparison of analytical and numerical results for a 2-D control model in electromagnetic induction–II. E-polarization calculations. Geophys. J. R. astr. Soc. **87**, 917–948.

Weaver, J.T. and Pu, X.H. (1988). Three dimensional modelling of induction porblems by finite differences. 9th Workshop on Electromagnetic Induction in the Earth and Moon. 24-31 Oct., 1988. Dagomys Complex, Sochi, USSR.

Weidelt, P. (1975a). Inversion of two-dimensional conductivity structures. Phys. Earth Planet. Inter. **10**, 282–291.

Weidelt, P. (1975b). Electromagnetic induction in three-dimensional structures. J. Geophys. **41**, 85–109.

Yee, E. (1985). The magnetotelluric impedance tensor-its reconstruction and analysis. Ph.D. theiss, University of Saskatchewan, saskatoon.

Yee, E. and Paulson, K.V. (1987). The canonical decomposition and its relationship to other forms of magnetotelluric impedance tensor analysis. J. Geophys. **61**, 173–189.

Zhao, G.Z. and Liu, G.D. (1990). A new inversion scheme for two-dimensional magnetotelluric modelling. J. Geomag. Geoelectr. **42**,

Zhdanov, M.S., Golubev, N.G., Spichak, V.V. and Varentsov, Iv. M. (1982). The construction of effective methods for electromagnetic modeling. Geophys. J. R. astr. Soc. **68**, 589–607.

# Appendix A

# INTEGRALS FOR BOUNDARY CONDITIONS IN THREE-DIMENSIONAL EM MODELLING

---

The contents in this appendix have also been published in separate as a CEOR report for easy reference (Pu, 1993).

Equations of the surface and bottom boundary conditions in the 3-D problem, (3.54), (3.55) and (3.56), involve three double integrals operators over the $x-y$ plane, $M_1$, $M_2$ and $M_d$; they are defined as

$$M_1 Z(\mathbf{r},0) = \frac{1}{2\pi}\int_{-\infty}^{\infty}\int_{-\infty}^{\infty} Z(u,v,0)\frac{x-u}{[(x-u)^2+(y-v)^2]}\,du\,dv, \quad \text{(A.1)}$$

$$M_2 Z(\mathbf{r},0) = \frac{1}{2\pi}\int_{-\infty}^{\infty}\int_{-\infty}^{\infty} Z(u,v,0)\frac{y-v}{[(x-u)^2+(y-v)^2]}\,du\,dv, \quad \text{(A.2)}$$

$$M_d \Phi(\mathbf{r},d) = \frac{1}{2\pi}\int_{-\infty}^{\infty} [\Phi(\mathbf{s},d)-\Phi(\mathbf{r},d)]\,Q(|\mathbf{r}-\mathbf{s}|)\,d\mathbf{s}, \quad \text{(A.3)}$$

where $\Phi$ stands for any magnetic component $X$, $Y$ or $Z$, $\mathbf{r}=(x,y)$, $\mathbf{s}=(u,v)$, $d\mathbf{s}=du\,dv$ and

$$Q(r) \equiv Q(\mathbf{r},0) = r^{-3}(1+r\alpha_0\sqrt{i})\exp(-r\alpha_0\sqrt{i}), \quad r=(x^2+y^2)^{1/2}. \quad \text{(A.4)}$$

For algebraic convenience in the following sections, we will ignore the constant factor $1/2\pi$ in the definitions of $M_1$, $M_2$ and $M_d$; it will be re-introduced into the formulae in the SUMMARY section.

Since the field values $Z$ and $\Phi$ are only defined at the grid nodes, we have to break the whole integral into a sum of sub-integrals over many rectangular cells. At the four corners of each cell, the field values are either defined as node values or as values given by the boundary conditions. The values at points between the grid nodes can be interpolated from these corner values by a specified

interpolation scheme. Thus the integrals over each cell can be evaluated, most of them analytically, but some have to be integrated numerically. The results are expressed in terms of the four node values at the corners of cells. When all these results are summed over the cells, the integral over the entire $x-y$ plane can be reduced to a linear combination of $F_{l,m}$, the values of $\Phi$ at the nodes $(x_l, y_m, 0)$ for $M_1$ and $M_2$, or $(x_l, y_m, d)$ for $M_d$, i.e.

$$M\,F(x_\lambda, y_\mu) = \sum_{l=1}^{L}\sum_{m=1}^{M} A_{\lambda\mu}^{lm} F_{lm} \tag{A.5}$$

where the coefficients $A_{\lambda\mu}^{lm}$ are composed of integrals over grid cells.

When the integrals are evaluated at a fixed node $(x_\lambda, y_\mu)$, the integrands are singular at the point $(x,y) = (x_\lambda, y_\mu)$, due to the presence of the factor $1/[(x_\lambda - x)^2 + (y_\mu - y)^2]^{3/2}$. This point will be referred to as the singularity or the singular point. Once the singularity has been fixed, the $x-y$ plane is decomposed into ten regions which are denoted by $\tilde{R}_0$, $R_0$ and $R_1$ to $R_8$ as shown in Fig (A.1) where we have defined

$$\begin{aligned} &x_0 = -\infty,\ \ x_{L+1} = +\infty,\ \ y_0 = -\infty,\ \ y_{M+1} = +\infty, \\ &g_l = x_{l+1} - x_l, \qquad\qquad h_m = y_{m+1} - y_m. \end{aligned} \tag{A.6}$$

The entire $x-y$ plane is thus covered by a mesh with nodes $(m,n)$, $0 \le m \le L+1$, $0 \le n \le M+1$. We call $\tilde{R}_0$ the singular region, which is defined as

$$\tilde{R}_0 = \{\mathbf{r} \mid -g_{\lambda-1} \le x - x_\lambda < g_\lambda;\ \ -h_{\mu-1} \le y - y_\mu < h_\mu\}. \tag{A.7}$$

It is composed of four individual singular cells surrounding the singular point $(x_\lambda, y_\mu)$. $R_0$ is the finite normal region, defined as

$$R_0 = \{\mathbf{r} \mid x_1 \le x < x_L;\ \ y_1 \le y < y_M\} - \tilde{R}_0. \tag{A.8}$$

$R_1$ to $R_4$ are infinite regions consisting of groups of infinite cells with one edge tending to infinity and $R_5$ to $R_8$ are infinite regions with two neighbouring edges

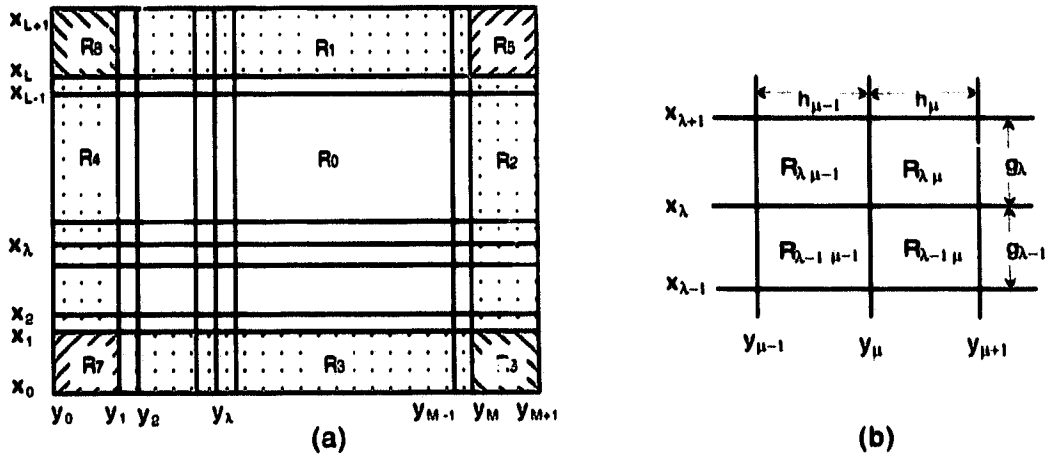


Figure A.1: (a) depicts the ten regions on the $xy$-plane; (b) is the singular region $\tilde{R}_0$.

approaching infinity. Sometimes, we also address an individual cell as $R_{lm}$ which is defined as $R_{lm} = \{\mathbf{r} \mid x_l \le x < x_{l+1};\ y_m \le y < y_{m+1}\}$.

Now, let us look at integral (A.1) first. For convenience, we define $D := [(x_\lambda - u)^2 + (y_\mu - v)^2]^{3/2}$ and also work with $-M_1 Z$ rather than $M_1 Z$. We have

$$\begin{aligned} -M_1 Z_{\lambda\mu} &= \int_{-\infty}^{\infty}\int_{-\infty}^{\infty} Z(u,v)\frac{u-x_\lambda}{D}\,du\,dv \\ &= \left[\oint_{\tilde{R}_0} + \int_{R_0} + \int_{R_1} + \ldots + \int_{R_8}\right] Z(u,v)\frac{u-x_\lambda}{D}\,du\,dv \\ &= \tilde{I}_0 + I_0 + I_1 + \ldots + I_8 \end{aligned} \tag{A.9}$$

where

$$\tilde{I}_0 = \oint_{\tilde{R}_0} Z(u,v)\frac{u-x_\lambda}{D}\,du\,dv = \oint_{x_\lambda - g_{\lambda-1}}^{x_\lambda + g_\lambda}\int_{y_\mu - h_{\mu-1}}^{y_\mu + h_\mu} Z(u,v)\frac{u-x_\lambda}{D}\,du\,dv \tag{A.10}$$

is interpreted as its Cauchy principal value. If we think in terms of each individual cell, we can also write

$$-M_1 Z_{\lambda\mu} = \sum_{l=0}^{L}\sum_{m=0}^{M} I_x^{lm} \tag{A.11}$$

where

$$I_x^{lm} := \int_{x_l}^{x_{l+1}}\int_{y_m}^{y_{m+1}} Z(u,v)\frac{u-x_\lambda}{D}\,du\,dv \tag{A.12}$$

## A.1 Contribution of Individual Cells

$I_x^{lm}$ is a typical integral over a single cell. The field values at the four corners of the cell are $Z_{lm}$, $Z_{l+1m}$, $Z_{lm+1}$ and $Z_{l+1m+1}$. For interpolating the values of $Z(u,v)$ at points between the nodes of the mesh, a bi-linear interpolation scheme will be employed here,

$$Z(u,v) = Z_{lm} + \frac{u-x_l}{g_l}(Z_{l+1m} - Z_{lm}) + \frac{v-y_m}{h_m}(Z_{lm+1} - Z_{lm}) + \frac{(u-x_l)(v-y_m)}{g_l h_m}(Z_{l+1m+1} + Z_{lm} - Z_{l+1m} - Z_{lm+1}). \quad \text{(A.13)}$$

To simplify the integrand in (A.12), we make the transformation

$$\alpha = u - x_\lambda, \qquad \beta = v - y_\mu, \quad \text{(A.14)}$$

and define

$$a_l = x_l - x_\lambda, \qquad b_m = y_m - y_\mu \quad \text{(A.15)}$$

$$T_1 = (Z_{l+1m} - Z_{lm})/g_l,\ T_2 = (Z_{lm+1} - Z_{lm})/h_m,$$

$$T_3 = (Z_{l+1m+1} + Z_{lm} - Z_{l+1m} - Z_{lm+1})/g_l h_m. \quad \text{(A.16)}$$

Then, we have

$$Z(u,v) = \tilde{Z}(\alpha,\beta) = Z_{lm} + T_1(\alpha - a_l) + T_2(\beta - b_m) + T_3(\alpha - a_l)(\beta - b_m),$$

$$D = [(x_\lambda - u)^2 + (y_\mu - v)^2]^{3/2} = (\alpha^2 + \beta^2)^{3/2}. \quad \text{(A.17)}$$

If we further define

$$\alpha_1 = a_l, \quad \alpha_2 = a_{l+1}; \quad \beta_1 = b_m, \quad \beta_2 = b_{m+1}, \quad \text{(A.18)}$$

then integral $I_x^{lm}$ becomes

$$I_x^{lm} = \int_{\alpha_1}^{\alpha_2}\int_{\beta_1}^{\beta_2} \tilde{Z}(\alpha,\beta)\frac{\alpha}{[\alpha^2+\beta^2]^{3/2}}\,d\alpha\,d\beta$$

$$= Z_{lm} I_\alpha^{lm} + T_1(I_{\alpha^2}^{lm} - a_l I_\alpha^{lm}) + T_2(I_{\alpha\beta}^{lm} - b_m I_\alpha^{lm}) + T_3(I_{\alpha^2\beta}^{lm} - a_l I_{\alpha\beta}^{lm} - b_m I_{\alpha^2}^{lm} + a_l b_m I_\alpha^{lm}), \quad \text{(A.19)}$$

or

$$I_x^{lm} = Z_{lm} I_\alpha^{lm} + T_1 A g_l + T_2 B h_m + T_3 C g_l h_m, \tag{A.20}$$

where

$$\begin{aligned} A &= (I_{\alpha^2}^{lm} - a_l I_\alpha^{lm})/g_l, \quad B = (I_{\alpha\beta}^{lm} - b_m I_\alpha^{lm})/h_m, \\ C &= (I_{\alpha^2\beta}^{lm} - a_l I_{\alpha\beta}^{lm} - b_m I_{\alpha^2}^{lm} + g_l h_m I_\alpha^{lm})/h_m g_l, \end{aligned} \tag{A.21}$$

and

$$\begin{aligned} I_\alpha^{lm} &= \int_{\alpha_1}^{\alpha_2}\int_{\beta_1}^{\beta_2} \frac{\alpha}{[\alpha^2+\beta^2]^{3/2}}\, d\alpha\, d\beta, \\ I_{\alpha^2}^{lm} &= \int_{\alpha_1}^{\alpha_2}\int_{\beta_1}^{\beta_2} \frac{\alpha^2}{[\alpha^2+\beta^2]^{3/2}}\, d\alpha\, d\beta, \\ I_{\alpha\beta}^{lm} &= \int_{\alpha_1}^{\alpha_2}\int_{\beta_1}^{\beta_2} \frac{\alpha\beta}{[\alpha^2+\beta^2]^{3/2}}\, d\alpha\, d\beta, \\ I_{\alpha^2\beta}^{lm} &= \int_{\alpha_1}^{\alpha_2}\int_{\beta_1}^{\beta_2} \frac{\alpha^2\beta}{[\alpha^2+\beta^2]^{3/2}}\, d\alpha\, d\beta. \end{aligned} \tag{A.22}$$

The integral $I_x^{lm}$ can also be written as

$$\begin{aligned} I_x^{lm} &= (Z_{lm} - T_1 a_l - T_2 b_m + T_3 a_l b_m) I_\alpha^{lm} \\ &\quad + (T_1 - T_3 b_m) I_{\alpha^2}^{lm} + (T_2 - T_3 a_l) I_{\alpha\beta}^{lm} + T_3 I_{\alpha^2\beta}^{lm}. \end{aligned} \tag{A.23}$$

It means that $I_x^{lm}$, a typical integral over a cell, can be broken into four sub-integrals, $I_\alpha^{lm}$, $I_{\alpha\beta}^{lm}$, $I_{\alpha^2}^{lm}$ and $I_{\alpha^2\beta}^{lm}$, over the same integration limits.

Insert the expressions for $T_1$, $T_2$ and $T_3$ into (A.20), so that $I_x^{lm}$ can be expressed in terms of the field value at nodes, i.e.

$$\begin{aligned} I_x^{lm} &= (I_\alpha^{lm} - A - B + C) Z_{l\,m} + (A - C) Z_{l+1\,m} \\ &\quad + (B - C) Z_{l\,m+1} - C Z_{l+1\,m+1} \\ &= Q_{lm}^{00} Z_{lm} + Q_{lm}^{10} Z_{l+1m} + Q_{lm}^{01} Z_{lm+1} + Q_{lm}^{11} Z_{l+1m+1} \\ &= \sum_{p=0}^{1}\sum_{q=0}^{1} Q_{lm}^{pq} Z_{l+p\,m+q}. \end{aligned} \tag{A.24}$$

$Q_{lm}^{pq}$ is the contribution of cell $R_{lm}$ to the coefficient of field value $Z_{l+p\,m+q}$. Inserting the expressions of $A$, $B$ and $C$ into $Q_{lm}^{pq}$ in the above formula and noting that $a_{l+1} = a_l + g_l$, $\quad b_{m+1} = b_m + h_m$, we have

$$\begin{aligned}
Q_{lm}^{00} &= (a_{l+1}b_{m+1}I_{\alpha}^{lm} - a_{l+1}I_{\alpha\beta}^{lm} - b_{m+1}I_{\alpha^2}^{lm} + I_{\alpha^2\beta}^{lm})/g_l\,h_m,\\
Q_{lm}^{10} &= -(a_l b_{m+1}I_{\alpha}^{lm} - a_l I_{\alpha\beta}^{lm} - b_{m+1}I_{\alpha^2}^{lm} + I_{\alpha^2\beta}^{lm})/g_l\,h_m,\\
Q_{lm}^{01} &= -(a_{l+1}b_m I_{\alpha}^{lm} - a_{l+1}I_{\alpha\beta}^{lm} - b_m I_{\alpha^2}^{lm} + I_{\alpha^2\beta}^{lm})/g_l\,h_m,\\
Q_{lm}^{11} &= (a_l b_m I_{\alpha}^{lm} - a_l I_{\alpha\beta}^{lm} - b_m I_{\alpha^2}^{lm} + I_{\alpha^2\beta}^{lm})/g_l\,h_m,
\end{aligned} \tag{A.25}$$

which can also be expressed by the general formula

$$Q_{lm}^{pq} = \frac{(-1)^{p+q}}{g_l\,h_m}\sum_{r=0}^{1}\sum_{s=0}^{1}(-1)^{r+s}(a_{l+1-p})^{1-r}(b_{m+1-q})^{1-s}I_{\alpha^{1+r}\beta^s}^{lm}. \tag{A.26}$$

## A.2 Integral Operator $M_1$

It is desirable to express the integral in the form of equation (A.5), i.e. in terms of the field values,

$$\begin{aligned}
-M_1\,Z_{\lambda\mu} &= \sum_{l=0}^{L}\sum_{m=0}^{M} I_x^{lm} = \sum_{l=0}^{L}\sum_{m=0}^{M}\sum_{p=0}^{1}\sum_{q=0}^{1} Q_{lm}^{pq} Z_{l+p\,m+q}\\
&= \sum_{l=0}^{L}\sum_{m=0}^{M}(Q_{lm}^{00}Z_{lm} + Q_{lm}^{10}Z_{l+1m} + Q_{lm}^{01}Z_{lm+1} + Q_{lm}^{11}Z_{l+1m+1})\\
&= \left[\sum_{l=0}^{L}\sum_{m=0}^{M} Q_{lm}^{00} + \sum_{l=1}^{L+1}\sum_{m=0}^{M} Q_{l-1m}^{10} + \sum_{l=0}^{L}\sum_{m=1}^{M+1} Q_{lm-1}^{01} + \sum_{l=1}^{L+1}\sum_{m=1}^{M+1} Q_{l-1m-1}^{11}\right] Z_{lm}\\
&= \left[\sum_{l=0}^{0}\sum_{m=0}^{0} + \sum_{l=0}^{0}\sum_{m=1}^{M} + \sum_{m=0}^{0}\sum_{l=1}^{L} + \sum_{l=1}^{L}\sum_{m=1}^{M}\right] Q_{lm}^{00} Z_{lm}\\
&+ \left[\sum_{l=L+1}^{L+1}\sum_{m=0}^{0} + \sum_{l=L+1}^{L+1}\sum_{m=1}^{M} + \sum_{m=0}^{0}\sum_{l=1}^{L} + \sum_{l=1}^{L}\sum_{m=1}^{M}\right] Q_{l-1m}^{10} Z_{lm}\\
&+ \left[\sum_{l=0}^{0}\sum_{m=M+1}^{M+1} + \sum_{l=0}^{0}\sum_{m=1}^{M} + \sum_{m=M+1}^{M+1}\sum_{l=1}^{L} + \sum_{l=1}^{L}\sum_{m=1}^{M}\right] Q_{lm-1}^{01} Z_{lm}\\
&+ \left[\sum_{l=L+1}^{L+1}\sum_{m=M+1}^{M+1} + \sum_{l=L+1}^{L+1}\sum_{m=1}^{M} + \sum_{m=M+1}^{M+1}\sum_{l=1}^{L} + \sum_{l=1}^{L}\sum_{m=1}^{M}\right] Q_{l-1m-1}^{11} Z_{lm}.
\end{aligned} \tag{A.27}$$

It gives

$$-M_1\,Z_{\lambda\mu} = \sum_{l=1}^{L}\sum_{m=1}^{M}(Q_{lm}^{00} + Q_{l-1m}^{10} + Q_{lm-1}^{01} + Q_{l-1m-1}^{11})Z_{lm}$$

$$
\begin{aligned}
&+ \sum_{l=1}^{L}(Q_{l0}^{00}+Q_{l-10}^{10})Z_{l0}+\sum_{l=1}^{L}(Q_{lM}^{01}+Q_{l-1M}^{11})Z_{lM+1}\\
&+ \sum_{m=1}^{M}(Q_{0m}^{00}+Q_{0m-1}^{01})Z_{0m}+\sum_{m=1}^{M}(Q_{Lm}^{10}+Q_{Lm-1}^{11})Z_{L+1m}\\
&+ Q_{00}^{00}Z_{00}+Q_{L0}^{10}Z_{L+10}+Q_{0M}^{01}Z_{0M+1}+Q_{LM}^{11}Z_{L+1M+1},
\end{aligned}
\tag{A.28}
$$

These summations group together the field value at nodes related to regions $(\tilde{I}_0+\tilde{\tilde{I}}_0)$, $I_3$, $I_1$, $I_4$, $I_2$, $I_7$, $I_8$, $I_6$ and $I_5$ respectively. At the boundary of the grid mesh, regions $R_1$ to $R_4$ and $R_5$ to $R_8$ are groups of cells with respectively one and two edges continued out to infinity. If no asymptotic boundary conditions are used, then the boundaries of the mesh ($x = x_1$ and $x = x_L$) must be sufficiently far away from the nearest conductivity contrast that, with the strike in the $y$-direction, $\partial F/\partial x \approx 0$ for all field components, i.e. $F(x) \approx F(x_1)$, for $x \leq x_1$ and $F(x) \approx F(x_L)$, for $x \geq x_l$. Thus we can pre-calculate the results for the limiting structures at infinity (either 2D or 1D) and use the results as the boundary conditions on the corresponding boundaries of the mesh during the computation of the 3D results, i.e.

$$
F(x_0,y_m)=F(x_0,y_m),\ F(x_L,y_m)=F(x_{L+1},y_m);\ m=1...M \tag{A.29}
$$

where $x_0 = -\infty$ and $x_{L+1} = +\infty$ are the same as defined before. The pre-calculated results are given at the grid nodes only. An interpolation scheme is needed for the variation along $y$-direction between the nodes; a linear variation is a reasonable assumption in this case. According to (A.17) , this linear variation may be written as

$$
F(\alpha,\beta)=F_{lm}+T_2(\beta-b_m),\ (x<x_1 \text{ or } x>x_L),\ y_m\leq y<y_{m+1}. \tag{A.30}
$$

Similarly, in $R_2$ and $R_4$ $|y_1|$ and $|y_M|$ must be large enough to satisfy $\partial F/\partial y \approx 0$ in $y \leq y_1$ or $y \geq y_m$, so that

$$
F(x_l,y_1)=F(x_l,y_0),\ F(x_l,y_M)=F(x_l,y_{M+1}),\ l=1...L \tag{A.31}
$$

can be applied along the $y$-direction with a linear variation in the $x$-direction.

In regions $R_5$ to $R_8$, the only natural choice is $\partial F/\partial x = \partial F/\partial y = 0$. Therefore, we can write

$$\begin{aligned}
F(x,y) = F(x_L, y_M) &= F(x_{L+1}, y_{M+1}), && (x,y) \in R_5 \\
F(x,y) = F(x_1, y_M) &= F(x_0, y_{M+1}), && (x,y) \in R_6 \\
F(x,y) = F(x_1, y_1) &= F(x_0, y_0), && (x,y) \in R_7 \\
F(x,y) = F(x_L\ y_1) &= F(x_{L+1}, y_0), && (x,y) \in R_8.
\end{aligned}$$

Since the only field component being integrated with $M_1$ is $Z$, from now on we will use $Z$ specifically instead of $F$ for the general case. In region $R_1$ and $R_3$, $Z$ is uniform in the $x$-direction and varies linearly in the $y$-direction. Thus $Z(x, y_m) = Z_{lm} = Z_{l+1\,m}$, $x_L \le x \le x_{L+1}$ or $x_0 \le x \le x_1$, and we can define $Z_{u\,m} = cZ_{lm} + (1-c)Z_{l+1\,m}$, $0 \le c \le 1$. Following the procedure which took (A.13) to (A.24), we obtain

$$\begin{aligned}
Z(u,v) &= Z_{u\,m} + \frac{v - y_m}{h_m}(Z_{u\,m+1} - Z_{u\,m}) = Z_{u\,m} + T_2(\beta - b_m) \\
I_x^{lm} &= \int_{\alpha_1}^{\alpha_2}\int_{\beta_1}^{\beta_2} [Z_{um} + T_2(\beta - b_m)] \frac{\alpha}{[\alpha^2+\beta^2]^{3/2}}\, d\alpha\, d\beta \\
&= Z_{um} I_\alpha^{lm} + T_2(I_{\alpha\beta}^{lm} - b_m I_\alpha^{lm}) = \frac{b_{m+1} I_\alpha^{lm} - I_{\alpha\beta}^{lm}}{h_m} Z_{um} - \frac{b_m I_\alpha^{lm} - I_{\alpha\beta}^{lm}}{h_m} Z_{u\,m+1}.
\end{aligned} \tag{A.32}$$

According to (A.24), when a bi-linear variation in the cell is assumed, the field values at all four corners of the cell have to be used to express $I_x^{lm}$, but here only two terms are needed because we have only a linear variation. Since we prefer to express the integrals in terms of the field values at finite grid nodes, we choose $c = 0$ for $Z_{um} = Z_{l+1m}$ when $l = 0$, and $c = 1$ for $Z_{um} = Z_{lm}$ when $l = L$. By comparison with (A.24), the integral $I_x^{lm}$ in region $R_1$, $R_3$ can then be written as

$$I_x^{lm} = \begin{cases} Q_{lm}^{00} Z_{l\,m} + Q_{lm}^{01} Z_{l\,m+1}, & l = L \\ Q_{lm}^{10} Z_{l+1\,m} + Q_{lm}^{11} Z_{l+1\,m+1}, & l = 0 \end{cases} \tag{A.33}$$

which leads to definitions

$$Q_{lm}^{00} = Q_{lm}^{01} = 0,\ Q_{lm}^{10} = \left(b_{m+1} I_{\alpha}^{lm} - I_{\alpha\beta}^{lm}\right)/h_m,\ Q_{lm}^{11} = -\left(b_m I_{\alpha}^{lm} - I_{\alpha\beta}^{lm}\right)/h_m$$
$$l = 0,\ \ m = 1 \ldots M-1 \qquad \text{(A.34)}$$

$$Q_{lm}^{10} = Q_{lm}^{11} = 0,\ Q_{lm}^{00} = \left(b_{m+1} I_{\alpha}^{lm} - I_{\alpha\beta}^{lm}\right)/h_m,\ Q_{lm}^{01} = -\left(b_m I_{\alpha}^{lm} - I_{\alpha\beta}^{lm}\right)/h_m$$
$$l = L,\ \ m = 1 \ldots M-1. \qquad \text{(A.35)}$$

Similarly in $R_2$ and $R_4$, we have $Z(\alpha, \beta) = Z_{lm} + T_1(\alpha - a_l)$.

Let $Z_{lv} = cZ_{lm} + (1-c)Z_{lm+1}$ , then

$$I_x^{lm} = Z_{lv} I_{\alpha}^{lm} + T_1(I_{\alpha^2}^{lm} - a_l I_{\alpha}^{lm}) = \frac{a_{l+1} I_{\alpha}^{lm} - I_{\alpha^2}^{lm}}{g_l} Z_{lv} - \frac{a_l I_{\alpha}^{lm} - I_{\alpha^2}^{lm}}{g_l} Z_{l+1\,v}$$
$$= \begin{cases} Q_{lm}^{00} Z_{l\,m} + Q_{lm}^{10} Z_{l+1\,m}, & m = M \quad (c=1) \\ Q_{lm}^{01} Z_{l\,m+1} + Q_{lm}^{11} Z_{l+1\,m+1}, & m = 0 \quad (c=0) \end{cases} \qquad \text{(A.36)}$$

and

$$Q_{lm}^{00} = Q_{lm}^{10} = 0,\ \ Q_{lm}^{01} = \left(a_{l+1} I_{\alpha}^{lm} - I_{\alpha^2}^{lm}\right)/g_l,\ \ Q_{lm}^{11} = -\left(a_l I_{\alpha}^{lm} - I_{\alpha^2}^{lm}\right)/g_l$$
$$l = 1 \ldots L-1,\ \ m = 0 \qquad \text{(A.37)}$$

$$Q_{lm}^{01} = Q_{lm}^{11} = 0,\ \ Q_{lm}^{00} = \left(a_{l+1} I_{\alpha}^{lm} - I_{\alpha^2}^{lm}\right)/g_l,\ \ Q_{lm}^{10} = -\left(a_l I_{c}^{lm} - I_{\alpha^2}^{lm}\right) g_l$$
$$l = 1 \ldots L-1,\ \ m = M \qquad \text{(A.38)}$$

For $R_5$ to $R_8$, it follows from $Z(\mathbf{r}) = 0$ that $I_5 = I_6 = I_7 = I_8 = 0$. We can therefore define

$$Q_{lm}^{00} = Q_{lm}^{10} = Q_{lm}^{01} = Q_{lm}^{11} = 0,\ \ (l,m) = (L,M),(0,M),(L,0),(0,0). \qquad \text{(A.39)}$$

In equation (A.28), the coefficients $Q_{lm}^{pq}$, which are related to the field values $Z_{l0}$, $Z_{l\,M+1}$, $Z_{0m}$, $Z_{l+1\,m}$ on the 2D boundaries at infinity and the field values $Z_{00}$, $Z_{L+1\,0}$, $Z_{0\,M+1}$, $Z_{L+1\,M+1}$ on the 1D corners at infinity, are now vanishing. This reduces (A.28) to

$$-M_1 Z_{\lambda\mu} = \sum_{l=1}^{L}\sum_{m=1}^{M} (Q_{lm}^{00} + Q_{l-1m}^{10} + Q_{lm-1}^{01} + Q_{l-1m-1}^{11}) Z_{lm}$$
$$= \sum_{l=1}^{L}\sum_{m=1}^{M} \left(\sum_{p=0}^{1}\sum_{q=0}^{1} Q_{l-p\,m-q}^{pq}\right) Z_{lm} = \sum_{l=1}^{L}\sum_{m=1}^{M} A_{\lambda\mu}^{lm} Z_{lm} \qquad \text{(A.40)}$$

If we let $Z_{lm} = 1$, some straightforward algebraic manipulation leads to the following grouping of $Q_{lm}^{pq}$:

$$\begin{aligned}
&\sum_{l=1}^{L}\sum_{m=1}^{M}(Q_{lm}^{00}+Q_{l-1m}^{10}+Q_{lm-1}^{01}+Q_{l-1m-1}^{11})\\
&=\sum_{l=1}^{L-1}\sum_{m=1}^{M-1}(Q_{lm}^{00}+Q_{lm}^{10}+Q_{lm}^{01}+Q_{lm}^{11})\\
&+\left(\sum_{l=L}\sum_{m=1}^{M-1}+\sum_{m=M}\sum_{l=1}^{L-1}+\sum_{l=L}\sum_{m=M}\right)Q_{lm}^{00}+\left(\sum_{l=0}\sum_{m=1}^{M-1}+\sum_{m=M}\sum_{l=1}^{L-1}+\sum_{l=0}\sum_{m=M}\right)Q_{lm}^{10}\\
&+\left(\sum_{l=L}\sum_{m=1}^{M-1}+\sum_{m=0}\sum_{l=1}^{L-1}+\sum_{l=L}\sum_{m=0}\right)Q_{lm}^{01}+\left(\sum_{l=0}\sum_{m=1}^{M-1}+\sum_{m=0}\sum_{l=1}^{L-1}+\sum_{l=0}\sum_{m=0}\right)Q_{lm}^{11}.
\end{aligned} \tag{A.41}$$

The definition of each grouping is

$$\begin{aligned}
Q_{lm}^{pq} &= \frac{(-1)^{p+q}}{g_l\,h_m}\sum_{r=0}^{1}\sum_{s=0}^{1}(-1)^{r+s}(a_{l+1-p})^{1-r}(b_{m+1-q})^{1-s}I_{\alpha^{1+r}\beta^{s}}\\
&\qquad p=0,1,\ q=0,1;\ \ l=1...L-1,\ m=1...M-1,
\end{aligned}$$

$$Q_{lm}^{00} = \begin{cases} (b_{m+1}I_{\alpha}^{lm}-I_{\alpha\beta}^{lm})/h_m, & l=L;\ \ m=1...M-1,\\ (a_{l+1}I_{\alpha}^{lm}-I_{\alpha^2}^{lm})/g_l, & m=M;\ \ l=1...L-1,\\ 0 & l=L;\ \ m=M,\end{cases}$$

$$Q_{lm}^{10} = \begin{cases} (b_{m+1}I_{\alpha}^{lm}-I_{\alpha\beta}^{lm})/h_m, & l=0;\ \ m=1...M-1,\\ -(a_{l}I_{\alpha}^{lm}-I_{\alpha^2}^{lm})/g_l, & m=M;\ \ l=1...L-1,\\ 0 & l=0;\ \ m=M,\end{cases}$$

$$Q_{lm}^{01} = \begin{cases} -(b_{m}I_{\alpha}^{lm}-I_{\alpha\beta}^{lm})/h_m, & l=L;\ \ m=1...M-1,\\ (a_{l+1}I_{\alpha}^{lm}-I_{\alpha^2}^{lm})/g_l, & m=0;\ \ l=1...L-1,\\ 0 & l=L;\ \ m=0,\end{cases}$$

$$Q_{lm}^{11} = \begin{cases} -(b_{m}I_{\alpha}^{lm}-I_{\alpha\beta}^{lm})/h_m, & l=0;\ \ m=1...M-1,\\ -(a_{l}I_{\alpha}^{lm}-I_{\alpha^2}^{lm})/g_l, & m=0;\ \ l=1...L-1,\\ 0 & l=0;\ \ m=0,\end{cases}$$

(A.42)

## A.3 Integral Operator $M_2$

Following the same procedure as for $M_1$, we have

$$-M_2 Z_{\lambda\mu} = \int_{-\infty}^{\infty}\int_{-\infty}^{\infty} Z(u,v)\frac{v-y_\mu}{D}\,du\,dv = \sum_{l=0}^{L}\sum_{m=0}^{M} I_y^{lm} \tag{A.43}$$

where

$$\begin{aligned} I_y^{lm} : &= \int_{x_l}^{x_{l+1}}\int_{y_m}^{y_{m+1}} Z(u,v)\frac{v-y_\mu}{D}\,du\,dv \\ &= \int_{\alpha_1}^{\alpha_2}\int_{\beta_1}^{\beta_2} \tilde{Z}(\alpha,\beta)\frac{\beta}{[\alpha^2+\beta^2]^{3/2}}\,d\alpha\,d\beta \\ &= Z_{lm} I_\beta^{lm} + T_1(I_{\alpha\beta}^{lm} - a_l I_\beta^{lm}) + T_2(I_{\beta^2}^{lm} - b_m I_\beta^{lm}) \\ &\quad + T_3(I_{\alpha\beta^2}^{lm} - a_l I_{\beta^2}^{lm} - b_m I_{\alpha\beta}^{lm} + a_l b_m I_\beta^{lm}) \\ &= R_{lm}^{00} Z_{lm} + R_{lm}^{10} Z_{l+1m} + R_{lm}^{01} Z_{lm+1} + R_{lm}^{11} Z_{l+1m+1} \\ &= \sum_{p=0}^{1}\sum_{q=0}^{1} R_{lm}^{pq} Z_{l+p\,m+q}, \end{aligned} \tag{A.44}$$

and

$$\begin{aligned} R_{lm}^{00} &= (a_{l+1}b_{m+1}I_\beta^{lm} - a_{l+1}I_{\beta^2}^{lm} - b_{m+1}I_{\alpha\beta}^{lm} + I_{\alpha\beta^2}^{lm})/g_l\,h_m, \\ R_{lm}^{10} &= -(a_l b_{m+1}I_\beta^{lm} - a_l I_{\beta^2}^{lm} - b_{m+1}I_{\alpha\beta}^{lm} + I_{\alpha\beta^2}^{lm})/g_l\,h_m, \\ R_{lm}^{01} &= -(a_{l+1}b_m I_\beta^{lm} - a_{l+1}I_{\beta^2}^{lm} - b_m I_{\alpha\beta}^{lm} + I_{\alpha\beta^2}^{lm})/g_l\,h_m, \\ R_{lm}^{11} &= (a_l b_m I_\beta^{lm} - a_l I_{\beta^2}^{lm} - b_m I_{\alpha\beta}^{lm} + I_{\alpha\beta^2}^{lm})/g_l\,h_m, \end{aligned} \tag{A.45}$$

which can also be expressed in the general formula

$$R_{lm}^{pq} = \frac{(-1)^{p+q}}{g_l\,h_m}\sum_{r=0}^{1}\sum_{s=0}^{1}(-1)^{r+s}(a_{l+1-p})^{1-r}(b_{m+1-q})^{1-s} I_{\alpha^r\beta^{1+s}}^{lm}. \tag{A.46}$$

The integrals are defined similarly to (A.22) as

$$\begin{aligned} I_\beta^{lm} &= \int_{\alpha_1}^{\alpha_2}\int_{\beta_1}^{\beta_2}\frac{\beta}{[\alpha^2+\beta^2]^{3/2}}\,d\alpha\,d\beta, \\ I_{\beta^2}^{lm} &= \int_{\alpha_1}^{\alpha_2}\int_{\beta_1}^{\beta_2}\frac{\beta^2}{[\alpha^2+\beta^2]^{3/2}}\,d\alpha\,d\beta, \\ I_{\alpha\beta^2}^{lm} &= \int_{\alpha_1}^{\alpha_2}\int_{\beta_1}^{\beta_2}\frac{\alpha\beta^2}{[\alpha^2+\beta^2]^{3/2}}\,d\alpha\,d\beta. \end{aligned} \tag{A.47}$$

The expressions for $R^{pq}_{lm}$ are similar to $Q^{pq}_{lm}$ except that the integrals $I^{lm}_{\alpha^{l+r}\beta^s}$ appearing in the expressions for $Q^{pq}_{lm}$ are replaced by $I^{lm}_{\alpha^r\beta^{l+s}}$ in $R^{pq}_{lm}$. The same replacements occur in (A.34), (A.35) and (A.37), (A.38). Therefore, if we define

$$R^{pq}_{lm} = \frac{(-1)^{p+q}}{g_l\, h_m}\sum_{r=0}^{1}\sum_{s=0}^{1}(-1)^{r+s}(a_{l+1-p})^{1-r}(b_{m+1-q})^{1-s} I_{\alpha^r\beta^{l+s}}.$$
$$p = 0,1,\ q = 0,1;\ \ l = 1...L-1,\ m = 1...M-1,$$

$$R^{00}_{lm} = \begin{cases} (b_{m+1}I^{lm}_{\beta} - I^{lm}_{\beta^2})/h_m, & l = L;\ \ m = 1...M-1, \\ (a_{l+1}I^{lm}_{\beta} - I^{lm}_{\alpha\beta})/g_l, & m = M;\ \ l = 1...L-1, \\ 0 & l = L;\ \ m = M, \end{cases}$$

$$R^{10}_{lm} = \begin{cases} (b_{m+1}I^{lm}_{\beta} - I^{lm}_{\beta^2})/h_m, & l = 0;\ \ m = 1...M-1, \\ -(a_l I^{lm}_{\beta} - I^{lm}_{\alpha\beta})/g_l, & m = M;\ \ l = 1...L-1, \\ 0 & l = 0;\ \ m = M, \end{cases}$$

$$R^{01}_{lm} = \begin{cases} -(b_m I^{lm}_{\beta} - I^{lm}_{\beta^2})/h_m, & l = L;\ \ m = 1...M-1, \\ (a_{l+1}I^{lm}_{\beta} - I^{lm}_{\alpha\beta})/g_l, & m = 0;\ \ l = 1...L-1, \\ 0 & l = L;\ \ m = 0, \end{cases}$$

$$R^{11}_{lm} = \begin{cases} -(b_m I^{lm}_{\beta} - I^{lm}_{\beta^2})/h_m, & l = 0;\ \ m = 1...M-1, \\ -(a_l I^{lm}_{\beta} - I^{lm}_{\alpha\beta})/g_l, & m = 0;\ \ l = 1...L-1, \\ 0 & l = 0;\ \ m = 0, \end{cases} \tag{A.48}$$

then (A.2) becomes

$$-M_2\, Z_{\lambda\mu} = \sum_{l=1}^{L}\sum_{m=1}^{M}\left(\sum_{p=0}^{1}\sum_{q=0}^{1} R^{pq}_{l-p\,m-q}\right) Z_{lm} = \sum_{l=1}^{L}\sum_{m=1}^{M} B^{lm}_{\lambda\mu} Z_{lm} \tag{A.49}$$

## A.4 Evaluation of the Integrals

The coefficients $Q^{pq}_{lm}$ and $R^{pq}_{lm}$ involve seven integrals $I^{lm}_{\alpha}$ $I^{lm}_{\beta}$ $I^{lm}_{\alpha^2}$ $I^{lm}_{\beta^2}$ $I^{lm}_{\alpha^2\beta}$ $I^{lm}_{\alpha\beta^2}$ and $I^{lm}_{\alpha\beta}$ all of which can be integrated analytically using the Maple symbolic computing system with program "TBCINT file". Since the results of $I^{lm}_{\beta}$ $I^{lm}_{\beta^2}$ and $I^{lm}_{\alpha\beta^2}$ can be simply obtained from that of $I^{lm}_{\alpha}$ $I^{lm}_{\alpha^2}$ and $I^{lm}_{\alpha^2\beta}$ by switching the roles of $\alpha$ and $\beta$, we sometimes omit $I^{lm}_{\beta}$ $I^{lm}_{\beta^2}$ and $I^{lm}_{\alpha\beta^2}$ and focus the discussion on $I^{lm}_{\alpha}$ $I^{lm}_{\alpha^2}$ $I^{lm}_{\alpha^2\beta}$ and $I^{lm}_{\alpha\beta}$ only. For $I^{lm}_{\alpha}$, $I^{lm}_{\alpha\beta}$ and $I^{lm}_{\alpha^2\beta}$, it does not matter over

which variable ($\alpha$ or $\beta$) the integration is first carried out, since both orders of integration yield the same results. But for $I^{lm}_{\alpha^2}$, we have to integrate it with respect to $\beta$ first followed by $\alpha$, as otherwise Maple is unable to complete the second step of the integration. The results obtained are

$$\begin{aligned}
I^{lm}_{\alpha} &= \ln\left[\left(\frac{\beta_2+\sqrt{\alpha_1^2+\beta_2^2}}{\beta_1+\sqrt{\alpha_1^2+\beta_1^2}}\right)\left(\frac{\beta_1+\sqrt{\alpha_2^2+\beta_1^2}}{\beta_2+\sqrt{\alpha_2^2+\beta_2^2}}\right)\right] \\
I^{lm}_{\alpha^2} &= \ln\left[\left(\frac{\alpha_2+\sqrt{\alpha_2^2+\beta_2^2}}{\alpha_1+\sqrt{\alpha_1^2+\beta_2^2}}\right)^{\beta_2}\left(\frac{\alpha_1+\sqrt{\alpha_1^2+\beta_1^2}}{\alpha_2+\sqrt{\alpha_2^2+\beta_1^2}}\right)^{\beta_1}\right] \\
I^{lm}_{\alpha\beta} &= \left(\sqrt{\alpha_2^2+\beta_1^2}-\sqrt{\alpha_2^2+\beta_2^2}\right)-\left(\sqrt{\alpha_1^2+\beta_1^2}-\sqrt{\alpha_1^2+\beta_2^2}\right) \\
I^{lm}_{\alpha^2\beta} &= \frac{1}{2}\left[\alpha_2\left(\sqrt{\alpha_2^2+\beta_1^2}-\sqrt{\alpha_2^2+\beta_2^2}\right)-\alpha_1\left(\sqrt{\alpha_1^2+\beta_1^2}-\sqrt{\alpha_1^2+\beta_2^2}\right)\right] \\
&\quad +\frac{1}{2}\ln\left[\left(\frac{\alpha_2+\sqrt{\alpha_2^2+\beta_2^2}}{\alpha_1+\sqrt{\alpha_1^2+\beta_2^2}}\right)^{\beta_2^2}\left(\frac{\alpha_1+\sqrt{\alpha_1^2+\beta_1^2}}{\alpha_2+\sqrt{\alpha_2^2+\beta_1^2}}\right)^{\beta_1^2}\right], \qquad \text{(A.50)}
\end{aligned}$$

and

$$\begin{aligned}
I^{lm}_{\beta}(\alpha_1,\alpha_2,\beta_1,\beta_2) &= I^{lm}_{\alpha}(\beta_1,\beta_2,\alpha_1,\alpha_2) \\
I^{lm}_{\beta^2}(\alpha_1,\alpha_2,\beta_1,\beta_2) &= I^{lm}_{\alpha^2}(\beta_1,\beta_2,\alpha_1,\alpha_2) \\
I^{lm}_{\beta^2\alpha}(\alpha_1,\alpha_2,\beta_1,\beta_2) &= I^{lm}_{\alpha^2\beta}(\beta_1,\beta_2,\alpha_1,\alpha_2) \qquad \text{(A.51)}
\end{aligned}$$

Since

$$\begin{aligned}
\ln\left(\alpha+\sqrt{\alpha^2+\beta^2}\right) &= \ln\left[\left(\alpha+\sqrt{\alpha^2+\beta^2}\right)\frac{\left(-\alpha+\sqrt{\alpha^2+\beta^2}\right)}{\left(-\alpha+\sqrt{\alpha^2+\beta^2}\right)}\right] \\
&= \ln\left(\frac{\beta^2}{-\alpha+\sqrt{\alpha^2+\beta^2}}\right), \qquad \text{(A.52)}
\end{aligned}$$

we deduce that

$$\ln\left(\frac{\alpha_1+\sqrt{\alpha_1^2+\beta^2}}{\alpha_2+\sqrt{\alpha_2^2+\beta^2}}\right)=\ln\left(\frac{-\alpha_2+\sqrt{\alpha_2^2+\beta^2}}{-\alpha_1+\sqrt{\alpha_1^2+\beta^2}}\right)=-\ln\left(\frac{-\alpha_1+\sqrt{\alpha_1^2+\beta^2}}{-\alpha_2+\sqrt{\alpha_2^2+\beta^2}}\right). \qquad \text{(A.53)}$$

Recalling that

$$\alpha_1 = x_l - x_\lambda,\ \alpha_2 = x_{l+1} - x_\lambda;\ \beta_1 = y_m - y_\mu,\ \beta_2 = y_{m+1} - y_\mu,$$

we can easily see that if $l \neq \lambda$ and $l+1 \neq \lambda$, then it is always true that

$$\mathrm{sgn}\,(\alpha_1) = \mathrm{sgn}\,(\alpha_2) = \mathrm{sgn}\,(\alpha).$$

Similarly,

$$\mathrm{sgn}\,(\beta_1) = \mathrm{sgn}\,(\beta_2) = \mathrm{sgn}\,(\beta),$$

if $m \neq \mu$ and $m+1 \neq \mu$. We can therefore write the identity (A.53) as

$$\begin{aligned} \ln\left(\frac{\alpha_1 + \sqrt{\alpha_1^2+\beta^2}}{\alpha_2 + \sqrt{\alpha_2^2+\beta^2}}\right) &= -\ln\left(\frac{-\alpha_1 + \sqrt{\alpha_1^2+\beta^2}}{-\alpha_2 + \sqrt{\alpha_2^2+\beta^2}}\right) \\ &= \mathrm{sgn}\,(\alpha)\ln\left(\frac{|\alpha_1| + \sqrt{\alpha_1^2+\beta^2}}{|\alpha_2| + \sqrt{\alpha_2^2+\beta^2}}\right). \end{aligned} \qquad \text{(A.54)}$$

These three expressions are identical from the mathematical point of view, but they differ significantly from numerical point of view. When $\beta \to 0$, in case of $\alpha_1 \leq 0$ and $\alpha_2 \leq 0$, the first expression approaches an expression which involves subtractions of nearly equal numbers, which not only causes the loss of significant figures but also introduces a $\log\frac{0}{0}$ uncertainty. In the case of $\alpha_1 \geq 0$ and $\alpha_2 \geq 0$, the second expression runs into the same problem. This difficulty does not arise with the third expression, however. We therefore re-write all the integrals in forms suitable for numerical computation as follows:

$$\begin{aligned} I_{\alpha}^{lm} &= \mathrm{sgn}\,(\beta)\ln\left[\left(\frac{|\beta_2| + \sqrt{\alpha_1^2+\beta_2^2}}{|\beta_1| + \sqrt{\alpha_1^2+\beta_1^2}}\right)\left(\frac{|\beta_1| + \sqrt{\alpha_2^2+\beta_1^2}}{|\beta_2| + \sqrt{\alpha_2^2+\beta_2^2}}\right)\right] \\ I_{\alpha^2}^{lm} &= \mathrm{sgn}\,(\alpha)\left[\beta_2\ln\frac{|\alpha_2| + \sqrt{\alpha_2^2+\beta_2^2}}{|\alpha_1| + \sqrt{\alpha_1^2+\beta_2^2}} + \beta_1\ln\frac{|\alpha_1| + \sqrt{\alpha_1^2+\beta_1^2}}{|\alpha_2| + \sqrt{\alpha_2^2+\beta_1^2}}\right] \\ I_{\alpha^2\beta}^{lm} &= \frac{1}{2}\left[\alpha_2\left(\sqrt{\alpha_2^2+\beta_1^2} - \sqrt{\alpha_2^2+\beta_2^2}\right) - \alpha_1\left(\sqrt{\alpha_1^2+\beta_1^2} - \sqrt{\alpha_1^2+\beta_2^2}\right)\right] \end{aligned}$$

$$
\begin{aligned}
&+ \frac{1}{2}\mathrm{sgn}\,(\alpha)\left[\beta_2^2 \ln \frac{|\alpha_2| + \sqrt{\alpha_2^2+\beta_2^2}}{|\alpha_1| + \sqrt{\alpha_1^2+\beta_2^2}} + \beta_1^2 \ln \frac{|\alpha_1| + \sqrt{\alpha_1^2+\beta_1^2}}{|\alpha_2| + \sqrt{\alpha_2^2+\beta_1^2}}\right] \\
I^{lm}_{\alpha\beta} &= \left(\sqrt{\alpha_2^2+\beta_1^2} - \sqrt{\alpha_2^2+\beta_2^2}\right) - \left(\sqrt{\alpha_1^2+\beta_1^2} - \sqrt{\alpha_1^2+\beta_2^2}\right) \\
I^{lm}_{\beta} &= \mathrm{sgn}\,(\alpha) \ln\left[\left(\frac{|\alpha_2| + \sqrt{\beta_1^2+\alpha_2^2}}{|\alpha_1| + \sqrt{\beta_1^2+\alpha_1^2}}\right)\left(\frac{|\alpha_1| + \sqrt{\beta_2^2+\alpha_1^2}}{|\alpha_2| + \sqrt{\beta_2^2+\alpha_2^2}}\right)\right] \\
I^{lm}_{\beta^2} &= \mathrm{sgn}\,(\beta)\left[\alpha_2 \ln \frac{|\beta_2| + \sqrt{\beta_2^2+\alpha_2^2}}{|\beta_1| + \sqrt{\beta_1^2+\alpha_2^2}} + \alpha_1 \ln \frac{|\beta_1| + \sqrt{\beta_1^2+\alpha_1^2}}{|\beta_2| + \sqrt{\beta_2^2+\alpha_1^2}}\right] \\
I^{lm}_{\alpha\beta^2} &= \frac{1}{2}\left[\beta_2\left(\sqrt{\beta_2^2+\alpha_1^2} - \sqrt{\beta_2^2+\alpha_2^2}\right) - \beta_1\left(\sqrt{\beta_1^2+\alpha_1^2} - \sqrt{\beta_1^2+\alpha_2^2}\right)\right] \\
&+ \frac{1}{2}\mathrm{sgn}\,(\beta)\left[\alpha_2^2 \ln \frac{|\beta_2| + \sqrt{\beta_2^2+\alpha_2^2}}{|\beta_1| + \sqrt{\beta_1^2+\alpha_2^2}} + \alpha_1^2 \ln \frac{|\beta_1| + \sqrt{\beta_1^2+\alpha_1^2}}{|\beta_2| + \sqrt{\beta_2^2+\alpha_1^2}}\right]
\end{aligned}
\tag{A.55}
$$

Two problematic situations may arise when evaluating the above integrals. In some areas the limits of integration may approach zero, giving rise to a singularity, and in others, the limits may approach infinity, thereby rendering the integral unsuitable for numerical computation. Attention must be paid to these special cases. We consider the singularity problem first.

### A.4.1 Integrals in Singular Cells

As shown in Fig (A-1b), there are four singular cells surrounding the singular point $(x_\lambda, y_\mu)$. We denote them by $\tilde{R}_{\lambda\mu}$, $\tilde{R}_{\lambda-1\mu}$, $\tilde{R}_{\lambda\mu-1}$ and $\tilde{R}_{\lambda-1\mu-1}$, defined by

$$
\begin{aligned}
\tilde{R}_{\lambda\mu} &= \{\mathbf{r}| \quad 0 \le x - x_\lambda \le g_\lambda; \quad 0 \le y - y_\mu \le h_\mu\}, \\
\tilde{R}_{\lambda-1\mu} &= \{\mathbf{r}| \quad -g_{\lambda-1} \le x - x_\lambda \le 0; \quad 0 \le y - y_\mu \le h_\mu\}, \\
\tilde{R}_{\lambda\mu-1} &= \{\mathbf{r}| \quad 0 \le x - x_\lambda \le g_\lambda; \quad -h_{\mu-1} \le y - y_\mu \le 0\}, \\
\tilde{R}_{\lambda-1\mu-1} &= \{\mathbf{r}| \quad -g_{\lambda-1} \le x - x_\lambda \le 0; \quad -h_{\mu-1} \le y - y_\mu \le 0\}.
\end{aligned}
\tag{A.56}
$$

When approaching the singular point, we encounter a difficulty in the integral $I_x^{lm}$ as given by expression (A.19) over each individual cell, because of the presence of the term $D = 1/(\alpha^2+\beta^2)^{3/2}$ in the integrand. For instance, in cell $\tilde{R}_{\lambda\mu}$,

we see that $\alpha_1 = \epsilon \to 0$ and $\beta_1 = \epsilon \to 0$. If we assume that $Z(\alpha, \beta) = 1$, then referring to (A.19), (A.22) and (A.55), we have

$$I_x^{lm} = \int_\epsilon^{g_\lambda} \int_\epsilon^{h_\mu} \frac{\alpha}{(\alpha^2 + \beta^2)^{3/2}} \, d\alpha \, d\beta = I_\alpha^{lm}|_{(\alpha_1=\epsilon, \beta_1=\epsilon)} = O(\log \epsilon) \qquad \text{(A.57)}$$

which diverges as $\epsilon \to 0$. Obviously, we cannot compute the integrals in each singular cell individually; instead, we compute the integration over the singular region $\tilde{R}_0$ as a whole, and anticipate that the singularity will be canceled out when the integral is interpreted as a Cauchy principal value. By comparison with (A.11) and (A.12), the integral defined by (A.10) over the singular region can also be written as

$$\begin{aligned}
\tilde{I}_0 &= \fint_{x_{\lambda-1}}^{x_{\lambda+1}} \fint_{y_{\mu-1}}^{y_{\mu+1}} Z(u,v) \frac{u - x_\lambda}{D} \, du \, dv = \fint_{-g_{\lambda-1}}^{g_\lambda} \fint_{-h_{\mu-1}}^{h_\mu} Z(\alpha, \beta) \frac{\alpha}{D} \, d\alpha \, d\beta \\
&= \lim_{\epsilon \to 0} \left[ \int_{-g_{\lambda-1}}^{-\epsilon} + \int_\epsilon^{g_\lambda} \right] \left[ \int_{-h_{\mu-1}}^{-\epsilon} + \int_\epsilon^{h_\mu} \right] Z(\alpha, \beta) \frac{\alpha}{(\alpha^2 + \beta^2)^{3/2}} \, d\alpha \, d\beta \\
&= \lim_{\epsilon \to 0} \left[ \int_{-g_{\lambda-1}}^{-\epsilon} \int_{-h_{\mu-1}}^{-\epsilon} + \int_\epsilon^{g_\lambda} \int_{-h_{\mu-1}}^{-\epsilon} + \int_{-g_{\lambda-1}}^{-\epsilon} \int_\epsilon^{h_\mu} + \int_\epsilon^{g_\lambda} \int_\epsilon^{h_\mu} \right] (\ldots) \\
&= \tilde{I}_x^{\lambda-1\,\mu-1} + \tilde{I}_x^{\lambda\mu-1} + \tilde{I}_x^{\lambda-1\,\mu} + \tilde{I}_x^{\lambda\mu} \qquad \text{(A.58)}
\end{aligned}$$

where $\tilde{I}_x^{\lambda-1\,\mu-1}$, $\tilde{I}_x^{\lambda-1\,\mu}$, $\tilde{I}_x^{\lambda\mu-1}$ and $\tilde{I}_x^{\lambda\mu}$ are integrals over the individual cells $\tilde{R}_{\lambda-1\,\mu-1}$, $\tilde{R}_{\lambda-1\,\mu}$, $\tilde{R}_{\lambda\,\mu-1}$ and $\tilde{R}_{\lambda\,\mu}$ respectively.

According to (A.23), each $\tilde{I}_x^{lm}$ in turn consists of four sub-integrals $\tilde{I}_\alpha^{lm}$, $\tilde{I}_{\alpha^2}^{lm}$, $\tilde{I}_{\alpha\beta}^{lm}$ and $\tilde{I}_{\alpha^2\beta}^{lm}$ integrated over the same cell. We can see that there is no singularity for the integral $\tilde{I}_{\alpha,\beta}^{lm}$, so that only the other three have to be considered.

Over the cell $\tilde{R}_{\lambda-1,\mu-1}$, we have

$$\alpha_1 = -g_{\lambda-1}, \; \alpha_2 = -\epsilon; \; \beta_1 = -h_{\mu-1}, \; \beta_2 = -\epsilon; \; \text{sgn}(\alpha) = -1, \; \text{sgn}(\beta) = -1;$$

thus

$$\tilde{I}_\alpha^{\lambda-1\,\mu-1} = -\lim_{\epsilon \to 0} \left[ \log \left( \frac{\epsilon + \sqrt{g_{\lambda-1}^2 + \epsilon^2}}{h_{\mu-1} + \sqrt{g_{\lambda-1}^2 + h_{\mu-1}^2}} \right) \left( \frac{h_{\mu-1} + \sqrt{\epsilon^2 + h_{\mu-1}^2}}{\epsilon + \sqrt{\epsilon^2 + \epsilon^2}} \right) \right]$$

$$= -\log \frac{2h_{\mu-1}}{h_{\mu-1}/g_{\lambda-1} + \sqrt{1 + h_{\mu-1}^2/g_{\lambda-1}^2}} + \lim_{\epsilon\to 0} \log\left(\epsilon + \sqrt{\epsilon^2+\epsilon^2}\right) \tag{A.59}$$

$$\begin{aligned}
\tilde{I}_{\alpha^2}^{\lambda-1\,\mu-1} &= -\lim_{\epsilon\to 0}\left[-\epsilon \log\left(\frac{\epsilon + \sqrt{\epsilon^2+\epsilon^2}}{g_{\lambda-1} + \sqrt{g_{\lambda-1}^2+\epsilon^2}}\right)\right] \\
&\quad -\lim_{\epsilon\to 0}\left[-h_{\mu-1}\log\left(\frac{g_{\lambda-1} + \sqrt{g_{\lambda-1}^2 + h_{\mu-1}^2}}{\epsilon + \sqrt{\epsilon^2 + h_{\mu-1}^2}}\right)\right] \\
&= h_{\mu-1}\log\left(\frac{g_{\lambda-1}}{h_{\mu-1}} + \sqrt{1 + \frac{g_{\lambda-1}^2}{h_{\mu-1}^2}}\right)
\end{aligned} \tag{A.60}$$

$$\begin{aligned}
\tilde{I}_{\alpha^2\beta}^{\lambda-1\,\mu-1} &= \frac{1}{2}\left[g_{\lambda-1}\left(\sqrt{g_{\lambda-1}^2 + h_{\mu-1}^2} - g_{\lambda-1}\right)\right] \\
&\quad -\frac{1}{2}\lim_{\epsilon\to 0}\left[\epsilon^2 \log\left(\frac{\epsilon + \sqrt{\epsilon^2+\epsilon^2}}{g_{\lambda-1} + \sqrt{g_{\lambda-1}^2+\epsilon^2}}\right)\right] \\
&\quad -\frac{1}{2}\lim_{\epsilon\to 0}\left[h_{\mu-1}^2 \log\left(\frac{g_{\lambda-1} + \sqrt{g_{\lambda-1}^2 + h_{\mu-1}^2}}{\epsilon + \sqrt{\epsilon^2 + h_{\mu-1}^2}}\right)\right] \\
&= -\frac{1}{2}\left[g_{\lambda-1}^2\left(1 - \sqrt{1 + \frac{h_{\mu-1}^2}{g_{\lambda-1}^2}}\right) + h_{\mu-1}^2 \log\left(\frac{g_{\lambda-1}}{h_{\mu-1}} + \sqrt{1 + \frac{g_{\lambda-1}^2}{h_{\mu-1}^2}}\right)\right].
\end{aligned} \tag{A.61}$$

Similarly, over $\tilde{R}_{\lambda\,\mu-1}$, we have

$$\alpha_1 = \epsilon,\ \alpha_2 = g_\lambda;\ \beta_1 = -h_{\mu-1},\ \beta_2 = -\epsilon;\ \mathrm{sgn}\,(\alpha) = +1,\ \mathrm{sgn}\,(\beta) = -1,$$

and

$$\tilde{I}_{\alpha}^{\lambda\,\mu-1} = \log \frac{2h_{\mu-1}}{h_{\mu-1}/g_\lambda + \sqrt{1 + h_{\mu-1}^2/g_\lambda^2}} - \lim_{\epsilon\to 0}\log\left(\epsilon + \sqrt{\epsilon^2+\epsilon^2}\right) \tag{A.62}$$

$$\tilde{I}_{\alpha^2}^{\lambda\,\mu-1} = h_{\mu-1}\log\left(\frac{g_\lambda}{h_{\mu-1}} + \sqrt{1 + \frac{g_\lambda^2}{h_{\mu-1}^2}}\right) \tag{A.63}$$

$$\tilde{I}_{\alpha^2\beta}^{\lambda\,\mu-1} = -\frac{1}{2}\left[g_\lambda^2\left(1 - \sqrt{1 + \frac{h_{\mu-1}^2}{g_\lambda}}\right) + h_{\mu-1}^2 \log\left(\frac{g_\lambda}{h_{\mu-1}} + \sqrt{1 + \frac{g_\lambda^2}{h_{\mu-1}^2}}\right)\right]; \tag{A.64}$$

over $\tilde{R}_{\lambda-1\,\mu}$, we have

$$\alpha_1 = -g_{\lambda-1},\ \alpha_2 = -\epsilon;\ \beta_1 = \epsilon,\ \beta_2 = h_\mu;\ \mathrm{sgn}\,(\alpha) = -1,\ \mathrm{sgn}\,(\beta) = +1,$$

and

$$\tilde{I}_{\alpha}^{\lambda-1\,\mu} = -\log \frac{2h_\mu}{h_\mu/g_{\lambda-1} + \sqrt{1 + h_\mu^2/g_{\lambda-1}^2}} + \lim_{\epsilon\to 0} \log\left(\epsilon + \sqrt{\epsilon^2+\epsilon^2}\right) \quad \text{(A.65)}$$

$$\tilde{I}_{\alpha^2}^{\lambda-1\,\mu} = h_\mu \log\left(\frac{g_{\lambda-1}}{h_\mu} + \sqrt{1 + \frac{g_{\lambda-1}^2}{h_\mu^2}}\right) \quad \text{(A.66)}$$

$$\tilde{I}_{\alpha^2\beta}^{\lambda-1\,\mu} = \frac{1}{2}\left[g_{\lambda-1}^2\left(1 - \sqrt{1 + \frac{h_\mu^2}{g_{\lambda-1}}}\right) + h_\mu^2 \log\left(\frac{g_{\lambda-1}}{h_\mu} + \sqrt{1 + \frac{g_{\lambda-1}^2}{h_\mu^2}}\right)\right]; \quad \text{(A.67)}$$

and finally over $\tilde{R}_{\lambda\,\mu}$, we have

$$\alpha_1 = \epsilon,\ \alpha_2 = g_\lambda;\ \beta_1 = \epsilon,\ \beta_2 = h_\mu;\ \mathrm{sgn}\,(\alpha) = +1,\ \mathrm{sgn}\,(\beta) = +1,$$

and

$$\tilde{I}_{\alpha}^{\lambda\,\mu} = \log \frac{2h_\mu}{h_\mu/g_\lambda + \sqrt{1 + h_\mu^2/g_\lambda^2}} - \lim_{\epsilon\to 0} \log\left(\epsilon + \sqrt{\epsilon^2+\epsilon^2}\right) \quad \text{(A.68)}$$

$$\tilde{I}_{\alpha^2}^{\lambda\,\mu} = h_\mu \log\left(\frac{g_\lambda}{h_\mu} + \sqrt{1 + \frac{g_\lambda^2}{h_\mu^2}}\right) \quad \text{(A.69)}$$

$$\tilde{I}_{\alpha^2\beta}^{\lambda\,\mu} = \frac{1}{2}\left[g_\lambda^2\left(1 - \sqrt{1 + \frac{h_\mu^2}{g_\lambda^2}}\right) + h_\mu^2 \log\left(\frac{g_\lambda}{h_\mu} + \sqrt{1 + \frac{g_\lambda^2}{h_\mu^2}}\right)\right]. \quad \text{(A.70)}$$

Well defined limits for the integrals $\tilde{I}_{\alpha^2}^{lm}$ and $\tilde{I}_{\alpha^2\beta}^{lm}$ exist when the singular point is approached, but not for $\tilde{I}_{\alpha}^{lm}$. We have to combine the contribution of $\tilde{I}_{\alpha}^{lm}$ over the four singular cells together to remove the singularity. Inserting expressions (A.24) for $\tilde{I}_{x}^{lm}$ into expression (A.58) for $\tilde{I}_0$, we have

$$\tilde{I}_0 = \tilde{I}_x^{\lambda-1\,\mu-1} + \tilde{I}_x^{\lambda\,\mu-1} + \tilde{I}_x^{\lambda-1\,\mu} + \tilde{I}_x^{\lambda\,\mu}$$

$$
\begin{aligned}
&= Z_{\lambda-1\,\mu-1}\tilde{Q}^{00}_{\lambda-1\,\mu-1} + Z_{\lambda+1\,\mu-1}\tilde{Q}^{10}_{\lambda\mu-1} + Z_{\lambda-1\,\mu+1}\tilde{Q}^{01}_{\lambda-1\,\mu} + Z_{\lambda+1\,\mu+1}\tilde{Q}^{11}_{\lambda\mu} \\
&+ Z_{\lambda-1\,\mu}(\tilde{Q}^{00}_{\lambda-1\,\mu} + \tilde{Q}^{01}_{\lambda-1\,\mu-1}) + Z_{\lambda+1\,\mu}(\tilde{Q}^{10}_{\lambda\mu} + \tilde{Q}^{11}_{\lambda\mu-1}) \\
&+ Z_{\lambda\mu-1}(\tilde{Q}^{00}_{\lambda\mu-1} + \tilde{Q}^{10}_{\lambda-1\,\mu-1}) + Z_{\lambda\mu+1}(\tilde{Q}^{01}_{\lambda\mu} + \tilde{Q}^{11}_{\lambda-1\,\mu}) \\
&+ Z_{\lambda\mu}(\tilde{Q}^{00}_{\lambda\mu} + \tilde{Q}^{10}_{\lambda-1\,\mu} + \tilde{Q}^{01}_{\lambda\mu-1} + \tilde{Q}^{11}_{\lambda-1\,\mu-1}) \qquad \text{(A.71)}
\end{aligned}
$$

where the coefficient of the term $Z_{\lambda\mu}$, $\tilde{Q}^{00}_{\lambda\mu} + \tilde{Q}^{10}_{\lambda-1\,\mu} + \tilde{Q}^{01}_{\lambda\mu-1} + \tilde{Q}^{11}_{\lambda-1\,\mu-1}$, is the combination of contributions from all four singular cells. According to (A.25), the collection of all the terms involved with $\tilde{I}^{lm}_{\alpha}$ in this coefficient is

$$
\begin{aligned}
&\left(a_{l+1}b_{m+1}\tilde{I}^{lm}_{\alpha}\right)/g_l h_m|_{(l,m)=(\lambda,\mu)} - \left(a_l b_{m+1}\tilde{I}^{lm}_{\alpha}\right)/g_l h_m|_{(l,m)=(\lambda-1,\mu)} \\
&- \left(a_{l+1}b_m\tilde{I}^{lm}_{\alpha}\right)/g_l h_m|_{(l,m)=(\lambda,\mu-1)} + \left(a_l b_m\tilde{I}^{lm}_{\alpha}\right)/g_l h_m|_{(l,m)=(\lambda-1,\mu-1)} \\
&= \tilde{I}^{\lambda\mu}_{\alpha} + \tilde{I}^{\lambda-1\,\mu}_{\alpha} + \tilde{I}^{\lambda\mu-1}_{\alpha} + \tilde{I}^{\lambda-1\,\mu-1}_{\alpha} \\
&= -\log\left(h_\mu/g_\lambda + \sqrt{1+h^2_\mu/g^2_\lambda}\right) + \log\left(h_\mu/g_{\lambda-1} + \sqrt{1+h^2_\mu/g^2_{\lambda-1}}\right) \\
&\quad -\log\left(h_{\mu-1}/g_\lambda + \sqrt{1+h^2_{\mu-1}/g^2_\lambda}\right) + \log\left(h_{\mu-1}/g_{\lambda-1} + \sqrt{1+h^2_{\mu-1}/g^2_{\lambda-1}}\right) \\
&= \sum_{p=0}^{1}\sum_{q=0}^{1}(-1)^{p+1}\log\left(h_{\mu-q}/g_{\lambda-p} + \sqrt{1+h^2_{\mu-q}/g^2_{\lambda-p}}\right) \\
&= \sum_{p=0}^{1}\sum_{q=0}^{1}\tilde{I}^{\lambda-p\,\mu-q}_{\alpha}, \qquad \text{(A.72)}
\end{aligned}
$$

so that we can define $\tilde{I}^{lm}_{\alpha}$ as

$$
\tilde{I}^{\lambda-p\,\mu-q}_{\alpha} = (-1)^{p+1}\log\left(h_{\mu-q}/g_{\lambda-p} + \sqrt{1+h^2_{\mu-q}/g^2_{\lambda-p}}\right),\ p=0,1;\ q=0,1. \qquad \text{(A.73)}
$$

We see that the singularity related to $I^{lm}_{\alpha}$ has been successfully canceled out. With this new definition, $\tilde{I}^{\lambda-p\,\mu-q}_{\alpha}$ has well defined limits in all four singular cells while the sum remains the same as the Cauchy principal value of the integral over the whole singular region $\tilde{R}_0$.

Since $\tilde{I}^{\lambda-p\,\mu-q}_{\alpha}$ appears in the coefficients of eight other nodes as well, we have to make sure that the new definition causes no conflicts there. In the singular cells, when $(x,y) \to (x_\lambda, y_\mu)$, we see that $a_l = a_{l+1} = O(\epsilon)$, $\epsilon \to 0$

and $b_m = b_\mu = O(\epsilon)$, $\epsilon \to 0$. From the original expressions (A.59), (A.62), (A.65) and (A.68), we deduce that $I_\alpha^{lm} = O(\log \epsilon)$, when $\epsilon \to 0$. In (A.71), the coefficeints of $Z_{\lambda-1\,\mu-1}$, $Z_{\lambda+1\,\mu-1}$, $Z_{\lambda-1\,\mu+1}$ and $Z_{\lambda+1\,\mu+1}$ are $\dot{Q}^{00}_{\lambda-1\,\mu-1}$, $\dot{Q}^{10}_{\lambda\,\mu-1}$, $\dot{Q}^{01}_{\lambda-1\,\mu}$ and $\dot{Q}^{11}_{\lambda\,\mu}$ respectively. By (A.25), each of these coefficients has one term involved with $I_\alpha^{lm}$, which is of the order $a_\lambda b_\mu I_\alpha^{lm} = O(\epsilon^2 \log \epsilon) \to 0$, when $\epsilon \to 0$. The coefficients of $Z_{\lambda-1\,\mu}$, $Z_{\lambda+1\,\mu}$, $Z_{\lambda\,\mu-1}$, and $Z_{\lambda\,\mu+1}$ are $\dot{Q}^{00}_{\lambda-1\,\mu} + \dot{Q}^{01}_{\lambda-1\,\mu-1}$, $\dot{Q}^{10}_{\lambda\,\mu} + \dot{Q}^{11}_{\lambda\,\mu-1}$, $\dot{Q}^{00}_{\lambda\,\mu-1} + \dot{Q}^{10}_{\lambda-1\,\mu-1}$ and $\dot{Q}^{01}_{\lambda\,\mu} + \dot{Q}^{11}_{\lambda-1\,\mu}$ respectively. Each of these $\dot{Q}$ terms is of the order $O(\epsilon \log \epsilon) \to 0$, when $\epsilon \to 0$. One can see that our new definition of $\tilde{I}_\alpha^{\lambda-p\,\mu-q}$ is of order $O(1)$; if we substitute $O(1)$ for $O(\epsilon)$, these $\dot{Q}$ terms still tend to the same limit — zero. So our new definition of $\tilde{I}_\alpha^{\lambda-p\,\mu-q}$, which is applied in the singular region only, works well with all the coefficients of the nodes in this region.

We can also write $\tilde{I}_{\alpha^2}^{\lambda-p\,\mu-q}$ and $\tilde{I}_{\alpha^2\beta}^{\lambda-p\,\mu-q}$ in the general formula as

$$\tilde{I}_{\alpha^2}^{\lambda-p\,\mu-q} = h_{\mu-q} \log\left(\frac{g_{\lambda-p}}{h_{\mu-q}} + \sqrt{1+\frac{g_{\lambda-p}^2}{h_{\mu-q}^2}}\right), \qquad p=0,1;\ q=0,1;$$

$$\tilde{I}_{\alpha^2\beta}^{\lambda-p\,\mu-q} = \frac{(-1)^q}{2}\left[g_{\lambda-p}^2\left(1-\sqrt{1+\frac{h_{\mu-q}^2}{g_{\lambda-p}^2}}\right)+h_{\mu-q}^2 \log\left(\frac{g_{\lambda-p}}{h_{\mu-q}}+\sqrt{1+\frac{g_{\lambda-p}^2}{h_{\mu-q}^2}}\right)\right]$$
$$p=0,1;\ q=0,1. \qquad (A.74)$$

Correspondingly, by exchanging the roles of $\alpha$ with $\beta$ and $h$ with $g$, we obtain the general formulae for $\tilde{I}_\beta^{\lambda-p\,\mu-q}$, $\tilde{I}_{\beta^2}^{\lambda-p\,\mu-q}$ and $\tilde{I}_{\beta^2\alpha}^{\lambda-p\,\mu-q}$ as

$$\tilde{I}_\beta^{\lambda-p\,\mu-q} = (-1)^{q+1} \log\left(g_{\lambda-p}/h_{\mu-q} + \sqrt{1+g_{\lambda-p}^2/h_{\mu-q}^2}\right), \quad p=0,1;\ q=0,1,$$

$$\tilde{I}_{\beta^2}^{\lambda-p\,\mu-q} = g_{\lambda-p} \log\left(\frac{h_{\mu-q}}{g_{\lambda-p}} + \sqrt{1+\frac{h_{\mu-q}^2}{g_{\lambda-p}^2}}\right), \qquad p=0,1;\ q=0,1,$$

$$\tilde{I}_{\beta^2\alpha}^{\lambda-p\,\mu-q} = \frac{(-1)^p}{2}\left[h_{\mu-q}^2\left(1-\sqrt{1+\frac{g_{\lambda-p}^2}{h_{\mu-q}^2}}\right)+g_{\lambda-p}^2 \log\left(\frac{h_{\mu-q}}{g_{\lambda-p}}+\sqrt{1+\frac{h_{\mu-q}^2}{g_{\lambda-p}^2}}\right)\right]$$
$$p=0,1;\ q=0,1. \qquad (A.75)$$

### A.4.2 Integrals in Infinite Cells

Integrals $I_{\alpha}^{lm}$, $I_{\alpha^2}^{lm}$, $I_{\beta}^{lm}$, $I_{\beta^2}^{lm}$ and $I_{\alpha\beta}^{lm}$ which appeared in (A.42) and (A.48) all have integration limits tending to infinity. To estimate the limits of these integrals, the following limits are useful:

$$\lim_{x\to\infty}\left(\sqrt{x^2+a^2}-\sqrt{x^2+b^2}\right)=0$$
$$\lim_{x\to\infty}\left(\frac{a+\sqrt{x^2+a^2}}{b+\sqrt{x^2+b^2}}\right)=1,\quad \lim_{x\to\infty}\left(\frac{a+\sqrt{x^2+a^2}}{b+\sqrt{x^2+b^2}}\right)^x=e^{\mathrm{sgn}\,(x)(a-b)}. \tag{A.76}$$

The first one is proved as follows:

$$\lim_{x\to\infty}\left(\sqrt{x^2+a^2}-\sqrt{x^2+b^2}\right)=\lim_{x\to\infty}|x|\left(\sqrt{1+\frac{a^2}{x^2}}-\sqrt{1+\frac{b^2}{x^2}}\right)$$
$$=\lim_{x\to\infty}|x|\left[\left((1+\frac{1}{2}\frac{a^2}{x^2}+O(\frac{1}{x^4})\right)-\left((1+\frac{1}{2}\frac{b^2}{x^2}+O(\frac{1}{x^4})\right)\right]$$
$$=\lim_{x\to\infty}\frac{a^2-b^2}{2|x|}=0. \tag{A.77}$$

The second one is obvious; for the third one,

$$\lim_{x\to\infty}\left(\frac{a+\sqrt{x^2+a^2}}{b+\sqrt{x^2+b^2}}\right)^x=\lim_{x\to\infty}\left(\frac{\frac{a}{|x|}+1+\frac{a^2}{2x^2}}{\frac{b}{|x|}+1+\frac{b^2}{2x^2}}\right)^{\mathrm{sgn}\,(x)|x|}$$
$$=\lim_{x\to\infty}\left[\left(1+\frac{a}{|x|}\right)^{\frac{|x|}{a}a}\left(1+\frac{b}{|x|}\right)^{-\frac{|x|}{b}b}\right]^{\mathrm{sgn}\,(x)}=e^{\mathrm{sgn}\,(x)(a-b)}. \tag{A.78}$$

Applying these limits to $I_{\alpha}^{lm}$, $I_{\alpha^2}^{lm}$, $I_{\beta}^{lm}$, $I_{\beta^2}^{lm}$ and $I_{\alpha\beta}^{lm}$, we obtain the following results:

in region $R_1$ where $l=L$, $\alpha_2=+\infty$, $\alpha_1>0$, $\mathrm{sgn}\,(\alpha)=+1$,

$$I_{\alpha}^{Lm} = \lim_{\alpha_2\to+\infty} I_{\alpha}^{lm}=\mathrm{sgn}\,(\beta)\log\frac{|\beta_2|+\sqrt{\alpha_1^2+\beta_2^2}}{|\beta_1|+\sqrt{\alpha_1^2+\beta_1^2}}$$
$$I_{\alpha\beta}^{Lm} = \lim_{\alpha_2\to+\infty} I_{\alpha\beta}^{lm}=-\left(\sqrt{\alpha_1^2+\beta_1^2}-\sqrt{\alpha_1^2+\beta_2^2}\right),$$

$$I_{\beta}^{Lm} = \lim_{\alpha_2 \to +\infty} I_{\beta}^{lm} = \log \frac{|\alpha_1| + \sqrt{\beta_2^2 + \alpha_1^2}}{|\alpha_1| + \sqrt{\beta_1^2 + \alpha_1^2}},$$

$$I_{\beta^2}^{Lm} = \lim_{\alpha_2 \to +\infty} I_{\beta^2}^{lm} = \operatorname{sgn}(\beta) \left[ |\beta_2| - |\beta_1| - \alpha_1 \log \frac{|\beta_2| + \sqrt{\beta_2^2 + \alpha_1^2}}{|\beta_1| + \sqrt{\beta_1^2 + \alpha_1^2}} \right],$$

$$l = L;\ m = 1 \ldots M - 1, \qquad (A.79)$$

in $R_3$ where $l = 0$, $\alpha_1 = -\infty$, $\alpha_2 < 0$, $\operatorname{sgn}(\alpha) = -1$,

$$I_{\alpha}^{0m} = \lim_{\alpha_1 \to -\infty} I_{\alpha}^{lm} = -\operatorname{sgn}(\beta) \log \frac{|\beta_2| + \sqrt{\alpha_2^2 + \beta_2^2}}{|\beta_1| + \sqrt{\alpha_2^2 + \beta_1^2}},$$

$$I_{\alpha\beta}^{0m} = \lim_{\alpha_1 \to -\infty} I_{\alpha\beta}^{lm} = \sqrt{\alpha_2^2 + \beta_1^2} - \sqrt{\alpha_2^2 + \beta_2^2},$$

$$I_{\beta}^{0m} = \lim_{\alpha_1 \to -\infty} I_{\beta}^{lm} = \log \frac{|\alpha_2| + \sqrt{\beta_2^2 + \alpha_2^2}}{|\alpha_2| + \sqrt{\beta_1^2 + \alpha_2^2}},$$

$$I_{\beta^2}^{0m} = \lim_{\alpha_1 \to -\infty} I_{\beta^2}^{lm} = \operatorname{sgn}(\beta) \left[ |\beta_2| - |\beta_1| + \alpha_2 \log \frac{|\beta_2| + \sqrt{\beta_2^2 + \alpha_2^2}}{|\beta_1| + \sqrt{\beta_1^2 + \alpha_2^2}} \right],$$

$$l = 0;\ m = 1 \ldots M - 1, \qquad (A.80)$$

in $R_2$ where $m = M$, $\beta_2 = +\infty$, $\beta_1 > 0$, $\operatorname{sgn}(\beta) = +1$,

$$I_{\alpha}^{lM} = \lim_{\beta_2 \to +\infty} I_{\alpha}^{lm} = \log \frac{|\beta_1| + \sqrt{\alpha_2^2 + \beta_1^2}}{|\beta_1| + \sqrt{\alpha_1^2 + \beta_1^2}},$$

$$I_{\alpha^2}^{lM} = \lim_{\beta_2 \to +\infty} I_{\alpha^2}^{lm} = \operatorname{sgn}(\alpha) \left[ |\alpha_2| - |\alpha_1| - \beta_1 \log \frac{|\alpha_2| + \sqrt{\alpha_2^2 + \beta_1^2}}{|\alpha_1| + \sqrt{\alpha_1^2 + \beta_1^2}} \right],$$

$$I_{\beta}^{lM} = \lim_{\beta_2 \to +\infty} I_{\beta}^{lm} = \operatorname{sgn}(\alpha) \log \frac{|\alpha_2| + \sqrt{\beta_1^2 + \alpha_2^2}}{|\alpha_1| + \sqrt{\beta_1^2 + \alpha_1^2}},$$

$$I_{\alpha\beta}^{lM} = \lim_{\beta_2 \to +\infty} I_{\alpha\beta}^{lm} = -\left( \sqrt{\alpha_1^2 + \beta_1^2} - \sqrt{\alpha_2^2 + \beta_1^2} \right),$$

$$l = 1 \ldots L - 1,\ m = M; \qquad (A.81)$$

in $R_4$ where $m = 0$, $\beta_1 = -\infty$, $\beta_2 < 0$, $\operatorname{sgn}(\beta) = -1$,

$$I_{\alpha}^{l0} = \lim_{\beta_1 \to -\infty} I_{\alpha}^{lm} = \log \frac{|\beta_2| + \sqrt{\alpha_2^2 + \beta_2^2}}{|\beta_2| + \sqrt{\alpha_1^2 + \beta_2^2}},$$

$$
\begin{aligned}
I^{l0}_{\alpha^2} &= \lim_{\beta_1 \to -\infty} I^{lm}_{\alpha^2} = \mathrm{sgn}\,(\alpha)\left[|\alpha_2| - |\alpha_1| + \beta_2 \log \frac{|\alpha_2| + \sqrt{\alpha_2^2 + \beta_2^2}}{|\alpha_1| + \sqrt{\alpha_1^2 + \beta_2^2}}\right], \\
I^{l0}_{\beta} &= \lim_{\beta_1 \to -\infty} I^{lm}_{\beta} = -\mathrm{sgn}\,(\alpha) \log \frac{|\alpha_2| + \sqrt{\beta_2^2 + \alpha_2^2}}{|\alpha_1| + \sqrt{\beta_2^2 + \alpha_1^2}}, \\
I^{l0}_{\alpha\beta} &= \lim_{\beta_1 \to -\infty} I^{lm}_{\alpha\beta} = \sqrt{\alpha_1^2 + \beta_2^2} - \sqrt{\alpha_2^2 + \beta_2^2}, \\
& \qquad\qquad l = 1 \ldots L-1,\ m = 0. \qquad\qquad \text{(A.82)}
\end{aligned}
$$

## A.5 Evaluation of $M_d$

The integral operator $M_d$ is defined as

$$M_d\, F(\mathbf{r}) = \int_{-\infty}^{\infty} [F(\mathbf{s}) - F(\mathbf{r})]\, Q(|\mathbf{r} - \mathbf{s}|)\, d\mathbf{s}, \qquad \text{(A.83)}$$

where $F(\mathbf{r})$ stands for any component of the magnetic field at the bottom boundary $z = d$, i.e. $X(\mathbf{r}, d)$, $Y(\mathbf{r}, d)$ or $Z(\mathbf{r}, d)$ and

$$Q(r) = \frac{(1 + \alpha_0\sqrt{ir})\exp(-\alpha_0\sqrt{ir})}{r^3}. \qquad \text{(A.84)}$$

Since numerical integration will be involved, it is better to scale the integral first to make it dimensionless and in proper numerical range. We choose a characteristic length $1/\alpha_0 = 1/\sqrt{\omega\mu_0\sigma_0}$ as the scaling factor. If we define the new variables as $\mathbf{r}' = \alpha_0\mathbf{r}$, then $\mathbf{r} = \mathbf{r}'/\alpha_0$, $r = r'/\alpha_0$ $d\mathbf{r} = dxdy = dx'dy'/\alpha_0^2 = d\mathbf{r}'/\alpha_0^2$ and

$$Q(r) = \frac{(1 + \alpha_0\sqrt{ir})\exp(-\alpha_0\sqrt{ir})}{r^3} = \frac{(1 + \sqrt{ir'})\exp(-\sqrt{ir'})}{(r'/\alpha_0)^3} =: \alpha_0^3\tilde{Q}(r')$$

We also rewrite (A.83) as

$$
\begin{aligned}
M_d\, F(\mathbf{r}) &= \lim_{R\to\infty} \int_{-R}^{R} [F(\mathbf{s}) - F(\mathbf{r})]\, Q(|\mathbf{r} - \mathbf{s}|)\, d\mathbf{s} \\
&= \lim_{R\to\infty} \int_{-\alpha_0 R}^{\alpha_0 R} [F(\mathbf{s}') - F(\mathbf{r}')]\, \alpha_0^3 \tilde{Q}(|\mathbf{r}' - \mathbf{s}'|)\, d\mathbf{s}'/\alpha_0^2 \\
&= \alpha_0\, \tilde{M}_d\, F(\mathbf{r}') \qquad\qquad \text{(A.85)}
\end{aligned}
$$

i.e. $M_d\,F(\mathbf{r}) = \alpha_0 \tilde{M}_d\,F(\mathbf{r}')$. If we drop the prime on $\mathbf{r}'$ and $\mathbf{s}'$ etc, but remember to convert $\mathbf{r}$ into $\mathbf{r}'$ by $\mathbf{r}' = \alpha_0\mathbf{r}$ etc. when estimating the above double integral, then $\tilde{M}_d\,F(\mathbf{r})$, i.e. $\tilde{M}_d\,F(\mathbf{r}')$, can be written as

$$\begin{aligned} \tilde{M}_d\,F(\mathbf{r}) &= \int_{\infty}^{\infty} [F(\mathbf{s}) - F(\mathbf{r})]\,\tilde{Q}(|\mathbf{r}-\mathbf{s}|)\,d\mathbf{s}, \\ \tilde{Q}(|\mathbf{r}-\mathbf{s}|) &= \frac{(1+\sqrt{i}|\mathbf{r}-\mathbf{s}|)\exp(-\sqrt{i}|\mathbf{r}-\mathbf{s}|)}{|\mathbf{r}-\mathbf{s}|^3}. \end{aligned} \tag{A.86}$$

Following the procedure for $M_1$ and $M_2$, we obtain

$$\tilde{M}_d\,F_{\lambda\mu} = \tilde{I}_0 + I_0 + I_1 + \ldots + I_8 = \sum_0^L \sum_0^M I_Q^{lm}$$

$$\begin{aligned} I_Q^{lm} &= \int_{x_l}^{x_{l+1}} \int_{y_m}^{y_{m+1}} [F(\mathbf{s}) - F(\mathbf{r})]\,\tilde{Q}(|\mathbf{r}-\mathbf{s}|)\,d\mathbf{s} \\ &= \int_{\alpha_1}^{\alpha_2} \int_{\beta_1}^{\beta_2} [F_{lm} + T_1(\alpha - a_l) + T_2(\beta - b_m) + T_3(\alpha - a_l)(\beta - b_m)]\tilde{Q}(\gamma)\,d\alpha\,d\beta \\ &\quad - F_{\lambda\mu} \int_{\alpha_1}^{\alpha_2} \int_{\beta_1}^{\beta_2} \tilde{Q}(\gamma)\,d\alpha\,d\beta \\ &= W_{lm}^{00} F_{lm} + W_{lm}^{10} F_{l+1m} + W_{lm}^{01} F_{lm+1} + W_{lm}^{11} F_{l+1m+1} - I_{00}^{lm} F_{\lambda\mu} \\ &= \sum_{p=0}^{1} \sum_{q=0}^{1} W_{lm}^{pq} F_{l+p\,m+q} - I_{00}^{lm} F_{\lambda\mu} \end{aligned} \tag{A.87}$$

where $\tilde{Q}(\gamma) = \tilde{Q}(\sqrt{\alpha^2 + \beta^2})$,

$$\begin{pmatrix} W_{lm}^{00} \\ W_{lm}^{10} \\ W_{lm}^{01} \\ W_{lm}^{11} \end{pmatrix} = \frac{1}{g_l\,h_m} \begin{pmatrix} a_{l+1}b_{m+1}I_{00}^{lm} - a_{l+1}I_{01}^{lm} - b_{m+1}I_{10}^{lm} + I_{11}^{lm} \\ -a_l b_{m+1} I_{00}^{lm} + a_l I_{01}^{lm} + b_{m+1} I_{10}^{lm} - I_{11}^{lm} \\ -a_{l+1} b_m I_{00}^{lm} + a_{l+1} I_{01}^{lm} + b_m I_{10}^{lm} - I_{11}^{lm} \\ a_l b_m I_{00}^{lm} - a_l I_{01}^{lm} - b_m I_{10}^{lm} + I_{11}^{lm} \end{pmatrix} \tag{A.88}$$

or

$$W_{lm}^{pq} = \frac{(-1)^{p+q}}{g_l\,h_m} \sum_{r=0}^{1} \sum_{s=0}^{1} (-1)^{r+s} (a_{l+1-p})^{1-r} (b_{m+1-q})^{1-s} I_{rs}^{lm}. \tag{A.89}$$

The double integrals $I_{00}^{lm}$, $I_{01}^{lm}$, $I_{10}^{lm}$ and $I_{11}^{lm}$ are defined as

$$I_{pq}^{lm} = \int_{\alpha_1}^{\alpha_2} \int_{\beta_1}^{\beta_2} \alpha^p \beta^q \tilde{Q}(\gamma)\,d\alpha\,d\beta,\ p = 0, 1;\ q = 0, 1. \tag{A.90}$$

As will be seen later, we no longer have the luxury of being able to evaluate all the integrals $I_{pq}^{lm}$ analytically. Therefore, the singularity cannot be cancelled out with the aid of analytical expressions. A bi-linear variation for the interpolation is no longer sufficient and we have to try a bi-quadratic variation instead.

### A.5.1 Bi-quadratic Variation

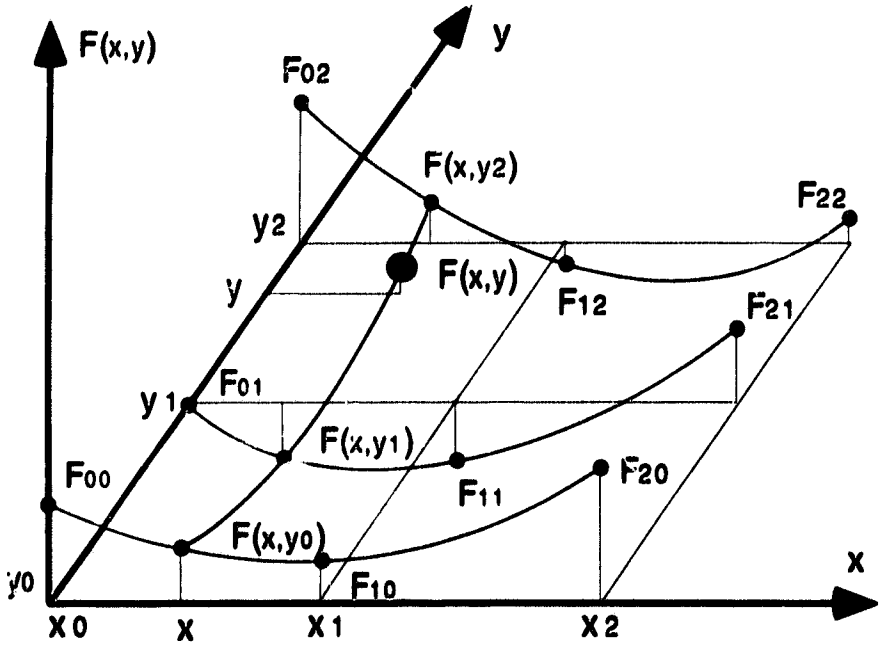


Figure A.2: Bi-quadratic variation.

A quadratic variation in the $x$-direction over two segments defined by three points $x_0$, $x_1$ and $x_2$ is

$$P(x) = l_0(x)f(x_0) + l_1(x)f(x_1) + l_2(x)f(x_2) = \sum_{p=0}^{2} l_p(x)f(x_p), \quad x_0 \leq x \leq x_2$$

where

$$l_0(x)=\frac{(x-x_1)(x-x_2)}{(x_0-x_1)(x_0-x_2)}, \; l_1(x)=\frac{(x-x_0)(x-x_2)}{(x_1-x_0)(x_1-x_2)}, \; l_2(x)=\frac{(x-x_0)(x-x_1)}{(x_2-x_0)(x_2-x_1)}, \quad \text{(A.91)}$$

which satisfy

$$l_p(x_q) = \delta_{pq} := \begin{cases} 1 & p = q \\ 0 & p \neq q. \end{cases}$$

Similarly, $m_0(y)$, $m_1(y)$ and $m_2(y)$ can be expressed in a corresponding manner for interpolation in the $y$-direction by substituting $y$ for $x$ in the above expressions. We say a function $f(x,y)$ has a bi-quadratic variation if it varies quadratically in both the $x$- and $y$- directions. Let $F_{pq}$ represent the field value at the nodal point $(x_p, y_q)$ and $F(x,y)$ represent the bi-quadratic interpolation of the field value at a general point $(x,y)$. As shown in figure (A.2), the field value at any general point along the three profiles, $y = y_0$, $y = y_1$ and $y = y_2$, are interpolated respectively by

$$\begin{aligned} F(x,y_0) &= l_0(x)F_{00} + l_1(x)F_{10} + l_2(x)F_{20} \\ F(x,y_1) &= l_0(x)F_{01} + l_1(x)F_{11} + l_2(x)F_{21} \\ F(x,y_2) &= l_0(x)F_{02} + l_1(x)F_{12} + l_2(x)F_{22} \end{aligned} \qquad (A.92)$$

or

$$(F(x,y_0), F(x,y_1), F(x,y_2)) = (l_0(x), l_1(x), l_2(x)) \begin{pmatrix} F_{00} & F_{01} & F_{02} \\ F_{10} & F_{11} & F_{12} \\ F_{20} & F_{21} & F_{22} \end{pmatrix}. \qquad (A.93)$$

$F(x,y_q)$, $q = 0,1,2$ can, in turn, be interpolated along the $y$-direction to give its value at any point $(x,y)$ in the form

$$\begin{aligned} F(x,y) &= m_0(y)F(x,y_0) + m_1(y)F(x,y_1) + m_2(y)F(x,y_2) \\ &= (l_0(x), l_1(x), l_2(x)) \begin{pmatrix} F_{00} & F_{01} & F_{02} \\ F_{10} & F_{11} & F_{12} \\ F_{20} & F_{21} & F_{22} \end{pmatrix} \begin{pmatrix} m_0(y) \\ m_1(y) \\ m_2(y) \end{pmatrix} \\ &= \sum_{p=0}^{2}\sum_{q=0}^{2} l_p(x)m_q(y)F_{pq}. \end{aligned} \qquad (A.94)$$

Using the notation of a local system, we let $(x_1, y_1) = (x_\lambda, y_\mu)$, so that $x_0 = x_{\lambda-1}$, $x_2 = x_{\lambda+1}$ and $y_0 = y_{\mu-1}$, $y_2 = y_{\mu+1}$. Then the integral over the singular region

$\tilde{I}_0$, similar to that of (A.10), becomes

$$\begin{aligned}\tilde{I}_0 &= \int_{x_0}^{x_2}\int_{y_0}^{y_2} [F(x,y) - F_{11}]\,\tilde{Q}\left(\sqrt{(x_1-x)^2+(y_1-y)^2}\right) dx dy \\ &= \int_{x_0}^{x_2}\int_{y_0}^{y_2} \left[\sum_{p=0}^{2}\sum_{q=0}^{2} l_p(x) m_q(y) F_{pq} - F_{11}\right] \tilde{Q}\left(\sqrt{(x_1-x)^2+(y_1-y)^2}\right) dx dy\end{aligned} \tag{A.95}$$

Transfering $(x,y)$ into $(\alpha,\beta)$ as in (A.14), and writing $g_0 = x_1 - x_0$, $g_2 = x_2 - x_1$, $g_{20} = g_2 - g_0$, $g_s = g_0 + g_2$, etc. we have $x - x_1 = \alpha$, $x - x_0 = \alpha + g_0$, $x - x_2 = \alpha - g_2$, etc. in (A.91). Thus $l_p(x)$, and by analogy $m_q(y)$, take the form

$$\begin{aligned} l_0(x) &= \tilde{l}_0(\alpha) = \tfrac{\alpha^2 - g_2\alpha}{g_0 g_s}, & m_0(y) &= \tilde{m}_0(\beta) = \tfrac{\beta^2 - h_2\beta}{h_0 h_s}, \\ l_1(x) &= \tilde{l}_1(\alpha) = 1 - \tfrac{\alpha^2 - g_{20}\alpha}{g_0 g_2}, & m_1(y) &= \tilde{m}_1(\beta) = 1 - \tfrac{\beta^2 - h_{20}\beta}{h_0 h_2}, \\ l_2(x) &= \tilde{l}_2(\alpha) = \tfrac{\alpha^2 + g_0\alpha}{g_2 g_s}, & m_2(y) &= \tilde{m}_2(\beta) = \tfrac{\beta^2 + h_0\beta}{h_2 h_s}. \end{aligned} \tag{A.96}$$

The above expression for $\tilde{I}_0$ becomes

$$\begin{aligned}\tilde{I}_0 &= \int_{-g_0}^{g_2}\int_{-h_0}^{h_2} \left[\sum_{p=0}^{2}\sum_{q=0}^{2} \tilde{l}_p(\alpha)\tilde{m}_q(\beta) F_{pq} - F_{11}\right] \tilde{Q}\left(\sqrt{\alpha^2+\beta^2}\right) d\alpha\, d\beta \\ &= \sum_{p=0}^{2}\sum_{q=0}^{2} F_{pq} \int_{-g_0}^{g_2}\int_{-h_0}^{h_2} \tilde{l}_p(\alpha)\tilde{m}_q(\beta)\tilde{Q}\left(\sqrt{\alpha^2+\beta^2}\right) d\alpha\, d\beta \\ &\quad - F_{11}\int_{-g_0}^{g_2}\int_{-h_0}^{h_2} \tilde{Q}\left(\sqrt{\alpha^2+\beta^2}\right) d\alpha\, d\beta \\ &= \sum_{p=0}^{2}\sum_{q=0}^{2} \dot{W}_{pq} F_{pq}.\end{aligned} \tag{A.97}$$

The coefficients $\dot{W}_{pq}$ are

$$\dot{W}_{pq} = \begin{cases} +\frac{I_{22} - h_2 I_{21} - g_2 I_{12} + g_2 h_2 I_{11}}{g_0 g_s h_0 h_s} & (p,q) = (0,0) \\ -\frac{I_{22} - h_{20} I_{21} - g_2 I_{12} + g_2 h_{20} I_{11}}{g_0 g_s h_0 h_2} + \frac{I_{20} - g_2 I_{10}}{g_0 g_s} & (0,1) \\ +\frac{I_{22} + h_0 I_{21} - g_2 I_{12} - g_2 h_0 I_{11}}{g_0 g_s h_2 h_s} & (0,2) \\ -\frac{I_{22} - h_2 I_{21} + g_{20} I_{12} - g_{20} h_2 I_{11}}{g_0 g_2 h_0 h_s} + \frac{I_{02} - h_2 I_{01}}{h_0 h_s} & (1,0) \\ +\frac{I_{22} - h_{20} I_{21} - g_{20} I_{12} + g_{20} h_{20} I_{11}}{g_0 g_s h_0 h_s} - \frac{I_{20} - g_{20} I_{10}}{g_0 g_2} - \frac{I_{02} - h_{20} I_{01}}{h_0 h_2} & (1,1) \\ -\frac{I_{22} + h_0 I_{21} - g_{20} I_{12} - g_{20} h_0 I_{11}}{g_0 g_2 h_2 h_s} + \frac{I_{02} + h_0 I_{01}}{h_2 h_s} & (1,2) \\ +\frac{I_{22} - h_2 I_{21} + g_0 I_{12} - g_0 h_2 I_{11}}{g_2 g_s h_0 h_s} & (2,0) \\ -\frac{I_{22} - h_{20} I_{21} + g_0 I_{12} - g_0 h_{20} I_{11}}{g_2 g_s h_0 h_2} + \frac{I_{20} + g_0 I_{10}}{g_2 g_s} & (2,1) \\ +\frac{I_{22} + h_0 I_{21} + g_0 I_{12} + g_0 h_0 I_{11}}{g_2 g_s h_2 h_s} & (2,2) \end{cases} \tag{A.98}$$

which consist of eight integrals $I_{01}$, $I_{10}$, $I_{11}$ $I_{02}$, $I_{20}$, $I_{12}$, $I_{21}$ and $I_{22}$ defined as

$$I_{pq} = \oint_{-g_0}^{g_2} \alpha^p \, d\alpha \oint_{-h_0}^{h_2} \beta^q \tilde{Q}\left(\sqrt{\alpha^2 + \beta^2}\right) d\beta. \qquad (A.99)$$

Note that there is no $I_{00}$ term involved in $\tilde{W}_{pq}$; it has been cancelled by the subtraction of the $F_{11} I_{00}$ term.

### A.5.2 Nine Double Integrals

There are nine double integrals involved in the coefficients $W_{lm}^{pq}$ from the regular cells, and the coefficients $\tilde{W}_{pq}$ from the singular cells; they are $I_{00}$, $I_{01}$, $I_{10}$, $I_{11}$, $I_{02}$, $I_{20}$, $I_{12}$, $I_{21}$ and $I_{22}$. We can denote these integrals by the general formula

$$I_{pq}(a_1, a_2; b_1, b_2) = \int_{a_1}^{a_2} x^p dx \int_{b_1}^{b_2} y^q \tilde{Q}(r) dy, \quad r := \sqrt{x^2 + y^2}. \qquad (A.100)$$

It follows that

$$I_{qp}(a_1, a_2; b_1, b_2) = \int_{a_1}^{a_2} x^q dx \int_{b_1}^{b_2} y^p \tilde{Q}(r) dy = \int_{b_1}^{b_2} x^p dx \int_{a_1}^{a_2} y^q \tilde{Q}(r) dy,$$

$$\text{i.e.} \qquad I_{qp}(a_1, a_2; b_1, b_2) = I_{pq}(b_1, b_2; a_1, a_2). \qquad (A.101)$$

It can also be readily verified that

$$\begin{aligned} I_{pq}(a_1, a_2; b_1, b_2) &= -I_{pq}(a_2, a_1; b_1, b_2) = (-1)^p I_{pq}(-a_2, -a_1; b_1, b_2), \\ I_{pq}(a_1, a_2; b_1, b_2) &= -I_{pq}(a_1, a_2; b_2, b_1) = (-1)^q I_{pq}(a_1, a_2; -b_2, -b_1). \end{aligned} \qquad (A.102)$$

By using these formulae, the integrals $I_{01}$, $I_{02}$ and $I_{21}$ can be obtained immediately from $I_{10}$, $I_{20}$ and $I_{12}$ respectively. We have found that whenever $p = 1$ or $q = 1$, an analytical integration can be carried out directly with respect to the variable to which the subscript refers, e.g. $I_{10}$ and $I_{12}$ can be integrated analytically once with respect to the first variable, while $I_{11}$ can be integrated analytically in both variables. The integrals $I_{00}$, $I_{20}$ and $I_{22}$ can also be integrated once analytically, but we have to convert them into polar coordinates, integrate them with respect to $r$, and then convert them back to the rectangular coordinates again.

With the help of Maple, $I_{11}$, $I_{10}$ and $I_{12}$ are evaluated as follows:

$$\begin{aligned}
I_{11}(a_1,a_2;b_1,b_2) &= \frac{1}{\sqrt{i}}\Big[\exp(-\sqrt{i}\sqrt{a_2^2+b_2^2}) - \exp(-\sqrt{i}\sqrt{a_2^2+b_1^2}) \\
&\quad - \exp(-\sqrt{i}\sqrt{a_1^2+b_2^2}) + \exp(-\sqrt{i}\sqrt{a_1^2+b_1^2})\Big] \\
I_{10}(a_1,a_2;b_1,b_2) &= -\int_{b_1}^{b_2}\left[\frac{\exp(-\sqrt{i}\sqrt{a_2^2+u^2})}{\sqrt{a_2^2+u^2}} - \frac{\exp(-\sqrt{i}\sqrt{a_1^2+u^2})}{\sqrt{a_1^2+u^2}}\right]du \\
I_{12}(a_1,a_2;b_1,b_2) &= -\int_{b_1}^{b_2}\left[a_2^2\frac{\exp(-\sqrt{i}\sqrt{a_2^2+u^2})}{\sqrt{a_2^2+u^2}} - a_1^2\frac{\exp(-\sqrt{i}\sqrt{a_1^2+u^2})}{\sqrt{a_1^2+u^2}}\right]du
\end{aligned} \tag{A.103}$$

Since we have to convert $I_{00}$, $I_{20}$ and $I_{22}$ into polar coordinates, it is convenient to look at $I_{pq}(a,\infty;b,\infty)$ first. As shown in figure (A.3), the transformation of

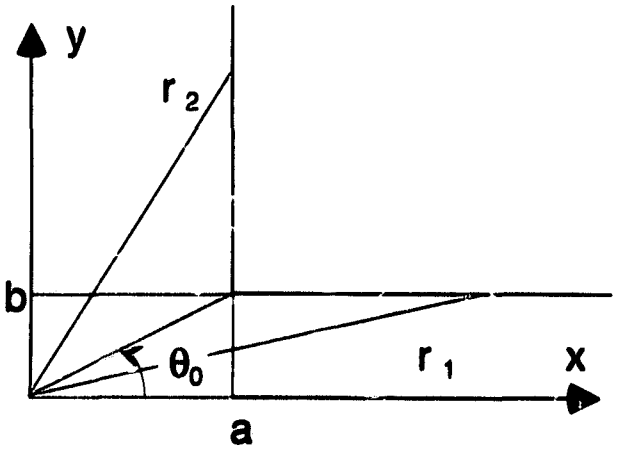


Figure A.3: Cartesian and polar coordinates.

the coordinates is

$$\begin{aligned}
r_1(\theta) &= \sqrt{x^2+b^2}, \cos\theta = \frac{x}{r},\ \sin\theta = \frac{b}{r},\ d\theta = -\frac{b}{r^2}dx,\ 0 < \theta \le \theta_0; \\
r_2(\theta) &= \sqrt{a^2+y^2}, \cos\theta = \frac{a}{r},\ \sin\theta = \frac{y}{r},\ d\theta = \frac{a}{r^2}dy,\ \theta_0 \le \theta < \frac{\pi}{2}; \\
\theta_0 &= \arctan(b/a),
\end{aligned} \tag{A.104}$$

yielding

$$I_{pq}(a,\infty;b,\infty) = \int_a^\infty x^p dx \int_b^\infty y^q \hat{Q}(r) dy$$

$$
\begin{aligned}
&= \left[\int_0^{\theta_0}\int_{r_1(\theta)}^{\infty} + \int_{\theta_0}^{\frac{\pi}{2}}\int_{r_2(\theta)}^{\infty}\right] \cos^p\theta \sin^q\theta\, r^{p+q-2}(1+\sqrt{i}r)\exp(-\sqrt{i}r)\, dr d\theta \\
&= \int_0^{\theta_0} \cos^p\theta \sin^q\theta f_{pq}(r_1)\, d\theta + \int_{\theta_0}^{\frac{\pi}{2}} \cos^p\theta \sin^q\theta f_{pq}(r_2)\, d\theta \\
&= \int_{\infty}^{a} \frac{x^p b^q}{r_1^{p+q}} f_{pq}(r_1)\frac{-b}{r_1^2}dx + \int_b^{\infty} \frac{a^p y^q}{r_2^{p+q}} f_{pq}(r_2)\frac{a}{r_2^2}dy \qquad \text{(A.105)}
\end{aligned}
$$

which can be written as

$$
I_{pq}(a,\infty;b,\infty) = \int_a^{\infty} \phi_{qp}(b,u)\, du + \int_b^{\infty} \phi_{pq}(a,u)\, du, \qquad \text{(A.106)}
$$

where

$$
\begin{aligned}
\phi_{pq}(x,y) &= \frac{x^{p+1}y^q}{r^{p+q+2}} f_{pq}(r), \quad r = \sqrt{x^2+y^2} \\
f_{pq}(r) &= \int_r^{\infty} u^{p+q-2}(1+\sqrt{i}u)\exp(-\sqrt{i}u)\, du. \qquad \text{(A.107)}
\end{aligned}
$$

The integral (A.107) gives

$$
\begin{aligned}
f_{00}(r) &= \frac{1}{r}\exp(-\sqrt{i}r) \\
f_{20}(r) &= f_{02}(r) = \frac{(2+\sqrt{i}r)}{\sqrt{i}}\exp(-\sqrt{i}r) \\
f_{22}(r) &= -\sqrt{i}\left[(\sqrt{i}r)^2(4+\sqrt{i}r) + 8(1+\sqrt{i}r)\right] \qquad \text{(A.108)}
\end{aligned}
$$

Using identity (A.106), we have

$$
\begin{aligned}
I_{pq}(a_1,a_2;b,\infty) &= \left(\int_{a_1}^{\infty} - \int_{a_2}^{\infty}\right)\int_b^{\infty}(\ldots) = \left(\int_{a_1}^{\infty}\int_b^{\infty} - \int_{a_2}^{\infty}\int_b^{\infty}\right)(\ldots) \\
&= I_{pq}(a_1,\infty;b,\infty) - I_{pq}(a_2,\infty;b,\infty) \\
&= \int_{a_1}^{a_2} \phi_{qp}(b,u)\, du + \int_b^{\infty}[\phi_{pq}(a_1,u) - \phi_{pq}(a_2,u)]\, du. \qquad \text{(A.109)}
\end{aligned}
$$

Similarly, we obtain

$$
\begin{aligned}
I_{pq}(a_1,a_2;b_1,b_2) &= \int_{a_1}^{a_2}[\phi_{qp}(b_1,u) - \phi_{qp}(b_2,u)]\, du \\
&+ \int_{b_1}^{b_2}[\phi_{pq}(a_1,u) - \phi_{pq}(a_2,u)]\, du \qquad \text{(A.110)}
\end{aligned}
$$

from which the integrals $I_{22}$, $I_{20}$, $I_{02}$ and $I_{00}$ can be calculated. For example,

$$f_{00}(r) = \exp(-\sqrt{i}r)/r, \quad \phi_{00}(x,y) = (x/r^3)\exp(-\sqrt{i}r),$$
$$I_{00}(a_1,a_2;b_1,b_2) = \int_{a_1}^{a_2}\left(b_1\frac{\exp(-\sqrt{i}\sqrt{b_1^2+u^2})}{(b_1^2+u^2)^{3/2}} - b_2\frac{\exp(-\sqrt{i}\sqrt{b_2^2+u^2})}{(b_2^2+u^2)^{3/2}}\right)du$$
$$+\int_{b_1}^{b_2}\left(a_1\frac{\exp(-\sqrt{i}\sqrt{a_1^2+u^2})}{(a_1^2+u^2)^{3/2}} - a_2\frac{\exp(-\sqrt{i}\sqrt{a_2^2+u^2})}{(a_2^2+u^2)^{3/2}}\right)du \tag{A.111}$$

Of the nine integrals, the coefficients $W_{lm}^{pq}$ for cells in the regular region $R_0$ require only four, viz. $I_{11}$, $I_{10}$, $I_{01}$ and $I_{00}$, while the coefficients $\tilde{W}_{pq}$ for cells in the singular region $\tilde{R}_0$ require eight (all but $I_{00}$). In regular cells, the integrals are integrated over each individual cell with integration limits $(a_1,a_2;b_1,b_2) = (x_l - x_\lambda, x_{l+1} - x_\lambda; y_m - y_\mu, y_{m+1} - y_\mu)$. We will denote these four integrals by $I_{pq}^{lm} := I_{pq}(a_1,a_2;b_1,b_2)$, $p = 0,1$, $q = 0,1$. In the singular region $\tilde{R}_0$, the integrals are taken over the entire region $\tilde{R}_0$ comprising four cells, the integration limits being

$(a_1,a_2;b_1,b_2) = (x_{\lambda-1} - x_\lambda, x_{\lambda+1} - x_\lambda; y_{\mu-1} - y_\mu, y_{\mu+1} - y_\mu) := (-g_0, g_2; -h_0, h_2)$. None of these four limits are zero; therefore, none of the denominators in the integrands will vanish. It follows that all the integrals in the singular region are free of singularities.

### A.5.3 Coefficients and Sub-integrals in Different Regions

In region $R_0$, we have

$$W_{lm}^{pq} = \frac{(-1)^{p+q}}{g_l\, h_m}\sum_{r=0}^{1}\sum_{s=0}^{1}(-1)^{r+s}(a_{l+1-p})^{1-r}(b_{m+1-q})^{1-s}I_{r\,s}^{lm}.$$
$$p = 0,1,\ q = 0,1;\ l = 1,\ldots L-1,\ m = 1,\ldots M-1$$
$$(l,m) \neq (\lambda,\mu),(\lambda-1,\mu),(\lambda,\mu-1),(\lambda-1,\mu-1); \tag{A.112}$$

and in the singular region $\hat{R}_0$, where $(l,m) = (\lambda,\mu)$, $(\lambda-1,\mu)$, $(\lambda,\mu-1)$ or $(\lambda-1\,\mu-1)$, we define

$$\begin{array}{llll} W^{00}_{\lambda\mu} = \hat{W}_{11}/4 & W^{00}_{\lambda-1\mu} = \hat{W}_{01}/2 & W^{00}_{\lambda\mu-1} = \hat{W}_{10}/2 & W^{00}_{\lambda-1\mu-1} = \hat{W}_{00} \\ W^{10}_{\lambda\mu} = \hat{W}_{21}/2 & W^{10}_{\lambda-1\mu} = \hat{W}_{11}/4 & W^{10}_{\lambda\mu-1} = \hat{W}_{20} & W^{10}_{\lambda-1\mu-1} = \hat{W}_{10}/2 \\ W^{01}_{\lambda\mu} = \hat{W}_{12}/2 & W^{01}_{\lambda-1\mu} = \hat{W}_{02} & W^{01}_{\lambda\mu-1} = \hat{W}_{11}/4 & W^{01}_{\lambda-1\mu-1} = \hat{W}_{01}/2 \\ W^{11}_{\lambda\mu} = \hat{W}_{22} & W^{11}_{\lambda-1\mu} = \hat{W}_{12}/2 & W^{11}_{\lambda\mu-1} = \hat{W}_{21}/2 & W^{11}_{\lambda-1\mu-1} = \hat{W}_{11}/4. \end{array} \tag{A.113}$$

In regions $R_1$, $R_3$ and $R_2$ $R_4$, as in (A.32) and (A.36), we have

$$\begin{aligned} I^{lm}_Q &= \int_{\alpha_1}^{\alpha_2}\int_{\beta_1}^{\beta_2} [Z_{um} + T_2(\beta - b_m)]\,\check{Q}\left(\sqrt{\alpha^2+\beta^2}\right) d\alpha\, d\beta \\ &= Z_{um} I^{lm}_{00} + T_2(I^{lm}_{01} - b_m I^{lm}_{00}) = \frac{b_{m+1} I^{lm}_{00} - I^{lm}_{01}}{h_m} Z_{um} - \frac{b_m I^{lm}_{00} - I^{lm}_{01}}{h_m} Z_{u\,m+1}, \\ I^{lm}_Q &= Z_{lv} I^{lm}_{00} + T_1(I^{lm}_{10} - a_l I^{lm}_{00}) = \frac{a_{l+1} I^{lm}_{00} - I^{lm}_{10}}{g_l} Z_{lv} - \frac{a_l I^{lm}_{00} - I^{lm}_{10}}{g_l} Z_{l+1\,v}. \end{aligned}$$

The final forms of the above two expressions could also have been obtained from (A.32) and (A.36) respectively by substituting $I^{lm}_{\alpha}$ for $I^{lm}_{00}$, $I^{lm}_{\alpha\beta}$ for $I^{lm}_{01}$ and $I^{lm}_{\alpha^2}$ for $I^{lm}_{10}$. Applying the same substitution to (A.34), (A.35), (A.37) and (A.38), we obtain

$$W^{00}_{lm} = W^{01}_{lm} = 0,\ W^{10}_{lm} = \left(b_{m+1} I^{lm}_{00} - I^{lm}_{01}\right)/h_m,\ W^{11}_{lm} = -\left(b_m I^{lm}_{00} - I^{lm}_{01}\right)/h_m$$
$$l = 0,\ \ m = 1 \ldots M-1 \tag{A.114}$$

$$W^{10}_{lm} = W^{11}_{lm} = 0,\ W^{00}_{lm} = \left(b_{m+1} I^{lm}_{00} - I^{lm}_{01}\right)/h_m\ \ W^{01}_{lm} = -\left(b_m I^{lm}_{00} - I^{lm}_{01}\right)/h_m,$$
$$l = L,\ \ m = 1 \ldots M-1 \tag{A.115}$$

$$W^{00}_{lm} = W^{10}_{lm} = 0,\ \ W^{01}_{lm} = \left(a_{l+1} I^{lm}_{00} - I^{lm}_{10}\right)/g_l,\ \ W^{11}_{lm} = -\left(a_l I^{lm}_{00} - I^{lm}_{10}\right)/g_l$$
$$l = 1 \ldots L-1,\ \ m = 0 \tag{A.116}$$

$$W^{01}_{lm} = W^{11}_{lm} = 0,\ \ W^{00}_{lm} = \left(a_{l+1} I^{lm}_{00} - I^{lm}_{10}\right)/g_l,\ \ W^{10}_{lm} = -\left(a_l I^{lm}_{00} - I^{lm}_{10}\right) g_l$$
$$l = 1 \ldots L-1,\ \ m = M \tag{A.117}$$

Unlike (A.39) for the surface boundary condition, the integrals in regions $R_5$ to $R_8$ are no longer zero; we obtain the following expressions: in $R_5$,

$$a_2 = +\infty,\ a_1 > 0;\ b_2 = +\infty,\ b_1 > 0;\ F(x,y) = F_{LM}$$

$$I_Q^{LM} = \int_{a_1}^{\infty}\int_{b_1}^{\infty}(F_{LM} - F_{\lambda\mu})\tilde{Q}(\sqrt{\alpha^2+\beta^2})\,d\alpha\,d\beta = (F_{LM} - F_{\lambda\mu})I_{00}^{LM}$$
$$= F_{LM}W_{LM}^{00} - F_{\lambda\mu}I_{00}^{LM}; \tag{A.118}$$

in $R_6$,

$$a_1 = -\infty,\ a_2 < 0;\ b_2 = +\infty,\ b_1 > 0;\ F(x,y) = F_{1M}$$
$$I_Q^{0M} = (F_{1M} - F_{\lambda\mu})I_{00}^{0M} = F_{1M}W_{0M}^{10} - F_{\lambda\mu}I_{00}^{0M}; \tag{A.119}$$

in $R_7$,

$$a_1 = -\infty,\ a_2 < 0;\ b_1 = -\infty,\ b_2 < 0;\ F(x,y) = F_{11}$$
$$I_Q^{00} = (F_{11} - F_{\lambda\mu})I_{00}^{00} = F_{11}W_{00}^{11} - F_{\lambda\mu}I_{00}^{00}; \tag{A.120}$$

and in $R_8$,

$$a_2 = +\infty,\ a_1 > 0;\ b_1 = -\infty,\ b_2 < 0;\ F(x,y) = F_{L1}$$
$$I_Q^{L0} = (F_{L1} - F_{\lambda\mu})I_{00}^{L0} = F_{L1}W_{L0}^{01} - F_{\lambda\mu}I_{00}^{L0}; \tag{A.121}$$

The coefficients $W_{lm}^{pq}$ given by (A.114) to (A.121), are summarized as

$$W_{lm}^{00} = \begin{cases} (b_{m+1}I_{00}^{lm} - I_{01}^{lm})/h_m, & l = L;\ m = 1...M-1, \\ (a_{l+1}I_{00}^{lm} - I_{10}^{lm})/g_l, & m = M;\ l = 1...L-1, \\ I_{00}^{LM}, & l = L;\ m = M, \end{cases}$$

$$W_{lm}^{10} = \begin{cases} (b_{m+1}I_{00}^{lm} - I_{01}^{lm})/h_m, & l = 0;\ m = 1...M-1, \\ -(a_lI_{00}^{lm} - I_{10}^{lm})/g_l, & m = M;\ l = 1...L-1, \\ I_{00}^{0M}, & l = 0;\ m = M, \end{cases}$$

$$W_{lm}^{01} = \begin{cases} -(b_mI_{00}^{lm} - I_{01}^{lm})/h_m, & l = L;\ m = 1...M-1, \\ (a_{l+1}I_{00}^{lm} - I_{10}^{lm})/g_l, & m = 0;\ l = 1...L-1, \\ I_{00}^{L0}, & l = L;\ m = 0, \end{cases}$$

$$W_{lm}^{11} = \begin{cases} -(b_mI_{00}^{lm} - I_{01}^{lm})/h_m, & l = 0;\ m = 1...M-1, \\ -(a_lI_{00}^{lm} - I_{10}^{lm})/g_l, & m = 0;\ l = 1...L-1, \\ I_{00}^{00}, & l = 0;\ m = 0, \end{cases} \tag{A.122}$$

and the integrals involved in these expressions are as follows:

in $R_1$, $l = L$, $a_2 = +\infty$, $a_1 > 0$, $m = 1...M-1$,

$$I_{pq}^{lm} = I_{pq}(a_1, +\infty; b_1, b_2) = I_{qp}(b_1, b_2; a_1, +\infty)$$

$$= \int_{b_1}^{b_2} \phi_{pq}(a_1, u)du + \int_{a_1}^{\infty} [\phi_{qp}(b_1, u) - \phi_{qp}(b_2, u)]\, du; \qquad (A.123)$$

in $R_3$, $l = 0$, $a_1 = -\infty$, $a_2 < 0$, $m = 1...M-1$,

$$I_{pq}^{lm} = I_{pq}(-\infty, a_2; b_1, b_2) = (-1)^p I_{qp}(b_1, b_2; |a_2|, +\infty)$$
$$= (-1)^p \left[ \int_{b_1}^{b_2} \phi_{pq}(|a_2|, u)du + \int_{|a_2|}^{\infty} [\phi_{qp}(b_1, u) - \phi_{qp}(b_2, u)]\, du \right]; \qquad (A.124)$$

in $R_2$, $m = M$, $b_2 = +\infty$, $b_1 > 0$, $l = 1...L-1$,

$$I_{pq}^{lm} = I_{pq}(a_1, a_2; b_1, +\infty)$$
$$= \int_{a_1}^{a_2} \phi_{qp}(b_1, u)du + \int_{b_1}^{\infty} [\phi_{pq}(a_1, u) - \phi_{pq}(a_2, u)]\, du; \qquad (A.125)$$

in $R_4$, $m = 0$, $b_1 = -\infty$, $b_2 < 0$, $l = 1...L-1$,

$$I_{pq}^{lm} = I_{pq}(a_1, a_2; -\infty, b_2) = (-1)^q I_{pq}(a_1, a_2; |b_2|, +\infty)$$
$$= (-1)^q \left[ \int_{a_1}^{a_2} \phi_{qp}(|b_2|, u)du + \int_{|b_2|}^{\infty} [\phi_{pq}(a_1, u) - \phi_{pq}(a_2, u)]\, du \right]. \qquad (A.126)$$

In regions from $R_5$ to $R_8$, we have

$$\begin{aligned}
I_{00}^{LM} &= I_{00}(a_1, \infty; b_1, \infty) \\
&= \int_{a_1}^{\infty} \phi_{00}(b_1, u)du + \int_{b_1}^{\infty} \phi_{00}(a_1, u)du \\
I_{00}^{0M} &= I_{00}(-\infty, a_2; b_1, \infty) = I_{00}(|a_2|, \infty; b_1, \infty) \\
&= \int_{|a_2|}^{\infty} \phi_{00}(b_1, u)du + \int_{b_1}^{\infty} \phi_{00}(|a_2|, u)du \\
I_{00}^{00} &= I_{00}(-\infty, a_2; -\infty, b_2) = I_{00}(|a_2|, \infty; |b_2|, \infty) \\
&= \int_{|a_2|}^{\infty} \phi_{00}(|b_2|, u)du + \int_{|b_2|}^{\infty} \phi_{00}(|a_2|, u)du \\
I_{00}^{L0} &= I_{00}(a_1, \infty; -\infty, b_2) = I_{00}(a_1, \infty; |b_2|, \infty) \\
&= \int_{a_1}^{\infty} \phi_{00}(|b_2|, u)du + \int_{|b_2|}^{\infty} \phi_{00}(a_1, u)du
\end{aligned} \qquad (A.127)$$

In terms of the coefficients $W_{lm}^{pq}$ defined above, the integral operator $M_d$ becomes

$$\begin{aligned} M_d F(\mathbf{r}) &= \alpha_0 \dot{M}_d F(\mathbf{r}') \\ &= \alpha_0 \sum_{l=1}^{L} \sum_{m=1}^{M} \left( \sum_{p=0}^{1} \sum_{q=0}^{1} W_{lm}^{pq} \right) F_{lm} - \alpha_0 F_{\lambda\mu} \sum_{l=0}^{L} \sum_{m=0}^{M} I_{00}^{lm} \\ \mathbf{r}' &= \alpha_0 \mathbf{r} \end{aligned} \tag{A.128}$$

## A.6 Summary

The results for the three integral operators $M_1$, $M_2$ and $M_d$ are summarised as follows. Note, however, that the constant factor $1/2\pi$ has now been included in the integral operators, so that $M_1$, $M_2$ and $M_d$ are again given by the original definitions quoted in (A.1), (A.2) and (A.3).

### A.6.1 Operators $M_1$ and $M_2$

Equations (A.1) and (A.2) become respectively

$$-M_1 Z_{\lambda\mu} = \frac{1}{2\pi}\sum_{l=1}^{L}\sum_{m=1}^{M} A^{lm}_{\lambda\mu} Z_{lm}; \quad -M_2 Z_{\lambda\mu} = \frac{1}{2\pi}\sum_{l=1}^{L}\sum_{m=1}^{M} B^{lm}_{\lambda\mu} Z_{lm} \qquad \text{(A.129)}$$

where

$$A^{lm}_{\lambda\mu} = Q^{00}_{lm} + Q^{10}_{l-1m} + Q^{01}_{lm-1} + Q^{11}_{l-1m-1} = \sum_{p=0}^{1}\sum_{q=0}^{1} Q^{pq}_{l-p\,m-q} \qquad \text{(A.130)}$$

$$B^{lm}_{\lambda\mu} = R^{00}_{lm} + R^{10}_{l-1m} + R^{01}_{lm-1} + R^{11}_{l-1m-1} = \sum_{p=0}^{1}\sum_{q=0}^{1} R^{pq}_{l-p\,m-q} \qquad \text{(A.131)}$$

$$\begin{cases} Q^{00}_{lm} = (a_{l+1}b_{m+1}I^{lm}_{\alpha} - a_{l+1}I^{lm}_{\alpha\beta} - b_{m+1}I^{lm}_{\alpha^2} + I^{lm}_{\alpha^2\beta})/g_l\,h_m \\ Q^{10}_{lm} = -(a_l b_{m+1}I^{lm}_{\alpha} - a_l I^{lm}_{\alpha\beta} - b_{m+1}I^{lm}_{\alpha^2} + I^{lm}_{\alpha^2\beta})/g_l\,h_m \\ Q^{01}_{lm} = -(a_{l+1}b_m I^{lm}_{\alpha} - a_{l+1}I^{lm}_{\alpha\beta} - b_m I^{lm}_{\alpha^2} + I^{lm}_{\alpha^2\beta})/g_l\,h_m \\ Q^{11}_{lm} = (a_l b_m I^{lm}_{\alpha} - a_l I^{lm}_{\alpha\beta} - b_m I^{lm}_{\alpha^2} + I^{lm}_{\alpha^2\beta})/g_l\,h_m \end{cases}$$

$$l = 1...L-1,\ m = 1...M-1, \qquad \text{(A.132)}$$

$$\begin{cases} R^{00}_{lm} = (a_{l+1}b_{m+1}I^{lm}_{\beta} - a_{l+1}I^{lm}_{\beta^2} - b_{m+1}I^{lm}_{\alpha\beta} + I^{lm}_{\alpha\beta^2})/g_l\,h_m \\ R^{10}_{lm} = -(a_l b_{m+1}I^{lm}_{\beta} - a_l I^{lm}_{\beta^2} - b_{m+1}I^{lm}_{\alpha\beta} + I^{lm}_{\alpha\beta^2})/g_l\,h_m \\ R^{01}_{lm} = -(a_{l+1}b_m I^{lm}_{\beta} - a_{l+1}I^{lm}_{\beta^2} - b_m I^{lm}_{\alpha\beta} + I^{lm}_{\alpha\beta^2})/g_l\,h_m \\ R^{11}_{lm} = (a_l b_m I^{lm}_{\beta} - a_l I^{lm}_{\beta^2} - b_m I^{lm}_{\alpha\beta} + I^{lm}_{\alpha\beta^2})/g_l\,h_m \end{cases}$$

$$l = 1...L-1,\ m = 1...M-1, \qquad \text{(A.133)}$$

$$
Q^{00}_{lm} = \begin{cases} (b_{m+1} I^{lm}_{\alpha} - I^{lm}_{\alpha\beta})/h_m, & l = L;\ m = 1 \ldots M-1, \\ (a_{l+1} I^{lm}_{\alpha} - I^{lm}_{\alpha^2})/g_l, & m = M;\ l = 1 \ldots L-1, \\ 0 & l = L;\ m = M, \end{cases}
$$

$$
Q^{10}_{lm} = \begin{cases} (b_{m+1} I^{lm}_{\alpha} - I^{lm}_{\alpha\beta})/h_m, & l = 0;\ m = 1 \ldots M-1, \\ -(a_l I^{lm}_{\alpha} - I^{lm}_{\alpha^2})/g_l, & m = M;\ l = 1 \ldots L-1, \\ 0 & l = 0;\ m = M, \end{cases}
$$

$$
Q^{01}_{lm} = \begin{cases} -(b_{m} I^{lm}_{\alpha} - I^{lm}_{\alpha\beta})/h_m, & l = L;\ m = 1 \ldots M-1, \\ (a_{l+1} I^{lm}_{\alpha} - I^{lm}_{\alpha^2})/g_l, & m = 0;\ l = 1 \ldots L-1, \\ 0 & l = L;\ m = 0, \end{cases}
$$

$$
Q^{11}_{lm} = \begin{cases} -(b_{m} I^{lm}_{\alpha} - I^{lm}_{\alpha\beta})/h_m, & l = 0;\ m = 1 \ldots M-1, \\ -(a_l I^{lm}_{\alpha} - I^{lm}_{\alpha^2})/g_l, & m = 0;\ l = 1 \ldots L-1, \\ 0 & l = 0;\ m = 0, \end{cases}
$$

$$
R^{00}_{lm} = \begin{cases} (b_{m+1} I^{lm}_{\beta} - I^{lm}_{\beta^2})/h_m, & l = L;\ m = 1 \ldots M-1, \\ (a_{l+1} I^{lm}_{\beta} - I^{lm}_{\alpha\beta})/g_l, & m = M;\ l = 1 \ldots L-1, \\ 0 & l = L;\ m = M, \end{cases}
$$

$$
R^{10}_{lm} = \begin{cases} (b_{m+1} I^{lm}_{\beta} - I^{lm}_{\beta^2})/h_m, & l = 0;\ m = 1 \ldots M-1, \\ -(a_l I^{lm}_{\beta} - I^{lm}_{\alpha\beta})/g_l, & m = M;\ l = 1 \ldots L-1, \\ 0 & l = 0;\ m = M, \end{cases}
$$

$$
R^{01}_{lm} = \begin{cases} -(b_{m} I^{lm}_{\beta} - I^{lm}_{\beta^2})/h_m, & l = L;\ m = 1 \ldots M-1, \\ (a_{l+1} I^{lm}_{\beta} - I^{lm}_{\alpha\beta})/g_l, & m = 0;\ l = 1 \ldots L-1, \\ 0 & l = L;\ m = 0, \end{cases}
$$

$$
R^{11}_{lm} = \begin{cases} -(b_{m} I^{lm}_{\beta} - I^{lm}_{\beta^2})/h_m, & l = 0;\ m = 1 \ldots M-1, \\ -(a_l I^{lm}_{\beta} - I^{lm}_{\alpha\beta})/g_l, & m = 0;\ l = 1 \ldots L-1, \\ 0 & l = 0;\ m = 0, \end{cases}
$$

(A.134)

$$
\begin{aligned}
I_{\alpha}^{lm} &= \operatorname{sgn}(\beta)\ln\left[\left(\frac{|\beta_2|+\sqrt{\alpha_1^2+\beta_2^2}}{|\beta_1|+\sqrt{\alpha_1^2+\beta_1^2}}\right)\left(\frac{|\beta_1|+\sqrt{\alpha_2^2+\beta_1^2}}{|\beta_2|+\sqrt{\alpha_2^2+\beta_2^2}}\right)\right]\\
I_{\alpha^2}^{lm} &= \operatorname{sgn}(\alpha)\left[\beta_2\ln\frac{|\alpha_2|+\sqrt{\alpha_2^2+\beta_2^2}}{|\alpha_1|+\sqrt{\alpha_1^2+\beta_2^2}}+\beta_1\ln\frac{|\alpha_1|+\sqrt{\alpha_1^2+\beta_1^2}}{|\alpha_2|+\sqrt{\alpha_2^2+\beta_1^2}}\right]\\
I_{\alpha^2\beta}^{lm} &= \frac{1}{2}\left[\alpha_2\left(\sqrt{\alpha_2^2+\beta_1^2}-\sqrt{\alpha_2^2+\beta_2^2}\right)-\alpha_1\left(\sqrt{\alpha_1^2+\beta_1^2}-\sqrt{\alpha_1^2+\beta_2^2}\right)\right]\\
&+ \frac{1}{2}\operatorname{sgn}(\alpha)\left[\beta_2^2\ln\frac{|\alpha_2|+\sqrt{\alpha_2^2+\beta_2^2}}{|\alpha_1|+\sqrt{\alpha_1^2+\beta_2^2}}+\beta_1^2\ln\frac{|\alpha_1|+\sqrt{\alpha_1^2+\beta_1^2}}{|\alpha_2|+\sqrt{\alpha_2^2+\beta_1^2}}\right]\\
I_{\beta}^{lm} &= \operatorname{sgn}(\alpha)\ln\left[\left(\frac{|\alpha_2|+\sqrt{\beta_1^2+\alpha_2^2}}{|\alpha_1|+\sqrt{\beta_1^2+\alpha_1^2}}\right)\left(\frac{|\alpha_1|+\sqrt{\beta_2^2+\alpha_1^2}}{|\alpha_2|+\sqrt{\beta_2^2+\alpha_2^2}}\right)\right]\\
I_{\beta^2}^{lm} &= \operatorname{sgn}(\beta)\left[\alpha_2\ln\frac{|\beta_2|+\sqrt{\beta_2^2+\alpha_2^2}}{|\beta_1|+\sqrt{\beta_1^2+\alpha_2^2}}+\alpha_1\ln\frac{|\beta_1|+\sqrt{\beta_1^2+\alpha_1^2}}{|\beta_2|+\sqrt{\beta_2^2+\alpha_1^2}}\right]\\
I_{\alpha\beta^2}^{lm} &= \frac{1}{2}\left[\beta_2\left(\sqrt{\beta_2^2+\alpha_1^2}-\sqrt{\beta_2^2+\alpha_2^2}\right)-\beta_1\left(\sqrt{\beta_1^2+\alpha_1^2}-\sqrt{\beta_1^2+\alpha_2^2}\right)\right]\\
&+ \frac{1}{2}\operatorname{sgn}(\beta)\left[\alpha_2^2\ln\frac{|\beta_2|+\sqrt{\beta_2^2+\alpha_2^2}}{|\beta_1|+\sqrt{\beta_1^2+\alpha_2^2}}+\alpha_1^2\ln\frac{|\beta_1|+\sqrt{\beta_1^2+\alpha_1^2}}{|\beta_2|+\sqrt{\beta_2^2+\alpha_1^2}}\right]\\
&l=1\ldots L-1,\quad m=1\ldots M-1,\\
&\qquad (l,m)\neq(\lambda,\mu),\ (\lambda-1,\mu),\ (\lambda,\mu-1),\ (\lambda-1,\mu-1)
\end{aligned}
$$

$$
\begin{aligned}
I_{\alpha\beta}^{lm} &= \left(\sqrt{\alpha_2^2+\beta_1^2}-\sqrt{\alpha_2^2+\beta_2^2}\right)-\left(\sqrt{\alpha_1^2+\beta_1^2}-\sqrt{\alpha_1^2+\beta_2^2}\right)\\
&\qquad l=1\ldots L-1,\quad m=1\ldots M-1
\end{aligned}
\tag{A.135}
$$

$$
\begin{aligned}
\tilde{I}_{\alpha}^{\lambda-p\,\mu-q} &= (-1)^{p+1}\log\left(h_{\mu-q}/g_{\lambda-p}+\sqrt{1+h_{\mu-q}^2/g_{\lambda-p}^2}\right)\\
\tilde{I}_{\alpha^2}^{\lambda-p\,\mu-q} &= h_{\mu-q}\log\left(\frac{g_{\lambda-p}}{h_{\mu-q}}+\sqrt{1+\frac{g_{\lambda-p}^2}{h_{\mu-q}^2}}\right)
\end{aligned}
$$

$$\tilde{I}^{\lambda-p\,\mu-q}_{\alpha^2\beta} = \frac{(-1)^q}{2}\left[g^2_{\lambda-p}\left(1-\sqrt{1+\frac{h^2_{\mu-q}}{g^2_{\lambda-p}}}\right)+h^2_{\mu-q}\log\left(\frac{g_{\lambda-p}}{h_{\mu-q}}+\sqrt{1+\frac{g^2_{\lambda-p}}{h^2_{\mu-q}}}\right)\right]$$

$$\tilde{I}^{\lambda-p\,\mu-q}_{\beta} = (-1)^{q+1}\log\left(g_{\lambda-p}/h_{\mu-q}+\sqrt{1+g^2_{\lambda-p}/h^2_{\mu-q}}\right)$$

$$\tilde{I}^{\lambda-p\,\mu-q}_{\beta^2} = g_{\lambda-p}\log\left(\frac{h_{\mu-q}}{g_{\lambda-p}}+\sqrt{1+\frac{h^2_{\mu-q}}{g^2_{\lambda-p}}}\right)$$

$$\tilde{I}^{\lambda-p\,\mu-q}_{\beta^2\alpha} = \frac{(-1)^p}{2}\left[h^2_{\mu-q}\left(1-\sqrt{1+\frac{g^2_{\lambda-p}}{h^2_{\mu-q}}}\right)+g^2_{\lambda-p}\log\left(\frac{h_{\mu-q}}{g_{\lambda-p}}+\sqrt{1+\frac{h^2_{\mu-q}}{g^2_{\lambda-p}}}\right)\right]$$

$$(l,m)=(\lambda-p,\mu-q);\quad p=0,1,\ q=0,1 \qquad \text{(A.136)}$$

$$I^{Lm}_{\alpha} = \lim_{\alpha_2\to+\infty} I^{lm}_{\alpha} = \operatorname{sgn}(\beta)\log\frac{|\beta_2|+\sqrt{\alpha_1^2+\beta_2^2}}{|\beta_1|+\sqrt{\alpha_1^2+\beta_1^2}}$$

$$I^{Lm}_{\alpha\beta} = \lim_{\alpha_2\to+\infty} I^{lm}_{\alpha\beta} = -\left(\sqrt{\alpha_1^2+\beta_1^2}-\sqrt{\alpha_1^2+\beta_2^2}\right),$$

$$I^{Lm}_{\beta} = \lim_{\alpha_2\to+\infty} I^{lm}_{\beta} = \log\frac{|\alpha_1|+\sqrt{\beta_2^2+\alpha_1^2}}{|\alpha_1|+\sqrt{\beta_1^2+\alpha_1^2}},$$

$$I^{Lm'}_{\beta^2} = \lim_{\alpha_2\to+\infty} I^{lm}_{\beta^2} = \operatorname{sgn}(\beta)\left[|\beta_2|-|\beta_1|-\alpha_1\log\frac{|\beta_2|+\sqrt{\beta_2^2+\alpha_1^2}}{|\beta_1|+\sqrt{\beta_1^2+\alpha_1^2}}\right],$$

$$l=L;\ m=1\ldots M-1, \qquad \text{(A.137)}$$

$$I^{0m}_{\alpha} = \lim_{\alpha_1\to-\infty} I^{lm}_{\alpha} = -\operatorname{sgn}(\beta)\log\frac{|\beta_2|+\sqrt{\alpha_2^2+\beta_2^2}}{|\beta_1|+\sqrt{\alpha_2^2+\beta_1^2}},$$

$$I^{0m}_{\alpha\beta} = \lim_{\alpha_1\to-\infty} I^{lm}_{\alpha\beta} = \sqrt{\alpha_2^2+\beta_1^2}-\sqrt{\alpha_2^2+\beta_2^2},$$

$$I^{0m}_{\beta} = \lim_{\alpha_1\to-\infty} I^{lm}_{\beta} = \log\frac{|\alpha_2|+\sqrt{\beta_2^2+\alpha_2^2}}{|\alpha_2|+\sqrt{\beta_1^2+\alpha_2^2}},$$

$$I^{0m}_{\beta^2} = \lim_{\alpha_1\to-\infty} I^{lm}_{\beta^2} = \operatorname{sgn}(\beta)\left[|\beta_2|-|\beta_1|+\alpha_2\log\frac{|\beta_2|+\sqrt{\beta_2^2+\alpha_2^2}}{|\beta_1|+\sqrt{\beta_1^2+\alpha_2^2}}\right],$$

$$l=0;\ m=1\ldots M-1, \qquad \text{(A.138)}$$

$$I^{lM}_{\alpha} = \lim_{\beta_2\to+\infty} I^{lm}_{\alpha} = \log\frac{|\beta_1|+\sqrt{\alpha_2^2+\beta_1^2}}{|\beta_1|+\sqrt{\alpha_1^2+\beta_1^2}},$$

$$
\begin{aligned}
I^{lM}_{\alpha^2} &= \lim_{\beta_2\to+\infty} I^{lm}_{\alpha^2} = \operatorname{sgn}(\alpha)\left[|\alpha_2| - |\alpha_1| - \beta_1 \log\frac{|\alpha_2| + \sqrt{\alpha_2^2+\beta_1^2}}{|\alpha_1| + \sqrt{\alpha_1^2+\beta_1^2}}\right],\\
I^{lM}_{\beta} &= \lim_{\beta_2\to+\infty} I^{lm}_{\beta} = \operatorname{sgn}(\alpha)\log\frac{|\alpha_2| + \sqrt{\beta_1^2+\alpha_2^2}}{|\alpha_1| + \sqrt{\beta_1^2+\alpha_1^2}},\\
I^{lM}_{\alpha\beta} &= \lim_{\beta_2\to+\infty} I^{lm}_{\alpha\beta} = -\left(\sqrt{\alpha_1^2+\beta_1^2} - \sqrt{\alpha_2^2+\beta_1^2}\right),\\
&\qquad\qquad l = 1\ldots L-1,\ m = M; \qquad\qquad (\Lambda.139)
\end{aligned}
$$

$$
\begin{aligned}
I^{l0}_{\alpha} &= \lim_{\beta_1\to-\infty} I^{lm}_{\alpha} = \log\frac{|\beta_2| + \sqrt{\alpha_2^2+\beta_2^2}}{|\beta_2| + \sqrt{\alpha_1^2+\beta_2^2}},\\
I^{l0}_{\alpha^2} &= \lim_{\beta_1\to-\infty} I^{lm}_{\alpha^2} = \operatorname{sgn}(\alpha)\left[|\alpha_2| - |\alpha_1| + \beta_2 \log\frac{|\alpha_2| + \sqrt{\alpha_2^2+\beta_2^2}}{|\alpha_1| + \sqrt{\alpha_1^2+\beta_2^2}}\right],\\
I^{l0}_{\beta} &= \lim_{\beta_1\to-\infty} I^{lm}_{\beta} = -\operatorname{sgn}(\alpha)\log\frac{|\alpha_2| + \sqrt{\beta_2^2+\alpha_2^2}}{|\alpha_1| + \sqrt{\beta_2^2+\alpha_1^2}},\\
I^{l0}_{\alpha\beta} &= \lim_{\beta_1\to-\infty} I^{lm}_{\alpha\beta} = \sqrt{\alpha_1^2+\beta_2^2} - \sqrt{\alpha_2^2+\beta_2^2},\\
&\qquad\qquad l = 1\ldots L-1,\ m = 0. \qquad\qquad (\Lambda.140)
\end{aligned}
$$

$$
\begin{aligned}
a_l &= x_l - x_\lambda, \quad \alpha_1 = a_l, \quad \alpha_2 = a_{l+1}, \quad g_l = x_{l+1} - x_l\\
b_m &= y_m - y_\mu, \quad \beta_1 = b_m, \quad \beta_2 = b_{m+1}, \quad h_m = y_{m+1} - y_m
\end{aligned}
\qquad (\Lambda.141)
$$

### A.6.2 Operator $M_d$

Equation (A.3) becomes: $\mathbf{r}' = \alpha_0 \mathbf{r}$, $M_d F(\mathbf{r}) = \alpha_0 \tilde{M}_d F(\mathbf{r}')$, and

$$\alpha_0 \tilde{M}_d F(\mathbf{r}'_{\lambda\mu}) = \frac{\alpha_0}{2\pi} \left( \sum_{l=1}^{L} \sum_{m=1}^{M} C_{\lambda\mu}^{lm} F_{lm} - F_{\lambda\mu} \sum_{l=0}^{L} \sum_{m=0}^{M} I_{00}^{lm} \right), \tag{A.142}$$

$$C_{\lambda\mu}^{lm} = W_{lm}^{00} + W_{l-1m}^{10} + W_{lm-1}^{01} + W_{l-1m-1}^{11} = \sum_{p=0}^{1} \sum_{q=0}^{1} W_{l-p\,m-q}^{pq} \tag{A.143}$$

$$\begin{pmatrix} W_{lm}^{00} \\ W_{lm}^{10} \\ W_{lm}^{01} \\ W_{lm}^{11} \end{pmatrix} = \frac{1}{g_l h_m} \begin{pmatrix} a_{l+1}b_{m+1}I_{00}^{lm} - a_{l+1}I_{01}^{lm} - b_{m+1}I_{10}^{lm} + I_{11}^{lm} \\ -a_l b_{m+1}I_{00}^{lm} + a_l I_{01}^{lm} + b_{m+1}I_{10}^{lm} - I_{11}^{lm} \\ -a_{l+1}b_m I_{00}^{lm} + a_{l+1}I_{01}^{lm} + b_m I_{10}^{lm} - I_{11}^{lm} \\ a_l b_m I_{00}^{lm} - a_l I_{01}^{lm} - b_m I_{10}^{lm} + I_{11}^{lm} \end{pmatrix}$$

$$l = 1...L-1, \quad m = 1, M-1,$$

$$(l,m) \neq (\lambda,\mu), (\lambda-1,\mu), (\lambda,\mu-1), (\lambda-1,\mu-1) \tag{A.144}$$

$$W_{lm}^{00} = \begin{cases} (b_{m+1}I_{00}^{lm} - I_{01}^{lm})/h_m, & l = L;\ m = 1...M-1, \\ (a_{l+1}I_{00}^{lm} - I_{10}^{lm})/g_l, & m = M;\ l = 1...L-1, \\ I_{00}^{LM}, & l = L;\ m = M, \end{cases}$$

$$W_{lm}^{10} = \begin{cases} (b_{m+1}I_{00}^{lm} - I_{01}^{lm})/h_m, & l = 0;\ m = 1...M-1, \\ -(a_l I_{00}^{lm} - I_{10}^{lm})/g_l, & m = M;\ l = 1...L-1, \\ I_{00}^{0M}, & l = 0;\ m = M, \end{cases}$$

$$W_{lm}^{01} = \begin{cases} -(b_m I_{00}^{lm} - I_{01}^{lm})/h_m, & l = L;\ m = 1...M-1, \\ (a_{l+1}I_{00}^{lm} - I_{10}^{lm})/g_l, & m = 0;\ l = 1...L-1, \\ I_{00}^{L0}, & l = L;\ m = 0, \end{cases}$$

$$W_{lm}^{11} = \begin{cases} -(b_m I_{00}^{lm} - I_{01}^{lm})/h_m, & l = 0;\ m = 1...M-1, \\ -(a_l I_{00}^{lm} - I_{10}^{lm})/g_l, & m = 0;\ l = 1...L-1, \\ I_{00}^{00}, & l = 0;\ m = 0, \end{cases}$$

$$\begin{array}{llll} W_{\lambda\mu}^{00} = \tilde{W}_{11}/4 & W_{\lambda-1\mu}^{00} = \tilde{W}_{01}/2 & W_{\lambda\mu-1}^{00} = \tilde{W}_{10}/2 & W_{\lambda-1\mu-1}^{00} = \tilde{W}_{00} \\ W_{\lambda\mu}^{10} = \tilde{W}_{21}/2 & W_{\lambda-1\mu}^{10} = \tilde{W}_{11}/4 & W_{\lambda\mu-1}^{10} = \tilde{W}_{20} & W_{\lambda-1\mu-1}^{10} = \tilde{W}_{10}/2 \\ W_{\lambda\mu}^{01} = \tilde{W}_{12}/2 & W_{\lambda-1\mu}^{01} = \tilde{W}_{02} & W_{\lambda\mu-1}^{01} = \tilde{W}_{11}/4 & W_{\lambda-1\mu-1}^{01} = \tilde{W}_{01}/2 \\ W_{\lambda\mu}^{11} = \tilde{W}_{22} & W_{\lambda-1\mu}^{11} = \tilde{W}_{12}/2 & W_{\lambda\mu-1}^{11} = \tilde{W}_{21}/2 & W_{\lambda-1\mu-1}^{11} = \tilde{W}_{11}/4 \end{array}$$

$$(l,m) = (\lambda,\mu), (\lambda-1,\mu), (\lambda,\mu-1), (\lambda-1,\mu-1) \tag{A.145}$$

$$\tilde{W}_{pq} = \begin{cases} +\frac{I_{22}-h_2 I_{21}-g_2 I_{12}+g_2 h_2 I_{11}}{g_0 g_s h_0 h_s} & (p,q)=(0,0) \\ -\frac{I_{22}-h_{20} I_{21}-g_2 I_{12}+g_2 h_{20} I_{11}}{g_0 g_s h_0 h_2} + \frac{I_{20}-g_2 I_{10}}{g_0 g_s} & (0,1) \\ +\frac{I_{22}+h_0 I_{21}-g_2 I_{12}-g_2 h_0 I_{11}}{g_0 g_s h_2 h_s} & (0,2) \\ -\frac{I_{22}-h_2 I_{21}+g_{20} I_{12}-g_{20} h_2 I_{11}}{g_0 g_2 h_0 h_s} + \frac{I_{02}-h_2 I_{01}}{h_0 h_s} & (1,0) \\ +\frac{I_{22}-h_{20} I_{21}-g_{20} I_{12}+g_{20} h_{20} I_{11}}{g_0 g_s h_0 h_s} - \frac{I_{20}-g_{20} I_{10}}{g_0 g_2} - \frac{I_{02}-h_{20} I_{01}}{h_0 h_2} & (1,1) \\ -\frac{I_{22}+h_0 I_{21}-g_{20} I_{12}-g_{20} h_0 I_{11}}{g_0 g_2 h_2 h_s} + \frac{I_{02}+h_0 I_{01}}{h_2 h_s} & (1,2) \\ +\frac{I_{22}-h_2 I_{21}+g_0 I_{12}-g_0 h_2 I_{11}}{g_2 g_s h_0 h_s} & (2,0) \\ -\frac{I_{22}-h_{20} I_{21}+g_0 I_{12}-g_0 h_{20} I_{11}}{g_2 g_s h_0 h_2} + \frac{I_{20}+g_0 I_{10}}{g_2 g_s} & (2,1) \\ +\frac{I_{22}+h_0 I_{21}+g_0 I_{12}+g_0 h_0 I_{11}}{g_2 g_s h_2 h_s} & (2,2) \end{cases} \qquad (\Lambda.146)$$

$$I_{11}^{lm} = \frac{1}{\sqrt{i}}\left[\exp(-\sqrt{i}\sqrt{a_2^2+b_2^2}) - \exp(-\sqrt{i}\sqrt{a_2^2+b_1^2}) - \exp(-\sqrt{i}\sqrt{a_1^2+b_2^2}) + \exp(-\sqrt{i}\sqrt{a_1^2+b_1^2})\right]$$
$$l = 1 \ldots L-1, \quad m = 1 \ldots M-1 \qquad (\Lambda.147)$$

$$I_{10}^{lm} = \int_{b_1}^{b_2} [f_{00}(a_1,u) - f_{00}(a_2,u)]\,du$$

$$I_{01}^{lm} = \int_{a_1}^{a_2} [f_{00}(b_1,u) - f_{00}(b_2,u)]\,du$$

$$I_{00}^{lm} = \int_{a_1}^{a_2} [\phi_{00}(b_1,u) - \phi_{00}(b_2,u)]\,du + \int_{b_1}^{b_2} [\phi_{00}(a_1,u) - \phi_{00}(a_2,u)]\,du$$
$$l = 1, \ldots L-1, \quad m = 1, \ldots M-1$$
$$(l,m) \neq (\lambda,\mu), (\lambda-1,\mu), (\lambda,\mu-1), (\lambda-1,\mu-1) \qquad (\Lambda.148)$$

$$I_{00}^{lm} = \begin{cases} \int_{b_1}^{b_2} \phi_{00}(|a_2|,u)du + \int_{|a_2|}^{\infty} [\phi_{00}(b_1,u) - \phi_{00}(b_2,u)]du, & l = 0 \\ \int_{b_1}^{b_2} \phi_{00}(a_1,u)du + \int_{a_1}^{\infty} [\phi_{00}(b_1,u) - \phi_{00}(b_2,u)]du, & l = L \\ & m = 1...M-1 \\ \int_{a_1}^{a_2} \phi_{00}(|b_2|,u)du + \int_{|b_2|}^{\infty} [\phi_{00}(a_1,u) - \phi_{00}(a_2,u)]du, & m = 0 \\ \int_{a_1}^{a_2} \phi_{00}(b_1,u)du + \int_{b_1}^{\infty} [\phi_{00}(a_1,u) - \phi_{00}(a_2,u)]du, & m = M \\ & l = 1...L-1 \\ \int_{|a_2|}^{\infty} \phi_{00}(|b_2|,u)du + \int_{|b_2|}^{\infty} \phi_{00}(|a_2|,u)du, & (l,m) = (0,0) \\ \int_{a_1}^{\infty} \phi_{00}(|b_2|,u)du + \int_{|b_2|}^{\infty} \phi_{00}(a_1,u)du, & (l,m) = (L,0) \\ \int_{|a_2|}^{\infty} \phi_{00}(b_1,u)du + \int_{b_1}^{\infty} \phi_{00}(|a_2|,u)du, & (l,m) = (0,M) \\ \int_{a_1}^{\infty} \phi_{00}(b_1,u)du + \int_{b_1}^{\infty} \phi_{00}(a_1,u)du, & (l,m) = (L,M) \end{cases} \tag{A.149}$$

$$I_{01}^{lm} = \begin{cases} \int_{b_1}^{b_2} \phi_{01}(|a_2|,u)du + \int_{|a_2|}^{\infty} [\phi_{10}(b_1,u) - \phi_{10}(b_2,u)]du, & l = 0 \\ \int_{b_1}^{b_2} \phi_{01}(a_1,u)du + \int_{a_1}^{\infty} [\phi_{10}(b_1,u) - \phi_{10}(b_2,u)]du, & l = L \\ & m = 1...M-1 \end{cases} \tag{A.150}$$

$$I_{10}^{lm} = \begin{cases} \int_{a_1}^{a_2} \phi_{01}(|b_2|,u)du + \int_{|b_2|}^{\infty} [\phi_{10}(a_1,u) - \phi_{10}(a_2,u)]du, & m = 0 \\ \int_{a_1}^{a_2} \phi_{01}(b_1,u)du + \int_{b_1}^{\infty} [\phi_{10}(a_1,u) - \phi_{10}(a_2,u)]du, & m = M \\ & l = 1...L-1 \end{cases} \tag{A.151}$$

$$(a_1,a_2,b_1,b_2) = (x_l - x_\lambda,\ x_{l+1} - x_\lambda,\ y_m - y_\mu,\ y_{m+1} - y_\mu) \tag{A.152}$$

$I_{pq}$ in $\tilde{W}_{pq}$ are given by

$$I_{pq} = \int_{a_1}^{a_2} [\phi_{qp}(b_1, u) - \phi_{qp}(b_2, u)]du + \int_{b_1}^{b_2} [\phi_{pq}(a_1, u) - \phi_{pq}(a_2, u)]du$$
$$p = 0, 1, 2;\ q = 0, 1, 2;\ (p, q) \neq (0, 0) \qquad (A.153)$$

$$(a_1, a_2, b_1, b_2) = (-g_{\lambda-1}, g_\lambda, -h_{\mu-1}, h_\mu). \qquad (A.154)$$

The functions $\phi_{pq}$ and $f_{00}$ are given by

$$\phi_{pq}(x, y) = \frac{x^{p+1} y^q}{r^{p+q+2}} f_{pq}(r),\ \ r = \sqrt{x^2 + y^2}$$
$$f_{pq}(r) = \int_r^\infty u^{p+q-2}(1 + \sqrt{i}u) \exp(-\sqrt{i}u)\, du \qquad (A.155)$$

where

$$f_{00}(r) = \frac{1}{r} \exp(-\sqrt{i}r)$$
$$f_{20}(r) = f_{02}(r) = \frac{(2 + \sqrt{i}r)}{\sqrt{i}} \exp(-\sqrt{i}r)$$
$$f_{22}(r) = -\sqrt{i} \left[ (\sqrt{i}r)^2 (4 + \sqrt{i}r) + 8(1 + \sqrt{i}r) \right]. \qquad (A.156)$$

All the integrals satisfy the relation

$$I_{pq}(a_1, a_2; b_1, b_2) = I_{qp}(b_1, b_2; a_1, a_2) \qquad (A.157)$$

# Appendix B

# INTEGRALS FOR BOUNDARY CONDITIONS IN TWO-DIMENSIONAL EM MODELLING

In this appendix we will discuss the integrals that arose from the Top-Boundary-Conditions (TBC) and the Bottom-Boundary-Conditions (BBC) for the 2D problems in Chapter 2.

## B.1 The Hilbert Transform

The Hilbert transform enters the Top-Boundary-Condition (TBC) at z=0- in the 2D E-polarization mode via equation (2.1). It is given by Weaver (1964) and can also be obtained from the TBC of the 3D problem, when the conductivity distribution is 2D, by integrating from $-\infty$ to $+\infty$ in the direction of the strike.

The definitions $y_0 = -\infty$ and $y_{M+1} = +\infty$ will be used throughout this appendix. For evaluating the integral numerically, we write the Hilbert transform at the point of $y = y_\mu$ as

$$\mathcal{H}Z_\mu = \frac{1}{\pi} \int\!\!\!\!\!\!- _{-\infty}^{\infty} \frac{Z(v)}{y_\mu - v} dv = -\frac{1}{\pi} I \tag{B.1}$$

where we have defined

$$\begin{aligned} I &:= \int\!\!\!\!\!\!- _{-\infty}^{\infty} \frac{Z(v)}{v - y_\mu} dv = \left[ \int_{y_0}^{y_1} + \int_{y_1}^{y_{\mu-1}} + \int\!\!\!\!\!\!- _{y_{\mu-1}}^{y_{\mu+1}} + \int_{y_{\mu+1}}^{y_M} + \int_{y_M}^{y_{M+1}} \right] \frac{Z(v)}{v - y_\mu} dv \\ &= I_0 + \sum_{m=1}^{\mu-2} I_m + I_s + \sum_{m=\mu+1}^{M-1} I_m + I_M \end{aligned} \tag{B.2}$$

in which

$$I_m = \int_{y_m}^{y_{m+1}} \frac{Z(v)}{v - y_\mu} dv, \quad I_s = \int\!\!\!\!\!\!- _{y_{\mu-1}}^{y_{\mu+1}} \frac{Z(v)}{v - y_\mu} dv. \tag{B.3}$$

Since we assume that 1D solutions are applied at $y = y_1$ and $y = y_M$ as the side boundary conditions where there is no variation in the $Z$-component, i.e. $Z \equiv 0$. Therefore, we have $Z \equiv 0$ for $y \leq y_1$ or $y \geq y_M$, whence $I_0 \equiv 0$ and $I_M \equiv 0$. We shall assume that $Z(v)$ varies linearly between any two consecutive nodal points, $y_m$ and $y_{m+1}$, i.e.

$$Z(v) = \frac{v - y_m}{h_m} Z_{m+1} + \frac{y_{m+1} - v}{h_m} Z_m, \quad y_m \leq v \leq y_{m+1}. \tag{B.4}$$

By defining

$$\beta = v - y_\mu, \qquad b_m = y_m - y_\mu, \tag{B.5}$$

we have

$$v - y_m = \beta - b_m, \quad v - y_{m+1} = \beta - b_{m+1}, \quad b_{m+1} = b_m + h_m. \tag{B.6}$$

Inserting (B.5) and (B.6) into (B.4), we obtain

$$Z(v) = Z(v(\beta)) = \frac{\beta - b_m}{h_m} Z_{m+1} - \frac{\beta - b_{m+1}}{h_m} Z_m. \tag{B.7}$$

It follows that

$$\begin{aligned} I_m &= \int_{y_m}^{y_{m+1}} \frac{Z(v)}{v - y_\mu} dv \\ &= \frac{Z_{m+1}}{h_m} \int_{b_m}^{b_{m+1}} \left(1 - \frac{b_m}{\beta}\right) d\beta - \frac{Z_m}{h_m} \int_{b_m}^{b_{m+1}} \left(1 - \frac{b_{m+1}}{\beta}\right) d\beta \\ &= \left(1 - \frac{b_m}{h_m} A_m\right) Z_{m+1} - \left(1 - \frac{b_{m+} }{h_m} A_m\right) Z_m \\ &= c_m^1 Z_{m+1} + c_m^0 Z_m \end{aligned} \tag{B.8}$$

where we have defined

$$c_m^1 = 1 - \frac{b_m}{h_m} A_m, \quad c_m^0 = -\left(1 - \frac{b_{m+1}}{h_m} A_m\right), \quad A_m = \ln \left| \frac{b_{m+1}}{b_m} \right|. \tag{B.9}$$

Using the transformation defined in (B.5) once more, we can write the integral in the neighbourhood of the singular point as

$$\begin{aligned} I_s = \fint_{y_{\mu-1}}^{y_{\mu+1}} \frac{Z(v)}{v - y_\mu} dv &= \lim_{\epsilon \to 0} \left[ \int_{y_{\mu-1}}^{y_\mu - \epsilon} + \int_{y_\mu + \epsilon}^{y_{\mu+1}} \right] \frac{Z(v)}{v - y_\mu} dv \\ &= \lim_{\epsilon \to 0} \left[ \int_{-h_{\mu-1}}^{-\epsilon} + \int_{\epsilon}^{h_\mu} \right] \frac{Z(v(\beta))}{\beta} d\beta \end{aligned} \tag{B.10}$$

For the first part of the above integral, in which $-h_{\mu-1} \le \beta \le -\epsilon$, we have

$$m = \mu - 1,\ b_m = -h_{\mu-1},\ b_{m+1} = -\epsilon,\ h_m = h_{\mu-1},\ Z_m = Z_{\mu-1},\ Z_{m+1} = Z_\mu$$

and, following (B.7),

$$\begin{aligned} Z(v) = Z(v(\beta)) &= \frac{\beta + h_{\mu-1}}{h_{\mu-1}} Z_\mu - \frac{\beta + \epsilon}{h_{\mu-1}} Z_{\mu-1} \\ &= \frac{Z_\mu - Z_{\mu-1}}{h_{\mu-1}} \beta + \left( Z_\mu - \frac{\epsilon}{h_{\mu-1}} Z_{\mu-1} \right). \end{aligned} \tag{B.11}$$

Similarly, for the second part of the integral, in which $\epsilon \le \beta \le h_\mu$, we have

$$m = \mu,\ b_m = \epsilon,\ b_{m+1} = h_\mu,\ h_m = h_\mu,\ Z_m = Z_\mu,\ Z_{m+1} = Z_{\mu+1}$$

and

$$\begin{aligned} Z(v) = Z(v(\beta)) &= \frac{\beta - \epsilon}{h_\mu} Z_{\mu+1} - \frac{\beta - h_\mu}{h_\mu} Z_\mu \\ &= \frac{Z_{\mu+1} - Z_\mu}{h_\mu} \beta + \left( Z_\mu - \frac{\epsilon}{h_\mu} Z_{\mu+1} \right). \end{aligned} \tag{B.12}$$

It follows that,

$$\begin{aligned} I_s &= \lim_{\epsilon \to 0} \left\{ \int_{-h_{\mu-1}}^{-\epsilon} \left[ \frac{Z_\mu - Z_{\mu-1}}{h_{\mu-1}} + \left( Z_\mu - \frac{\epsilon}{h_{\mu-1}} Z_{\mu-1} \right) \frac{1}{\beta} \right] d\beta \right. \\ &\qquad \left. + \int_{\epsilon}^{h_\mu} \left[ \frac{Z_{\mu+1} - Z_\mu}{h_\mu} + \left( Z_\mu - \frac{\epsilon}{h_\mu} Z_{\mu+1} \right) \frac{1}{\beta} \right] d\beta \right\} \\ &= Z_{\mu+1} - Z_{\mu-1} + \lim_{\epsilon \to 0} [Z_\mu \ln |\epsilon / h_{\mu-1}| + Z_\mu \ln |h_\mu / \epsilon|] \\ &= Z_{\mu+1} - Z_{\mu-1} + Z_\mu \lim_{\epsilon \to 0} \ln |(h_\mu / \epsilon)(\epsilon / h_{\mu-1})| \\ &= -Z_{\mu-1} + Z_\mu \ln |h_\mu / h_{\mu-1}| + Z_{\mu+1}. \end{aligned} \tag{B.13}$$

Since $h_\mu > 0$, $h_{\mu-1} > 0$, we can also write

$$I_s = -Z_{\mu-1} + Z_\mu \ln(h_\mu / h_{\mu-1}) + Z_{\mu+1}. \tag{B.14}$$

Now we can write $I$ as

$$I = \sum_{m=1}^{\mu-2} I_m + I_s + \sum_{m=\mu+1}^{M-1} I_m$$

$$
\begin{aligned}
&= \sum_{m=1}^{\mu-2}(c_m^1 Z_{m+1} + c_m^0 Z_m) - Z_{\mu-1} + \ln(h_\mu/h_{\mu-1})Z_\mu + Z_{\mu+1} \\
&+ \sum_{m=\mu+1}^{M-1}(c_m^1 Z_{m+1} + c_m^0 Z_m) \\
&= \sum_{m=2}^{\mu-1} c_{m-1}^1 Z_m + \sum_{m=1}^{\mu-2} c_m^0 Z_m - Z_{\mu-1} + (\ln h_\mu/h_{\mu-1})Z_\mu + Z_{\mu+1} \\
&+ \sum_{m=\mu+2}^{M} c_{m-1}^1 Z_m + \sum_{m=\mu+1}^{M-1} c_m^0 Z_m \\
&= c_1^0 Z_1 + \sum_{m=2}^{\mu-2}(c_{m-1}^1 + c_m^0)Z_m + (c_{\mu-2}^1 - 1)Z_{\mu-1} + (-\ln h_{\mu-1} + \ln h_\mu)Z_\mu \\
&+ (1 + c_{\mu+1}^0)Z_{\mu+1} + \sum_{m=\mu+2}^{M-1}(c_{m-1}^1 + c_m^0)Z_m + c_{M-1}^1 Z_M \\
&= \sum_{m=1}^{M}(c_{m-1}^1 + c_m^0)Z_m = \sum_{m=1}^{M} H_{\mu m} Z_m
\end{aligned}
\tag{B.15}
$$

where

$$
H_{\mu m} = c_{m-1}^1 + c_m^0 \tag{B.16}
$$

with $c_m^1$ and $c_m^0$ redefined as

$$
c_m^0 = \begin{cases} 0 & m = 0 \\ (1 - A_m b_m/h_m) & m = 1 \ldots \mu - 2 \\ -1 & m = \mu - 1 \\ \ln h_\mu & m = \mu \\ (1 - A_m b_m/h_m) & m = \mu + 1 \ldots M - 1 \end{cases} \tag{B.17}
$$

$$
c_m^1 = \begin{cases} -(1 - A_m b_{m+1}/h_m) & m = 1 \ldots \mu - 2 \\ -\ln h_{\mu-1} & m = \mu - 1 \\ 1 & m = \mu \\ -(1 - A_m b_{m+1}/h_m) & m = \mu + 1 \ldots M - 1 \\ 0 & m = M \end{cases} \tag{B.18}
$$

and $A_m$ still given by (B.9) as $A_m = \ln|b_{m+1}/b_m|$. The Hilbert transform can therefore be written as

$$
\mathcal{H}Z_\mu = \frac{1}{\pi}\int_{-\infty}^{\infty} \frac{Z(v)}{y_\mu - v} dv = -\frac{1}{\pi}\sum_{m=1}^{M} H_{\mu m} Z_m. \tag{B.19}
$$

## B.2 Integrals in the Bottom Boundary Conditions

The following type of integral was used in equation (2.24) for the 2D bottom boundary conditions:

$$I = \int_{-\infty}^{\infty} [F(v) - F(y_\mu)] \frac{K_1(|y_\mu - v|\alpha_0\sqrt{i})}{|y_\mu - v|} dv. \tag{B.20}$$

It can be broken up as

$$I = \left[ \int_{y_0}^{y_1} + \sum_{m=1}^{\mu-2} \int_{y_m}^{y_{m+1}} + \int_{y_{\mu-1}}^{y_{\mu+1}} + \sum_{m=\mu-1}^{M-1} \int_{y_m}^{y_{m+1}} + \int_{y_M}^{y_{M+1}} \right] [F(v) - F_\mu] \frac{K_1(|y_\mu - v|\alpha_0\sqrt{i})}{|y_\mu - v|} dv \tag{B.21}$$

where we have denoted $F(y_\mu)$ by $F_\mu$.

Since $|y_1|$ and $|y_M|$ must be sufficiently large, $F$ is assumed to be constant in the regions $y < y_1$ and $y > y_M$, and linear variations in the regions $y_m \leq y \leq y_{m+1}$ for $m = 1, ..., \mu - 2$ and $m = \mu + 1, ..., M - 1$ are assumed. In the neighbourhood of the singular point, $y_{\mu-1} \leq y \leq y_{\mu+1}$, $F$ is expanded in a Taylor series to second order. Therefore, we can write

$$F(v) = \begin{cases} F_1 & y \leq y_1 \\ \frac{1}{h_m}(v - y_m)F_{m+1} + \frac{1}{h_m}(y_{m+1} - v)F_m & v \in [y_m, y_{m+1}], \\ & m = 1, ..., \mu - 2 \\ F_\mu + (v - y_\mu)F'_\mu + \frac{1}{2}(v - y_\mu)^2 F''_\mu & v \in [y_{\mu-1}, y_{\mu+1}] \\ \frac{1}{h_m}(v - y_m)F_{m+1} + \frac{1}{h_m}(y_{m+1} - v)F_m & v \in [y_m, y_{m+1}], \\ & m = \mu + 1, ..., M - 1 \\ F_M & y \geq y_M. \end{cases} \tag{B.22}$$

The transformation $\beta = v - y_\mu$ and definition $b_m := y_m - y_\mu$ take $F$ into the form

$$F(\beta) = \begin{cases} F_1 & \beta \leq b_1 \\ \frac{\beta - b_m}{h_m} F_{m+1} + \frac{b_{m+1} - \beta}{h_m} F_m & \beta \in [b_m, b_{m+1}], \\ & m = 1, ..., \mu - 2 \\ F_\mu + \beta F'_\mu + \frac{1}{2}\beta^2 F''_\mu & \beta \in [b_{\mu-1}, b_{\mu+1}] \\ \frac{\beta - b_m}{h_m} F_{m+1} + \frac{b_{m+1} - \beta}{h_m} F_m & \beta \in [b_m, b_{m+1}], \\ & m = \mu + 1, ..., M - 1 \\ F_M & \beta \leq b_M. \end{cases} \tag{B.23}$$

The integral (B.21) then becomes

$$I = \left[\int_{b_0}^{b_1} + \sum_{m=1}^{\mu-2}\int_{b_m}^{b_{m+1}} + \int_{b_{\mu-1}}^{b_{\mu+1}} + \sum_{m=\mu-1}^{M-1}\int_{b_m}^{b_{m+1}} + \int_{b_M}^{b_{M+1}}\right] [F(\beta) - F_\mu]\frac{K_1(|\beta|\alpha_0\sqrt{i})}{|\beta|}d\beta$$

$$= I_0 + \sum_{m=1}^{\mu-2} I_m + I_s + \sum_{m=\mu-1}^{M-1} I_m + I_M. \tag{B.24}$$

Since for integral $I_0$, $b_0 = -\infty$, $b_1 = y_1 - y_\mu < 0$, it follows that $\beta < 0$. We then have,

$$I_0 = \int_{b_0}^{b_1}(F_1 - F_\mu)\frac{K_1(|\beta|\alpha_0\sqrt{i})}{|\beta|}d\beta = (F_1 - F_\mu)p_0^0 \tag{B.25}$$

where

$$p_0^0 = \int_{b_0}^{b_1}\frac{K_1(|\beta|\alpha_0\sqrt{i})}{|\beta|}d\beta = \int_{-|b_0|}^{-|b_1|}\frac{K_1(|\beta|\alpha_0\sqrt{i})}{|\beta|}d\beta = -\int_{|b_0|}^{|b_1|}\frac{K_1(\beta\alpha_0\sqrt{i})}{\beta}d\beta. \tag{B.26}$$

In the integral $I_M$, we have $b_M = y_M - y_\mu > 0$, $y_{M+1} = +\infty > 0$, so that $\beta > 0$ and

$$I_M = \int_{b_M}^{b_{M+1}}(F_M - F_\mu)\frac{K_1(|\beta|\alpha_0\sqrt{i})}{|\beta|}d\beta = (F_M - F_\mu)p_M^0 \tag{B.27}$$

where

$$p_M^0 = \int_{b_M}^{b_{M+1}}\frac{K_1(|\beta|\alpha_0\sqrt{i})}{|\beta|}d\beta = \int_{|b_M|}^{|b_{M+1}|}\frac{K_1(\beta\alpha_0\sqrt{i})}{\beta}d\beta. \tag{B.28}$$

For the integral $I_m$, $m = 1, ..., \mu - 2$ or $m = \mu + 1, ..., M - 1$, we have

$$I_m = \int_{b_m}^{b_{m+1}}\left(\frac{\beta - b_m}{h_m}F_{m+1} - \frac{\beta - b_{m+1}}{h_m}F_m - F_\mu\right)\frac{K_1(|\beta|\alpha_0\sqrt{i})}{|\beta|}d\beta$$

$$= B_m^1 F_{m+1} + B_m^0 F_m - p_m^0 F_\mu \tag{B.29}$$

where

$$B_m^1 = (p_m^1 - b_m p_m^0)/h_m, \quad B_m^0 = -(p_m^1 - b_{m+1}p_m^0)/h_m \tag{B.30}$$

and

$$p_m^0 = \int_{b_m}^{b_{m+1}}\frac{K_1(|\beta|\alpha_0\sqrt{i})}{|\beta|}d\beta, \quad p_m^1 = \int_{b_m}^{b_{m+1}}\frac{\beta K_1(|\beta|\alpha_0\sqrt{i})}{|\beta|}d\beta. \tag{B.31}$$

For $m = 1, ..., \mu - 2$, we note that $b_m < \beta < b_{m+1} < 0$, whence

$$p_m^0 = \int_{-|b_m|}^{-|b_{m+1}|} \frac{K_1(|\beta|\alpha_0\sqrt{i})}{|\beta|} d\beta = -\int_{|b_m|}^{|b_{m+1}|} \frac{K_1(\beta\alpha_0\sqrt{i})}{\beta} d\beta, \tag{B.32}$$

$$p_m^1 = \int_{-|b_m|}^{-|b_{m+1}|} \frac{\beta K_1(|\beta|\alpha_0\sqrt{i})}{|\beta|} d\beta = \int_{|b_m|}^{|b_{m+1}|} K_1(\beta\alpha_0\sqrt{i}) d\beta; \tag{B.33}$$

while for $m = \mu + 1, ..., M - 1$, we have $0 < b_m < \beta < b_{m+1}$, and

$$p_m^0 = \int_{|b_m|}^{|b_{m+1}|} \frac{K_1(\beta\alpha_0\sqrt{i})}{\beta} d\beta, \quad p_m^1 = \int_{|b_m|}^{|b_{m+1}|} K_1(\beta\alpha_0\sqrt{i}) d\beta. \tag{B.34}$$

Combining (B.26), (B.28), (B.32), (B.33) and (B.34), we can write generally

$$\begin{aligned} p_m^0 &= \operatorname{sgn}(\beta) \int_{|b_m|}^{|b_{m+1}|} \frac{K_1(\beta\alpha_0\sqrt{i})}{\beta} d\beta, \ m = 0, ..., \mu - 2, \mu + 1, ..., M; \\ p_m^1 &= \int_{|b_m|}^{|b_{m+1}|} K_1(\beta\alpha_0\sqrt{i}) d\beta, \quad m = 1, ..., \mu - 2, \ \mu + 1, ..., M - 1; \\ p_m^0 &= p_m^1 \equiv 0, \qquad\qquad m = \mu - 1, \ \mu. \end{aligned} \tag{B.35}$$

Since $b_{\mu-1} = y_{\mu-1} - y_\mu = -h_{\mu-1}$ and $b_{\mu+1} = y_{\mu+1} - y_\mu = h_\mu$ for the integral $I_s$, it follows that

$$I_s = \int_{-h_{\mu-1}}^{h_{\mu+1}} (\beta F'_\mu + \frac{1}{2}\beta^2 F''_\mu) \frac{K_1(|\beta|\alpha_0\sqrt{i})}{|\beta|} d\beta = F'_\mu I'_s + \frac{1}{2} F''_\mu I''_s. \tag{B.36}$$

The integral $I'_s$ can be written as

$$\begin{aligned} I'_s &= \int_{-h_{\mu-1}}^{h_{\mu+1}} \frac{K_1(|\beta|\alpha_0\sqrt{i})}{|\beta|} d\beta = \int_{h_{\mu-1}}^{h_{\mu+1}} K_1(\beta\alpha_0\sqrt{i}) d\beta \\ &= -\frac{1}{\alpha_0\sqrt{i}} [K_0(h_\mu\alpha_0\sqrt{i}) - K_0(h_{\mu-1}\alpha_0\sqrt{i})]. \end{aligned} \tag{B.37}$$

where in the last step, the relation

$$K_1(z) = -K'_0(z) \tag{B.38}$$

given in Olver (1964, 9.6.27, p376) together with the definition $z := \beta\alpha_0\sqrt{i}$ have been used. Similarly, with definitions

$$z_{\mu-1} := h_{\mu-1}\alpha_0\sqrt{i}, \quad z_\mu := h_\mu\alpha_0\sqrt{i}, \tag{B.39}$$

we have

$$\begin{aligned} I_s'' &= \int_{-h_{\mu-1}}^{h_{\mu+1}} \frac{\beta^2 K_1(|\beta|\alpha_0\sqrt{i})}{|\beta|} d\beta = \frac{1}{\alpha_0^2 i}\left[\int_0^{z_{\mu-1}} + \int_0^{z_\mu}\right] z K_1(z) dz \\ &= \frac{1}{\alpha_0^2 i}[H(z_{\mu-1}) - z_{\mu-1}K_0(z_{\mu-1}) + H(z_\mu) - z_\mu K_0(z_\mu)] \end{aligned} \tag{B.40}$$

where $H(z_m) = \int_0^{Z_m} K_0(z)dz$. Replacing the derivatives in $I_s$ by their corresponding finite difference expressions, we obtain

$$\begin{aligned} I_s &= F_\mu' I_s' + \frac{1}{2}F_\mu'' I_s'' \\ &= I_s'\left(\frac{h_{\mu-1}}{h_\mu h_\mu^+}F_{\mu+1} + \frac{h_\mu^-}{h_{\mu-1}h_\mu}F_\mu - \frac{h_\mu}{h_{\mu-1}h_\mu^+}F_{\mu-1}\right) \\ &+ \frac{1}{2}I_s''\left(\frac{2}{h_\mu h_\mu^+}F_{\mu+1} - \frac{2}{h_{\mu-1}h_\mu}F_\mu + \frac{2}{h_{\mu-1}h_\mu^+}F_{\mu-1}\right) \\ &= B_{\mu-1}^0 F_{\mu-1} + (B_{\mu-1}^1 + B_\mu^0)F_\mu + B_\mu^1 F_{\mu+1} \end{aligned} \tag{B.41}$$

where

$$\begin{aligned} B_{\mu-1}^0 &= \frac{-h_\mu I_s' + I_s''}{h_{\mu-1}h_\mu^+},\ B_{\mu-1}^1 = B_\mu^0 = \frac{h_\mu^- I_s' - I_s''}{2h_{\mu-1}h_\mu},\ B_\mu^1 = \frac{h_{\mu-1}I_s' + I_s''}{h_\mu h_\mu^+}, \\ h_\mu^+ &= h_\mu + h_{\mu-1},\quad h_\mu^- = h_\mu - h_{\mu-1}. \end{aligned} \tag{B.42}$$

Taking all these results into account, we see that (B.24) becomes

$$\begin{aligned} I &= I_0 + \sum_{m=1}^{\mu-2} I_m + I_s + \sum_{m=\mu-1}^{M-1} I_m + I_M \\ &= (F_1 - F_\mu)p_0^0 + \sum_{m=1}^{\mu-2}(B_m^1 F_{m+1} + B_m^0 F_m - F_\mu p_m^0) \\ &+ B_{\mu-1}^0 F_{\mu-1} + (B_{\mu-1}^1 + B_\mu^0)F_\mu + B_\mu^1 F_{\mu+1} \\ &+ \sum_{m=\mu+1}^{M-1}(B_m^1 F_{m+1} + B_m^0 F_m - F_\mu p_m^0) + (F_M - F_\mu)p_M^0 \\ &= (p_0^0 + B_1^0)F_1 + \sum_{m=2}^{\mu-2}(B_{m-1}^1 + B_m^0)F_m \\ &+ (B_{\mu-2}^1 + B_{\mu-1}^0)F_{\mu-1} + (B_{\mu-1}^1 + B_\mu^0)F_\mu + (B_\mu^1 + B_{\mu+1}^0)F_{\mu+1} \\ &+ \sum_{m=\mu+2}^{M-1}(B_{m-1}^1 + B_m^0)F_m + (B_{M-1}^1 + p_M^0)F_M - F_\mu \sum_{m=0}^{M} p_m^0 \end{aligned}$$

$$= \sum_{m=1}^{M} (B_{m-1}^1 + B_m^0) F_m - F_\mu \sum_{m=0}^{M} p_m^0. \tag{B.43}$$

By defining

$$C_{\mu m} = B_{\mu-1}^1 + B_\mu^0 \tag{B.44}$$

and re-definining $B_m^0$ and $B_m^1$ as

$$B_m^0 = \begin{cases} 0 & m = 0 \\ -(p_m^1 - b_{m+1} p_m^0)/h_m & m = 1, \ldots, \mu - 2 \\ (-h_\mu I_s' + I_s'')/(h_{\mu-1} h_\mu^+) & m = \mu - 1 \\ \frac{1}{2}[(h_\mu^- I_s' - I_s'')/(h_{\mu-1} h_\mu) - S] & m = \mu \\ -(p_m^1 - b_{m+1} p_m^0)/h_m & m = \mu + 1, \ldots, M - 1 \\ p_m^0 & m = M, \end{cases} \tag{B.45}$$

$$B_m^0 = \begin{cases} p_0^0 & m = 0 \\ (p_m^1 - b_m p_m^0)/h_m & m = 1, \ldots, \mu - 2 \\ \frac{1}{2}[(h_\mu^- I_s' - I_s'')\,'(h_{\mu-1} h_\mu) - S] & m = \mu - 1 \\ (h_{\mu-1} I_s' + I_s'')/(h_\mu h_\mu^+) & m = \mu \\ (p_m^1 - b_m p_m^0)/h_m & m = \mu + 1, \ldots, M - 1 \\ 0 & m = M. \end{cases} \tag{B.46}$$

where

$$S = \sum_{m=0}^{M} p_m^0, \tag{B.47}$$

we can finally write the integral (B.24), and hence (B.20), as

$$I = \int_{-\infty}^{\infty} [F(v) - F(y_\mu)] \frac{K_1(|y_\mu - v|\alpha_0\sqrt{i})}{|y_\mu - v|} dv = \sum_{m=1}^{M} C_{\mu m} F_m. \tag{B.48}$$